(2)

PROJECT SUMMARY
TO THE
OFFICE OF NAVAL RESEARCH

OF A WORK ENTITLED

DEPHASING PROCESSES IN III-V SEMICONDUCTORS

UNDER THE DIRECTION OF
DR. GUY D. GILLILAND, PRINCIPAL INVESTIGATOR

ASSISTANT PROFESSOR
IN THE
DEPARTMENT OF PHYSICS AND ASTRONOMY
OF
EMORY UNIVERSITY

PROJECT SUMMARY
TO THE
OFFICE OF NAVAL RESEARCH

OF A WORK ENTITLED

DEPHASING PROCESSES IN III-V SEMICONDUCTORS

UNDER THE DIRECTION OF
DR. GUY D. GILLILAND, PRINCIPAL INVESTIGATOR

ASSISTANT PROFESSOR
IN THE
DEPARTMENT OF PHYSICS AND ASTRONOMY
OF
EMORY UNIVERSITY

R&T Number: 414r008---04
Contract/Grant Number: N00014-92-J-1927
Contract Dates: 1 October 1992 through 30 September 1993

Dr. Guy D. Gilliland Soc. Sec. No.446-60-0874

EMORY UNIVERSITY
ATLANTA, GEORGIA 30322

DEPHASING PROCESSES IN III-V SEMICONDUCTORS

PROJECT SUMMARY

Our study has dealt with both experimental and theoretical studies of electronic "dephasing" processes in a variety of model semiconductor systems, all based upon III-V materials and heterostructures. Attention has been primarily given to dephasing processes in excitonic systems, however, free-carrier dynamics have not been ignored. We have studied the following model systems: exciton-polaritons in GaAs, 3D bulk excitons in GaAs, quasi-2D interface excitons in $GaAs/Al_xGa_{1-x}As$ heterostructures, excitons in type-II $GaAs/Al_xGa_{1-x}As$ structures, and excitons and free-carriers in ordered $In_xGa_{1-x}P$. Experimental techniques utilized include: photoluminescence (PL), PL-excitation, PL decay kinetics, time-resolved PL-excitation, resonant Raman scattering, time-resolved spectroscopies, resonant Brillioun scattering, and all-optical carrier transport measurements. Our theoretical studies have included: modeling of carrier transport and capture into shallow excitonic states, rate equation modeling of free-exciton and free-carrier radiative decay, modeling of excitonic transport, localization, and trapping, and modeling of nonradiative energy transfer and decay processes.

1. Introduction.

With a goal of improving our understanding of dephasing processes in semiconductors, progress has been made towards this end with support from the Office of Naval Research under the current contract, N00014-92-J-1927, from May 1, 1992 through the present, and ending on September 30, 1993. This work has been performed in collaboration with Dr. D.J. Wolford at the IBM T.J. Watson Research Center.

The general scope of our effort concerns dephasing processes in III-V semiconductors. Dephasing refers to the stochastic interaction between a coherent, photoexcited ensemble of carriers or excitons and their crystalline environment. This interaction may assume many forms, including: multiphonon emission, carrier-phonon scattering, carrier-carrier scattering, interface scattering, scattering at alloy and/or potential fluctuations, spectral and spatial diffusion, and radiative emission. These processes may be quite complex and interconnected with other processes, and generally occur, in these systems, on a very fast time scale ($\leq$ 500 ps), necessitating utilization of complex time-resolved (fs/ps) experiments together with complementary experiments designed to give a complete picture of all dynamical processes.

We have investigated the optical and dephasing properties of exciton-polaritons in GaAs, 3D bulk excitons in GaAs, 2D excitons in GaAs/$Al_xGa_{1-x}As$ quantum-wells, quasi-2D interface excitons in GaAs/$Al_xGa_{1-x}As$ heterostructures, and excitons in type-II GaAs/$Al_xGa_{1-x}As$ structures. Additionally, we have made some preliminary measurements of the transport of excitons and free-carriers in ordered $In_xGa_{1-x}P$. Also, importantly, we have investigated the quality of all materials prior to any detailed study of dephasing processes, thus insuring that the observed dynamics truly represent the effects of a wholly intrinsic or specifically desired extrinsic process. These studies may include assessing the quality of heterointerfaces, effects of residual strain on carrier dynamics, wavefunctions, and energies in an epi-layer, and the effects of bulk or interface impurities/defects.

We have used a variety of experimental techniques to study these systems. These include photoluminescence (PL), PL-excitation (PLE), time-resolved PL, time- and spatially-resolved PL, and time-resolved "spatial-expansion" measurements to characterize and quantify dynamics in these systems. These experimental results have been modeled theoretically in an effort to gain further insight into the observed results. Such theory includes modeling of wavefunctions and ground-state energies of excitons, and excitonic diffusion, localization, and trapping, and time-dependent bandbending and screening influencing excitonic transport.

2. Results.

The following is a list of the systems studied during the term of this contract.

- Cross-Interface Exciton Transport in Type-II GaAs/AlAs Short-Period Superlattices.
- Direct Electron-Hole Plasma Transport in Type-II GaAs/AlAs Short-Period Superlattices.
- Screening and Heterointerfacial Bandbending Influenced Quasi-2D Excitonic Transport.
- Free-Exciton Recombination in Bulk GaAs.
- Photoexcited Carrier Transport in Ordered $In_xGa_{1-x}P$.

Here, we will describe in more detail the progress and results obtained for each of these model systems.

2.1 Cross-Interface Exciton Transport in Type-II GaAs/AlAs Short-Period Superlattices.

We have reported the *first*, as far as we are aware, direct experimental determination of excitonic transport properties in type-II GaAs/AlAs short-period superlattices. We have *demonstrated conclusively and directly* that the transport is governed by the thermal activation from localized states to highly-mobile states, a conclusion which heretofor has only been indirectly hypothesized. Further, from such measurements we have quantified the heterointerfacial disorder which is most probably responsible for the observed excitonic localization.

We have also observed temperature invariant PL lineshapes, which suggests that the type-II radiative recombination only occurs from localized states, otherwise, the recombination of excitons in the higher-energy mobile states would yield a distinct high-energy tail in the PL spectra. Since spatially separated electrons and holes are attracted, via the Coulomb potential, to the heterointerface, and, therefore, are intimate contact with the heterointerface, their optical and electronic properties should be very sensitive to any possible heterointerfacial disorder. Thus, we conclude that the localization results from disorder in the heterointerfacial potential, and that this heterointerface roughness is vital to the recombination mechanism. The PL spectrum is indicative of the distribution of localized states. Our results also suggest that the mobile states are ~ 6.8 meV higher than the distribution of localized states. The temperature-dependent transport probably results from the temperature-dependent excitonic occupation of mobile versus stationary localized states, rather than from a temperature-dependence of the diffusivity of mobile excitons alone. We have thus proposed the following model: (1) at low-temperatures ($kT << \Delta E$) all excitons are localized and recombine radiatively with the PL indicative of this distribution of localized states, (2) as temperature is increased ($kT \sim \Delta E$) excitons may be thermally-detrapped yielding a significant, temperature-dependent population in the mobile states, (3) these mobile excitons may then spatially diffuse, but do not radiate from these states, (4) as these mobile

excitons diffuse they may become trapped at a nonradiative defect, and thus disappear, and (5) the mobile excitons may also spatially diffuse and become relocalized in the lower-energy sites and subsequently recombine. This model explains all of the experimental observations.

We have derived a microscopic model for nonradiative decay in type-II superlattices. This model combines our measured temperature-dependent diffusion with trapping at heterointerfacial defects, resulting in temperature-dependent PL decay-kinetics and efficiencies. Using this model we calculate, for the first time, a nonradiative defect sheet density of ~ $\mathbf{1.2x10^7\ cm^{-2}}$. This nonradiative defect density is also consistent with the temperature-independent diffusion lengths of ~ 3 μm, derived from our transport and kinetic measurements. This relatively small density of nonradiative defects is consistent with possible heterointerfacial oxygen incorporation and/or interfacial dislocations, but this is only speculation.

Our temperature-dependent transport alludes to a higher-lying energy level in which cross-interface excitons are highly mobile, and a distribution of localized states governing the PL lineshape. One possible explanation for such an electronic energy-level system might be due to the nondegenerate X_Z and $X_{X,Y}$ states. Excitons in the lower energy X_Z state, with momentum perpendicular to the layer, may be localized, whereas excitons in the $X_{X,Y}$ states, with momentum parallel to the layer and in the plane of observation, may lie ~ 7 meV higher in energy and be highly mobile. We also recognize that our experiments actually excite excitons at all interfaces, and thus our diffusion constants, nonradiative trap densities, etc., are indicative of an average over all interfaces.

In summary we have reported a direct observation of the, heretofore only postulated, temperature-dependent, spatial localization of cross-interface excitons in type-II superlattices. We have also developed a quantitative model relating the excitonic decay kinetics to their transport. Our model accurately predicts the observed PL decay kinetics using the measured diffusivities. From this model we may characterize the heterointerface quality in terms of the density of nonradiative traps, which for this sample is about $1.2x10^7$ cm^{-2}. This is, to our knowledge, the *first optical determination of quantitative heterointerfacial nonradiative defect sheet densities.*

2.2 Direct Electron-Hole Plasma Transport in Type-II GaAs/AlAs Short-Period Superlattices.

We have measured the time- and space-resolved Photoluminescence (PL) at high laser-excitation densities in GaAs/AlAs Short-Period Superlattices made naturally type-II through appropriate choice of well and barrier layer thicknesses. At high excitation-densities ($>10^{18}$ cm^{-3}) we observe a luminescence feature at higher energies than the zero-phonon, X_Z-Γ type-II cross-interface excitonic recombination. This PL emission decays exponentially

in < 1 ns, and dominates the PL spectra at early times. We attribute this PL to the recombination of a *direct electron-hole plasma,*due to this short lifetime, and the fact that this emission only occurs at low-temperatures and high excitation-densities. We find, using a confocal PL imaging technique, that the transport of the this direct electron-hole plasma is very rapid - expanding from ≈ 5 μm to ≈ 30 μm in 2-3 ns (near sound-velocity), and may affect the observed transport of the spatially indirect cross-interface excitons.

Recently MacKay, et al.[1] have studied the PL from highly-excited type-II structures, such as ours. From detailed time-dependent PL spectra, they derive an electron-hole plasma density versus time, and find that the density is almost constant, whereas the peak PL emission intensity drops by more than an order-of-magnitude on the same time-scale. They conclude, based upon these observations, that there may possibly be electron-hole condensation (i.e. liquid) in this system. For this to be true, it would require that the spatial distribution of carriers must contract spatially with time. We find in our structures that this is not the case, in contrast we observe a rapid spatial expansion of the carrier distribution. Our results therefore disagree with the conclusions of MacKay, et al.[1]. However, because we haven't examined a wide variety of type-II structures to date, we cannot say that electron-hole condensation does not occur for all type-II systems. Indeed MacKay, et al.[1] note that their results are not obtained for all type-II structures, but only for a select few. Therefore, this study clearly requires more work to make any universal statements. At this point, all we can say is that condensation does not occur for the samples that we have examined.

1. J.L. Mackay, M.D. Sturge, M.H. Meynadier, M.C. Tamargo, and J.L. deMiguel, J. of Lumin. **48,49**, 731 (1991).

2.3 Screening and Heterointerfacial Bandbending Influenced Quasi-2D Excitonic Transport.

We have measured spatially, temporally, and spectrally resolved quasi-2D exciton recombination, the so-called H-band emission, in a bulk GaAs/Al_xGa_{1-x}As double heterostructures. We have directly measured the time- and injected carrier-density dependent heterointerfacial bandbending, and thus demonstrate the importance of this bandbending on the lateral spatial transport of excitons localized at the GaAs/Al_xGa_{1-x}As heterointerfaces. This time-dependence originates from the time-dependent exciton density (due to radiative recombination) and the screening of the built-in equilibrium heterointerface field by the highly polarized (in the growth direction) interface excitions. These conclusions are further confirmed through numerical modeling of the dynamical, time-dependent electrostatics - relying heavily on our previous kinetic results. The observed transport is macroscopic, expanding from an initial width of ≈ 3 μm to over 400 μm during the interface exciton lifetime. We find instantaneous diffusivities of 3600 cm^2/s initially, to 50 cm^2/s asymptotically.

From our kinetics measurements and numerical modeling, we have concluded that the H-band PL emission energy is indicative of the heterointerfacial bandbending. At high carrier-densities (early times, near the center of the laser spot) the built-in bandbending is reduced due to the screening of the built-in heterointerfacial electric-field by the photoexcited carriers. At low carrier-densities (late times, or at the edges of the spatial distribution) the built-in bandbending asymptotically approaches static equilibrium. We have directly measured the time- and carrier-density-dependent heterointerfacial bandbending. This time-dependent bandbending may be viewed as a force which is calculated from the spatial gradient of the H-band PL emission energy. We find that the bandbending force decreases monotonically in time, and becomes negligible 20 ns after the laser pulse, indicating the return to static bandbending uniformly along the interface.

The time-dependent bandbending of the conduction and valence bands near the heterointerface is a direct consequence of the time-dependences of the photoexcited carrier densities, and the density-dependent screening of the heterointerface field. In our transport measurements, initial photoexcitation creates a spatially nonuniform, Gaussian spatial distribution of carriers, which concomitantly induces a spatially nonuniform bandbending in the plane of the heterointerface, and thus a force which is only indirectly electrostatic in origin. We have modeled this bandbending force in terms of the electrostatics of a spatially nonuniform distribution of *aligned dipoles,* (the hole component of the exciton is always localized closest to the heterointerface), a classical approximation to the highly-polarized interface excitons. We solve the diffusion equation (in cylindrical symmetry) using this force as a driving term. Here, the effects of Coulomb screening are included using a simple Thomas-Fermi screening model. The Coulomb screening causes the maximum force to decrease with density at high densities, and simulates the reduction in bandbending force at high densities ($F \sim n \exp(-n\alpha)$) when "flat-band" conditions are realized, thereby limiting the maximum force for increasing densities. We find that the long-time transport is dominated by diffusive motion with $D \approx 50$ cm^2/s, and the initial transport is driven by the bandbending force with $\mu \approx 20{,}000{,}000$ cm^2/Vs and screening length of 0.3 μm. Also, assuming a peak exciton sheet density $n_0 = 10^{11}$ cm^{-2}, and characteristic width $\Delta_0 \approx 30$ μm, we deduce that $F_{max} \approx 2000$ meV/μm, in excellent agreement with our data.

Thus, we have measured and quantified, for the first time as far as we are aware, the time- and carrier-density-dependent bandbending at GaAs/Al_xGa_{1-x}As heterointerfaces, and have observed its direct influence upon the interface exciton lateral transport. We find the diffusive mobility of 316,000 cm^2/Vs in good agreement with the currently standing record, low-temperature hole-mobility of ~300,000 cm^2/Vs obtained in p-type modulation-doped MBE-structures, where the similarity between exciton and modulation-doped hole transport is due to the similarity in mass and the reduction in sensitivity to

charged-center scattering. Recognizing that these interface excitons are necessarily confined to intimate contact with the heterointerface, our observed transport should also be especially sensitive to interface-roughness scattering. This may suggest that interface scattering and/or ionized impurity scattering of our photoexcited interface excitons is negligible in our OMVPE-structures; an observation also supported by our other optical studies of these samples.

2.4 Free-Exciton Recombination in Bulk GaAs.

We have studied free-exciton recombination kinetics in the prototypical direct-gap semiconductor, GaAs. In our work, we extend the lifetime measurements to higher temperatures but focus on the low temperature phenomena. We have compared our data with a kinetic theory of interacting electrons, holes, excitons, dopants, and traps. We find that the exciton lifetime is very strongly determined by the creation rate for excitons. In fact, the data can be explained by the temperature dependence of the creation and destruction kinetics alone. Thus, we simply assume a temperature-independent radiative lifetime, and explain the entire temperature dependence of the data in terms of the temperature dependence obtained from the kinetics. This modeling was accomplished by simultaneous solutions of the nonlinear rate equations governing the kinetics. We have found that our model requires the introduction of excitonic localization into shallow traps. Such localization improves the agreement between theory and experiment, especially at low temperatures. Thus, the temperature-dependent data has forced us to interpret "free" exciton decay as decay of weakly bound excitons. This mechanism is also suggested by examination of the defect lines observed in our resonant spectra. We also rule out the polariton mechanism as a candidate for governing the observed kinetics due to our thickness dependence studies which slow little variation in radiative lifetime for a wide range of sample thicknesses.

2.5 Photoexcited Carrier Transport in Ordered $In_xGa_{1-x}P$.

We have studied the time- and space-resolved Photoluminescence (PL) from optically excited free-carriers and/or free-excitons in highly-ordered $In_xGa_{1-x}P$ alloys grown on grooved-substrates. Chen and Stringfellow[1] have shown the highest degree of ordering in such structures - with the largest domains typically several μm square by the entire length of the groove (cm). The PL from such structures has a spectral width of 48 meV, centered at 1.914 eV. Time-resolved spectra reveal that this emission actually redshifts with time. Corresponding PL time-decay kinetics show fast, exponential decay kinetics ($\tau \approx 1$ ns) on the high-energy side, whereas at lower energies the decays are nonexponential and much longer ($\tau > 1$ μs), possibly indicative of spectral migration. We have measured the transport properties of such photoexcited carriers, and find that these carriers indeed move spatially. These results demonstrate the spatial and spectral migration of free-carriers in ordered

$In_xGa_{1-x}P$ alloys. In the future we hope to be able to distinguish between carrier transport in ordered versus disordered domains.

1. G.S. Chen and G.B. Stringfellow, Appl. Phys. Lett. **59**, 324 (1991).

3. Conclusions and Summary.

Our goal in this study has been to further our understanding of dephasing processes in a variety of model semiconductor systems. In particular, here, we have examined the transport properties of photoexcited carriers. We find the transport, in all cases, to be diffusive under certain conditions (i.e. low pump-power, long-times, or low-temperatures). Under these conditions, we may then use the Einstein relation to calculate mobilities from our measured diffusivities. The mobility is proportional to the scattering time, and inversely proportional to the mass. This scattering is a possible source of dephasing. For example, the scattering time for free-excitons in bulk GaAs, which were found to have a peak diffusivity of 1000 cm^2/s at 1.8 K, is ~ 200 ps. In comparison, time-resolved dephasing measurements have determined the exciton dephasing time in bulk GaAs to be 7 ps. It therefore appears that our scattering is not the dominant dephasing mechanism in this system. Similarly, for cross-interface excitonic transport in type-II systems, the scattering time corresponding to our maximum diffusivity of 7 cm^2/s at 30 K is ~ 100 fs. In this case our results are indicative of the transport of these excitons along the heterointerface, and the scattering time is possibly indicative of heterointerfacial induced scattering.

We have made much progress towards our goal of further understanding dephasing processes in III-V semiconductor structures. However, there is clearly more which may be done, both experimentally and theoretically, Experimentally, this includes; (1) Additional measurements of cross-interface exciton transport in type-II samples with different well and barrier layer thicknesses should be done to empirically clarify the role of heterointerfacial scattering. (2) Direct dephasing time measurements in type-II structures may be compared to our scattering times derived from transport measurements. (3) The emission wavelength dependence of observed transport in type-II structures may show the existence of a mobility edge. (4) Transport measurements of the direct-gap electron-hole plasma in type-II structures will clarify the importance of this recombination pathway upon the formation and decay dynamics of the cross-interface excitons. (5) Transport and recombination kinetics measurements of quasi-2D excitons, which give rise to H-band emission, versus pressure will elucidate the effects band-structure changes have on these excitons. (6) Resonantly excited transport and recombination kinetics measurements of free-excitons in bulk GaAs structures may further support our hypothesis regarding weak localization of these excitons. (7) Examine the transport and time-resolved PL properties of highly-excited type-II structures for possible electron-hole liquid formation. (8) Lastly,

we intend to measure photoexcited-carrier transport in additional ordered-alloys in an effort to understand the optical and electrical properties of these structures (i.e. the effect of a periodic potential as opposed to a random one on the scattering and dephasing of carriers). Theoretically, this additional work includes; (1) More detailed modeling of transport in type-II structures will assist in our understanding of heterointerfacial localization and scattering. (2) Theoretical analysis of our transport in all systems and how the derived scattering times relate to dephasing times (i.e. in type-II systems this may be compared to thermally-activated hopping transport). (3) Modeling of the dynamics of direct electron-hole plasma formation and decay in type-II structures may elucidate the complex dynamics of cross-interface excitons and Γ-X scattering in these structures. (4) Further modeling of screening will enhance our understanding that this has on the band-structure of heterostructures. (5) We intend to finish our rate-equation modeling of free-exciton recombination kinetics. (6) Modeling of dispersive transport in ordered-alloys. All of this will be undertaken in the future.

Publications Supported in part by
the
Office of Naval Research
under
Contract N00014-92-J-1927

PAPERS SUBMITTED BUT NOT YET PUBLISHED.

Submitted to Physical Review Letters.

DIRECT MEASUREMENT OF HEAVY-HOLE EXCITON TRANSPORT IN TYPE-II GaAs/AlAs SUPERLATTICES

G.D. Gilliland,† A. Antonelli,† D.J. Wolford,§ K.K. Bajaj,† J. Klem,‡ and J.A. Bradley§
§IBM T.J. Watson Research Center, P.O. Box 218
Yorktown Heights, NY 10598
†Emory University, Department of Physics
Atlanta, GA 30322
‡Sandia National Laboratories
Albuquerque, NM 87185

Abstract

We have directly measured the transport of heavy-hole excitons in a type-II GaAs/AlAs superlattice. We find these excitons to be highly localized at low-temperatures, and more mobile by more than 3 orders-of-magnitude with increasing temperature. Our results constitute the first direct confirmation of exciton localization in type-II structures and thermal activation to more mobile states. We have also developed a quantitative model to explain our transport and kinetics results, and have obtained the nonradiative interfacial defect density.

Band-structure engineering of semiconductor materials may drastically change the optical and electronic properties from those normally observed in the bulk depending on whether electrons and holes are confined in the same layer (type-I superlattices and quantum-wells) or in different layers (type-II superlattices).[1-4] For type-II superlattices, these structure-induced changes may enhance certain processes, including: intersubband scattering, real-space transfer, spatially-indirect recombination, excitonic localization, and carrier-scattering at potential fluctuations caused by interfacial disorder.[5-14] In spite of these studies, a quantitative understanding of exciton kinetics in type-II structures is still lacking. Additionally, characterization of excitonic transport properties has been problematical due to their electrical neutrality which precludes the use of conventional electrical transport techniques.

$GaAs/Al_xGa_{1-x}As$ short-period superlattices may be made type-II through judicious choice of both GaAs and $Al_xGa_{1-x}As$ layer thicknesses (as well as $Al_xGa_{1-x}As$ composition), or through the application of hydrostatic pressure.[3,13]. For the $(GaAs)_m/(AlAs)_n$ system, type-II band-alignment results for GaAs-layer thicknesses < 35 Å ($m<13$) and AlAs-layer thicknesses > 15 Å ($n>6$).[3,5] In such structures, it is generally agreed that the hole ground-state is in the GaAs-layer (at the Γ-point), whereas, in contrast, there has been considerable controversy concerning the nature of the electronic ground-state.[6-12] Part of the difficulty has arisen due to the three-fold degeneracy of X-electron states in the AlAs layers, which may be lifted by several processes, such as: strain-induced splitting of X_Z and $X_{X,Y}$ [$m_e(X_Z)=1.1m_0$ and $m_e(X_{X,Y})=0.19m_0$], Γ-X mixing due to the superlattice potential, and interface disorder or roughness induced potential fluctuations.[6-12,15] Also, the recombination mechanism is not well-understood since the transition is doubly-indirect (real-space and momentum-space) and the relative importance of each of the above mechanisms remains unresolved. Nevertheless, there is some

consensus regarding one hypothesis; namely, the universally observed rapid decrease in photoluminescence (PL) lifetime with increasing temperature results from thermal activation from localized states. *However, this has never been shown experimentally.*

In this letter we report, to our knowledge, the *first* direct experimental determination of excitonic transport in type-II superlattices, specifically, GaAs/AlAs short-period superlattices. Additionally, we have quantitatively modeled the temperature dependence of both the exciton kinetics and transport. We *demonstrate directly* that the transport is governed by the thermal activation from localized states to highly-mobile states. Furthermore, we quantify the heterointerfacial disorder that is most probably responsible for the observed excitonic localization as well as the interfacial nonradiative defect density.

In order to measure excitonic transport we have resorted to an all-optical analog of the classic Haynes-Shockley experiment,[16] whereby, excitonic PL is spatially and temporally resolved.[17,18] There are several varieties of this basic technique, and ours relies on confocal laser excitation and imaging of the photoexcited excitons. PL was excited by a synchronously pumped cavity-dumped dye laser (1 ps pulsewidth) pumped by a frequency-doubled cw mode-locked Nd^{3+}:YAG laser. Time-resolution is achieved using time-correlated single photon counting. With this experimental arrangement, near diffraction-limited laser spot sizes (~ 3 μm) are achievable, with a temporal and spectral resolution of ~ 50 ps and ~ 0.1 meV, respectively.

The sample used in this study was a MBE-prepared $(GaAs)_{11}/(AlAs)_{19}$ superlattice with 55 periods. GaAs layers are 30 Å thick and the AlAs layers are 50 Å thick. Most studies[6-9] have concluded that the lowest electronic bound state is X_Z for thin structures, whereas for superlattices with AlAs barriers > 60 Å thick the lowest state is $X_{X,Y}$. Jaros, et al.[19] have found that X_Z is the ground state

regardless of the structure. Thus, the prevailing view is that X_Z is the electronic ground-state of our structure.

Figure 1 shows the cw PL spectra versus temperature from 2 to 30 K. The X_Z-Γ no-phonon line is clearly evident and the lower-energy phonon replicas are much weaker. These cw spectra show the remarkable temperature invariant PL lineshape of the X_Z-Γ no-phonon line - with no shift in peak emission energy, very little broadening of the PL line, and a small decrease in emission intensity. With pulsed excitation (at a repetition rate slower than the longest decay time) we find that the PL intensity decreases drastically - by more than 3 orders-of-magnitude - while the lineshape again remains invariant. The linewidth of the X_Z-Γ no-phonon line is ~ 5.5 meV at 1.8 K and only increases to ~ 5.8 meV at 30 K, whereas kT at 30 K is 2.6 meV.

Figure 2 shows PL time-decays versus temperature for the X_Z-Γ no-phonon line. At low temperatures the decays are nonexponential and very slow, whereas, for increasing temperature the decays become exponential (over 3 decades) and much faster. These decays may be quantified by their lifetimes deduced from the long-time exponential tail of the decays - yielding lifetimes ranging from ~ 21 μs at 1.8 K to ~ 15 ns at 30 K.

Using our time-resolved confocal PL-imaging technique, we have obtained the time-dependent spatial profile of the radiating carriers. We observe a clear and systematic expansion of the luminescence from the initial laser spot-size of ~ 5 μm to over 30 μm at high-temperatures. We find, under our excitation conditions (photon flux of $< 10^{12}$ cm^{-2}), that the transport is diffusive, with diffusion coefficients versus temperature shown in Fig. 3. There is more than a 3 order-of-magnitude *increase* of diffusion constant, D, with temperature - from ~ 2×10^{-3} cm^2/s at 1.8 K to ~ 7 cm^2/s at 30 K. An Arrhenius plot of the diffusion constant yields an activation energy of ~ 6.8 ± 1.5 meV.

Based upon PL kinetics alone, most reports[4,9-11] have concluded that the temperature dependence arises from the thermally activated detrapping of excitons from localized states to mobile states. However, this hypothesis has never been proven since the spatial transport of these cross-interface excitons has never been measured. Our results demonstrate the temperature-dependent transport of these cross-interface excitons, which is crucial to the localization model previously hypothesized. Furthermore, the observed temperature-independent PL lineshapes suggest that the type-II radiative recombination only occurs from localized states, otherwise, the recombination of excitons in the higher-energy mobile states would yield a distinct high-energy tail in the PL spectra. Since spatially separated electrons and holes are in intimate contact with the heterointerface due to their mutual Coulomb attraction, their optical and electronic properties should be very sensitive to any possible heterointerfacial disorder. Thus, we conclude that the localization most probably results from heterointerfacial disorder, and that this is vital to the recombination mechanism. The PL spectrum (lineshape) is indicative of the distribution of localized states. Also, our results suggest that the mobile states are ~ 6.8 ± 1.5 meV higher in energy than the distribution of localized states.

The temperature-dependent transport probably results from the temperature-dependent excitonic occupation of mobile versus stationary localized states, rather than from a temperature-dependence of the diffusivity of mobile excitons alone. We may thus extend the previously proposed model as follows: (1) at low-temperatures ($kT << \Delta E$) all excitons are localized and recombine radiatively with the PL indicative of this localized state distribution, (2) as temperature is increased ($kT \sim \Delta E$) excitons may be thermally-detrapped yielding a significant, temperature-dependent population in the mobile states (3) these mobile excitons may then spatially diffuse, without radiating from these states, (4) as these mobile excitons diffuse they may become trapped at a nonradiative defect, and (5) the mobile

excitons may spatially diffuse, become relocalized in the lower-energy sites, and subsequently recombine. This model explains all the experimental observations.

Based on the premises above and using as a starting point the theory by Chandrasekhar,[20] which treated the theory of coagulation in colloids, we developed a quantitative model to compare with our experimental results. Here, we divide the photoexcited 2D excitonic population into two categories, localized n_l and mobile n_m ($N=n_l + n_m$), where the relative populations are related by a Arrhenius term, $\exp(-\Delta E_a/kT)$. The mobile population is free to diffuse, and possibly become trapped at a perfectly absorbing nonradiative defect. PL decay kinetics and efficiencies are affected by this trapping and concomitant nonradiative decay of these mobile excitons. We have solved the diffusion equation for the mobile excitons in 2D using the Wigner-Seitz method[21,22] with the following boundary conditions: $n_m=C_0$ at t=0, and $n_m=0$ at $r=r_1$, $\frac{\partial n_m}{\partial r}=0$ at $r=r_2$ for $t \geq 0$, where r_1 is the radius of the perfectly absorbing defect and $2r_2$ is the mean separation between defects. This yields the time-dependent density of mobile excitons

$$n_m(t)=\frac{\pi^2 C_0 r_1}{2}\sum_{n=1}^{\infty}\left[\frac{\alpha_n J_0^2(\alpha_n r_1)}{J_0^2(\alpha_n r_1)-J_1^2(\alpha_n r_2)}\right]\left\{Y_1(\alpha_n r_2)J_1(\alpha_n r_1)-J_1(\alpha_n r_2)Y_1(\alpha_n r_1)\right\}, \quad (1)$$
$$\times U(\alpha_n r)e^{-D\alpha_n^2 t}$$

where $U(\alpha_n r)$ is defined as

$$U(\alpha_n r)=\left\{Y_1(\alpha_n r_2)J_0(\alpha_n r)-J_1(\alpha_n r_2)Y_0(\alpha_n r)\right\}, \quad (2)$$

and α_n are the zeros of $U(\alpha_n r)$. Here, J_i and Y_i (i=0,1) are the Bessel and Modified Bessel functions of order i. Using Klein, Sturge, and Cohen (KSC) theory[23] for radiative decay in an alloy (distribution of radiative rates), which approximates the heterointerface disorder induced randomness in this type-II excitonic system, the PL decay kinetics may be modeled as

$$I(t)=I_0 e^{-\int_0^t w_{nr}dt'}\left(1+e^{-w_r t}\right)^{-3/2} \quad (3)$$

where

$$w_{nr}(t) = \frac{-2\pi D r_1 \left(\frac{\partial n_m(r,t)}{\partial r} \right)\Big|_{r=r_1}}{2\pi \int_{r_1}^{r_2} n_m(r,t) r dr}, \qquad (4)$$

and w_r and w_{nr} are the radiative a ıd nonradiative rates, respectively.

We have derived a microscopic model for nonradiative decay in type-II superlattices, thus extending the KSC theory to specifically model this process. Figure 4 shows results of our model calculation compared with our experimental measurements, using only r_1 and r_2 as adjustable parameters. We find good agreement between experiment and theory for r_1= 115 Å and r_2=2.9 μm. This implies a nonradiative defect sheet density of ~ 1.2×10^7 cm^{-2}. We have assumed that r_1 is equal to the 2D exciton Bohr radius.[24] This nonradiative defect density is also consistent with the temperature-independent diffusion lengths of ~ 3 μm derived from our transport-and kinetic measurements. This relatively small density of nonradiative defects is consistent with possible heterointerfacial oxygen incorporation and/or interfacial dislocations,[25] but this is only speculation.

This model combines our measured temperature-dependent diffusion with trapping at defects resulting in temperature-dependent PL decay-kinetics. The model more accurately agrees with our data at high temperatures, and this may be due to other nonradiative decay mechanisms (i.e., nonradiative decay from localized states) becoming as important at low temperatures as the nonradiative trap mechanism described here. Eq. (3) clearly gives nonexponential decays at low-temperatures (when D and w_{nr} are small), due to the heterointerfacial disorder induced randomness in the cross-interface excitonic wavefunctions, and exponential decays at higher temperatures (when D and w_{nr} are large).

Our temperature-dependent transport alludes to a higher-lying energy level in which cross-interface excitons are highly mobile, and a distribution of localized states

governing the PL lineshape. One possible explanation for such an electronic energy-level system might be due to the nondegenerate X_Z and $X_{X,Y}$ states. Excitons in the lower energy X_Z state, with momentum perpendicular to the layer, may be localized, whereas excitons in the $X_{X,Y}$ states, with momentum parallel to the layer and in the plane of observation, may lie ~ 7 meV higher in energy and be highly mobile. We also recognize that our experiments actually excite excitons at all interfaces, and thus our diffusion constants, nonradiative trap densities, etc., are indicative of an average over all interfaces.

In summary we report here a direct observation of the, heretofore only postulated, temperature-dependent, spatial localization of cross-interface excitons in type-II superlattices. We have also developed a quantitative model relating the excitonic decay kinetics to their transport. Our model accurately predicts the observed PL decay kinetics using the measured diffusivities. From this model we may characterize the heterointerface quality in terms of the density of nonradiative traps, which for this sample is about 1.2×10^7 cm^{-2}.

Acknowledgments

This work was supported in party by ONR under contracts N00014-90-C-0077 and N00014-92-J-1927, and AFOSR under grant AFOSR-91-0056.

REFERENCES

1. R. Dingle, A.C. Gossard, and W. Wiegmann, Phys. Rev. Lett. **34**, 1327 (1975).
2. A.C. Gossard, P.M. Petroff, W. Weigmann, R. Dingle, and A. Savage, Appl. Phys. Lett. **29**, 323 (1976).
3. E. Finkman, M.D. Sturge, M.H. Meynadier, R.E. Nahory, M.C. Tamargo, D.M. Hwang, and C.C. Chang, J. of Lumin. **39**, 57 (1987).
4. B.A. Wilson, IEEE J. Quantum Elect. **QE-24**, 1763 (1988).
5. K.J. Moore, P. Dawson, and C.T. Foxon, Phys. Rev. B **38**, 3368 (1988).

6. P. Dawson, C.T. Foxon, and H.W. van Kesteren, Semicond. Sci. Technol. **3**, 54 (1990).
7. W. Ge, M.D. Sturge, W.D. Schmidt, L.N. Pfeiffer, and K.W. West, Appl. Phys. Lett. **57**, 55 (1990).
8. H.W. van Kesteren, E.C. Cosman, P. Dawson, K.J. Moore, C.T. Foxon, Phys. Rev. B **39**, 13426 (1989).
9. D. Scalbert, J. Cernogora, C. Benoit a la Guillaume, M. Maaref, F.F. Charfi, and R. Planel, Surface Science **229**, 464 (1990).
10. F. Minami, K. Hirata, K. Era, T. Yao, Y. Masumoto, Phys. Rev. B **36**, 2875 (1987).
11. E. Finkman, M.D. Sturge, and M.C. Tamargo, Appl. Phys. Lett. **49**, 1299 (1986).
12. J. Ihm, Appl. Phys. Lett. **50**, 1068 (1987).
13. T.W. Steiner, D.J. Wolford, T.F. Kuech, and M. Jaros, Superlattices and Microstructures **4**, 227 (1988); D.J. Wolford, T.F. Kuech, J.A. Bradley, M.A. Gell, D. Ninno, and M. Jaros, J. Vac. Sci. Technol. B **4**, 1043 (1986).
14. J. Feldmann, R. Sattmann, E.O. Göbel, J. Kuhl, J. Hebling, K. Ploog, R. Muralidharan, P. Dawson, and C.T. Foxon, Phys. Rev. Lett. **62**, 1892 (1989).
15. T.J. Drummond, E.D. Jones, H.P. Hjalmarson, and B.L. Doyle, Growth of Compound Semiconductors, SPIE **796**, 2 (1987).
16. J.R. Haynes and W. Shockley, Phys. Rev. **81**, 835 (1951).
17. G.D. Gilliland, D.J. Wolford, T.F. Kuech, and J.A. Bradley, Appl. Phys. Lett. **59**, 216 (1991).
18. D.J. Wolford, G.D. Gilliland, T.F. Kuech, J.A. Bradley, and H.P. Hjalmarson, Phys. Rev. B, (in press).
19. L.D.L. Brown, M. Jaros, and D.J. Wolford, Phys. Rev. B **40**, 6413 (1989).
20. S. Chandrasekhar, Rev. Mod. Physics **15**, 1 (1943).

21. M. Muskat, *The Flow of Homogeneous Fluids Through Porous Media*, (McGraw-Hill, New York 1937).

22. V.M. Agranovitch and M.D. Galanin, *Electronic Excitation Energy Transfer in Condensed Matter*, (North-Holland, New York 1982).

23. M.V. Klein, M.D. Sturge, and E. Cohen, Phys. Rev. B **25**, 4331 (1982).

24. J. Cen, S.V. Branis, and K.K. Bajaj, Phys. Rev. B **44**, 12848 (1991).

25. M.T. Asom, M. Geva, R.E. Leibenguth, and S.N.G. Chu, Appl. Phys. Lett. **59**, 976 (1991).

FIGURE CAPTIONS

Fig. 1. PL spectra versus temperature after cw excitation at 4579 Å. All spectra are normalized. Inset shows X_Z-Γ no-phonon transition.

Fig. 2. X_Z-Γ PL decay kinetics versus temperature after pulsed excitation at 6000 Å.

Fig. 3. Temperature dependence of diffusivity and lifetimes derived from our transport and PL decay kinetics measurements.

Fig. 4. Comparison of model calculation of nonradiative decay rates as a function of diffusivity versus experimentally determined values. The best fit is obtained for $r_2/r_1 \approx 250$.

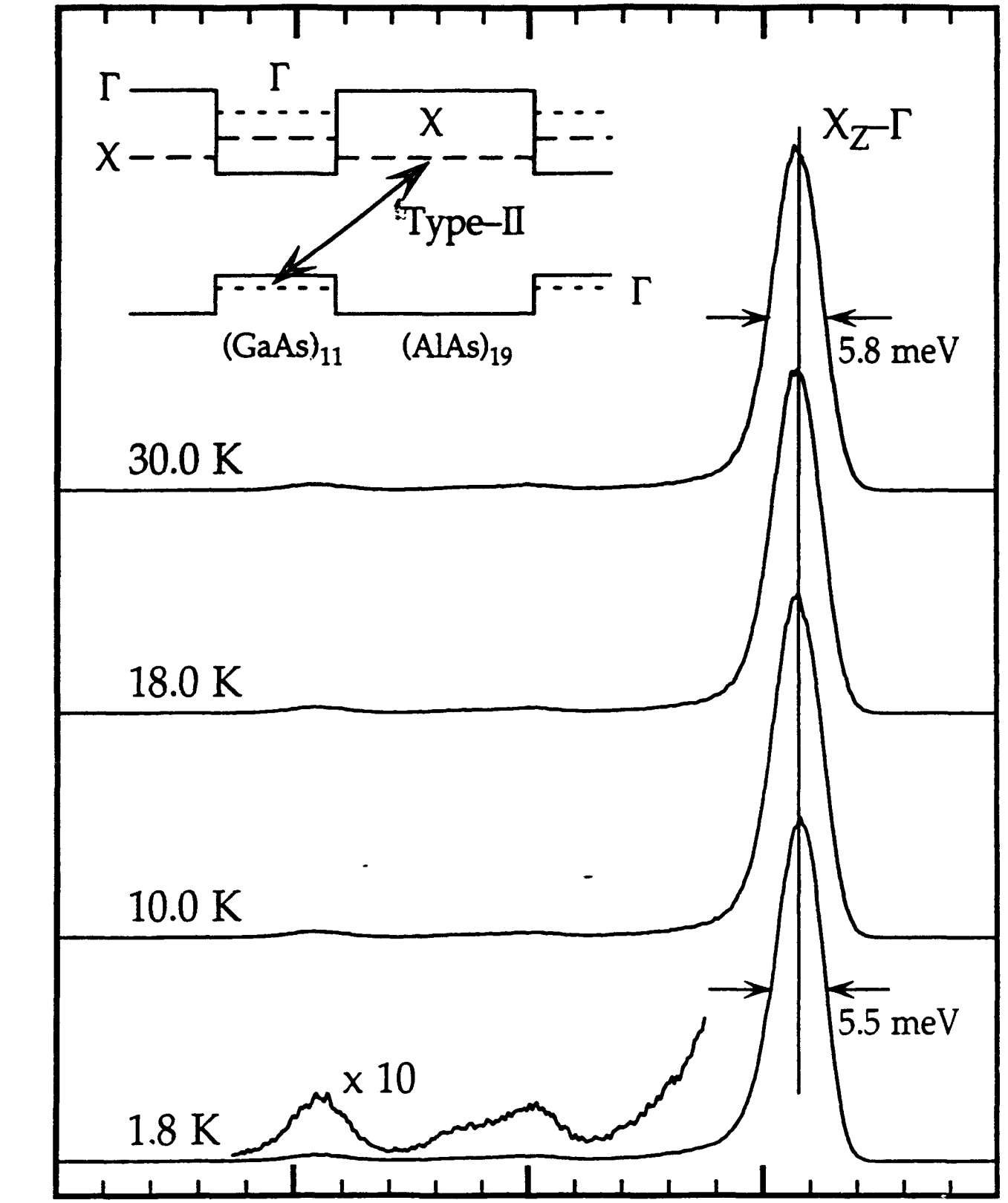
Γ
Γ
X
X
Type–II
Γ
(GaAs)11
(AlAs)19
X_Z–Γ
5.8 meV
30.0 K
18.0 K
10.0 K
5.5 meV
x 10
1.8 K
7400
7200
7000
WAVELENGTH (Å)

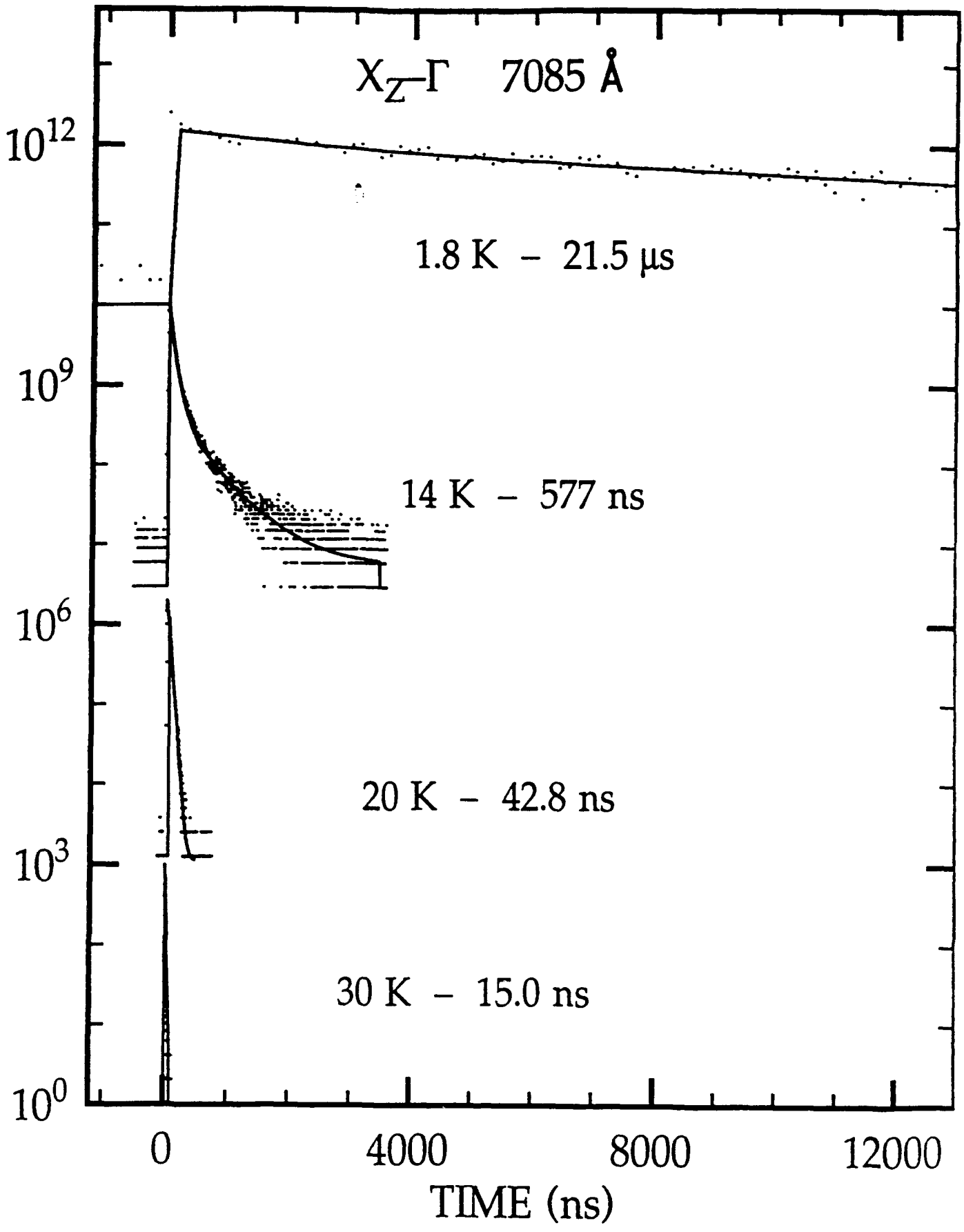
X_Z–Γ 7085 Å
10^{12}
1.8 K – 21.5 μs
10^{9}
14 K – 577 ns
10^{6}
20 K – 42.8 ns
10^{3}
30 K – 15.0 ns
10^{0}
0
4000
8000
12000
TIME (ns)

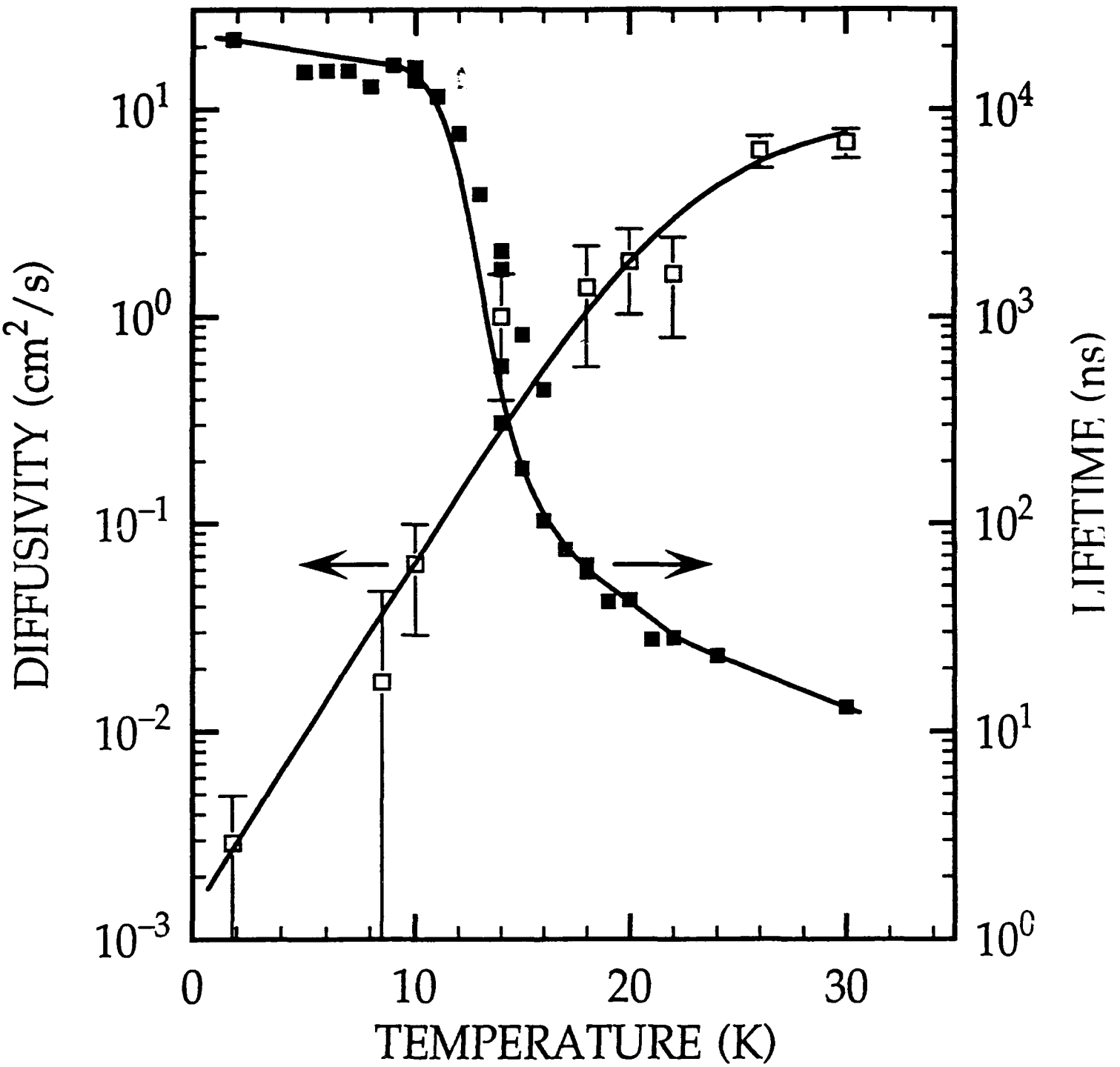
DIFFUSIVITY (cm²/s)
10¹
10⁰
10⁻¹
10⁻²
10⁻³
LIFETIME (ns)
10⁴
10³
10²
10¹
10⁰
0
10
20
30
TEMPERATURE (K)

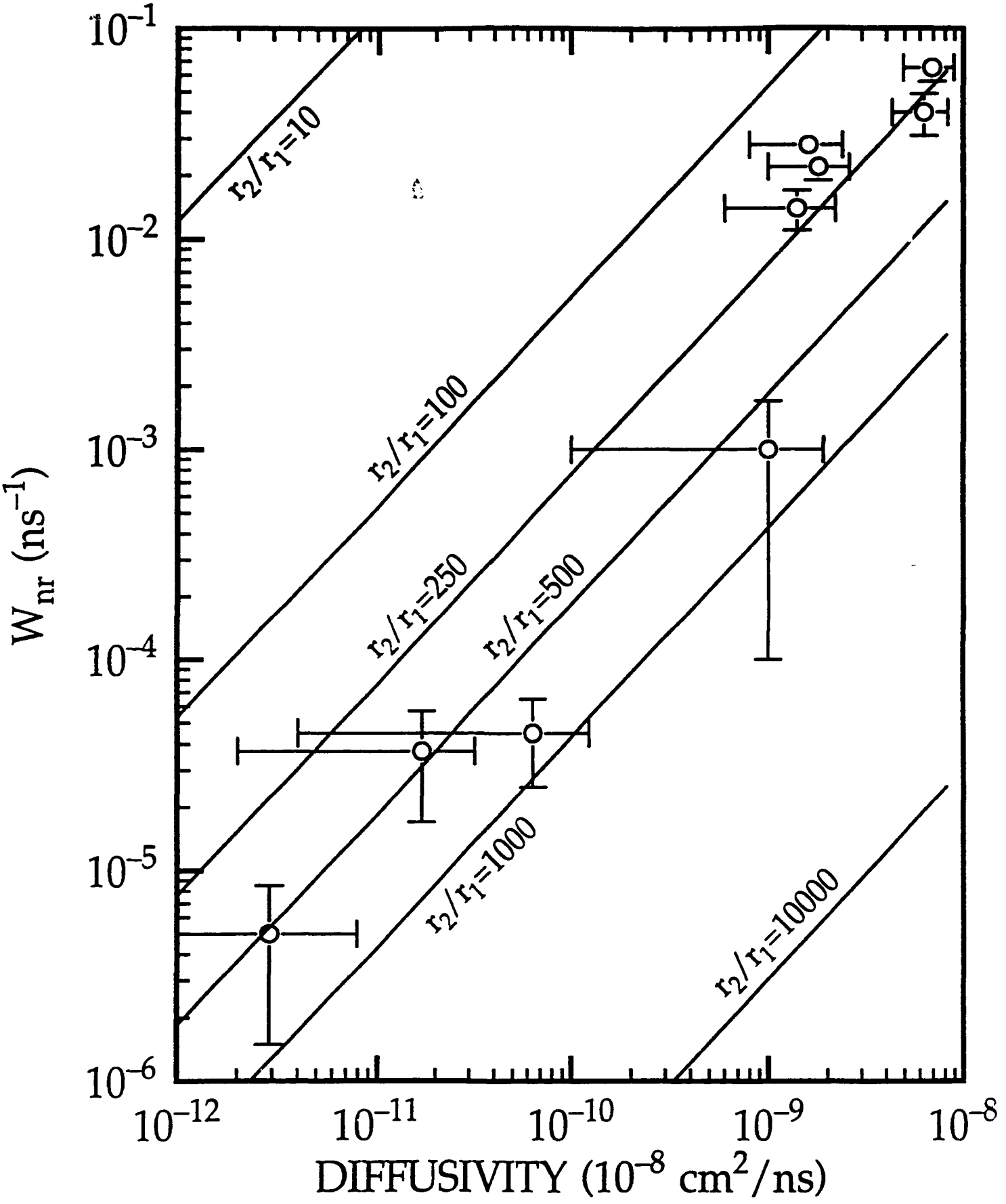
10^{-1}
10^{-2}
10^{-3}
10^{-4}
10^{-5}
10^{-6}
W_{nr} (ns^{-1})
r_2/r_1=10
r_2/r_1=100
r_2/r_1=250
r_2/r_1=500
r_2/r_1=1000
r_2/r_1=10000
10^{-12}
10^{-11}
10^{-10}
10^{-9}
10^{-8}
DIFFUSIVITY (10^{-8} cm^2/ns)

Acta Physica Polonica.
accepted for publication.

OPTICALLY-DETERMINED EXCITON TRANSPORT IN GaAs STRUCTURES

G.D. Gilliland,[a] D.J. Wolford,[b] H.P. Hjalmarson,[c] M.S. Petrovic,[b] J. Klem,[c] T.F. Kuech,[b] G.A. Northrop,[b] and J.A. Bradley[b]

[a]Emory University, Physics Dept.
Atlanta, GA 30322
[b]IBM T.J. Watson Research Center, P.O. Box 218
Yorktown Heights, NY 10598
[c]Sandia National Laboratories
Albuquerque, NM 87185

Abstract

We have used an all-optical Photoluminescence-imaging technique to measure excitonic transport in three types of GaAs structures in which the excitonic transitions vary from allowed direct-gap excitons to forbidden, doubly-indirect Type-II excitons. We find remarkable differences in the transport properties of these excitons. Our studies show that bulk free-exciton transport exhibits an anomalous laser power-dependent diffusivity, whereas quasi-2D interfacial excitons and Type-II cross-interface excitons do not. Additionally, we observe localization of cross-interface excitons at the potential disorder induced by the heterointerface roughness.

PACS Numbers: 78.47.+p, 78.65.Fa, and 72.80.Ey

I. Introduction.

In recent years excitonic properties have received increased attention due to their possible use in nonlinear optoelectronic devices.[1,2] Some of these devices rely upon the transport or scattering of excitonic species; however, the electrical neutrality of excitons precludes the use of conventional electrical transport techniques for characterization of some of these transport and/or scattering processes. This problem has been circumvented through the use of all-optical imaging of the excitonic Photoluminescence (PL) to derive diffusivities.[3-6] There are many variations on this general technique, all of which rely upon the diffusion of carriers in either their own concentration gradient or an externally applied potential gradient. Perhaps the most notable example is the demonstration of phonon-wind driven transport of the electron-hole droplets in both Silicon and Germanium.[3] Additionally, they have recently proven useful in measuring lateral free-carrier transport in bulk GaAs structures,[6-8] free-exciton transport in GaAs quantum-wells,[5,9] excitonic transport in Cu_2O,[4] and electron-hole plasma transport in GaAs structures,[10] to mention only a few.

In this paper we intend to outline the results of our studies of excitonic transport in three model systems, highlighting the differences in the physical processes influencing the observed transport. Our three model systems include: (1) free-excitons in bulk GaAs structures,[9] (2) quasi-2D excitons in $Al_xGa_{1-x}As$/GaAs double heterostructures,[11,12] and (3) cross-interface excitons in Type-II GaAs/AlAs short-period superlattices.[13,14] The differences between these systems are related, first, to the nature of the exciton (direct in both real- and momentum-space, indirect in real-space and direct in momentum-space, and indirect in both real- and momentum-space, respectively) and, secondly, to their sensitivity to the heterointerface potential and possible scattering there.

II. Experiment and Samples.

We have used an all-optical PL-imaging technique analogous to the classical Haynes-Shockley experiment[15] to measure excitonic transport in these model systems. Our technique[7,8] relies on the confocal laser excitation and imaging of the photoexcited carriers. PL was excited by a synchronously pumped cavity-dumped dye laser pumped by a frequency-doubled cw mode-locked Nd^{3+}:YAG laser. Laser pulsewidths are ~1 ps with a variable repetition rate up to 76 MHz. Time-resolution is achieved using time-correlated single photon counting, and a spectrometer disperses the PL to obtain spectral resolution. With careful alignment, this experimental arrangement yields near diffraction-limited laser spot sizes (~ 3 μm), a temporal resolution of ~ 50 ps, and a spectral resolution of ≤ 0.1 meV.

Our samples were prepared by both organometallic-vapor-phase-epitaxy (OMVPE) and molecular-beam-epitaxy (MBE). Our OMVPE samples are simple $GaAs/Al_{0.3}Ga_{0.7}As$ double heterostructures with GaAs layer thicknesses from 50 Å to 10 μm. Unintentional doping yields a p-n-p structure with a background GaAs doping of ~ 10^{15} cm^{-3}. Our MBE sample is a $(GaAs)_{11}/(AlAs)_{19}$ superlattice with 55 periods. GaAs layers are 30 Å thick whereas AlAs layers are 50 Å thick.

III. Results.

A. Bulk Free-Exciton Transport.

We have observed prominent free-exciton emission in the low-temperature PL spectra of our bulk OMVPE structures, and have fully characterized the excitonic recombination kinetics previously.[16] Typical results are shown in Figure 1. Our results confirm the relatively high-purity and "surface-free" quality of these samples. We have measured spatially- and temporally-resolved free-exciton PL distributions for our OMVPE samples at 1.8 K. Fits to these spatial PL distributions with gaussian lineshapes allows a quantification of the characteristic width of the PL distribution and hence possible transport. The temporal dependence of the full-width-at-half-maximum (FWHM) squared is shown in Fig. 2. We find that at low-temperatures (≤ 50 K), where excitonic effects become important, the transport is laser power-

dependent with PL distributions which are still gaussian.[14] This power-dependence is not observed at higher temperatures. Diffusion constants may be derived from the slopes of such curves, yielding ~ 1 cm^2/s to 1300 cm^2/s at 1.8 K, for the sample shown. Additionally, we find that peak diffusivities are sample dependent. Figure 3 shows a summary of our measured diffusivities versus temperature and versus laser power for 2 samples.

These results may be understood only through a detailed study of free-exciton recombination kinetics. We find free-carriers play a very important role in the recombination of free-excitons,[16] and may even totally dominate the observed kinetics, depending upon sample purity, temperature, excitation density, and excitation wavelength. Excitons thermally couple to free-carriers even at 1.8 K, though weakly, and this coupling leads to a temperature-dependent joint transport of both species of carrier. Thus, even though spectrally resolving the free-exciton PL only, our observations reflect the joint transport of both free-excitons and free-carriers.

B. Quasi-2D Exciton Transport.

Several years ago, a new PL emission was observed by Yuan et al.[17] in $GaAs/Al_xGa_{1-x}As$ heterostructures, and labeled by them as the H-band. We have observed a similar emission in the low-temperature PL spectra of our OMVPE double-heterostructures,[18] shown in Fig. 1, and conducted experiments parallel to those of Yuan et al.[17] to verify H-band emission in our structures. Time-resolved PL studies together with detailed numerical modeling of the observed H-band recombination kinetics, in our structures, suggest that the Coulomb interaction between electrons and holes is very important to a full understanding of the observations. Thus, we conclude that H-band emission, in our structures, arises from the radiative recombination of quasi-2D excitons, with the hole component of the exciton quantum-mechanically bound to the heterointerface in the potential notch there.

Our results show the rich nature of the H-band kinetics (i.e. time-dependent red-shifts, lifetimes ~ 50 μs, and a structural dependence to the observed kinetics). In an effort to further our understanding of H-band kinetics, we have used the PL-imaging technique described above, taking advantage of the spectral resolution, to characterize quasi-2D exciton transport.[11,12] Discrimination between bulk, 3D free-exciton transport and quasi-2D exciton transport is accomplished through spectral windowing of the H-band PL only, denoted by vertical lines in Fig. 1. We find time-resolved PL spatial distributions with clear, macroscopic expansion, from ~ 30 μm to ~ 400 μm in just 250 ns. Figure 4 shows the characteristic width of the PL distributions versus time. The nonlinear behavior is indicative of non-diffusive transport, and the derived instantaneous diffusivities decrease monotonically with time from 3600 cm^2/s to 50 cm^2/s.

In an effort to understand this quasi-2D exciton transport, we have made detailed time- and space-resolved measurements of the PL spectra using the same PL-imaging apparatus. We find that there exists a nonuniform, time-dependent bandbending due to the additional photoexcited carriers which may locally screen the built-in heterointerfacial field. We find the peak bandbending force is 1750 meV/cm, decreasing monotonically with time, going essentially zero within 20 ns. In Fig. 4 it is clear that most of the nonlinear expansion occurs within the first 50 ns. So a possible explanation for this transport is that the quasi-2D excitons are initially driven by the time- and carrier-density dependent heterointerfacial bandbending. In actuality, the quasi-2D exciton dynamics are much more complicated. We find that there is a continuous evolution of this quasi-2D exciton from the spherical, bulk 3D free-exciton discussed in the previous session to a highly-polarized quasi-2D exciton, and possibly to full ionization into spatially separated 2D and 3D carriers. Lastly, we conclude that the asymptotic diffusivity of 50 cm^2/s, or an equivalent mobility of 300,000 cm^2/Vs (using the Einstein relation), represents the true, purely diffusive motion of these carriers.

C. Cross-Interface Exciton Transport.

In recent years the optical and electronic properties of GaAs/AlAs short-period superlattices have been extensively studied.[19] These studies have shown the doubly-indirect nature of the excitons in these systems (indirect in real-space and momentum-space - electron at X in the AlAs layer and hole at Γ in the GaAs layer, and thus cross-interface). In particular, time-resolved studies have shown that the radiative recombination of these cross-interface excitons is very slow and nonexponential at low temperatures (from μs to ms), and rapidly becomes faster (ns) and exponential with increasing temperature. The conclusion almost universally reached is that these excitons are localized at low-temperatures and become thermally-detrapped at higher temperatures. This conclusion is inferred indirectly from these PL time-decay measurements, and has never been proven directly. Here, we show directly that this localization does indeed exist, and we have quantified the transport, including versus temperature, of these cross-interface excitons.[13,14]

Fig. 5 shows the cw PL spectra for our MBE short-period superlattice versus temperature. Remarkably, we observe no discernable change in the X_Z-Γ PL lineshape versus temperature (with pulsed excitation we find the intensity drops precipitiously with increasing temperature), and a PL linewidth of ~ 5.5 meV. PL decay kinetics of the same emission yield long, nonexponential decay kinetics at low-temperatures (21 μs at 1.8 K) and a monotonic decrease in lifetime (13 ns at 30 K) with a concomitant change to exponential decays.

We have measured the time-resolved PL spatial distributions of the X_Z-Γ no-phonon emission at low laser-powers, fit each distribution with a gaussian, and calculated the diffusion constant versus temperature, as outlined above. We find diffusive transport which may be characterized by a single diffusion constant, shown in Fig. 6. *These results clearly and unmistakably demonstrate the heretofor only hypothesized localization of the cross-interface excitons at low-temperatures and the thermal-detrapping which occurs at higher temperatures.* Diffusivities derived from

these measurements range from $\leq 2 \times 10^{-3}$ cm^2/s at 1.8 K to 7.0 cm^2/s at 30 K, a 5×10^3 change in just 30 K. We believe that these localized states most probably result from the potential disorder due to heterointerface roughness since the Coulomb attraction between electrons and holes forces them to be in intimate contact with the heterointerface.

IV. Discussion.

The above results may now be used to compare and contrast the transport properties of the three species of excitons studied here. We find that the transport of bulk free-excitons is strongly laser-power dependent, whereas quasi-2D excitons exhibit a weaker power dependence, and cross-interface excitons do not exhibit any power dependence (at powers less than that required to create an electron-hole plasma). The relative binding energies and coupling to free-carriers are responsible for these differences. Bulk free-excitons ($E_B \sim 4.2$ meV) may more readily couple and be influenced by free-carriers than either quasi-2D excitons ($E_B \sim 5$ meV and localized near the heterointerfaces[18]) or cross-interface excitons ($E_B \sim$ 8-9 meV[20]). Quasi-2D excitons are strongly influenced by the laser-induced changes in bandbending which occur for absorbed photon densities comparable to the background doping and may eventually evolve into spatially separated electrons and holes.

Each of these three systems also differ in their sensitivity to heterointerfacial scattering. We find that bulk, 3D free excitons are relatively insensitive to any potential disorder caused by interface roughness in these structures. This is due to the high-quality heterointerfaces of our OMVPE structures as well as the fact that these excitons are not confined in close physical contact with the heterointerfaces. Quasi-2D excitons are more sensitive to the heterointerface potential since at least one component of the exciton (holes in our samples) is confined next to the heterointerface. The transport is sensitive to gradients in the heterointerface built-in field along the heterointerface. Cross-interface excitons in Type-II structures are the

most strongly influenced by the electronic structure of the heterointerface. The Coulomb interaction between electrons and holes restricts both species to be in intimate contact with the interface. Indeed, we have demonstrated the spatial localization of these excitons and conclude that this localization most probably results from interface disorder.

V. Conclusions.

We have demonstrated the utility of our all-optical PL-imaging technique in characterizing excitonic transport. Our studies of three model systems reveal distinct differences in the observed excitonic transport which are reasonably understood on the basis of known differences in the nature of the excitonic transition (direct versus indirect in both real- and momentum-space) and the proximity of each excitonic species to the heterointerface.

VI. Acknowledgements.

This work was supported in part by ONR under contracts N00014-90-C-0077, N00014-91-J-1697, and N00014-92-J-1927. The work at Sandia was supported by U.S. DOE under contract DE-AC04-76DP00789.

REFERENCES

1. S. Schmitt-Rink, D.S. Chemla, and D.A.B. Miller, Phys. Rev. B **32**, 6601 (1985).
2. S. Schmitt-Rink and D.S. Chemla, Phys. Rev. Lett. **57**, 2752 (1986).
3. J.P. Wolfe, J. Lumin. **30**, 82 (1985).
4. D.P. Trauernicht and J.P. Wolfe, Phys. Rev. B **33**, 8506 (1986).
5. H. Hilmer, A. Forchel, S. Hansmann, M. Morohashi, E. Lopez, H.P. Meier, and K. Ploog, Phys. Rev. B **39**, 10901 (1989).
6. A. Olsson, D.J. Erskine, Z.Y. Xu, A. Schremer, and C.L. Tang, Appl. Phys. Lett. **41**, 659 (1982).
7. G.D. Gilliland, D.J. Wolford, T.F. Kuech, and J.A. Bradley, Appl. Phys. Lett. **59**, 216 (1991).

8. D.J. Wolford, G.D. Gilliland, T.F. Kuech, J.A. Bradley, and H.P. Hjalmarson, Phys. Rev. B to be published.
9. D.J. Wolford, G.D. Gilliland, T.F. Kuech, J.A. Bradley, and H.P. Hjalmarson, Proc. of the 18th Int. Symp. on Gallium Arsenide and Rel. Comp., Seattle, WA, Sept. 9-12, 1991, Inst. Phys. Conf. Ser. **120**, (IOP Bristol, 1992), p. 271.
10. K.T. Tsen and H. Morkoc, Inst. Phys. Conf. Ser. **83**, 337 (1986).
11. G.D. Gilliland, D.J. Wolford, G.A. Northrop, M.S. Petrovic, T.F. Kuech, and J.A. Bradley, J. Vac. Sci. Technol. B **10**, 1959 (1992).
12. G.D. Gilliland, D.J. Wolford, G.A. Northrop, T.F. Kuech, and J.A. Bradley, Proc. of the 18th Int. Symp. on Gallium Arsenide and Rel. Comp., Seattle, WA, Sept. 9-12, 1991, Inst. Phys. Conf. Ser. **120**, (IOP Bristol, 1992), p. 413.
13. G.D. Gilliland, D.J. Wolford, J.A. Bradley, and J. Klem, Proc. of the 20th Phys. and Chem. of Semiconductor Interfaces Conference, Williamsburg, VA, Jan 25-29, 1993, J. Vac. Sci. Tech. B to be published.
14. G.D. Gilliland, D.J. Wolford, J.A. Bradley, and J. Klem, Proc. of the 21st Int. Conf. on the Physics of Semiconductors, Beijing China, (World Scientific), to be published.
15. J.R. Haynes and W. Shockley, Phys. Rev. **81**, 835 (1951).
16. D.J. Wolford, G.D. Gilliland, T.F. Kuech, J.A. Bradley, H.P. Hjalmarson, and J. Klem, Proc. of the 21st Int. Conf. on the Physics of Semiconductors, Beijing China, (World Scientific), to be published.
17. Y.R. Yuan, K. Mohammed, M.A.A. Puednski, and J.L. Merz, Appl. Phys. Lett. **45**, 739 (1984).
18. G.D. Gilliland, D.J. Wolford, T.F. Kuech, and J.A. Bradley, Phys. Rev. B **43**, 14251 (1991).
19. B.A. Wilson, IEEE J. Quantum Elect. **QE-24**, 1763 (1988).
20. J. Cen, S.V. Branis, and K.K. Bajaj, Phys. Rev. B **44**, 12848 (1991).

FIGURE CAPTIONS

Fig. 1. 1.8 K PL spectrum for our 0.3 μm thick OMVPE GaAs/$Al_{0.3}Ga_{0.7}As$ double heterostructure. Arrows denote energies at which PL-imaging measurements were made.

Fig. 2. Δ^2 versus time at 1.8 K for various laser pump powers at free-exciton peak emission energy.

Fig. 3. Summary of diffusivities versus temperature derived from PL-imaging experiments for two OMVPE double heterostructures.

Fig. 4. Δ^2 versus time at 1.8 K obtained by spectrally resolving H-band PL only.

Fig. 5. 1.8 K cw PL spectra of MBE Type-II short-period superlattice versus temperature.

Fig. 6. Diffusion constant of cross-interface excitons versus temperature.

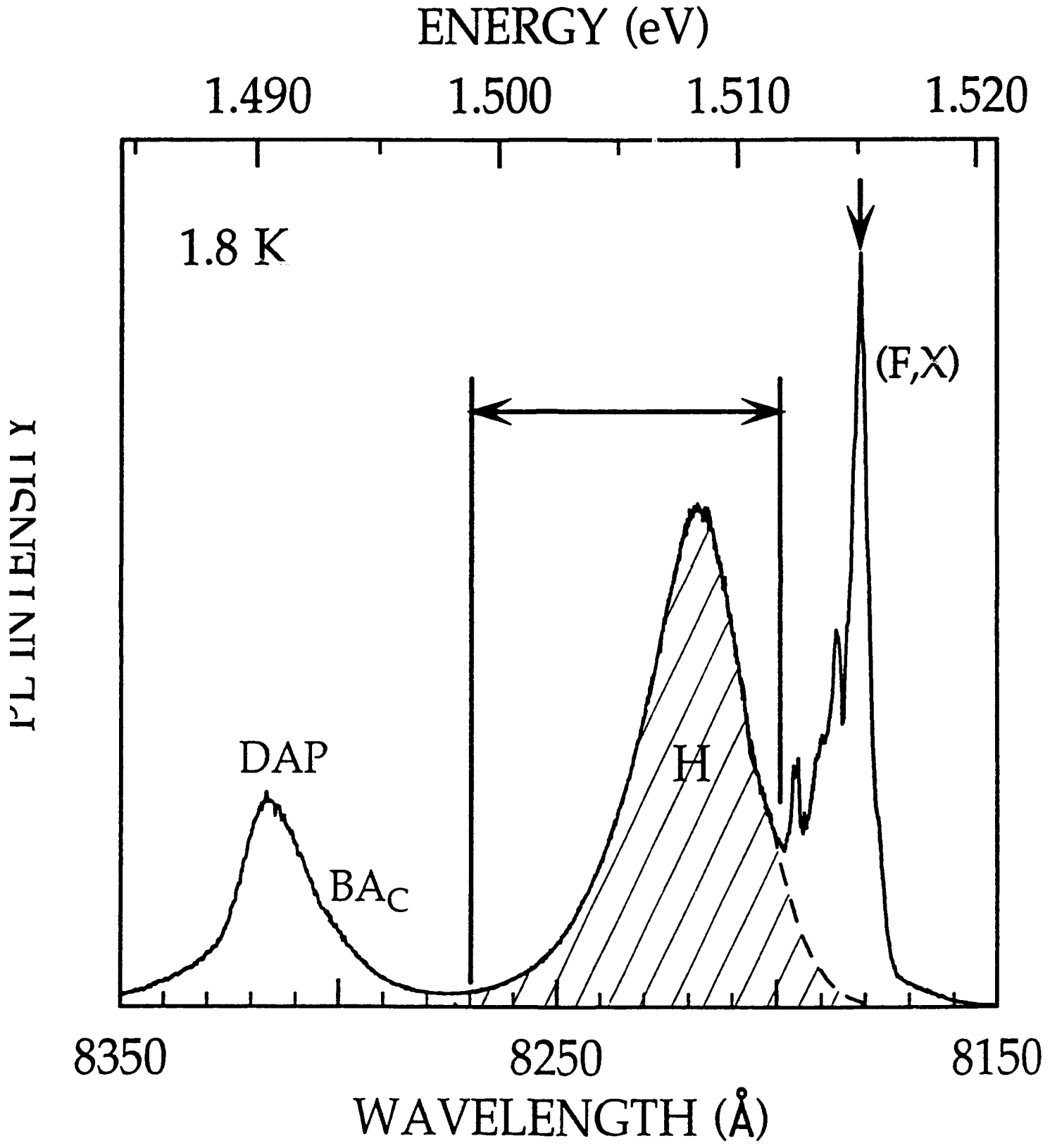
ENERGY (eV)
1.490
1.500
1.510
1.520
1.8 K
(F,X)
H
DAP
BA$_C$
PL INTENSITY
8350
8250
8150
WAVELENGTH (Å)

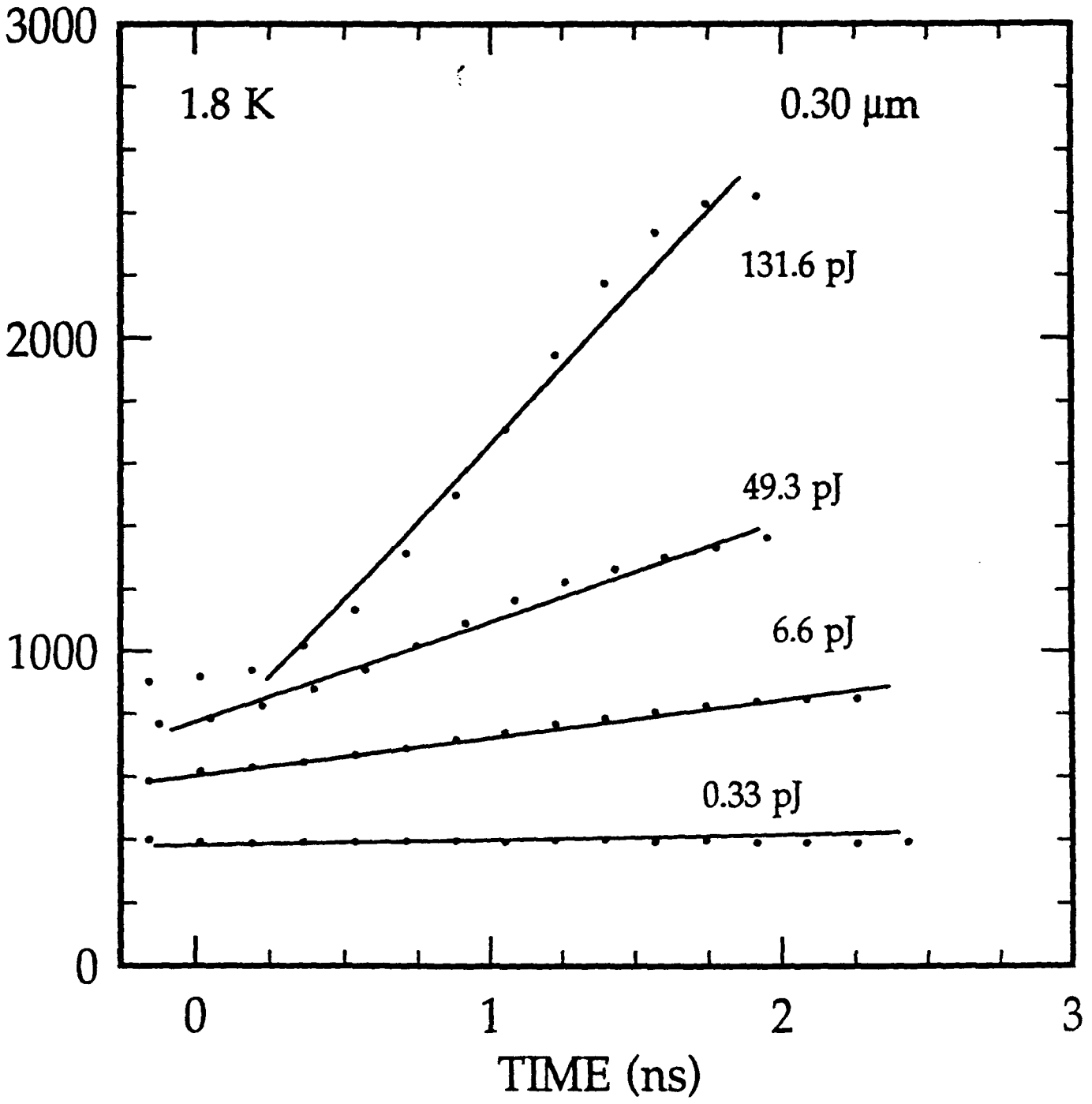
3000
2000
1000
0
1.8 K
0.30 µm
131.6 pJ
49.3 pJ
6.6 pJ
0.33 pJ
0
1
2
3
TIME (ns)

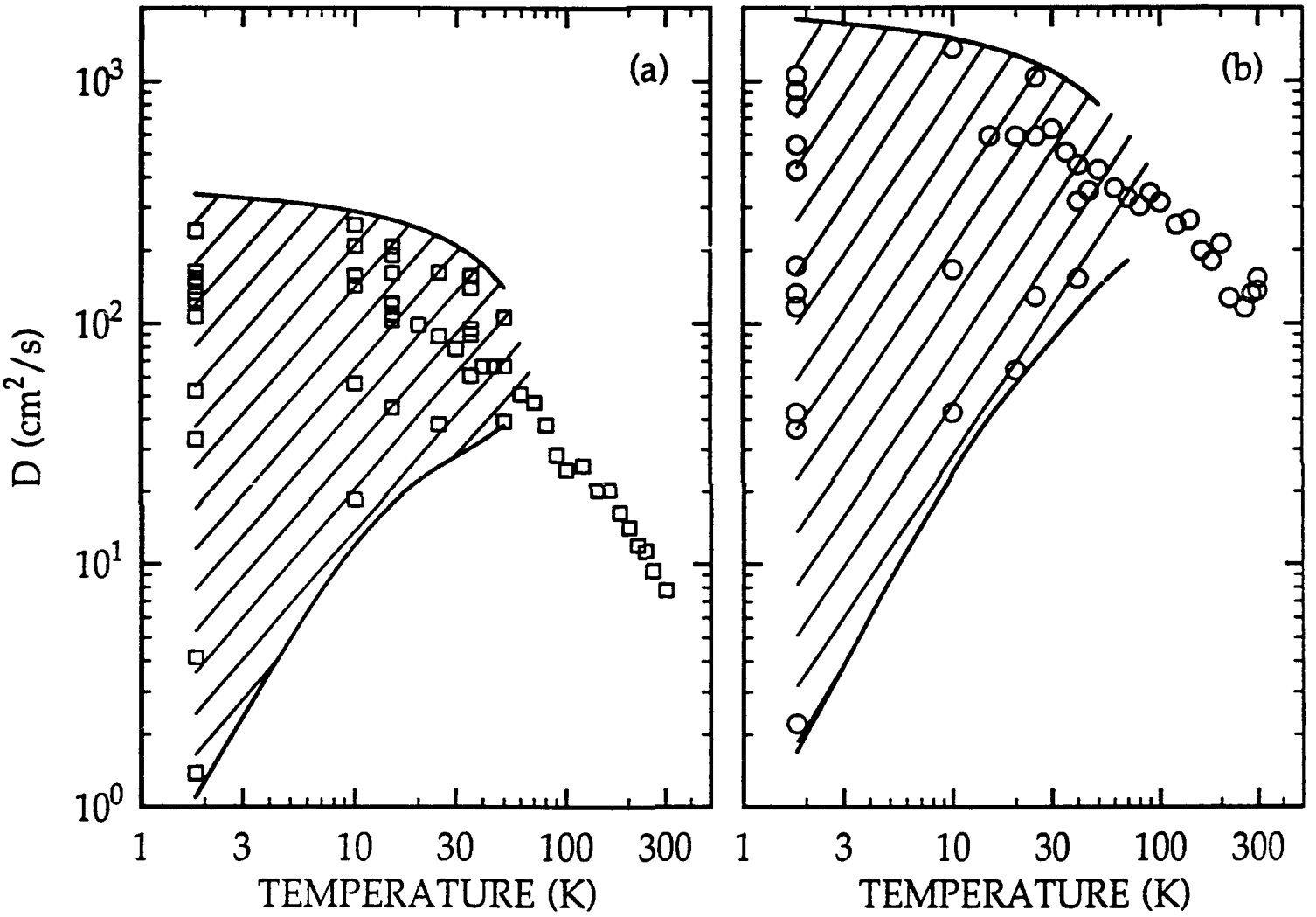
(a)
(b)
10^3
10^2
10^1
10^0
D (cm^2/s)
1
3
10
30
100
300
TEMPERATURE (K)

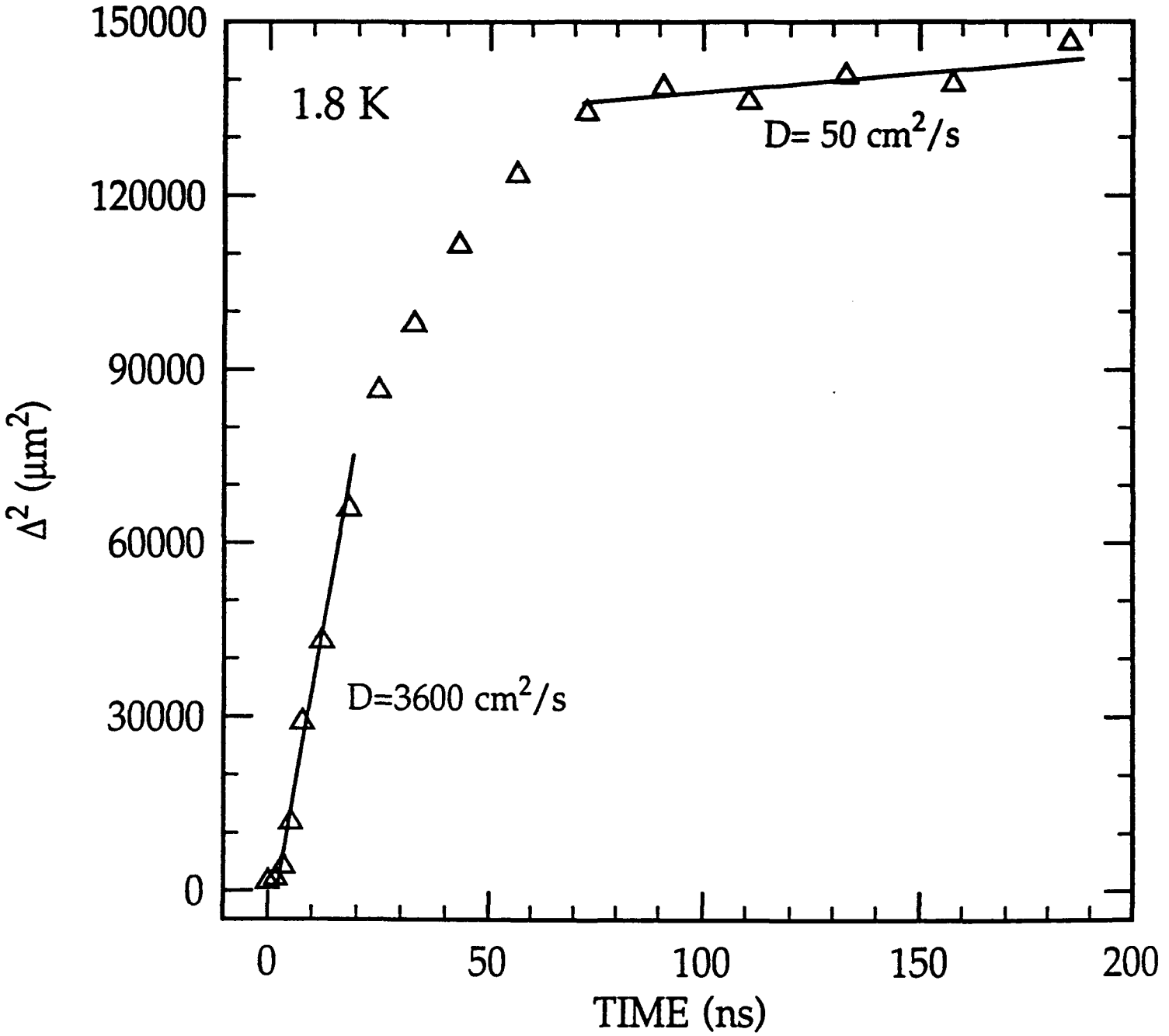
150000
120000
90000
60000
30000
0
1.8 K
D= 50 cm²/s
D=3600 cm²/s
Δ² (μm²)
0
50
100
150
200
TIME (ns)

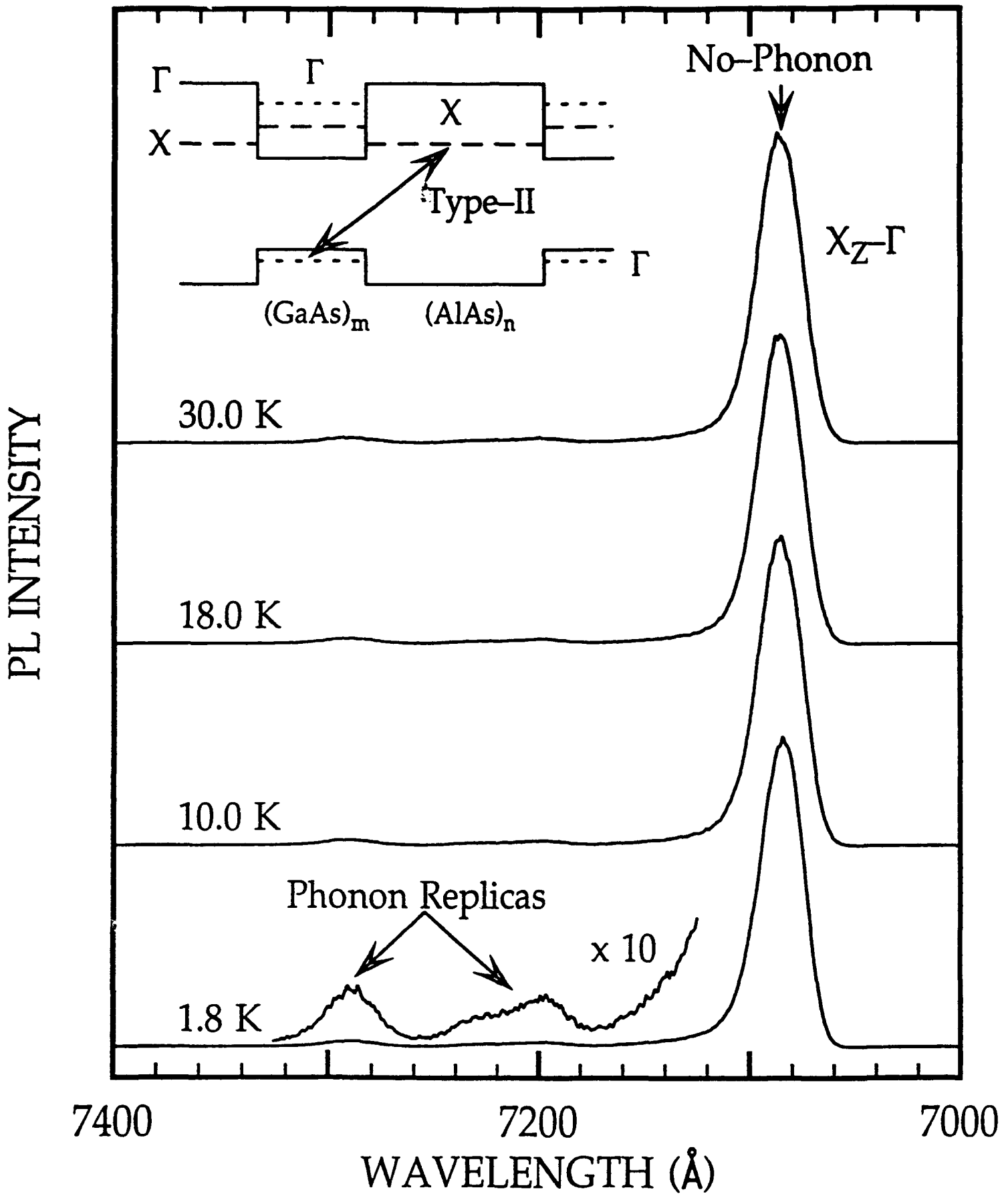
Γ
Γ
X
X
Type–II
Γ
(GaAs)m
(AlAs)n
No–Phonon
XZ–Γ
30.0 K
18.0 K
10.0 K
Phonon Replicas
x 10
1.8 K
PL INTENSITY
7400
7200
7000
WAVELENGTH (Å)

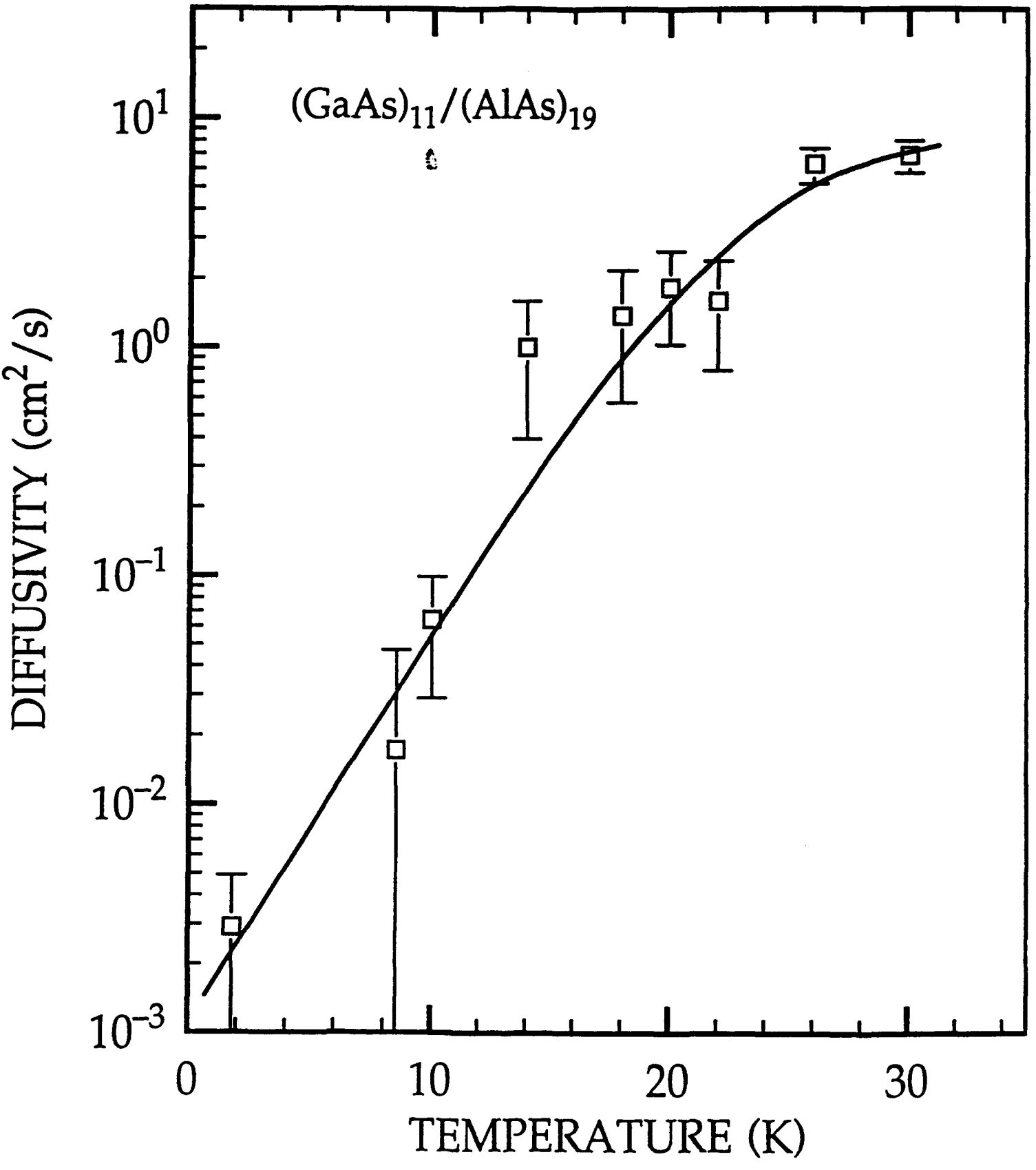
$(GaAs)_{11}/(AlAs)_{19}$
10^1
10^0
10^{-1}
10^{-2}
10^{-3}
DIFFUSIVITY (cm^2/s)
0
10
20
30
TEMPERATURE (K)

Submitted to Applied Physics Letters.

COMPARISON OF TRANSPORT, RECOMBINATION, AND INTERFACIAL QUALITY IN MBE AND OMVPE GaAs/$Al_xGa_{1-x}As$ STRUCTURES

D.J. Wolford,[a] G.D. Gilliland,[b] T.F. Kuech,[a,†] J.F. Klem,[c] H.P. Hjalmarson,[c] J.A. Bradley,[a] C.F. Tsang,[a] and J. Martinsen[a]

[a]IBM Research Division, T.J. Watson Research Center
P.O. Box 218
Yorktown Heights, New York 10598
[b]Emory University, Physics Department
Atlanta, GA 30322
[c]Sandia National Laboratory
Albuquerque, NM 87185

Abstract

We have studied free-carrier recombination and transport in GaAs structures prepared by different epitaxial growth techniques and with different "surface-barriers" - all aimed at eliminating interfacial recombination - including Molecular Beam Epitaxy (MBE) and Organo Metallic Vapor Phase Epitaxy (OMVPE) prepared undoped, symmetric GaAs/$Al_{0.3}Ga_{0.7}As$ double heterostructures and these same structures after etch-removing the top $Al_{0.3}Ga_{0.7}As$ layer and repassivating with Na_2S. We find 300 K lifetimes of $\geq$ 2.5 μs (350 ns), and interface recombination velocities of 40 cm/s (250 cm/s) for our OMVPE (MBE) structures. Identical measurements for Na_2S and bare surfaces yield interface recombination velocities of 5500 cm/s and 34,000 cm/s, respectively. Free-carrier transport in both types of structures is diffusive with hole-mobilities of ~ 350 cm^2/Vs.

PACS numbers: 78.20.-e, 78.30.Fs, 78.47+p, 78.55.-m, and 78.65.Fa.

Nonradiative decay at surfaces or interfaces may drastically reduce photoluminescence (PL) efficiencies and lifetimes in GaAs structures,[1-5] and may dominate minority-carrier kinetics, thereby, limiting the performance of minority-carrier GaAs optoelectronic devices such as injection lasers, LEDs, photodetectors, etc..[3,5-8] Consequently, there has been substantial interest in passivation of the notoriously bad GaAs surface,[3-10] with a wide variety of materials,[3,7-13] and the passivating effects of these materials have been characterized by many different experimental techniques.[3-13] However, studies of such surface passivants quantified by many of these techniques are not conclusive, due, in part, to the lack of a "surface-free" standard for comparison, lack of complete characterization of complex recombination processes, the inaccuracy and *relative* nature of most of these measurement techniques, and the absence of free-carrier transport quantification.

In our study the transport and recombination of free-carriers and the effects of GaAs/$Al_xGa_{1-x}As$ heterointerfaces on free-carrier dynamics is compared for MBE- and OMVPE-prepared epitaxial layers. Our test structures were symmetric GaAs/$Al_{0.3}Ga_{0.7}As$ double heterostructures, which, due to their simple design, eliminate many of the complications of more complex device structures, thereby allowing an assessment of the *intrinsic* free-carrier dynamics of these undoped materials (intentionally doped structures have been studied elsewhere[14,15]). We use PL time-decay measurements to quantify free-carrier kinetics - perhaps the most quantitative means for assessment of nonradiative recombination, with the distinct advantage over other techniques in its *absolute* rather than relative nature. Most surface recombination measurements rely on relative PL efficiency measurements which are not only relative in nature but also difficult to perform accurately, whereas PL time-decays yield precise and absolute (rather than relative) quantities. Free-carrier transport was quantified through an all-optical PL imaging technique described elsewhere.[16]

We have examined band-to-band recombination in these GaAs structures,[17] enabling an accurate and absolute comparison of $Al_xGa_{1-x}As$ passivation layers versus preparation technique (MBE vs. OMVPE), and a further comparison with Na_2S passivating layers. We find that characterization of GaAs layers and $Al_xGa_{1-x}As$ and Na_2S passivating layers requires an exhaustive study of the minority-carrier recombination kinetics (including versus temperature).[17] We find that lifetime measurements alone are not sufficient for accurate interface characterization - commonly quantified as an interface recombination velocity (a phenomenological term which arises as a boundary condition to the diffusion equation, and relates the nonradiative decay rate at each interface to their separation).[18]

Samples used in this study were OMVPE-prepared (MBE-prepared) $Al_{0.3}Ga_{0.7}As$/GaAs double heterostructures, grown at 750 °C (740 °C) with growth interruptions at each heterointerface to promote interfacial abruptness. $Al_{0.3}Ga_{0.7}As$ cladding layers were nominally 0.5 μm thick, undoped, and p-type ~ 3×10^{16} cm^{-3} (p-type ~ 10^{15} cm^{-3}). GaAs layers were n-type ~ 1×10^{15} cm^{-3} (p-type ~ $1\text{-}2 \times 10^{14}$ cm^{-3}), with thicknesses from 10 μm to 50 Å (4 μm to 50 Å). By varying only the GaAs-layer thickness, we may thus deduce the effects of interface and bulk nonradiative recombination. PL was excited by a variable repetition rate cavity-dumped dye laser (1 ps pulsewidth) with near-resonant wavelength to yield essentially uniform, bulk excitation. The extremely small laser fluences used in the PL decay experiments ($\leq 5 \times 10^{10}$ cm^{-2}) were obtained by defocusing the laser spot to ~ 3 mm diameter, whereas the transport measurements required tight focusing of the laser spot to ~ 3 μm diameter.

Comparison of Na_2S passivants with the original $Al_{0.3}Ga_{0.7}As$ layers required the removal of the top $Al_{0.3}Ga_{0.7}As$ layer - thus enabling a comparison of passivants for a single interface. This was achieved through chemical etching with a 3:1:50 solution of H_3PO_4:H_2O_2:H_2O at 0 °C. Resulting surfaces had < 5% deviation from the target thickness over lateral distances of ≥ 500 μm, thereby leaving the GaAs-layer thickness unchanged, as determined from surface profilimiter, SEM, and TEM measurements. Standard techniques were used for application of the Na_2S passivation layer,[8] and all measurements were performed in the dry He-gas atmosphere of the optical cryostat within several hours of application to minimize possible degradation of the hygroscopic Na_2S layer.

The 300 K PL of all structures exhibited the expected Boltzmann tail on the high-energy side, indicating that the recombination is of thermalized carriers.[17] In addition, peak PL energies are identical for all bulk samples. Decay kinetics versus GaAs-layer thickness are, however, quite different, both qualitatively and quantitatively. For OMVPE-prepared structures,[17] PL decays are highly-nonexponential and bimolecular for thick samples, and rigorously exponential for thin samples (d ≤ 0.5 μm) - changing *systematically* from bimolecular to exponential for decreasing GaAs-layer thickness. Decay kinetics in all MBE-prepared structures are bimolecular. Lifetimes, in general, decrease with decreasing GaAs-layer thickness in all structures. These kinetics were fit to the rate equation for band-to-band recombination

$$\frac{dp}{dt} = -B(np + n_0 p + p_0 n) - \frac{p}{\tau_{nr}} - \frac{(S_1 + S_2)p}{d}, \qquad (1)$$

p (n) is the photoexcited hole (electron) density, p_0 (n_0) is the built-in hole (electron) density, τ_{nr} represents bulk nonradiative decay, d is the GaAs layer thickness, and S_i (i=1,2) is the interface recombination velocity at each interface. B is the bimolecular decay constant, (2×10^{-10} cm^3/s).[3]

Our initially bimolecular decays in thick OMVPE and all MBE structures,[19] eventually become dominated by interface recombination at long-times, yielding exponential decays. Results for thinner OMVPE structures (≤ 0.5 μm) are, in contrast, always exponential. We have found in our optical transport measurements that our thin OMVPE structures become *effectively p-type modulation doped* due to the accumulation of holes in the GaAs layer from both $Al_{0.3}Ga_{0.7}As$ layers.[16] Thus, lifetimes obtained in these thin OMVPE samples are accordingly limited by the majority-hole density (the term Bp_0n), and the minority-carriers are electrons. In contrast the higher-purity MBE structures exhibit bimolecular decays with exponential long-time tails indicative of interface recombination.

Measured lifetimes may be used to calculate interface recombination velocities for these samples. S_1 and S_2 are related to the measured lifetime as

$$\frac{1}{\tau} = \frac{1}{\tau_{nr}} + \frac{(S_1 + S_2)}{d} + B(n_0 + p_0), \qquad (2)$$

(assuming that $(S_1 + S_2) \ll (\pi^2 D)/d$, where D is the diffusivity).[17] Therefore, $S = 1/2(S_1 + S_2)$ may be calculated from lifetimes versus GaAs-layer thickness. Our results are shown in Fig. 1, yielding $S \approx 40$ cm/s and $S \approx 250$ cm/s for OMVPE and MBE structures, respectively. We find that S for our OMVPE structures may only be determined from the thick structures (≥ 0.5 μm), due to complications arising in thinner structures, as noted above. Moreover, we find that bulk nonradiative decay is negligible in the OMVPE structures ($\tau_{nr} \geq 3$ μs), and larger in the MBE structures ($\tau_{nr} \approx 800$ ns).

After finding virtually "surface-free" interfacial quality for the OMVPE structures, we proceeded with Na_2S surface-passivant studies of these samples. Figure 2 shows PL spectra and lifetimes for OMVPE structures with an $Al_{0.3}Ga_{0.7}As$ surface, a "bare" surface, and a Na_2S passivated surface. Using Eq. 2, we obtain interface recombination velocities of 34,000 cm/s and 5500 cm/s for single "bare" and Na_2S interfaces, respectively. Corresponding PL efficiencies are ~ 900 and ~ 30 times weaker than the original 9.82 μm $GaAs/Al_{0.3}Ga_{0.7}As$ double heterostructure, respectively. Thus, the increased nonradiative surface recombination is accompanied by reduced lifetimes and PL efficiencies.

Recently we have reported measurements of free-carrier transport in these OMVPE structures using a time-resolved PL imaging technique[16] (these measurements are not possible in the Na_2S and bare surface structures due to the weak PL emission). We observed[16] a time-dependent and GaAs-layer thickness dependent change from ambipolar to free-electron dominated diffusion that is quantitatively understood in terms of the known unintentional doping of both GaAs and $Al_{0.3}Ga_{0.7}As$ l yers. We report here similar measurements of free-carrier transport in our MBE structures, with the results for both OMVPE and MBE structures shown in Fig. 3. In contrast to the complex OMVPE results, free-carrier transport in the MBE structures is purely ambipolar, yielding hole diffusion constants (D_h = 1/2 D_a) and corresponding mobilities from the Einstein relation, as shown. These results are consistent with the higher purity of the isotype MBE structures compared to the OMVPE structures. Further, obtained minority hole mobilities in this n-type GaAs are in good agreement with majority hole Hall measurements in comparable p-type GaAs samples.

These measured minority-carrier lifetimes and diffusivities may be further used to characterize the heterointerfacial quality via calculations of minority-carrier diffusion lengths. Defined as $L_D = \sqrt{D\tau}$, we find hole diffusion lengths $\geq$ 37 μm and $\geq$ 18 μm for the OMVPE and MBE structures, respectively. Also, we find electron diffusion lengths $\geq$ 120 μm in the thin OMVPE structures. These results are shown in Fig. 4 together with the number of heterointerface reflections for each structure, ~ 140 and 50, respectively (calculated from the ratio of L_D to d). More free-carrier heterointerface reflections are indicative of higher interfacial quality.

In this study we have thus determined and compared the passivating effects of MBE- and OMVPE-prepared $Al_xGa_{1-x}As$ layers, as well as Na_2S passivating layers on a single GaAs surface, since (1) we have *fully* characterized the back heterointerface ($GaAs/Al_{0.3}Ga_{0.7}As$) and find it to be "surface-free" (thus minority-carriers are almost totally unaffected by the back heterointerface), and (2) we have quantified minority-carrier transport in these structures. We find the passivating effects and optical quality of MBE-prepared $Al_{0.3}Ga_{0.7}As$ and GaAs layers and heterointerfaces, although of extremely high-quality, to be less than those of OMVPE-prepared $Al_{0.3}Ga_{0.7}As$ and GaAs layers and heterointerfaces - a surprising result in view of the typically higher mobility of MBE structures compared to OMVPE structures. Moreover, we find bulk nonradiative decay is more significant in MBE than OMVPE structures. We confirm that Na_2S passivants are inferior to high-quality $Al_{0.3}Ga_{0.7}As$ layers. Further, all intrinsic band-to-band recombination kinetics are fully described by the band-to-band recombination rate equation. From our analysis, we also conclude that photon recycling is negligible in these structures based

upon three observations: (1) lifetimes are consistent with known sample purity and radiative B coefficient,[20] (2) PL spectra exhibit no redshift versus GaAs-layer thickness,[14,21] and (3) all transport is in good agreement with electrically measured mobilities. Lastly, our OMVPE lifetimes (2.5 μs for the 9.82 μm structure) and interface recombination velocities (40 cm/s) are among the *longest* and *lowest*, respectively, for any GaAs/$Al_xGa_{1-x}As$ structure to date.

This work was supported in part by ONR under contracts N00014-90-C-0077, N00014-91-J-1697, and N00014-92-J-1927, and the U.S. DOE under contract DE-AC04-76DP00789.

REFERENCES

†Present Address: Univ. of Wisconsin, Dept. of Chem. Eng., Madison, WI 53706.

1. G. Lasher and F. Stern, Phys. Rev. **133**, 553 (1964).
2. H.C. Casey, Jr. and F. Stern, J. Appl. Phys. **47**, 631 (1976).
3. R.J. Nelson and R.G. Sobers, J. Appl. Phys. **49**, 6103 (1978).
4. E. Yablonovitch, R. Bhat, J.P. Harbison, and R.A. Logan, Appl. Phys. Lett. **50**, 1197 (1987).
5. L.M. Smith, D.J. Wolford, J. Martinsen, R. Venkatasubramanian, and S.K. Ghandi, J. Vac. Sci. Technol. B **8**, 787 (1990).
6. C.J. Sandroff, R.N. Nottenburg, J.C. Bischoff, and R. Bhat, Appl. Phys. Lett. **51**, 33 (1987).
7. M.G. Mauk, S. Xu, D.J. Arent, R.P. Mertens, and G. Borghs, Appl. Phys. Lett. **54**, 213 (1989).
8. B.J. Skromme, C.J. Sandroff, E. Yablonovitch, and T. Gmitter, Appl. Phys. Lett. **51**, 2022 (1987).
9. L.W. Molenkamp and H.F.J. van't Blik, J. Appl. Phys. **64**, 4253 (1988).
10. P. Dawson and K. Woodbridge, Appl. Phys. Lett. **45**, 1227 (1984).
11. S.K. Ghandi, S. Tyagi, and R. Venkatasubramanian, Appl. Phys. Lett. **53**, 1308 (1988).
12. K.C. Hwang, and S.S. Li, J. Appl. Phys. **67**, 2162 (1990).
13. S.D. Offsey, J.M. Woodall, A.C. Warren, P.D. Kirchner, T.I. Chappell, and G.D. Pettit, Appl. Phys. Lett. **48**, 415 (1986).
14. R.K. Ahrenkiel, B.M. Keyes, and D.J. Dunlavy, J. Appl. Phys. **70**, 225 (1991).
15. G.B. Lush, M.R. Melloch, M.S. Lundstrom, H.F. MacMillan, B.M. Keyes, D.H. Levi, and R.K. Ahrenkiel, submitted to J. Appl. Phys.
16. G.D. Gilliland, D.J. Wolford, T.F. Kuech, and J.A. Bradley, Appl. Phys. Lett. **59**, 216 (1991).

17. D.J. Wolford, G.D. Gilliland, T.F. Kuech, L.M. Smith, J. Martinsen, J.A. Bradley, C.F. Tsang, R. Venkatasubramanian, S.K. Ghandi, and H.P. Hjalmarson, J. Vac. Sci. Technol. B **9**, 2369 (1991).
18. G.S. 'tHooft and C. van Opdorp, J. Appl. Phys. **60**, 1065 (1986).
19. At still lower excitation levels, the decays become exponential with a lifetime equivalent to the long-time tail.
20. According to Lush et al.[15] PR will manifest itself in a negative curvature when lifetimes are plotted as $1/\tau$ vs. $1/d$. In our OMVPE samples this curvature is positive, and there is no curvature for our MBE samples.
21. S.D. Lester, T.S. Kim, and B.G. Streetman, J. Appl. Phys. **63**,853 (1988).

17. D.J. Wolford, G.D. Gilliland, T.F. Kuech, L.M. Smith, J. Martinsen, J.A. Bradley, C.F. Tsang, R. Venkatasubramanian, S.K. Ghandi, and H.P. Hjalmarson, J. Vac. Sci. Technol. B **9**, 2369 (1991).
18. G.S. 'tHooft and C. van Opdorp, J. Appl. Phys. **60**, 1065 (1986).
19. At still lower excitation levels, the decays become exponential with a lifetime equivalent to the long-time tail.
20. According to Lush et al.[15] PR will manifest itself in a negative curvature when lifetimes are plotted as $1/\tau$ vs. 1/d. In our OMVPE samples this curvature is positive, and there is no curvature for our MBE samples.
21. S.D. Lester, T.S. Kim, and B.G. Streetman, J. Appl. Phys. **63**,853 (1988).

FIGURE CAPTIONS

Fig. 1. 300 K lifetimes obtained for the OMVPE-prepared $Al_{0.3}Ga_{0.7}As/GaAs/Al_{0.3}Ga_{0.7}As$ double heterostructures •, MBE-prepared $Al_{0.3}Ga_{0.7}As/GaAs/Al_{0.3}Ga_{0.7}As$ double heterostructures o, $Na_2S/GaAs/Al_{0.3}Ga_{0.7}As$ heterostructures Δ, and "bare" $GaAs/Al_{0.3}Ga_{0.7}As$ heterostructure ♦, versus GaAs layer thickness.

Fig. 2. (a) 300-K PL for 9.82-μm $Al_{0.3}Ga_{0.7}As/GaAs/Al_{0.3}Ga_{0.7}As$ double heterostructure, Na_2S passivated structure, and a "bare" $GaAs/Al_{0.3}Ga_{0.7}As$ structure. (b) Corresponding 300-K PL decays for these same structures, with derived lifetimes.

Fig. 3. Electron and hole diffusion constants and mobilities, versus GaAs layer thickness for OMVPE- (squares) and MBE-prepared (circles) structures.

Fig. 4. (a) 300 K diffusion lengths obtained from our transport and time-decay results for all $GaAs/Al_{0.3}Ga_{0.7}As$ double heterostructures. (b) Corresponding number of free-carrier heterointerface reflections for these structures.

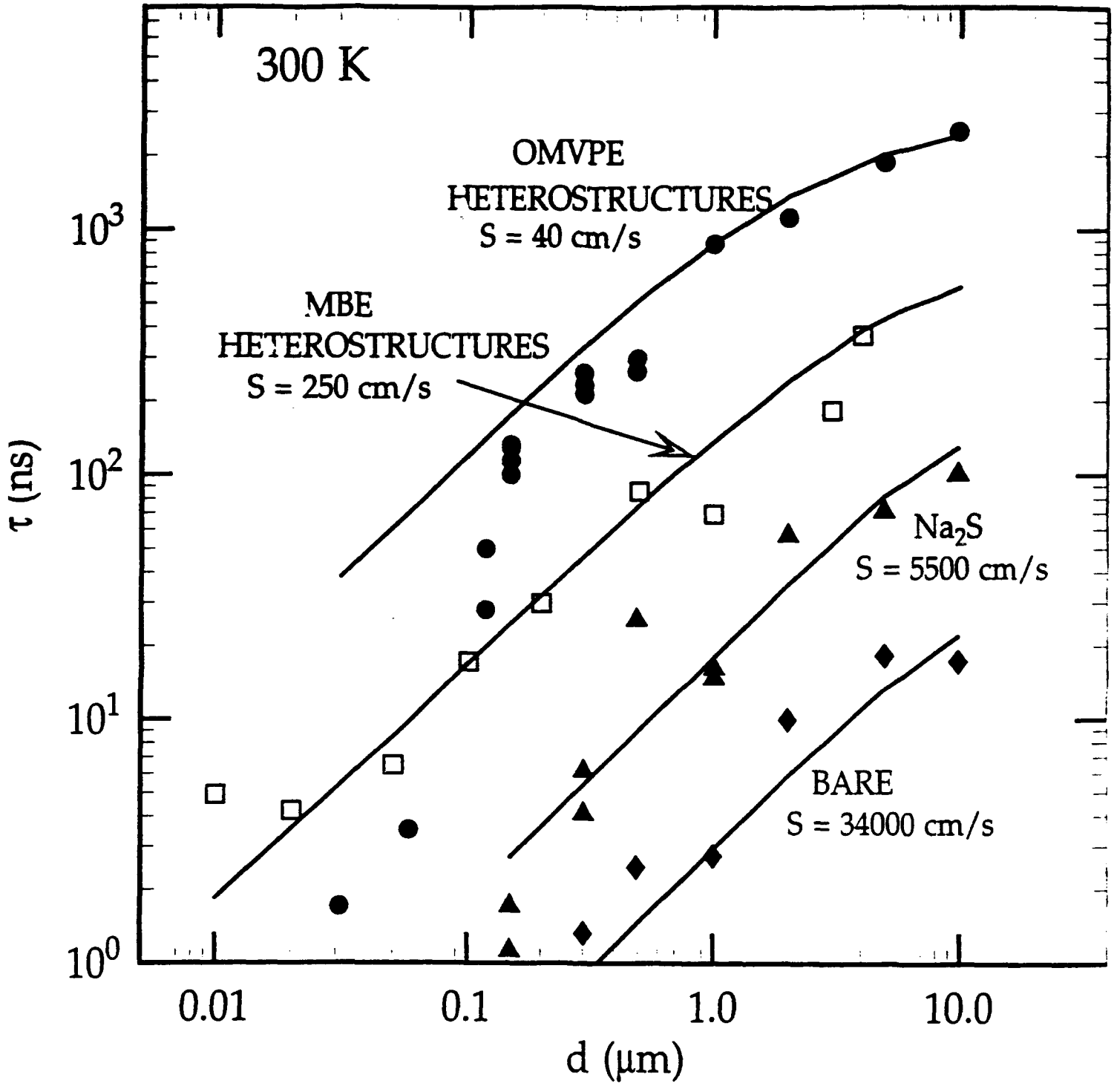
300 K
OMVPE
HETEROSTRUCTURES
S = 40 cm/s
MBE
HETEROSTRUCTURES
S = 250 cm/s
Na2S
S = 5500 cm/s
BARE
S = 34000 cm/s
τ (ns)
10^3
10^2
10^1
10^0
0.01
0.1
1.0
10.0
d (μm)

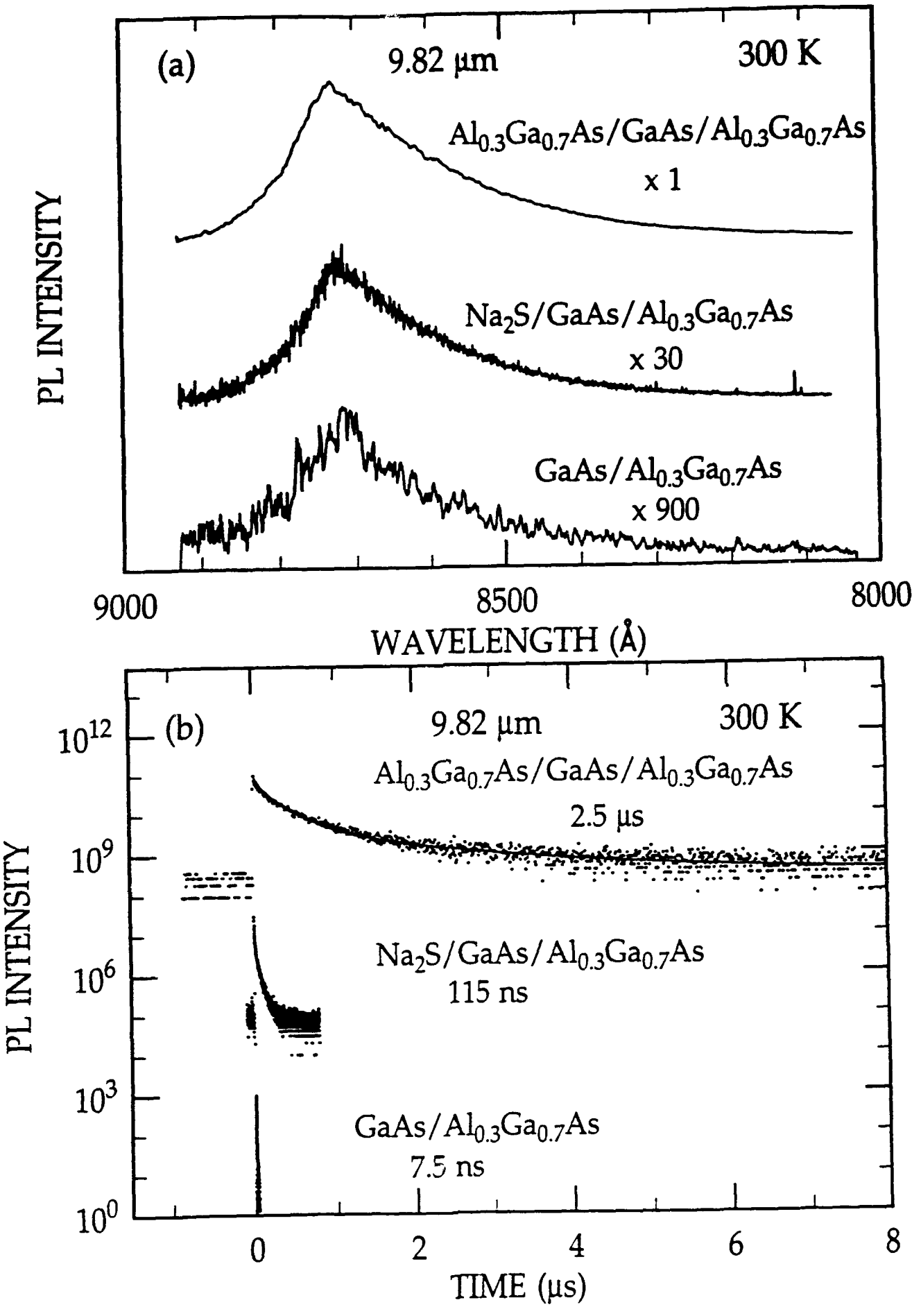
(a)
9.82 μm
300 K
$Al_{0.3}Ga_{0.7}As/GaAs/Al_{0.3}Ga_{0.7}As$
x 1
$Na_2S/GaAs/Al_{0.3}Ga_{0.7}As$
x 30
$GaAs/Al_{0.3}Ga_{0.7}As$
x 900
PL INTENSITY
9000
8500
8000
WAVELENGTH (Å)
(b)
9.82 μm
300 K
$Al_{0.3}Ga_{0.7}As/GaAs/Al_{0.3}Ga_{0.7}As$
2.5 μs
$Na_2S/GaAs/Al_{0.3}Ga_{0.7}As$
115 ns
$GaAs/Al_{0.3}Ga_{0.7}As$
7.5 ns
PL INTENSITY
10^{12}
10^{9}
10^{6}
10^{3}
10^{0}
0
2
4
6
8
TIME (μs)

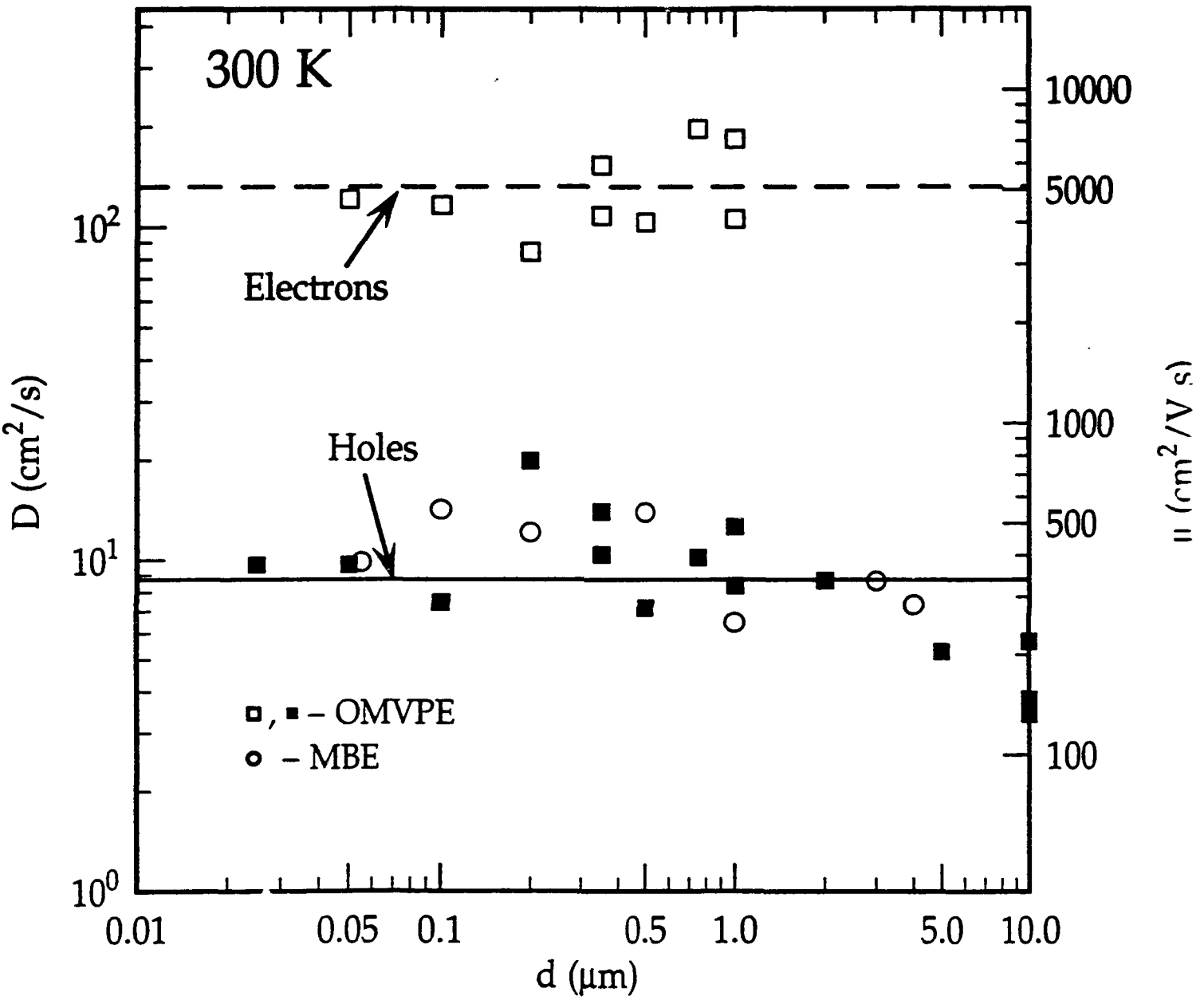
300 K
10000
5000
10^2
Electrons
1000
Holes
D (cm^2/s)
500
10^1
□, ■ – OMVPE
○ – MBE
100
10^0
0.01
0.05
0.1
0.5
1.0
5.0
10.0
d (μm)

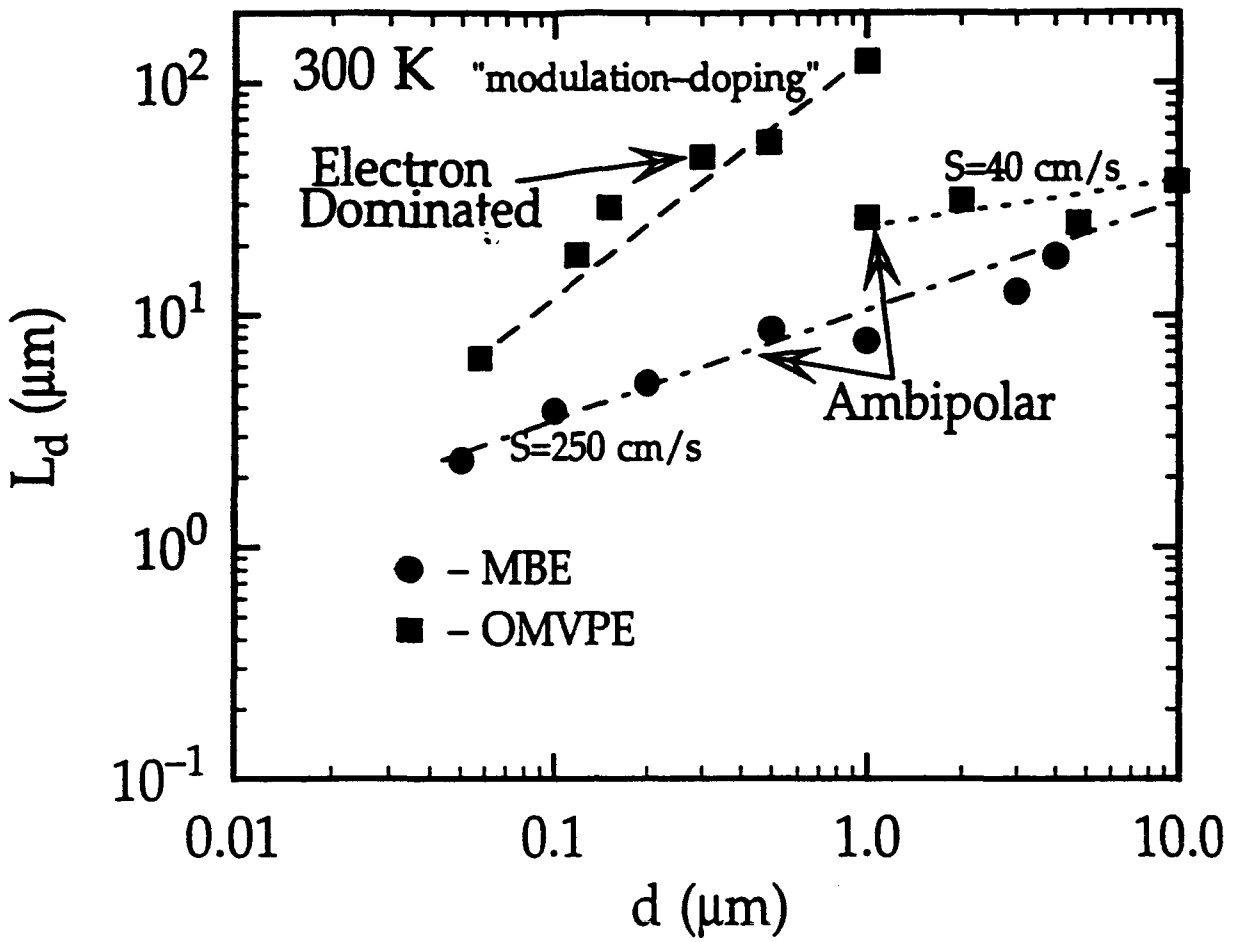
300 K "modulation-doping"
Electron Dominated
S=40 cm/s
Ambipolar
S=250 cm/s
● – MBE
■ – OMVPE
L_d (μm)
10^2
10^1
10^0
10^{-1}
0.01
0.1
1.0
10.0
d (μm)

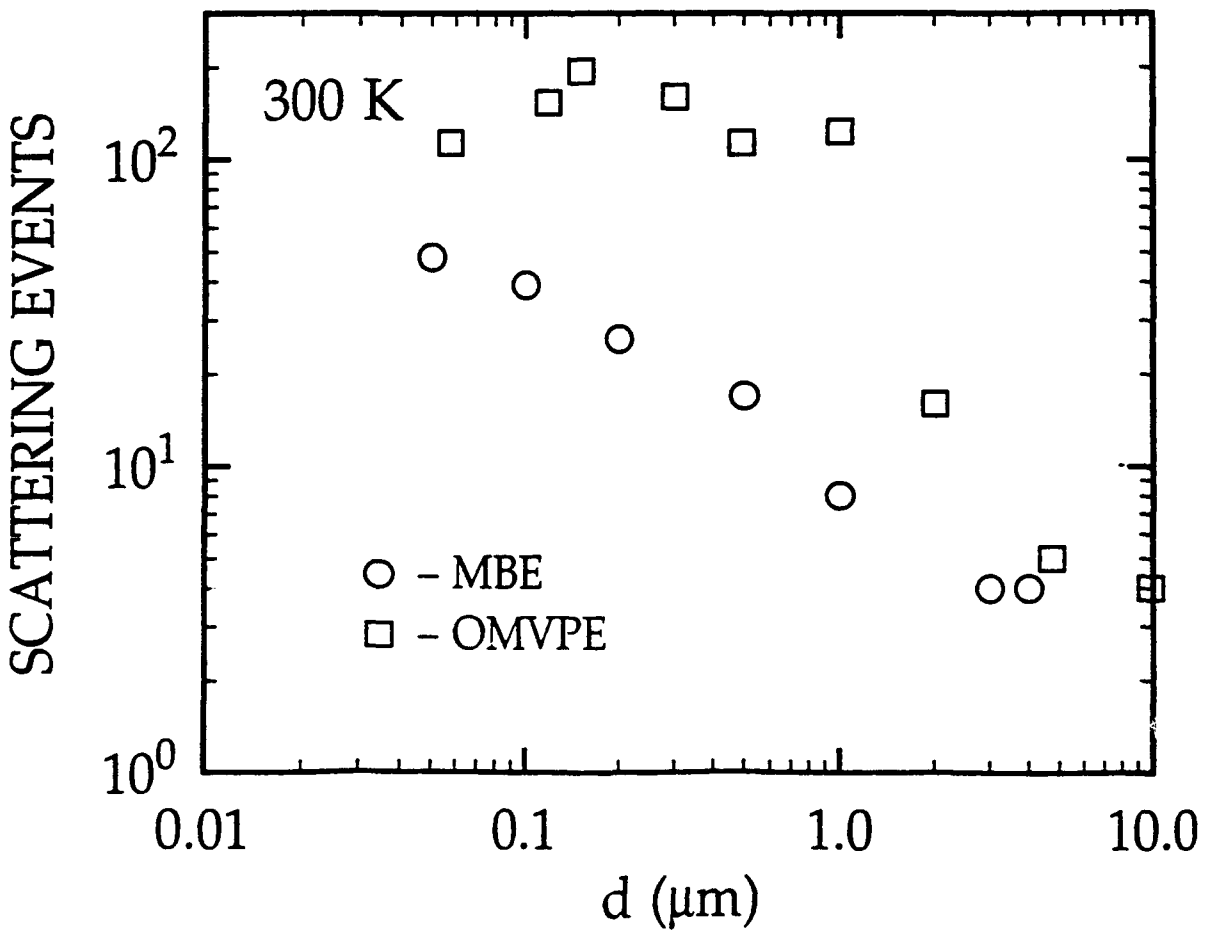
300 K
○ – MBE
□ – OMVPE
SCATTERING EVENTS
10^2
10^1
10^0
0.01
0.1
1.0
10.0
d (μm)

Submitted to Physical Review B.

LUMINESCENCE KINETICS OF INTRINSIC EXCITONIC STATES QUANTUM-MECHANICALLY BOUND NEAR HIGH-QUALITY GaAs(n^-)/$Al_xGa_{1-x}As$(p) HETEROINTERFACES

G.D. Gilliland, D.J. Wolford, T.F. Kuech,† and J.A. Bradley

IBM Research Division, T.J. Watson Research Center

P.O. Box 218

Yorktown Heights, New York 10598

Abstract

Recently, an optical emission process, termed the H-band, has been observed in GaAs/$Al_xGa_{1-x}As$ heterostructures which has been related to the regions surrounding the heterointerfaces. We show here that the mechanism responsible for this new H-band photoluminescence (PL) in our structures, is the recombination of quasi-2D excitons — and not due to either the recombination of carriers bound at impurities/defects, or recombination of 2D carriers with 3D free-carriers. We have used such PL in high-purity, virtually "interface-free" GaAs(n^-)/$Al_{0.3}Ga_{0.7}As$(p) double heterostructures to study H-band decay dynamics, and thus prove these excitations in our structures are "intrinsic" and arise from quantum-mechanically bound quasi-2D excitons. Time-resolved PL spectra show emission to be spectrally non-stationary, with lifetimes across the band varying from a few ns to more than 50 μs. Further, we find that large interfacial recombination velocities, in inferior samples, may mask the truly intrinsic H-band recombination dynamics. Our accompanying quantum-mechanical numerical modeling of such 2D-excitons interprets and reproduces virtually all of our experimental observations. Indeed, they demonstrate H-band PL cannot be impurity-induced, but instead arises from the recombination of intrinsic excitonic states bound at both heterointerfaces. Hence, we find that in

thinner structures, these excitonic states may be simultaneously associated with both interfaces, with a critical GaAs-thickness at which this "exciton sharing" between heterointerfaces becomes significant of $\sim 0.5\ \mu m$. We also discuss the time-evolution of the initially photo-excited 3D "bulk" excitons as they acquire this subsequent 2D-character, through a mechanism at the interfaces analogous to the Quantum Confined Stark Effect in quantum wells. Our combined experimental and theoretical modeling, in these virtually "interface-free," samples therefore, provide, perhaps, a direct, "pure" measure and full quantum-mechanical explanation of the temporal evolution of these intrinsic 2D-excitons — from 3D-formation to 2D-recombination — as undistorted by the deleterious influence of carrier trapping and nonradiative decay (in both the bulk and at interfaces), which may otherwise dominate the usually "more-imperfect" typical heterostructure. The results presented here are for specific, high-quality, "interface-free" GaAs/$Al_{0.3}Ga_{0.7}As$ heterostructures, however these measurement and analysis techniques may also be applicable to other types of structures.

I. INTRODUCTION.

Modern epitaxy of structured materials now makes possible detailed, analytical study of the structural and electronic properties of high-electronic-quality, abrupt heterostructure interfaces.[1-4] Molecular beam epitaxy (MBE) and organometallic vapor phase epitaxy (OMVPE) are most recently capable of producing truly abrupt heterointerfaces, with interfacial fluctuations of one-to-two monolayers.[5-7] Moreover, relative material purity has also drastically improved, as these separate growth techniques have matured and higher-purity sources have become available. As a result, the intrinsic properties of heterointerfaces — e.g., spikes and notches in the energy-band-edges at the heterointerface — might now be studied spectroscopically, virtually unimpeded by the effects of graded interfaces, or consequential residual impurity/defect concentrations either in the bulk, or at the interfaces. We thus report here the first detailed results of extensive static and dynamical study of formation and decay of quantum-mechanical excitonic states, bound intrinsically at such high-quality GaAs/$Al_xGa_{1-x}As$ heterointerfaces in double heterostructures.

Recently, optical studies of GaAs/$Al_xGa_{1-x}As$ structures have resulted in the observation of a new and distinct, near-edge photoluminescence (PL) process.[8] Referred to as the H-band, this PL lies energetically between the edge-bound excitons and the band-to-acceptor (and/or donor-acceptor pair) emissions, and has been observed in both n-p and n-n heterostructures. Indeed, such H-band PL has been reported for samples prepared by a variety of techniques, including liquid phase epitaxy (LPE),[8] MBE,[9-21] and OMVPE.[22-28] Furthermore, some PL H-band studies conducted in electric[14,16,19] and magnetic[10,12,17,18] fields have suggested that this recombination may be spatially related to the heterointerface, and possibly the electrostatic band-bending generally induced there. However, to date, no complete and systematic study of H-band temporal evolution (dynamics) has been reported, especially in heterostructures proven to be electronically optimum. Hence, in our view, a truly adequate and compelling explanation

for the excitations responsible for this unique PL — capable of accounting for all of its static and dynamic properties — has not been available.

Previous studies have, for instance, shown (mostly through cw-PL) relatively complex, power- and temperature-dependences for H-band emission. In its first observation, Yuan et al.[8] concluded this new H-band PL must arise from the GaAs/$Al_xGa_{1-x}As$ heterointerface — a supposition supported mostly by chemically removing one of the $Al_xGa_{1-x}As$ barriers, and observing either diminishment or total loss of the H-band. Nonetheless, these workers also found accompanying H-band peak-energy-shifts to be more-or-less proportional to the log of the excitation-laser power density, and that H-band PL intensity seemed to qualitatively diminish with increasing temperature, from 1.8-K to near disappearance above ~ 15 K. Further, electric-field studies[14,16,19] indicated a tendency for H-band PL to shift in energy with applied field. In contrast, magnetic-field studies[10,12,17,18] found the H-band to split into several peaks, whose magnitudes varied as roughly the cosine of the angle between the field and the growth direction, thus indicating a possible two-dimensionality for this excitation, and implicating the heterointerfaces with its possible origin. Moreover, the PL also appeared to shift to higher energies with applied magnetic-field (by as much as 10 meV at 10 Tesla), but inconclusively the associated "diamagnetic shift" appeared linear in applied magnetic-field in some studies,[10,12] while appearing nonlinear in field in others.[17,18] Lastly, limited study of H-band temporal decays suggested an increased lifetime with applied magnetic-field,[17,18] thus making H-band temporal evolution very complex.

Thus, despite many such luminescence and perturbative H-band studies, much controversy still remains concerning the physical origin of this excitation and recombination process. As an example, Alferov et al.[12] have concluded this PL (found in their MBE-structures) was due to the recombination between donor impurities in the narrow-gap material, with unspecified "acceptor-like" surface states arising from within the barrier materials. More recently, others[13,17,18] have attributed virtually this same PL to yet other unspecified defect-pair recom-

bination, in which one of the defects is located precisely at the GaAs/$Al_xGa_{1-x}As$ interface. Nonetheless, most studies[8,10,14,19,20,27] have yielded to the conclusion that the H-band may arise from the recombination between a free carrier and a carrier (not necessarily quantum-mechanically) confined near hetero-interfacial band-bending. However, to date, numerous experimental observations still remain incompletely or inadequately explained by any truly definitive physical model or system photoexcitation.

In contrast, here we show that the H-band emission, in our structures, is not impurity induced, but instead results from an "intrinsic" 2-D excitonic emission. As will be shown, this becomes apparent through detailed dynamical behavior found by time-resolving the H-band PL in a series of otherwise identical, virtually "interface-free" GaAs/$Al_{0.3}Ga_{0.7}As$ double heterostructures, in which the GaAs-layer thickness is made the single and most important structurally varied sample parameter. We then offer an analytical and numerically solved, fully quantum-mechanical, model for the H-band excitation and simulation of its subsequent temporal evolution, and definitively show observed decays, in our structures, may only be explained by the combined effect of both double heterointerfaces. Our calculations thus explain virtually all of our experimentally observed static and dynamic properties of low-temperature H-band emission.

2. EXPERIMENTAL METHODS.

Samples used were OMVPE-prepared GaAs/$Al_{0.3}Ga_{0.7}As$ double heterostructures, with GaAs thicknesses ranging from 0.1 μm to 2.0 μm. $Al_{0.3}Ga_{0.7}As$ layers were 0.5-μm thick in all samples, and were unintentionally, p-type (carbon) doped at $\sim 3 \times 10^{16} cm^{-3}$, whereas GaAs layers were nominally undoped, n-type at $\sim 1 \times 10^{15} cm^{-3}$. All heterostructures were prepared at 750°C, at V/III ratios of 40, with undoped (*n*-type) 0.5-μm-thick GaAs buffer layers, on semi-insulating substrates. To help promote interfacial abruptness, all samples were prepared with growth interruptions at each heterointerface.

Photoluminescence experiments were performed in a variable-temperature optical cryostat, allowing detailed studies versus temperatures between 1.8 and 50 K. Samples were mounted "strain-free" with rubber cement to the sample probe, with the temperature monitored by a Si-diode mounted (in the same fashion) to the probe backside. Luminescence was excited by a synchronously-pumped, cavity-dumped DCM (4-Dicyanomethylene-2-methyl-6-p-dimethylaminostyryl-4H-pyran) dye laser, with a pulse-width of 1.0-ps, and tunable from 6400 to 7000 Å. The luminescence was collected and then dispersed by a 0.85-meter double-grating spectrometer, and detected by a chilled RCA C31034A photomultiplier. Time-decays were collected using the time-correlated single-photon-counting technique;[29] care was taken to insure photon-pile-up did not occur, by keeping detection rates at least 2-orders-of-magnitude below the laser repetition rate; total system time resolution was better than 0.5 ns. Photoexcited carrier densities for all kinetics studies were $\sim 10^{15} - 10^{16} cm^{-3}$.

3. EXPERIMENTAL RESULTS.

Because our study may relate to the $GaAs/Al_xGa_{1-x}As$ heterointerfaces, careful first characterization of these interfaces is of ultimate importance. Without such thorough study of the interface and bulk properties, one may never be certain that observed processes are not related to — if not totally originating from — poor interfacial and/or bulk properties. We have thus thoroughly characterized all samples by measuring the absolute interface quality,[30-33] as "quantified" by the interface recombination velocity, S, representing the nonradiative decay of carriers at each heterointerface. Such generally nonradiative and uncontrollable decay may drastically alter PL efficiencies and lifetimes, and is usually calculated from PL efficiency and/or lifetime measurements.[30-35] We have therefore calculated S from room-temperature lifetime measurements of all samples, finding $S \lesssim \underline{40\ cm/s}$ [30-33] — among the lowest reported (by detailed GaAs-thickness dependences) for any $GaAs/Al_xGa_{1-x}As$ structure,[35] to date — with

room-temperature band-to-band recombination lifetimes of over 2.5 μs. [30 – 33] Such high-quality interfaces should therefore allow carriers to reside near to them, for long times, without decaying nonradiatively; we may thus be assured that ensuing dynamics found are not adversely affected (or distorted) by the interface. In addition, our long observed lifetimes indicate that bulk nonradiative recombination in our samples may be neglected, as well.

A typical low-temperature (1.8-K) PL spectrum of a 0.3-μm-thick GaAs-layer double heterostructure is shown in Fig. 1. All samples, regardless of GaAs thickness, show the same general features — luminescence dominated by free-excitons peaking near 1.51515 eV (8180.8 Å),[30 – 33] with much weaker emission peaking near 1.490 and 1.492 eV attributable to donor-acceptor pair (DAP) and band-to-carbon acceptor (BA_C) recombination. The unusually high sample quality is confirmed by this rare dominance of free-excitonic emission, in preference to the usually intense shallow-impurity-bound excitons found in even the purist epitaxial GaAs;[36 – 39] indeed, in our samples, such "intrinsic" excitonic PL associated with both residual donors and acceptors is found only weakly in the PL spectra, just below the free-exciton (Fig. 1). The broader PL feature located between these edge-excitons and the band-to-acceptor was first identified by Yuan et al.,[8] and termed the "H-band." It is important to recognize that this emission lies energetically between all the known shallow band-edge-excitons[40] and the shallowest band-to-acceptor luminescence (from carbon).[41] Thus, one may conclude the H-band may not be attributed to the recombination of carriers at impurities solely within the GaAs layer itself.

Also shown in Fig. 1 is the PL excitation (PLE) spectra, detected at the peak of the H-band emission. Clearly, the dominant PLE peak exactly coincides with the free-exciton PL. This is indicative of the importance of free-excitons to a full-understanding of H-band kinetics (i.e. formation). Also evident in the PLE spectra is the band-to-band absorption which subsequently leads to H-band emission. This same feature is evident in the free-exciton PLE (detector set at free-exciton emission energy 8180.8 Å). Thus, the band-to-band absorption may lead to H-band

emission through the intermediate formation of free-excitons.

Figure 2 shows 1.8-K PL spectra for a representative set of such samples, with varying GaAs-layer thicknesses. All spectra show the same general features, namely, free-exciton PL, edge-bound exciton PL, and relatively strong H-band PL; these spectral features are reproducible in all samples. Thus, the high-quality of these structures — as evidenced by the rare, distinct free exciton emission — is consistently uniform. Moreover, we find free exciton emission to be absent upon chemical removal of the top $Al_{0.3}Ga_{0.7}As$ layer[30-32] (giving rise to the well-known "double-humped" structure,[42] with a dip at the free excitonic resonance (1.51515 eV) which is generally associated with exciton-polariton[43] and "dead-layer" effects[44-46]), a result most probably linked to the high-interfacial quality experienced by both the free excitons and the H-band excitations.

We find in all of our heterostructure samples that H-band intensity also decreases dramatically with increasing temperature, as illustrated in Fig. 3. As an example, H-band PL is, in fact, fully quenched and undetectable from the background at just $\gtrsim$ 14 K. The impurity-induced transitions, i.e. (DAP),(BA_C), (D^0,X), etc., are, however, still present in the spectra above 14 K, and do not decrease in intensity with increasing temperature nearly as drastically as the H-band. As further documentation of this rapid quenching, Fig. 4 shows the spectrally-integrated H-band intensity versus temperature. Thus, by plotting such data versus inverse temperature (an Arrhenius plot) an activation energy for this emission process may then be extracted (through least-squares fitting) — with the best fit to our data yielding $\sim$ 0.75 meV; similarly, all other samples yield activation energies $\lesssim$ 1 meV. This unusually small activation energy compared to shallow edge-excitons (e.g., $\sim$ 5 meV for a donor-bound-exciton[40]), together with the unique energetic H-band peak position, argue against the H-band PL process being associated with the "extrinsic" recombination of carriers trapped at residual impurities/defects either in the GaAs, or precisely at the GaAs/$Al_{0.3}Ga_{0.7}As$ heterointerfaces.

Yuan et al.[8] have shown that H-band peak position after cw excitation may also be power

dependent, moving to higher energies as the log of the excitation power density in their LPE-structures; this, we have also verified in all of our OMVPE-heterostructure samples as further proof of H-band observation and identification. This "static" H-band behavior may be understood as being due to the changes in interfacial band-bending resulting from the addition of free photo-carriers (and/or excitons), as will be shown in detail later. We also find that H-band PL is absent upon chemical removal of the top $Al_{0.3}Ga_{0.7}As$ layer,[22 – 26] as in Fig. 2, thus again showing qualitative verification of H-band identity, parallel to those of Yuan et al..[8] Having thus confirmed H-band activity in all of our heterostructures, we proceeded to the previously sparsely studied,[19 – 21,28] dynamical time-evolution characteristic of the H-band recombination process.[22 – 26]

Because the H-band peak-energy critically depends upon a variety of experimental conditions, and because very little may be inferred from cw PL about such possible dynamics of the H-band, detailed time-resolved PL measurements were performed, aimed at understanding the emission kinetics.[22 – 26] Figure 5 shows such time-resolved PL of a 0.2-μm structure, with each successive spectrum having been taken at 150-ns intervals. These data immediately demonstrate the H-band is not stationary in time, but, in fact, moves toward decreasing emission energies, as time goes by — with total (cumulative) shift being $\gtrsim$ 25 meV.

Such H-band time-evolution may be further quantified by measuring the detailed intensity versus time (time-decay) at discrete energies throughout the emission spectrum. Hence, Figs. 6(a) and 6(b) show such decay kinetics at various emission energies for 2.0- and 0.2-μm samples, respectively — with all decays being highly-nonexponential, [22 – 26] but readily fit to a "bimolecular" decay of the form[30 – 35]

$$I(t) = \frac{Ae^{-t/\tau}}{1 + C[1 - e^{-t/\tau}]} . \qquad (1)$$

Such an implied PL intensity time-dependence results from solution of the differential

equation[30 – 35]

$$\frac{dp(t)}{dt} = -\alpha p^2. \tag{2}$$

where

$$\alpha p_0 = \frac{1}{\tau}. \tag{3}$$

Implicit in these equations are the conditions n = p, where n (p) is the total electron (hole) densities (photo-injected, plus built-in) and n_0 (p_0) is the built-in electron (hole) density. Least-squares fits to the data, using Eq.(1), lead to well-defined and eminently comparable decay lifetimes (representative of the asymptotic exponential decay); these long, nonexponential decays (with systematic trends versus emission energy) are typical of all of our heterostructure samples.

By measuring our derived lifetime (τ) versus emission energy and versus GaAs thickness, the direct influence of this "active" GaAs-layer on H-band dynamics may be straight-forwardly deduced. (Such lifetimes were only measured at energies either well-above the band-to-acceptor luminescence or well-below the edge-excitonic luminescence, so as to minimize the influence of two spectrally overlapping processes in the decays.) Figure 7 shows these lifetimes, as deduced from nonlinear-least-squares fits to Eq. (1) versus emission energy, for all double heterostructures studied. (Note the thinnest structure - 300 Å - shows the effects of quantum confinement and the concomitant blue-shift in emission energy.) Quite generally, we find lifetimes increase exponentially with decreasing emission energy,[22 – 26] with results for thicker structures (e.g., 0.5 μm, 1.0 μm, and 2.0 μm) being virtually identical at all emission energies, and with lifetimes ranging from several ns to more than 50 μs. As the GaAs-layer thickness decreases below ~ 0.5 μm, however, significant, systematic differences rapidly become evident, appearing only on the low-energy-side of each H-emission band. We thus find the significant result that H-band lifetimes appear to saturate at different values for different GaAs thicknesses, with the onset of

saturation occurring at higher energies for thinner GaAs layers.[22 – 26] The fact that different structures (with similar purities and virtually identical interfaces — as determined by the interface recombination velocity) have differing emission dynamics further supports the notion that H-band emission may indeed be of "intrinsic" origin and, hence, not impurity-induced. Further, we find experimentally that structurally identical, but electronically and optically "inferior" samples, with larger interfacial recombination velocities, yield drastically shorter, nonexponential H-band kinetics and corresponding lifetimes while showing virtually identical H-band PL, Fig. 8; hence, their behavior versus time may not be trusted to be truly indicative of an "intrinsic" decay process, but instead would presumably reflect the irrelevant (and unwanted) dynamics of the unidentified competing "extrinsic" nonradiative recombination associated with an electronically (and possibly atomically) inferior interface.

4. THEORETICAL-MODEL RESULTS.

The electronic structure of heterojunctions has been the subject of much attention since the early 1960's.[47 – 52] Much work focussed on electrostatic bending of the conduction and valence bands at the heterointerfaces, which results from differences in properties of the two materials composing the heterojunction — including electron affinities, dielectric constants, band gaps, doping type, and doping densities. It has generally been recognized that this band-bending may confine carriers next to the interface in the notch formed by such band-bending.[53] The specie of such carriers which may become quantum-mechanically confined (electron or hole) depends on the type of heterojunction (i.e., n-n or p-n, respectively), while the confined carrier is two-dimensional (2D), and is restricted in movement to directions parallel to the interface. Much work has been done on the 2-dimensional electron gas (2DEG) which may form in these electrostatic potential notches,[53] especially in relation to high-mobility or HEMT structures.

Yuan et al.[8] have postulated that the H-band emission, in their n-n double heterostructures arises from the recombination of a 2D confined-electron with a 3D free-hole. Such recombi-

nation might then occur by tunneling in the tails of the high-field regions of the GaAs layers; disturbingly, however, such mechanisms can not explain all experimental II-band observations (i.e., temperature dependence, etc.). Alternatively, emission from such states might also be interpreted as the recombination of a quasi-2D exciton; and indeed Balslev[54] adopted such a view as a means of including a possible existing electron-hole Coulomb interaction (within the scheme proposed by Yuan et al.[8]). In this picture, the photo-excited free carriers and highly-mobile 3D-excitons, which form in < 1 ns,[55] must diffuse (or be field-driven) to the GaAs high-field interfacial regions; the exciton energy then decreases, due to the quadratic Stark shift[56] and the field-induced polarization of the exciton perpendicular to the interface. Thus, the photoexcited excitons might become "attracted" for a variety of reasons to the heterointerface, and steadily evolve into quasi-2D excitons — with the II-band emission then being the result of radiative recombination of these 2D, intrinsically bound excitons. Hence, this II-band PL may be thought of as resulting from an intrinsic Quantum Confined Stark Effect,[57 – 59] wherein the field results from the heterojunction, and the quantum confinement is due to the sharp electrostatic potential profile at the heterointerfaces.[53]

Such regions adjoining the heterointerfaces are the high-field regions of the heterostructure, with a peak field sufficiently great to possibly ionize any free-excitons which might gravitate toward those interfaces. It, therefore, might be questioned whether these quasi-2D excitons may be allowed to exist, as the field required to ionize bulk free excitons in GaAs is only 4.5 kV/cm.[59] (It will be shown below that these quasi-2D excitons may, indeed, exist in these structures, albeit in the high-field tail.) In connection with this, Köhler et al.[59] have found that 2D-excitons in quantum-wells may survive in electrostatic fields of up to 100 kV/cm, largely as a result of the quantum-confinement accompanying the reduction in dimensionality from 3D to 2D.

Thus, here, the first step in modeling II-band emission along these lines is to determine the electronic bands of the entire structure. Figure 9 shows such a self-consistent solution of

Poisson's equation, obtained numerically, for the 0.5-μm structure. (Our structures form p-n heterojunctions; therefore, the discussion throughout the rest of this paper will be restricted to this case, unless otherwise explicitly noted.) In modeling this band structure, and — hence, the H-band emission — it is thus imperative to include both heterointerfaces, thus causing the GaAs-layer thickness to become an important, if not critical parameter.[22-26]

Laser photoexcitation, generic to all of these PL H-band experiments, generates additional free carriers which may alter the resultant band structure. In this context, photoexcited holes will diffuse and drift to the high-field region near the interface, thereby altering (self-consistently) the electrostatic fields determining the entire heterostructure band structure. Since these photoexcited carriers must decay both radiatively and perhaps nonradiatively, the total carrier density — and hence, the band structure — must change drastically with time, especially near the heterointerface. In view of this, any realistic physical model must consist of self-consistent, time-dependent, simultaneous solutions of: (1) Poisson's equation, (2) the Boltzmann equation, governing carrier transport and decay, (3) Schrödinger's equation, and (4) the electron-hole Coulomb interaction. Such a complete model is indeed most complex and thus beyond the scope of this work. Nonetheless, we find a more calculationally simplistic (but still realistic) physical model may be adopted, and readily solved, in which we "parameterize" the time evolution (dynamics) of the entire heterostructure, while neglecting the details of the actual carrier transport. In this spirit, the band structure of Fig. 9 was approximated by fitting it to an expression of the form

$$\phi_v(z) = F_i d_i^{eq} a_n e^{-\left(\frac{|z|}{d_i a_n}\right)} \tag{4}$$

and

$$\phi_c(z) = \phi_v(z) + E_g, \tag{5}$$

where i = 1,2 correspond to the GaAs and $Al_{0.3}Ga_{0.7}As$ layers, respectively. Here also, F_i re-

presents the maximum field at the heterointerface in each layer, d_i^{eq} becomes a characteristic "screening length" parameter, as measured in units of the simpler, 3D-exciton Bohr radius (a_B), and z is the growth direction.

This admittedly non-(explicitly) time-dependent approach provides a physical and realistic starting point for numerical calculation, and essentially corresponds to the case of no photoexcitation, or the long-time limit ($t \rightarrow \infty$). In the opposite extreme (i.e., creation of a large number of electron-hole pairs in the GaAs layer), these additional carriers are available to screen the heterointerface electrostatic field, thereby reducing the heterointerface band-bending; thus, as $t \rightarrow 0$, the conduction and valence bands of the GaAs layer should approach a "flat-banded" condition. Such dynamics (and their intermediate cases) may thus be modeled by parameterizing d_1, the screening length, in the GaAs layer as a virtual (relative) time parameter following pulsed photoexcitation. Since the actual photoexcitation was performed energetically below the $Al_{0.3}Ga_{0.7}As$ band-gap (thereby, only generating additional carriers in the GaAs layer), as a first approximation, its band structure may be considered constant. Thus, as $d_1 \rightarrow 0$ corresponds to short-times after the "delta-function" photo-excitation pulse, so to, $d_1 \rightarrow d_1^{eq}$ time-simulates the decay of the photoexcited carriers in the long-time limit.

The envelope function for the quasi-2D exciton (subject to the potentials of Eqs. (4) and (5)) may then be determined by numerically solving Schrödinger's equation, with the appropriate Hamiltonian. Assuming that the total solution may be factored into separable electron and hole solutions, the total Hamiltonian thus becomes[54]

$$\mathcal{H} = \mathcal{H}_e + \mathcal{H}_h, \tag{6}$$

where the corresponding wavefunction must be a product of electron and hole envelope wavefunctions

$$\Psi = \sqrt{\frac{2}{\pi}}\, a_\perp^{-1} \Phi_e(z_e)\Phi_h(z_h) e^{-\left(\frac{|\vec{r}_\perp|}{a_\perp} + i\vec{K}_\perp \cdot \vec{R}_\perp\right)}, \tag{7}$$

where $\vec{r}_\perp$ and $\vec{R}_\perp$ are the relative and center-of-mass exciton coordinates, respectively, projected onto the x-y plane (plane of the interface). Correspondingly, $\vec{K}_\perp$ is the wavevector of the resultant quasi-2D exciton, $a_\perp$ is its Bohr radius, and Φ_e and Φ_h, are the separate electron and hole envelope wavefunctions (assumed normalized). The wavefunction of the confined particle, the hole, may then be readily found from

$$\mathscr{H}_h\Phi_h(z_h) = E_h\Phi_h(z_h). \tag{8}$$

where

$$\mathscr{H}_h = -\frac{\hbar^2}{2m_h}\frac{\partial^2}{\partial z_h^2} - \phi_v(z_h), \tag{9}$$

and Eqs. (8) and (9) may be straight-forwardly solved numerically for $\Phi_h(z_h)$ and E_h. In this view, the "mean position" for the hole along the direction perpendicular to the heterointerface may then be defined as

$$\bar{z}_h = \int z[\Phi_h(z)]^2 dz. \tag{10}$$

The corresponding quantum-mechanical solution for the "free" particle, the electron, is correspondingly found from

$$\mathscr{H}_e\Phi_e(z_e) = E_e\Phi_e(z_e) \tag{11}$$

and

$$\mathscr{H}_e = -\frac{\hbar^2}{2m_e}\frac{\partial^2}{\partial z_e^2} - V_{eff}(z_e), \tag{12}$$

where

$$V_{eff}(z_e) = -\phi_c(z_e) - \frac{e^2}{4\pi\varepsilon_0}\frac{2}{\pi a_\perp^2}\int_0^\infty \frac{e^{\left(-2\frac{r_\perp}{a_\perp}\right)}2\pi r_\perp dr_\perp}{[r_\perp^2 + (z_e - \bar{z}_h)^2]^{1/2}}, \tag{13}$$

accounts for the static, Coulomb interaction between electrons and holes. Direct influences of the sharply changing (and time-dependent) electric fields at the heterointerfaces are thus included in the calculation solely through the "band-bending" described by $\phi_c(z_e)$ and $\phi_v(z_h)$. (In contrast to the p-n-p structures studied in our experiments, corresponding n-n-n or n-p-n structures, may be solved by reversing the role of electrons and holes in the above model.)

For both particles, the ground-state envelope wavefunctions are the final bound-state solutions sought, and $a_\perp$ may then be systematically varied to minimize the total energy; and because these are one-dimensional attractive potentials, there must therefore be at least one bound-state for both the electron and hole. By comparing these resultant bound-state energies with kT, we may then subsequently determine whether or not excitons may form. Since all of our time-decay measurements were performed at 1.8 K, where kT ~ 0.15 meV, we may assume the electron and hole excited-states may therefore be safely neglected. (In this context, we find that the energy spacing of the first excited-state of the hole confined in the heterointerface potential notch is ~ 3 meV for $d_1 \rightarrow d_1^{eq}$, and the corresponding spacing for the electron is ~ 0.6 meV.) Perhaps significantly (or fortuitously) our experiments show no evidence of such excited states in the PL spectra; indeed, for the calculation, these additional states only become important for $d_1 \rightarrow 0$ and/or for samples with wide GaAs layers. We have also made the simplification that the Coulomb-potential-energy between electrons and holes, which is responsible for binding them together to form the quasi-2D exciton, is much smaller than the hole confinement energy in the heterointerface notch — this then limits the validity of our model to the parameter space of $d_1 \gtrsim 1$.

Figures 10(a) and 10(b) show our calculated results for screening lengths, d_1, from 0.5 to 12 and 0.5 to 9, respectively. Figure 10(a), with $d_1 = d_1^{eq} \simeq 12$, corresponds to the case of no photoexcitation — or equivalently $t \rightarrow \infty$ — in which the conduction and valence band potentials were taken from the self-consistent solutions of Poisson's equation in Fig. 9. The time-dependent H-band dynamics are, therefore, modeled here by parameterizing d_1 such that <u>increasing</u>

time after pulsed excitation corresponds to increasing d_1. In this connection, there are several important points to note in the figures: (1) For small d_1 (short-times) the band-bending is indeed quite small, and the photoexcited electrons and holes appear uniformly distributed throughout the GaAs layer; this situation corresponds to "bulk" excitation, with accompanying fast diffusion of carriers throughout the GaAs layer yielding an effectively (instantaneous) homogeneous carrier distribution. (2) As d_1 increases (increasing time) the band-bending at the heterointerfaces increases, thus forming heterointerfacial potential notches which rapidly confine the mobile holes. (3) The additional Coulomb interaction between electrons and holes causes the distribution of electrons to follow that of the holes — thereby, early-on moving the photoexcited electrons also toward the heterointerfaces. (4) As d_1 increases further, the conduction band-bending, resulting from the high-field at the heterointerface, next forces the electrons back toward the center of the GaAs layers — and away from the holes, which become increasingly quantum-confined near the heterointerface. (5) Finally, the electrons and holes reach their maximum separation, corresponding to one-half of the total GaAs-layer thickness, a long-time result occurring for $d_1 < d_1^{eq}$. The relatively striking differences between results in Figs. 10(a) and 10(b) should be especially noted here, namely that the carriers appear to reach their maximum separation both for smaller values of d_1 and for thinner GaAs layers. These analytical results therefore display at least the "qualitative" time-evolutional dependences of H-band dynamics abundantly clear in our experiment versus GaAs thickness. For more realistic comparison, Figs. 11(a) and 11(b) show the same calculated electron and hole envelope-wavefunctions as in Figs. 10(a) and 10(b), but with the electron and hole envelope-wavefunctions properly scaled to reflect proper charge conservation.

Importantly for direct comparison with data, the H-band-emission transition energy and quasi-2D exciton binding energy may also be readily calculated from the approach in Figs. 10, with results shown in Fig. 12 (the transition energy is measured from the optical band-gap, at the measurement temperature). Here, the transition energy is equal to the total valence band

band-bending minus the sum of electron and hole confinement energies, E_e and E_h in Figs. 10(a) and 10(b), respectively. E_B is calculated from solutions for the ground-state energy with and without the Coulomb potential in Eq. 13. Our model calculation thus predicts the H-emission energy to decrease linearly with increasing d_i (or "simulated" time). It also predicts that the maximum PL-energy shift for the 5000-Å structure will be ~ 25 meV, and for the 2000-Å structure about 20 meV. Further, we find the quasi-2D exciton binding energy, E_B^{2D}, to continuously vary with d_i (or time), and to always be less than the experimental 3D-exciton binding energy, $E_B^{3D} = 4.2$ meV,[42,56] approached for large d_i. For small d_i, however, E_B^{2D} approaches E_B^{3D}; as it should, but as d_i increases, E_B^{2D} decreases asymptotically to ~ 0.45 meV. Results for the 2000-Å-layer thickness are similar, although here E_B^{2D} saturates near 1.0 meV, instead.

With the envelope wavefunctions for both electrons and holes properly deduced, the relative II-band transition lifetime may then be readily calculated. Since the oscillator strength of the transition, f, is directly related to this spatial electron-hole wavefunction overlap (which composes the exciton, Eq. 7) — thus, implicitly including exciton effects — as

$$f \sim |\langle \Psi_h | \Psi_e \rangle|^2 \, f_0, \tag{14}$$

and the lifetime of the transition is related to the oscillator strength as

$$\tau^{-1} \sim f, \tag{15}$$

then the relative change in oscillator strength, and hence lifetime, may be straight-forwardly deduced. (Here, f_0 represents the transition oscillator strength when the envelope wavefunctions of the carriers are perfectly overlapped as bulk, 3D-exciton.) Figure 13 shows the calculated results for the 2000-Å structure, compared directly against the corresponding experimental results of Fig. 7, with agreement being quite good. Theoretical bandstructure for 4 different transition energies (taken from Figures 10 and 11) are also shown in relation to the relative oscillator strength calculated. Thus, our simple (time-simulated) physical model appears to accurately and quantitatively predict, the saturation-behavior found experimentally in our thin

structures; correspondingly, calculation for a thicker structure does not result in saturation (Fig. 14), again in agreement with our experiments. The discrepancy found between the measured lifetimes and the calculated oscillator strengths for the 5000-Å structure of Fig. 14 is undoubtedly a result of a variety of simplifying factors in our model, especially neglection of both electron and hole excited-states.

An important result also coming directly from our calculation shows our observed lifetime-saturation, occurring at higher energies for thinner structures, must arise from the finite size of the GaAs layer — or, equivalently, to the effects of the "companion" heterointerface. Thus, the quantum-confined electrons and holes reach their maximum separation, equal to half of the GaAs-layer thickness, at progressively smaller values of d_l — thus, higher energies — as the GaAs-layer thickness decreases. This result is therefore equivalent to the 2D-excitons being effectively "shared" by both heterointerfaces, hence causing the spatial wavefunction overlap to become approximately constant, hence yielding our observed lifetime saturation.[22 – 26] Further, the calculation shows that the transition is "indirect" in real-space (recombination of quasi-2D excitons with a continuous distribution of radii), which explains our observed long, nonexponential H-band time-decays.

Yuan et al.[8] have reported the H-band has a recombination lifetime of ~ 1.3 ns. Nonetheless, their actual decay kinetics were measured at only a single emission energy (1.5079 eV, 8220 Å) — a result considerably shorter than we find (Fig. 7). Also, Zhao et al.[14] report H-band lifetimes in a GaAs/$Al_xGa_{1-x}As$ double heterostructures (with a 500-Å GaAs-layer thickness) in which observed lifetimes increase with decreasing emission energy — but again lifetimes at any given energy are significantly shorter than those reported here (by a factor of 500 at the lowest emission energies). Further, these authors[14] also reported exponential intensity decays for H-band emission, a result which is difficult to reconcile with models based on of the recombination of a quasi-2D exciton with a continuous distribution of radii, or on a 2D-carrier recombining with a free 3D-carrier. An additional significant fact to note is that, in our expe-

rience, samples of poorer interfacial quality (as determined by the interface recombination velocity)[30-33] yield shorter lifetimes than we quote in Fig. 7, as demonstrated in Fig. 8, while neither of these previous studies[8,14] included any form of interface characterization. The results of these two previous studies might, therefore, may have been adversely affected (or inadvertently dominated) by nonradiative interfacial recombination. Further, the saturation in lifetime we find and explain as being associated with a small (or finite) GaAs-layer thickness proves additionally that these earlier studies, basically confined to narrow structures, must not have been reflecting true H-band "intrinsic" dynamics.

5. DISCUSSION.

Because of the obvious complexity of the H-band dynamics reported both here, and in the literature, it is difficult to make any universal conclusions concerning the exact physical mechanism responsible for this emission, in all structures. It may, therefore, be possible that different *heterostructures may yield nearly identical emission, but as a result of entirely different physical* mechanisms. This may, in fact, be part of the observed structural dependences reported thus far: In particular, heavily doped structures, or single heterostructures, may yield H-band emission through the model originally proposed by Yuan et al.[8] (2D-carrier recombining with a free 3D-carrier), and excitonic effects, as we emphasize here, may not be present due to the electrostatic screening accompanying heavy doping. Indeed, we find that for wide structures, $E_B^{2D} \rightarrow kT$, thus thermally ionizing free excitons into free carriers. In addition, there are certain reports of slightly different H-band behavior from that originally reported by Yuan et al.[8] An example is Zhao et al.[19] who show the H-band to persist to temperatures $\gtrsim$ 30 K, in their heavily doped, single-sided heterostructures; this may be further proof of the above-noted issues. In any case, we find from our current perspective that nearly all reported results refute the H-band emission as arising from impurities or defects.

The experimental results presented here regarding the H-band, and the excellent agreement

between these data and our calculation, prove conclusively this emission in our structures to be of "intrinsic" origin and not impurity-induced. The dominance of free-excitons in both the PL and PLE spectra shows the high-purity of our samples, and is circumstantial proof of the importance of excitonic effects in any emission process at low temperatures. Taken together, all of our results can only lead to a quantum-mechanical, 2D-excitonic description for the H-band, in our samples.

Thus, in summary, we may put forth as fact the following experimental observations for our samples:[22 – 26] (1) H-band emission weakens with increasing temperature and is not detectable in any PL above 15 K, whereas the PL bands associated with both donors and acceptors, (D^0,X), (DAP), (BA_C), etc., persist to higher temperatures. (2) Time-resolved PL spectra reveal H-band emission to be spectrally dynamic. (3) Lifetimes measured at various emission energies show that the precise physical structure of the double heterostructures (in particular, the GaAs-layer thickness) drastically influences emission dynamics. (4) Extrapolation of these lifetimes to higher energies is in good agreement with the expected 1.8-K GaAs band-edge of 1.5194 eV,[42,56] and its corresponding excitonic lifetime of $\lesssim$ 1 ns.[60] As for our model calculations, the following may also be observed:[22 – 26] (1) H-band activation energies are indeed quite small ($\lesssim$ 1 meV). Transition energies extend to 25 meV below the bandgap, and are dependent on sample structure. (3) Oscillator strengths increase for decreasing emission energies, with saturation evident in thin structures. Thus, we may again emphasize that our combined experiment and theory are all entirely consistent with this emission as being intrinsic, and not impurity-induced.[22 – 26]

The temperature dependence of the H-band PL and the derived activation energy (Fig. 4) are in good agreement with the binding energy of our quasi-2D exciton, as calculated from our physical model. E_B^{2D}, as calculated from the model, and shown in Fig. 12, is a smoothly varying function of d_1 — and hence, time, with early times (or small d_1) leading to almost insignificantly small band-bending at the heterointerface. Next, with carrier decay the screening of the heter-

ointerface field is reduced and the potential notch in the valence band at the heterointerface begins to form. Holes quantum-confined in this notch then electrostatically attract electrons toward the interfaces through the Coulomb interaction, and the resulting quantum-confined exciton acquires two-dimensional character, with a binding energy approaching 4 meV — the bulk free-exciton binding energy. As time (or d_i) increases still further, the separation between carriers (as calculated from the mean position of the electrons and holes as in Eq. (10)) begins to increase, until it reaches maximum separation equal to precisely half the GaAs-layer width. Thus, as the exciton evolves from a 3D entity into a quasi-2D quantum mechanically interfacially-bound exciton, the wavefunction changes from spherical to ellipsoidal, with a concomitant increasing of the effective "radius" of the quasi-2D exciton. The binding energy, E_B^{2D}, decreases as a result of the inverse relation between the binding energy of the exciton and its "radius," as displayed in Fig. 12, and indeed saturates at $\lesssim$ 1.0 meV, resulting from the saturation in carrier separation.

An additional fact to be noted is that H-band emission occurs at energies just below the band-gap, and extends up to 25 meV[22-26] below the GaAs band-gap (1.5194 eV).[42,56] Our model predicts, to first order, the same maximum energy shift of the PL (Fig. 12), and a direct proportionality between the transition energy and the screening length, d_i. This PL transition energy is determined virtually entirely by the hole-confinement energy, and is almost insignificantly affected by the excitonic binding energy ($\lesssim$ 1.0 meV). Our calculation also predicts maximum PL energy shifts to be dependent on the GaAs-layer thickness; hence, thinner structures should have a smaller maximum energy shift. However, since the experimentally determined H-band position at the maximum energy shift lies close to the band-to-acceptor PL, such subtle differences are beyond our ability to spectroscopically resolve.

The energy at which saturation in the lifetime occurs (as discussed in relation to Fig. 7) is also predicted by our model. This energy may be deduced by finding the screening length at which the carriers reach their maximum separation, and by then recalculating the transition

energy for this screening length. As a case in point, for the double heterostructure with a 0.5-μm GaAs-layer thickness, the carriers should reach a maximum separation for $d_I \simeq 8$. The corresponding calculated transition energy is then $E_T \simeq 20$meV (1.499 eV), which is in surprisingly good agreement with the data of Fig. 7. For thicker structures the corresponding emission energies at which saturation occurs are even lower, whereas, for thinner structures the carriers reach maximum separation for smaller values of d_I, and thus higher energies. This is again confirmed in the data in Fig. 7, which clearly show that the lifetime saturation for the 0.1-μm double heterostructure occurs at a higher emission energy than for the corresponding 0.2-μm structure, just as theoretically expected.

Further, we find from calculation that without excitonic electron-hole Coulomb interaction, the relative change in lifetime which may be predicted over the H-emission band is entirely insufficient to account for our data. For example, in our p-n-p structures the electron wavefunction would, at all simulated times (all d_I), be centered in the n-type GaAs layer. The electron wavefunction therefore never becomes attracted toward the heterointerface and the holes residing there. This non-physical situation would necessarily result in exceedingly long radiative lifetimes (fully spatially indirect free carriers), a finding inconsistent with our observations.

Given our above intrinsic excitonic description of H-band processes, further details of dynamics may be elaborated and speculated upon. For example, extrapolation of measured lifetimes to higher energies (as shown in Fig. 7, and discussed above) directly signify the physical origins of the H-band, in that H-emission energies nearest the band gap (and at earliest times) result from conduction- and valence-band potentials which must be flat, due to the electrostatic screening from the large number of photoexcited carriers. Hence, following pulsed excitation, carrier evolution eventually contributing to H-emission would have to be envisioned as follows: First, electron-hole pairs photoexcited within the GaAs layers generates free carriers, which in turn may quickly condense into bulk 3D-excitons. Next, these excitons and free carriers may

diffuse and drift towards the high-field regions of the material — both heterointerfaces — where the very presence of such large numbers of excitons and free carriers would reduce the interfacial band-bending. However, as these very excitons migrate toward the interfaces, the field they experience there may become sufficient to reionize them into free carriers. Hence, large numbers of free electrons and holes drawn to the heterointerfaces further add to (or prolong) the "flat-banding." Next, these carriers would be expected to radiatively recombine, near the band-gap energy, with a lifetime determined by the high electron-hole gas density. Then, as the carrier concentrations diminish due to recombination, band-bending at the heterointerfaces becomes increasingly restored which would then serve to quantum-confine the holes in the heterointerface potential, and ultimately form the quasi-2D excitons. At this point the field at the interface, and the subsequent band-bending, may be considered sufficiently reduced that these quasi-2D excitons may appear "3D-like," but nonetheless weakly confined; this explains why our quasi-2D exciton binding energy approaches that of a 3D-exciton for small d_1. (However, for $d_1 \simeq 0$, an exciton picture breaks down and is inappropriate near the heterointerfaces.) Finally, at longest times these quasi-2D excitons would be expected to continue to recombine, all-the-while increasing (restoring) the band-bending, and with these excitons become increasingly more oriented perpendicular to the interface (polarized), and with their PL energy becoming increasingly smaller until the remaining photoexcited carriers had all decayed. (We should note here that our small calculated binding energies of these quasi-2D excitons directly includes these electric-field changes, through their influence upon the conduction and valence band potentials.) Thus, these arguments suggest that quantum confinement, together with the finite GaAs-layer thickness, would actually eventually prevent the 2D excitons bound at the interfaces from being ionized by the still relatively strong heterointerfacial fields.

As for the steadily and dramatically increasing H-band exciton lifetimes as emission energy decreases (Figs. 7, 13, and 14), this arises naturally in our picture as being due to the steadily increasing (as time goes on) field-induced charge separation, and the corresponding decrease in

electron-hole overlap. Thus, the field is intrinsic to the heterojunction region of the structure, with the band-bending resulting from this field causing a time- and energy-dependent "red-shift"; at the same time, this band-bending also serves to partially confine the exciton, thus imparting to it 2D-character. We might thus refer to the mechanism responsible for H-band as an intrinsic Quantum-Confined Stark Effect. [57 – 59,61] Here, unlike in traditional quantum-well experiments under applied electric-field, no externally applied field is necessary — the heterojunction instead provides it all. Similar types of behavior (PL red-shift and increasing lifetimes with increasing field) in quantum-well systems with applied fields have indeed been observed and adequately explained by such mechanisms.[59,61]

6. CONCLUSIONS.

Previous theoretical work[54] relating to the H-band has only considered the effect of a single heterointerface on a quasi-2D exciton. The complex dynamics of quasi-2D-excitonic motion, evolution, and recombination have not, therefore, been considered in detail previously. As noted above, the importance of the companion interface in double heterostructures cannot be neglected, or even underestimated, in exciton recombination kinetics. Therefore, a complete study of the dynamics of H-band PL, as unencumbered by complicating effects, can only be done in wide structures. This conclusion is in contrast to some earlier work on near-quantum-well size structures.[19 – 21] Further, the interfaces must be of demonstrably high-quality, as quantified by, for example, interface recombination velocity studies, as at least one species of carrier may reside at the interface for long periods of time — as long as tens of μs. We have made measurements of the recombination dynamics and modeled the carrier dynamics responsible for the H-band PL in ideal, high-purity structures. Our simple theoretical model shows that the Coulomb interaction between electrons and holes (forming excitons) is essential to adequately describe our observed H-band decay dynamics versus emission energy. Our combined results thus explain the detailed dynamics of excitons quantum-confined at a single GaAs/

$Al_xGa_{1-x}As$ heterointerface, and prove these dynamics may be readily understood with a simple quantum-confined, 2D-excitonic description.

Acknowledgements

We thank G.A. Northrop and L.M. Smith for valuable discussions, J. Martinsen for help in computer-data acquisition and analysis, and A.C. Warren for use of a "Poisson-solver" program (HETMOD) to provide initial, static band-bending simulations. Supported, in part, by the U.S. Office of Naval Research, under contracts N00014-85-C-0868, N00014-90-C-0077, and N00014-91-J-1697.

REFERENCES

†Present Address: University of Wisconsin, Dept. of Chemical Engineering, 1415 Johnson Drive, Madison WI 53706.

1. J. Hegarty, L. Goldner, and M.D. Sturge, Phys. Rev. B **30**, 7346 (1984).
2. L. Schultheis, A. Honold, J. Kuhl, K. Köhler, and C.W. Tu, Phys. Rev. B **34**, 9027 (1986).
3. M. Kohl, D. Heitmann, S. Tarucha, K. Leo, and K. Ploog, Phys. Rev. B **39**, 7736 (1989).
4. K. Fujiware, K. Kanamoto, and N. Tsukada, Phys. Rev. B **40**, 9698 (1989).
5. D. Bimberg, J. Christen, T. Fukunaga, H. Nakashima, D.E. Mars, and J.N. Miller, J. Vac. Sci. Technol. B **5**, 1191 (1987); S. Munnnix, R.K. Bauer, D. Bimberg, J.S. Harris, Jr., R. Köhrbrück, E.C. Larkins, Ch. Maierhofer, D.E. Mars, and J.N. Miller, J. Vac. Sci. Technol. B **7**, 704 (1989); R. Köhrbrück, S. Munnix, D. Bimberg, E.C. Larkins, and J.S. Harris, Jr., Appl. Phys. Lett. **54**, 623, (1989).
6. A. Ourmazd, D.W. Taylor, J. Cunningham, and C.W. Tu, Phys. Rev. Lett. **62**, 933, (1989).
7. K. Wada, A. Kozen, Y. Hasumi, and J. Temmyo, Appl. Phys. Lett. **54**, 436 (1989).
8. Y.R. Yuan, K. Mohammed, M.A.A. Pudensi, and J.L. Merz, Appl. Phys. Lett. **45**, 739

(1984); Y.R. Yuan, M.A.A. Pudenski, G.A. Vawter, and J.L. Merz, J. Appl. Phys. **58**, 397 (1985); Y.R. Yuan, J.L. Merz, and G.A. Vawter, J. Lumin. **40,41**, 755 (1988).

9. A.M. Vasil'ev, P.S. Kop'ev, V.P. Kochereshko, N.N. Ledentsov, B.Ya. Mel'tser, I.N. Ural'tsev, V.M. Ustinov, and D.R. Yakovlev, Sov. Phys. Semicond. **20**, 220 (1986).
10. W. Ossau, E. Bangert, and G. Weimann, Solid State Communications **64**, 711 (1987).
11. I.V. Kukushkin, K.V. Klitzing, and K. Ploog, Phys. Rev. B 37, 8509 (1988).
12. Zh.I. Alferov, A.M. Vasil'ev, P.S. Kop'ev, V.P. Kochereskho, I.N. Ural'tsev, Al.L. Efros, and D.R. Yakovlev, JETP Lett. Vol. **43**, 570 (1986).
13. L.W. Molenkamp, G.W. 'tHooft, W.A.J.A. van der Poel, and C.T. Foxon, J. de Physique Colloque **C5**, 217 (1987); G.W. 'tHooft, W.A.J.A. van der Poel, L.W. Molenkamp, and C.T. Foxon, Appl. Phys. Lett. **50**, 1388 (1987).
14. Q.W. Zhao, J.P. Bergman, P.O. Holtz, B. Monemar, C. Hallin, M. Sundaram, J.L. Merz, and A.C. Gossard, Mat. Res. Soc. Symp. Proc. Vol. 163 (1990), ed. D.J. Wolford, J. Bernholc, and E.E. Haller, p. 337.
15. E.S. Koteles and J.Y. Chi, Superlattices and Microstructures **2**, 421 (1986).
16. C.H. Yang, S.A. Lyon, and C.W. Tu, Superlattices and Microstructures **3**, 269 (1987).
17. P.S. Kop'ev, V.P. Kochereshko, I.N. Uraltsev, Al.L. Efros, and D.R. Yakovlev, J. Lumin. **40,41**, 747 (1988).
18. P.O. Kop'ev, I.N. Uraltsev, V.M. Ustinov, and A.M. Vasil'ev, Inst. Phys. Conf. Ser. **95**, 57 (1988).
19. Q.X. Zhao, J.P. Bergman, P.O. Holtz, B. Monemar, C. Hallin, M. Sundaram, J.L. Merz, and A.C. Gossard, Semicond. Sci. Technol. **5**, 884 (1990).
20. J.P. Bergman, Q.X. Zhao, P.O. Holtz, B. Monemar, M. Sundaram, J.L. Merz, and A.C. Gossard, Phys. Rev. B **43**, 4771 (1991).
21. Q.X. Zhao, Y. Fu, P.O. Holtz, B. Monemar, J.P. Bergman, K.A. Chao, M. Sundaram, J.L. Merz, and A.C. Gossard, Phys. Rev. B **43**, 5035 (1991).

22. G.D. Gilliland, D.J. Wolford, and T.F. Kuech, American Physical Society Meeting, Annaheim, CA, March 1990. Bull. Am. Phys. Soc. 35, 486 (1990).

23. G.D. Gilliland, D.J. Wolford, T.F. Kuech, and J.A. Bradley, Proc. of the 20th Int. Conf. on the Physics of Semiconductors, Thessaloniki Greece, (World Scientific, 1990) p. 1577.

24. G.D. Gilliland, D.J. Wolford, T.F. Kuech, and J.A. Bradley, Phys. Rev. B 43, 14251 (1991).

25. G.D. Gilliland, D.J. Wolford, T.F. Kuech, and J.A. Bradley, J. Vac. Sci. Technol. B 9, 2377 (1991).

26. G.D. Gilliland, D.J. Wolford, G.A. Northrop, T.F. Kuech, and J.A. Bradley, in Gallium Arsenide and Related Compounds, edited by G. Stringfellow, Inst. Phys. Conf. Ser. 120, (IOP Bristol, 1992), p. 413.

27. J.L. Bradshaw, W.J. Choyke, R.P. Devaty, and R.L. Messham, American Physical Society Meeting, Annaheim, CA, March 1990. Bull. Am. Phys. Soc. 35, 761 (1990).

28. W.M. Chen, Q.X. Zhao, M. Ahlström, and B. Monemar, Proc. 19th Int. Conf. on the Physics of Semiconductors, Ed. W. Zawadzki (Institute of Physics, Polish Academy of Sciences, Warsaw, 1988), p. 279.

29. W. Demtröder, *Laser Spectroscopy*, (Springer, New York 1982) p. 560.

30. D.J. Wolford, G.D. Gilliland, L.M. Smith, T.F. Kuech, M. Heiblum, and J. Martinsen, American Physical Society Meeting, Annaheim, CA, March 1990. Bull. Am. Phys. Soc. 35, 238 (1990); G.D. Gilliland, D.J. Wolford, T.F. Kuech, J.A. Bradley, and H.P. Hjalmarson, American Physical Society Meeting, Cincinnati, OH, March 1991. Bull. Am. Phys. Soc. 36, 649 (1991).

31. D.J. Wolford, G.D. Gilliland, T.F. Kuech, L.M. Smith, J. Martinsen, J.A. Bradley, C.F. Tsang, R. Venkatasubramanian, S.K. Ghandi, and H.P. Hjalmarson, J. Vac. Sci. Technol. B 9, 2369 (1991).

32. D.J. Wolford, G.D. Gilliland, T.F. Kuech, J. Martinsen, C.F. Tsang, J.A. Bradley, and H.P. Hjalmarson, in Gallium Arsenide and Related Compounds, edited by G. Stringfellow, (IOP

Bristol, 1992), p. 401.

33. G.D. Gilliland, D.J. Wolford, T.F. Kuech, L.M. Smith, J. Martinsen, and I.A. Bradley, unpublished.

34. L.M. Smith, D.J. Wolford, R. Venkatasubramanian, and S.K. Ghandhi, Appl. Phys. Lett. **57**, 1572 (1990).

35. R.J. Nelson and R.G. Sobers, Appl. Phys. Lett. **32**, 761 (1978); R.J. Nelson and R.G. Sobers, J. Appl. Phys. **49**, 6103 (1978).

36. G.W. 'tHooft, W.A.J.A. van der Poel, L.W. Molenkamp, and C.T. Foxon, Phys. Rev. B **35**, 8281 (1987).

37. E.S. Koteles, B.S. Elman, and S.A. Zemon, S.S. Commun. **62**, 703 (1987).

38. B.S. Elman, E.S. Koteles, S.A. Zemon, and Y.J. Chi, J. Vac. Sci. Technol. B **5**, 757 (1987).

39. M. Heiblum, E.E. Mendez, and L. Osterling, J. Appl. Phys. **54**, 6982 (1983).

40. E.H. Bogardus and H.B. Bebb, Phys. Rev. **176**, 993 (1961); A.M. White, P.J. Dean, L.L. Taylor, R.C. Clarke, D.J. Ashen, and J.B. Mullin, J. Phys. **C5**, 1727 (1972); H. Venghaus, J. Lumin. **16**, 331 (1978).

41. D.J. Ashen, P.J. Dean, D.T.J. Hurle, J.B. Mullin, A.M. White, and P.D. Greene, J. Phys. Chem. Solids **36**, 1041 (1975).

42. D.D. Sell, S.E. Stokowski, R. Dingle, and J.V. DiLorenzo, Phys. Rev. B **7**, 4568 (1973).

43. R.G. Ulbricht and C. Weisbuch, Phys. Rev. Lett. **38**, 865 (1977).

44. P.Y. Yu, *Topics of Current Physics — Excitons*, (Springer-Verlag, New York 1979). **14**, 211 (1979).

45. E.S. Koteles, J. Lee, J.P. Salerno, and M.O. Vassell, Phys. Rev. Lett. **55**, 867 (1985); T. Steiner, M.L.W. Thewalt, E.S. Koteles, and J.P. Salerno, Phys. Rev. B **34**, 1006 (1986).

46. E.I. Rashba and M.D. Sturge, *Excitons*, (North-Holland, Amsterdam, 1982).

47. D.T. Cheung, S.Y. Chiang, and G.L. Pearson, Solid State Electronics **18**, 263 (1975).

48. H.J.A. Bluyssen, L.J. Van Ruyven, and F. Williams, Solid State Electronics **22**, 573 (1979).

49. R.L. Anderson, Solid State Electronics 5, 341 (1962).

50. W.G. Oldham and A.G. Milnes, Solid State Electronics 6, 121 (1963).

51. G.A. Baraff and J.A. Appelbaum, Phys. Rev. B 5, 4891 (1972).

52. F. Stern, Phys. Rev. B 5, 4891 (1972).

53. T. Ando, A.B. Fowler, and F. Stern, Reviews of Modern Physics 54 (1982).

54. I. Balslev, Semicond. Sci. Technol. 2, 437 (1987); I. Balslev, in *Excitons in Confined Systems*, Proc. of International Meeting on Excitons in Confined Systems, Rome, Italy, edited by R. Del Sole, A.D'Andrea, and A. Lapiccirella, (Springer-Verlag, New York 1987) p. 87.

55. T.C. Damen, J. Shah, D.Y. Oberli, D.S. Chemla, J.E. Cunningham, and J.M. Kuo, Proc. of SPIE Conference on Advances in Semiconductors and Superconductors: Physics Toward Device Applications, San Diego, CA, March 17-21, 1990.

56. D.C. Reynolds and T.C. Collins, *Excitons Their Properties and Uses*, (Academic Press, New York 1981).

57. D.A.B. Miller, D.S. Chemla, T.C. Damen, A.C. Gossard, W.Wiegmann, T.H. Wood, and C.A. Burrus, Phys. Rev. Lett. 53, 217 (1984).

58. H.J. Polland, L. Schultheis, J. Kuhl, E.O. Göbel, and C.W. Tu, Phys. Rev. Lett. 55, 2610 (1985).

59. K. Köhler, H.J. Polland, L. Schultheis, and C.W. Tu, Phys. Rev. B 38, 5496 (1988).

60. D.J. Wolford, G.D. Gilliland, T.F. Kuech, J.A. Bradley, and H.P. Hjalmarson, Bull. Am. Phys. Soc. 36, 648 (1991).

61. S. Charbonneau, M.L.W. Thewalt, E.S. Koteles, and B. Elman, Phys. Rev. B 38, 6287 (1988).

FIGURE CAPTIONS

Fig. 1. Low-temperature (1.8 K), time-integrated PL spectra of a typical 0.3-μm thick GaAs-layer double heterostructure. Free-excitons (F,X) dominate. PL-excitation spectra at 1.8 K is also shown for detection of H-band emission at the peak of the H-band emission (dashed line).

Fig. 2. Low-temperature (1.8 K), time-integrated PL spectra for 2.0-μm, 1.0-μm, 0.3-μm, and 0.2-μm GaAs-layer thicknesses. Bottom spectra is for a 2.0-μm thick sample, with the top $Al_{0.3}Ga_{0.7}As$ layer chemically removed.

Fig. 3. Time-integrated PL spectra versus temperature. Hatched regions represent the H-band emission.

Fig. 4. Arrhenius plot of spectrally integrated H-band PL, taken from the time-integrated spectra of Fig. 2. The solid line represents the best least-squares fit to the data, with an activation energy of $\sim$ 0.75 meV.

Fig. 5. Time-resolved PL spectra of a double heterostructure with a 0.2-μm GaAs-layer thickness, taken at 1.8 K. Each successive spectra (from top to bottom) are at 220-ns time intervals following the excitation pulse (spectral resolution is $\simeq$ 2.0 Å).

Fig. 6. Photoluminescence-decay kinetics at 1.8 K, versus emission energy for (a) 2.0-μm and (b) 0.2-μm structures. Fits (solid lines) were obtained using Eq. (1).

Fig. 7. Measured time-decay lifetimes at different energies across the H-band. Data for all structures were taken under identical conditions, and the lifetimes obtained using Eq. (1), are those shown in Fig. 5.

Fig. 8. (a) 1.8 K photoluminescence spectra of two comparable 0.5-μm double heterostructures. (b) Measured time-decay lifetimes at different energies across the H-band for the same 0.5-μm double heterostructures. Surface recombination velocities, S, were determined for both samples from 300-K band-to-band recombination lifetime measurements.

Fig. 9. Results of our model, numerical calculation for the "static limit." Conduction- and valence-band potentials for the GaAs layer were obtained from self-consistent solution of Poisson's equation; carrier-envelope wavefunctions were obtained from solutions of Schrödinger's equation, as described in the text. E_T is the transition energy referenced to the band edge, and E_B is the exciton binding energy. (Note: energy scales are correct, with the energy-gap between conduction and valence bands having, for convenient illustration, been reduced.)

Fig. 10(a). Model calculation results for a structure with a 0.5-μm GaAs-layer thickness. Only the GaAs band structure is shown (solid). Dotted lines and hatched areas represent hole-envelope wavefunctions, while dashed lines and shaded areas represent electron-envelope wavefunctions. E_B is the 2D exciton binding energy, E_e and E_h are the electron and hole confinement energies, respectively, and f is the electron-hole wavefunction overlap integral. (Note: the energy scales are correct, with the energy-gap between conduction and valence bands having, for convenient illustration, been reduced).

Fig. 10(b). Model calculation results for a structure with a 0.2-μm GaAs-layer thickness. Only the GaAs band structure is shown (solid). Dotted lines and hatched areas represent hole-envelope wavefunctions, while dashed lines and shaded areas represent electron-envelope wavefunctions. E_B is the 2D exciton binding energy, E_e and E_h are the electron and hole confinement energies, respectively, and f is the electron-hole wavefunction overlap integral. (Note: the energy scales are correct, with the energy-gap between conduction and valence bands having, for convenient illustration, been reduced).

Fig. 11(a). Model calculation results from Fig. 9(a) for a structure with a 0.5-μm GaAs-layer thickness, with wavefunctions scaled to show "charge conservation." Only the GaAs band structure is shown (solid). Dotted lines and hatched areas represent hole-envelope wavefunctions, while dashed lines and shaded areas represent electron-envelope wavefunctions. (Note: the energy scales are correct, with the energy-gap between conduction

and valence bands having, for convenient illustration, been reduced).

Fig. 11(b). Model calculation results from Fig. 9(b) for a structure with a 0.2-μm GaAs-layer thickness, with wavefunctions scaled to show "charge conservation." Only the GaAs band structure is shown (solid). Dotted lines and hatched areas represent hole-envelope wavefunctions, while dashed lines and shaded areas represent electron-envelope wavefunctions. (Note: the energy scales are correct, with the energy-gap between conduction and valence bands having, for convenient illustration, been reduced).

Fig. 12. PL transition energy (E_T) and binding energy of the quasi-2D exciton (E_B) as obtained from model calculation, with transition energies being referenced to the optical band-gap (1.5194 eV). (a) Results for 0.5-μm structure, and (b) results for 0.2-μm structure.

Fig. 13. Comparison of results between model calculation and experimental results for a double heterostructure with a 0.2-μm GaAs-layer thickness. Solid symbols represent the model calculation, while open symbols represent experiment. Theoretical bandstructure for several transition energies are shown in surrounding figures.

Fig. 14. Comparison of model calculation results for the 0.5-μm and 0.2-μm structures, with inverse oscillator strength of the optical transition being proportional to the square of the envelope overlap integrals.

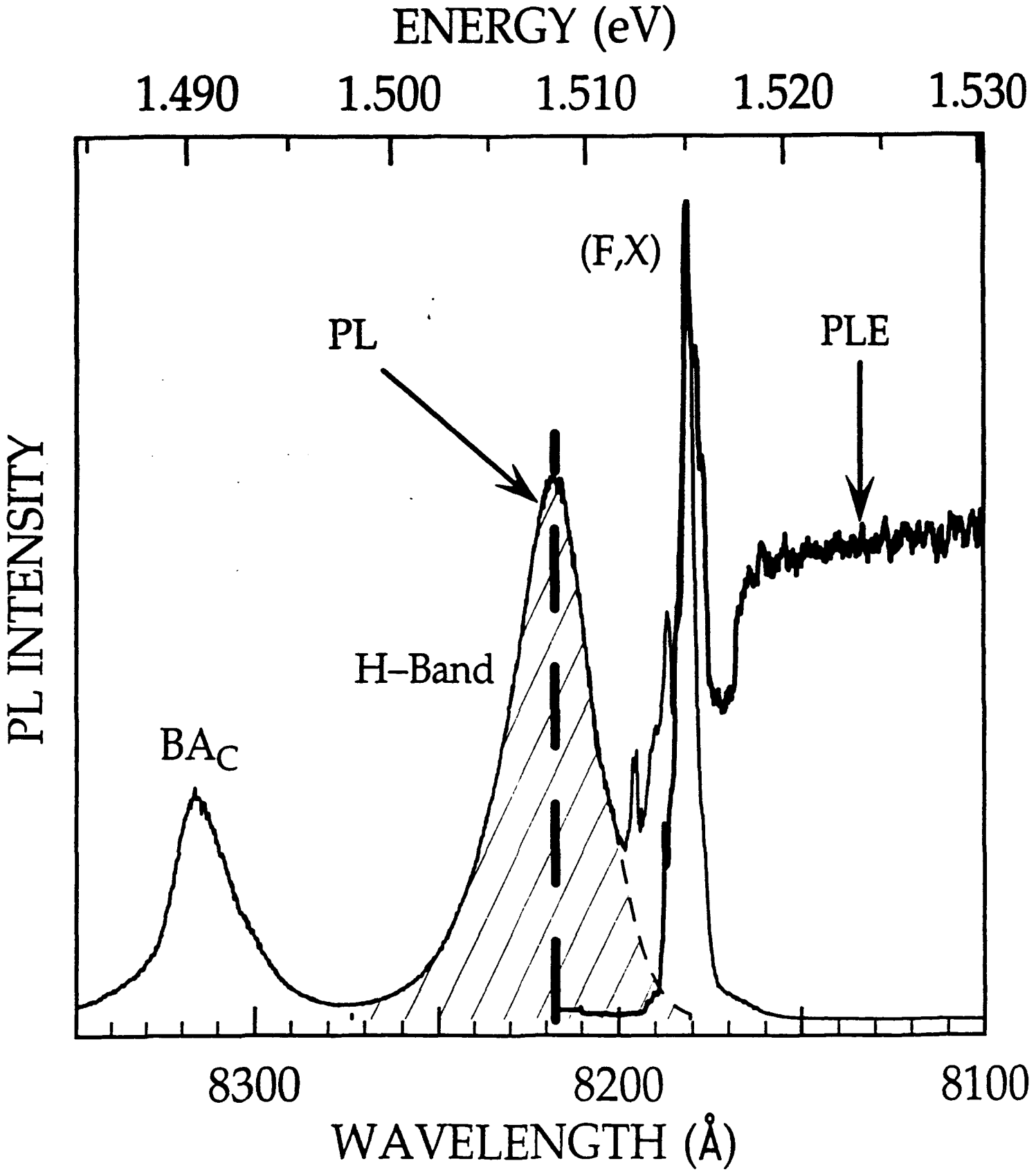
ENERGY (eV)
1.490
1.500
1.510
1.520
1.530
(F,X)
PL
PLE
H–Band
BA_C
PL INTENSITY
8300
8200
8100
WAVELENGTH (Å)

FIG 1

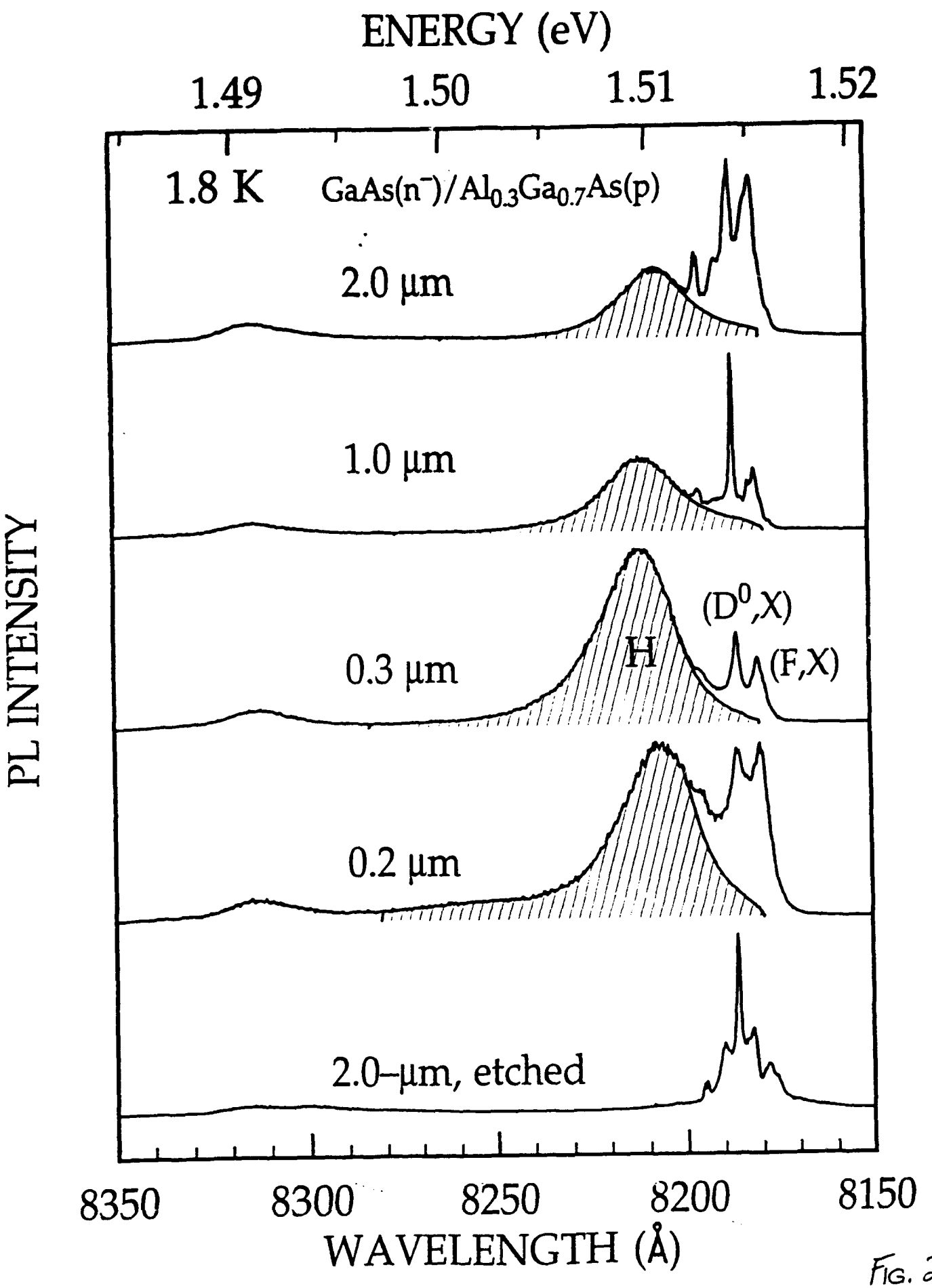
ENERGY (eV)
1.49
1.50
1.51
1.52
1.8 K
GaAs(n⁻)/Al0.3Ga0.7As(p)
2.0 μm
1.0 μm
0.3 μm
(D0,X)
H
(F,X)
0.2 μm
2.0–μm, etched
PL INTENSITY
8350
8300
8250
8200
8150
WAVELENGTH (Å)

FIG. 2

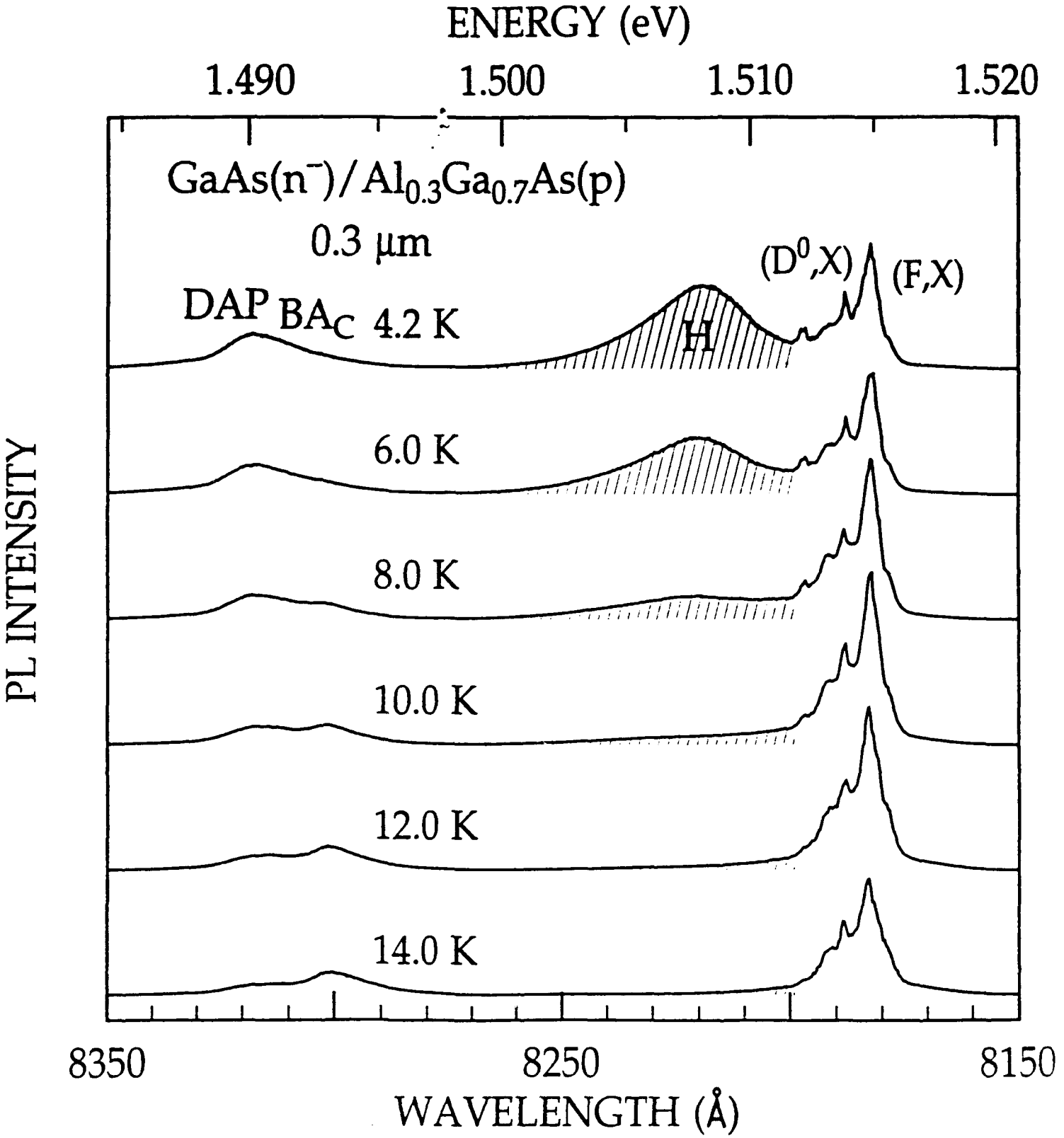
ENERGY (eV)
1.490
1.500
1.510
1.520
GaAs(n⁻)/Al0.3Ga0.7As(p)
0.3 μm
DAP
BAC
4.2 K
H
(D0,X)
(F,X)
6.0 K
8.0 K
10.0 K
12.0 K
14.0 K
PL INTENSITY
8350
8250
8150
WAVELENGTH (Å)

FIG. 3

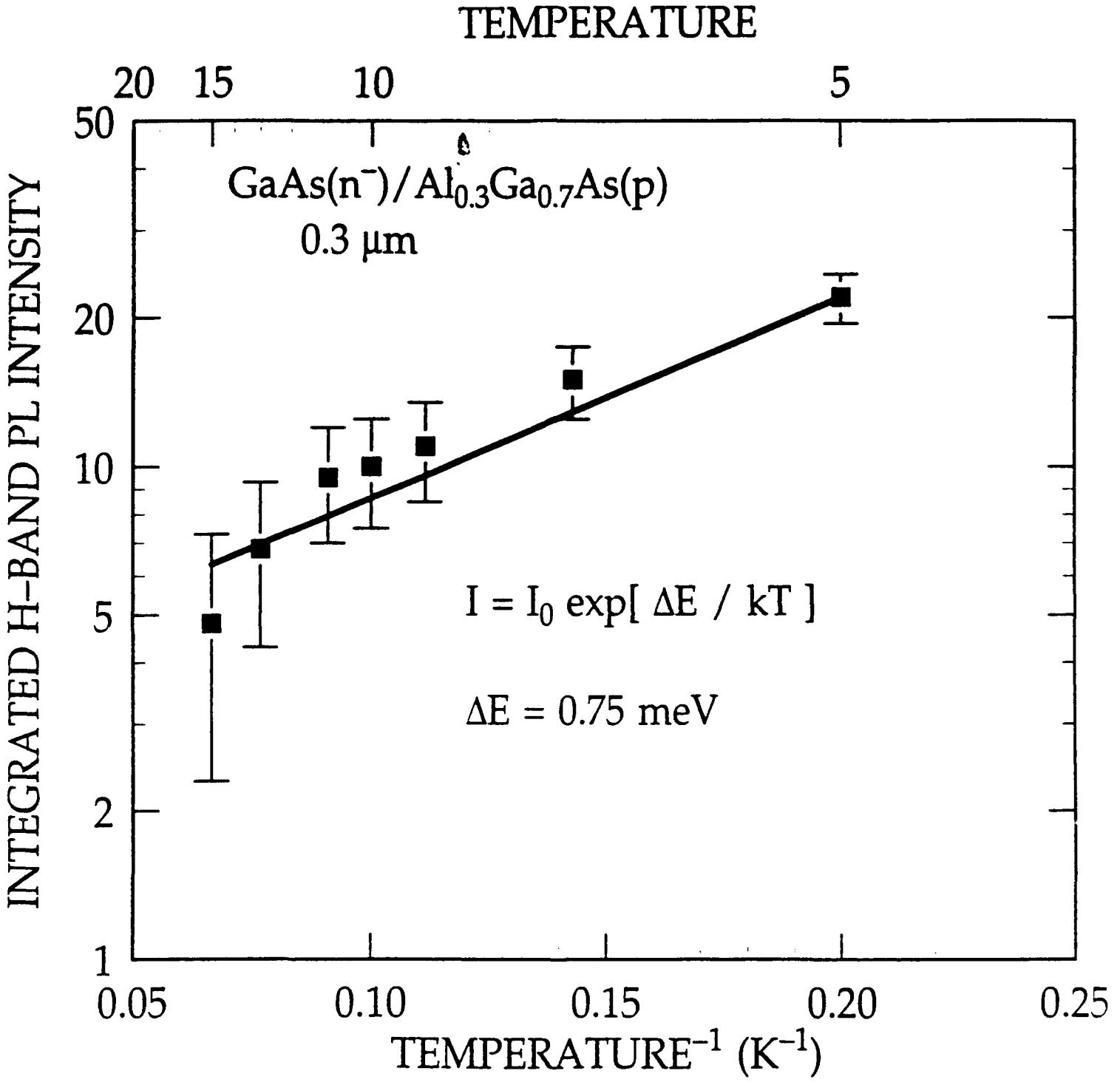
TEMPERATURE
20
15
10
5
50
20
10
5
2
1
GaAs(n⁻)/Al0.3Ga0.7As(p)
0.3 μm
I = I0 exp[ΔE / kT]
ΔE = 0.75 meV
INTEGRATED H-BAND PL INTENSITY
0.05
0.10
0.15
0.20
0.25
TEMPERATURE⁻¹ (K⁻¹)

FIG. 4

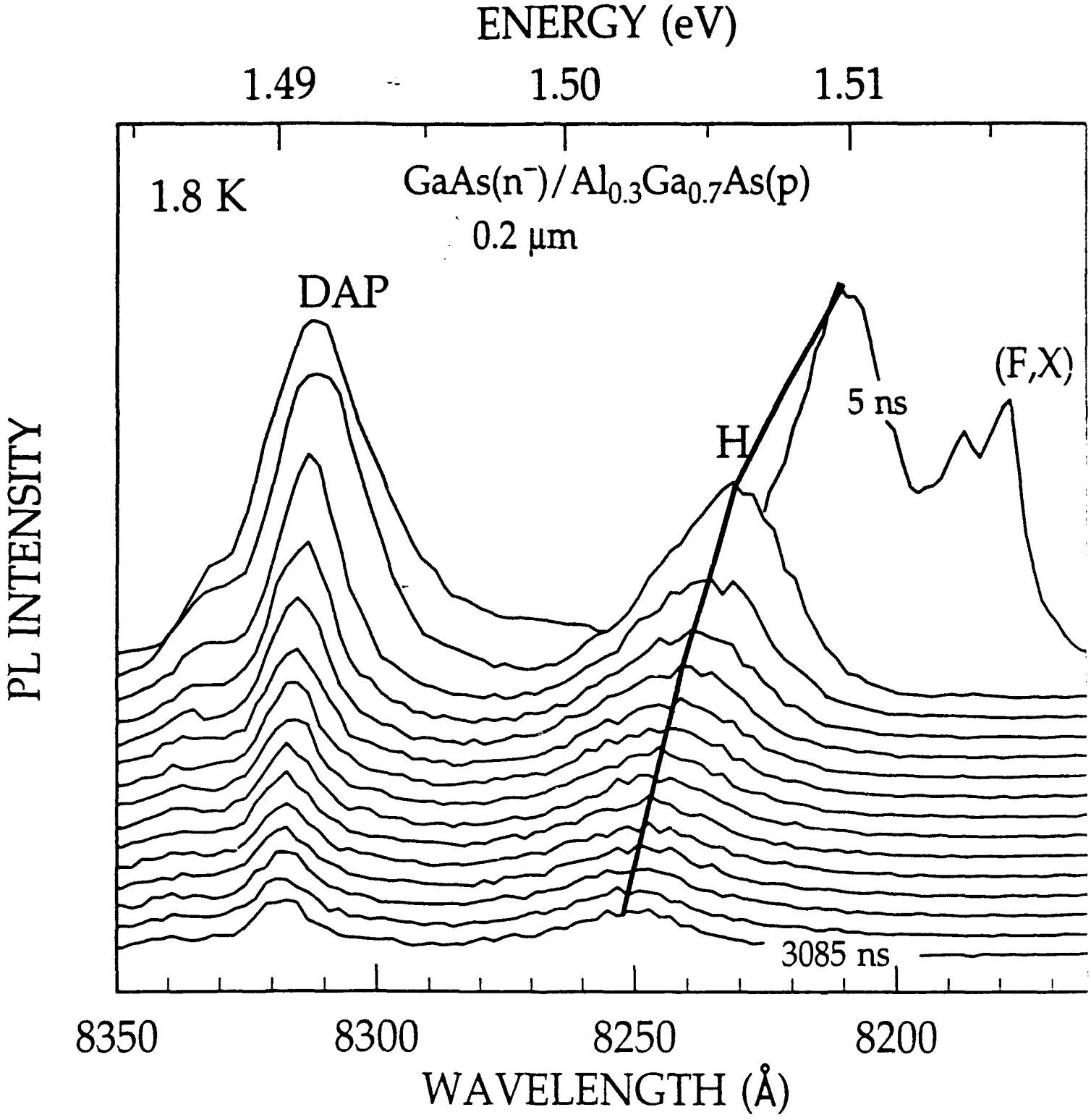
ENERGY (eV)
1.49
1.50
1.51
1.8 K
GaAs(n⁻)/Al0.3Ga0.7As(p)
0.2 μm
DAP
H
5 ns
(F,X)
3085 ns
PL INTENSITY
8350
8300
8250
8200
WAVELENGTH (Å)

FIG. 5

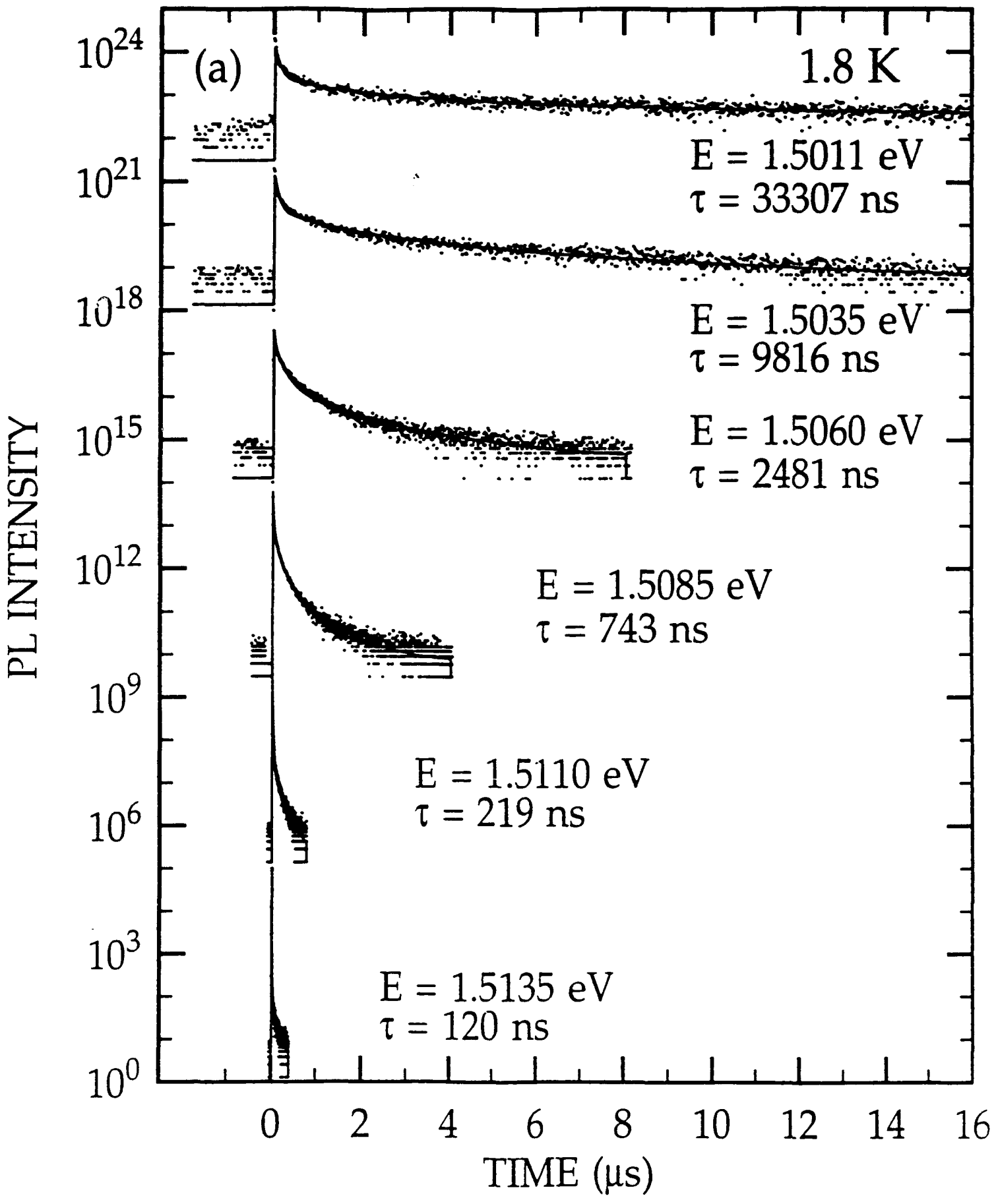
(a)
1.8 K
E = 1.5011 eV
τ = 33307 ns
E = 1.5035 eV
τ = 9816 ns
E = 1.5060 eV
τ = 2481 ns
E = 1.5085 eV
τ = 743 ns
E = 1.5110 eV
τ = 219 ns
E = 1.5135 eV
τ = 120 ns
PL INTENSITY
10^{24}
10^{21}
10^{18}
10^{15}
10^{12}
10^{9}
10^{6}
10^{3}
10^{0}
0
2
4
6
8
10
12
14
16
TIME (μs)

FIG. 6a

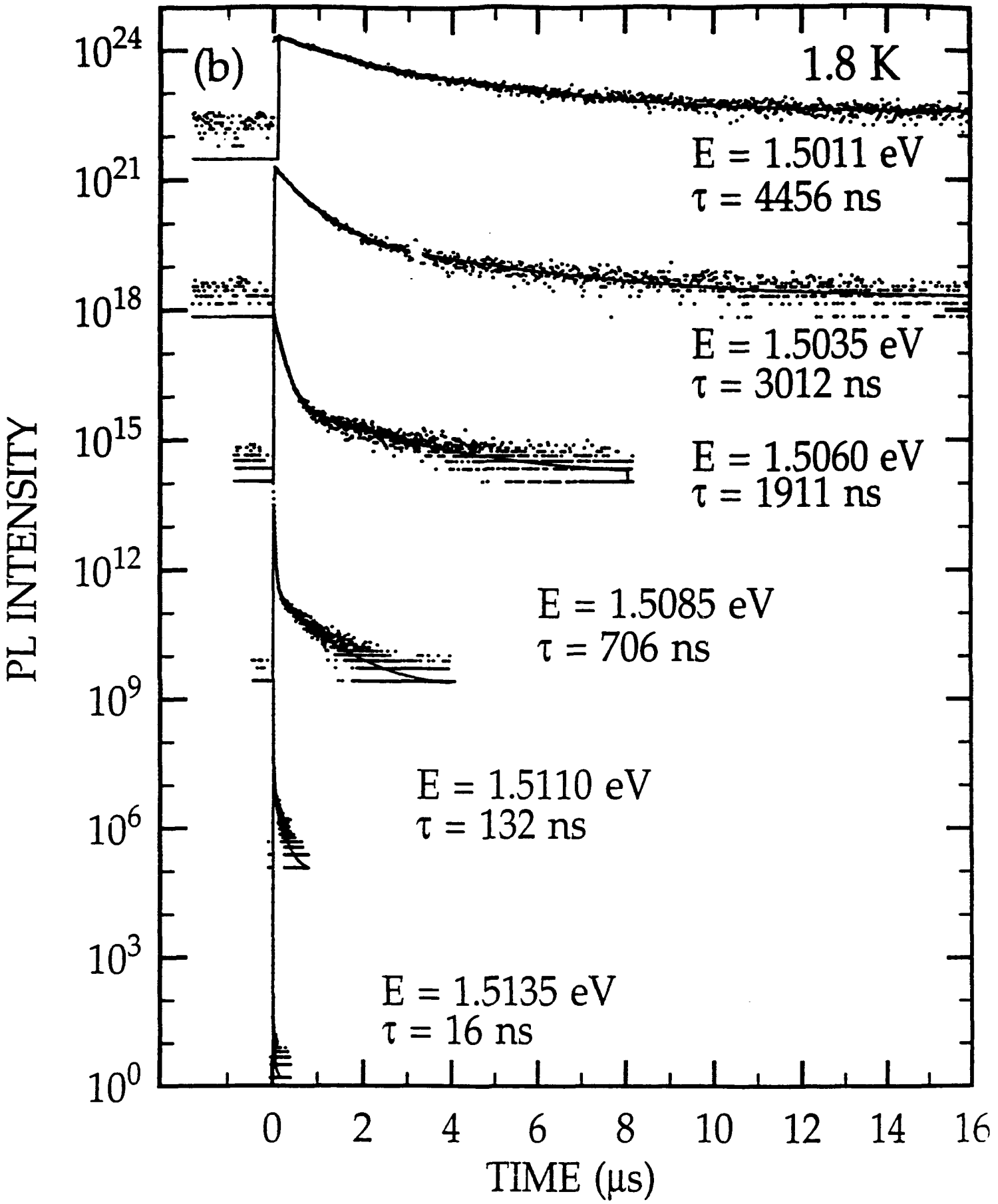
(b)
1.8 K
E = 1.5011 eV
τ = 4456 ns
E = 1.5035 eV
τ = 3012 ns
E = 1.5060 eV
τ = 1911 ns
E = 1.5085 eV
τ = 706 ns
E = 1.5110 eV
τ = 132 ns
E = 1.5135 eV
τ = 16 ns
PL INTENSITY
10^{24}
10^{21}
10^{18}
10^{15}
10^{12}
10^{9}
10^{6}
10^{3}
10^{0}
0
2
4
6
8
10
12
14
16
TIME (μs)

Fig. 6b

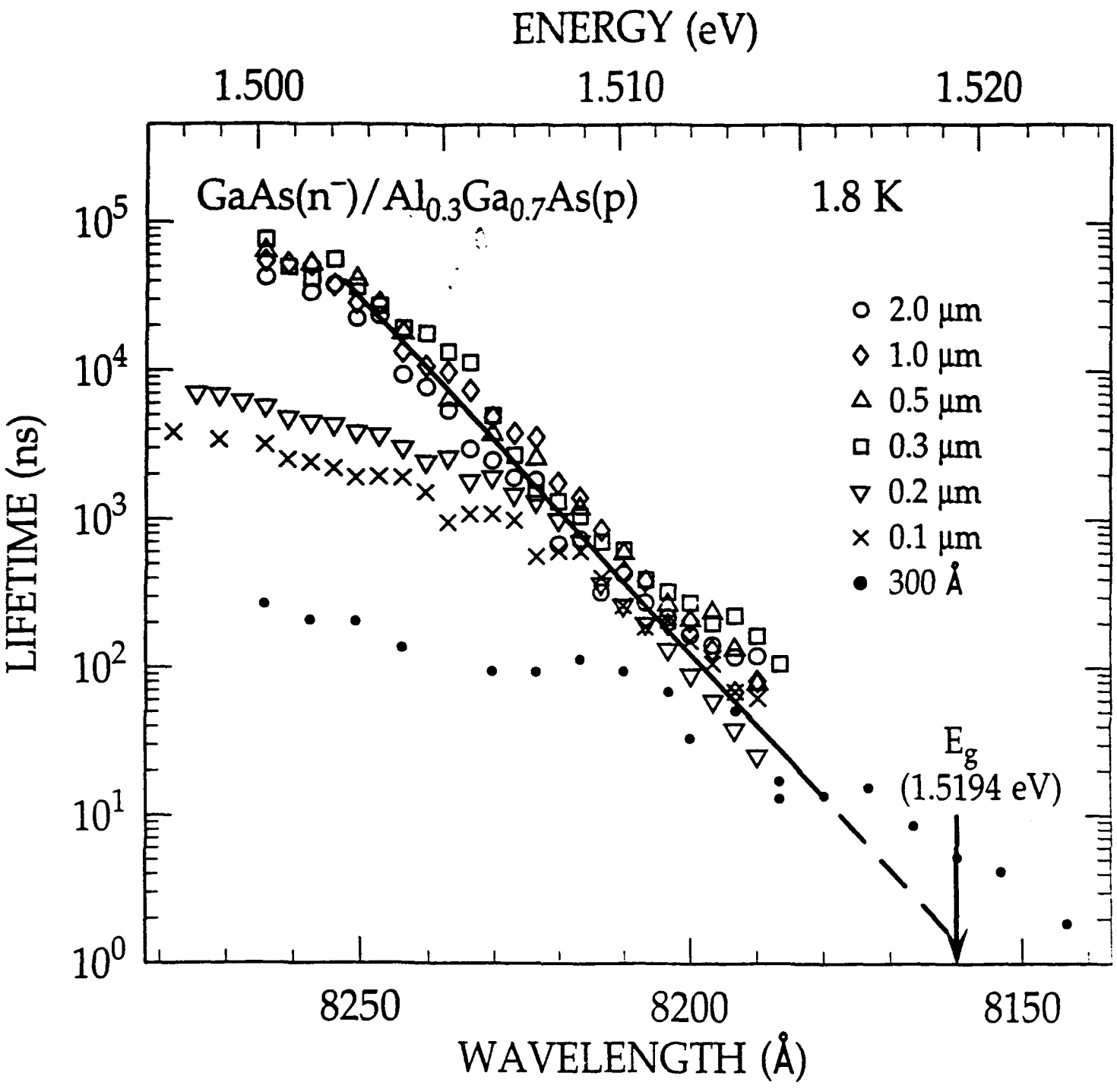
ENERGY (eV)
1.500
1.510
1.520
GaAs(n⁻)/Al0.3Ga0.7As(p)
1.8 K
2.0 μm
1.0 μm
0.5 μm
0.3 μm
0.2 μm
0.1 μm
300 Å
LIFETIME (ns)
10^5
10^4
10^3
10^2
10^1
10^0
Eg
(1.5194 eV)
8250
8200
8150
WAVELENGTH (Å)

FIG. 7

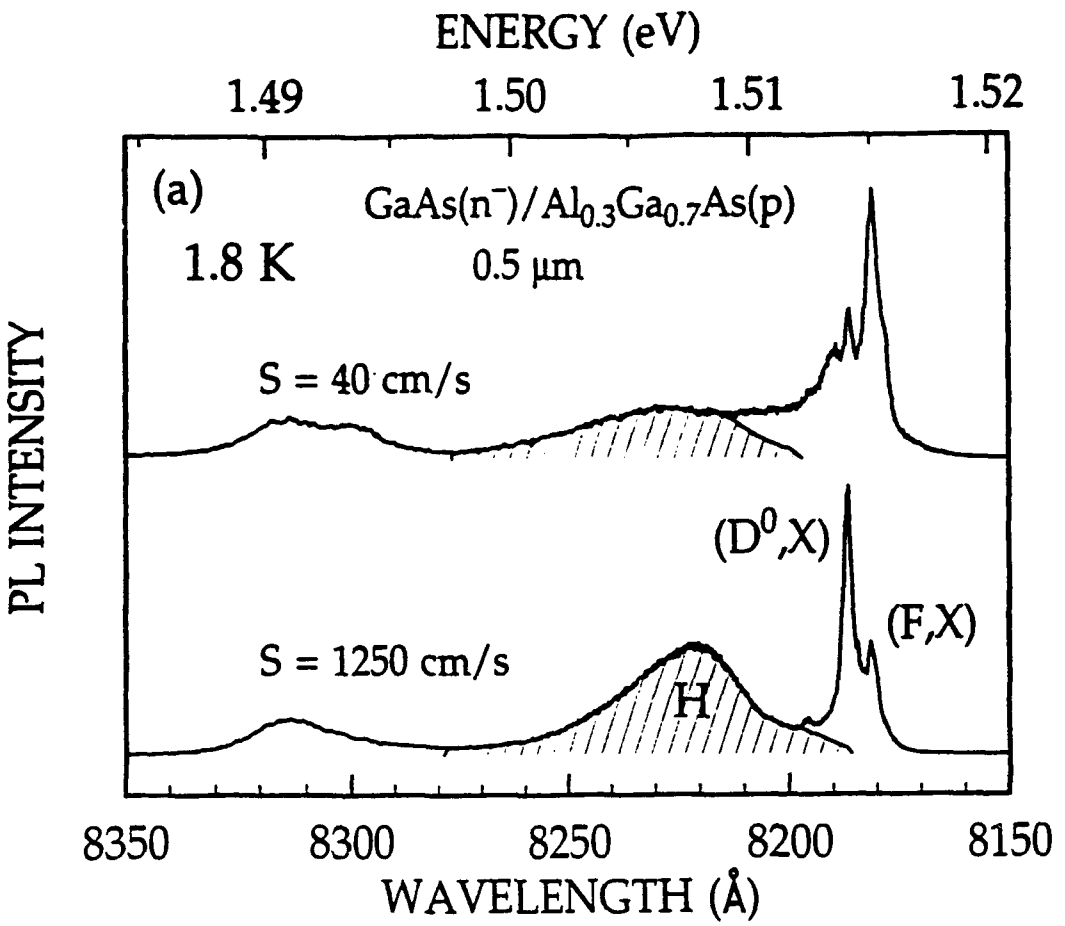
ENERGY (eV)
1.49
1.50
1.51
1.52
(a)
GaAs(n⁻)/Al0.3Ga0.7As(p)
1.8 K
0.5 μm
S = 40 cm/s
PL INTENSITY
(D0,X)
(F,X)
S = 1250 cm/s
H
8350
8300
8250
8200
8150
WAVELENGTH (Å)

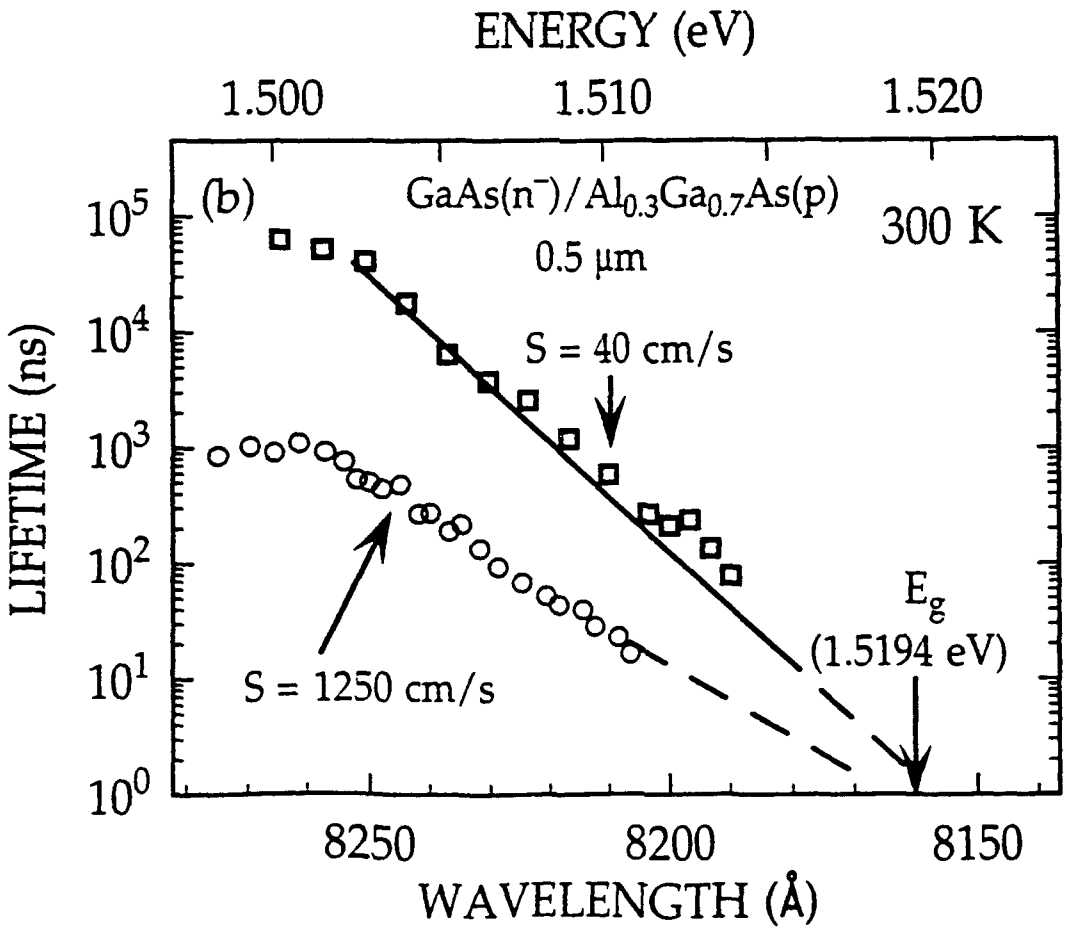
ENERGY (eV)
1.500
1.510
1.520
(b)
GaAs(n⁻)/Al0.3Ga0.7As(p)
0.5 μm
300 K
S = 40 cm/s
LIFETIME (ns)
10⁵
10⁴
10³
10²
10¹
10⁰
Eg
(1.5194 eV)
S = 1250 cm/s
8250
8200
8150
WAVELENGTH (Å)

Fig. 8

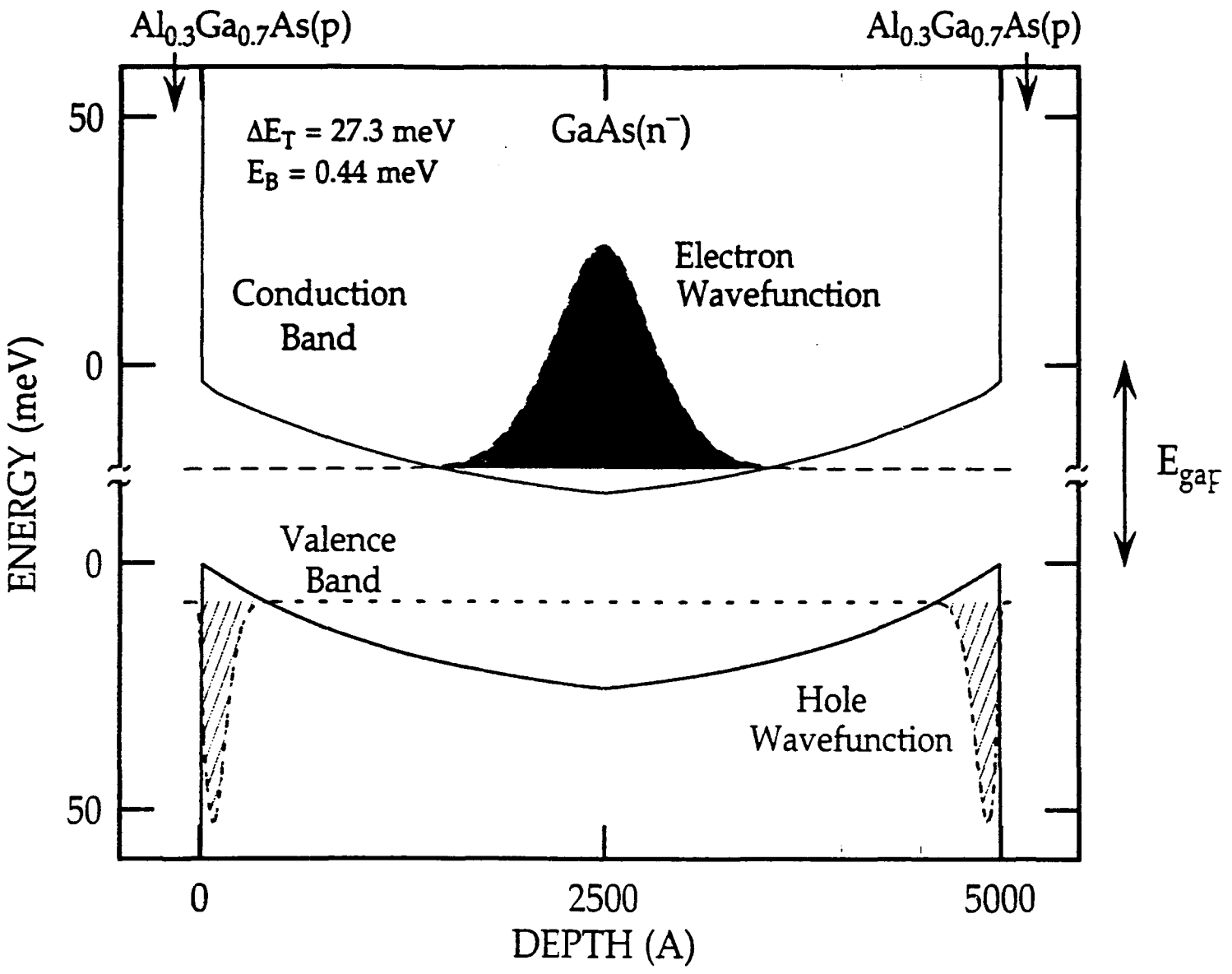
$Al_{0.3}Ga_{0.7}As(p)$
$Al_{0.3}Ga_{0.7}As(p)$
50
ΔE_T = 27.3 meV
E_B = 0.44 meV
$GaAs(n^-)$
Electron
Wavefunction
Conduction
Band
0
E_{gap}
ENERGY (meV)
0
Valence
Band
Hole
Wavefunction
50
0
2500
5000
DEPTH (A)

Fig. 9

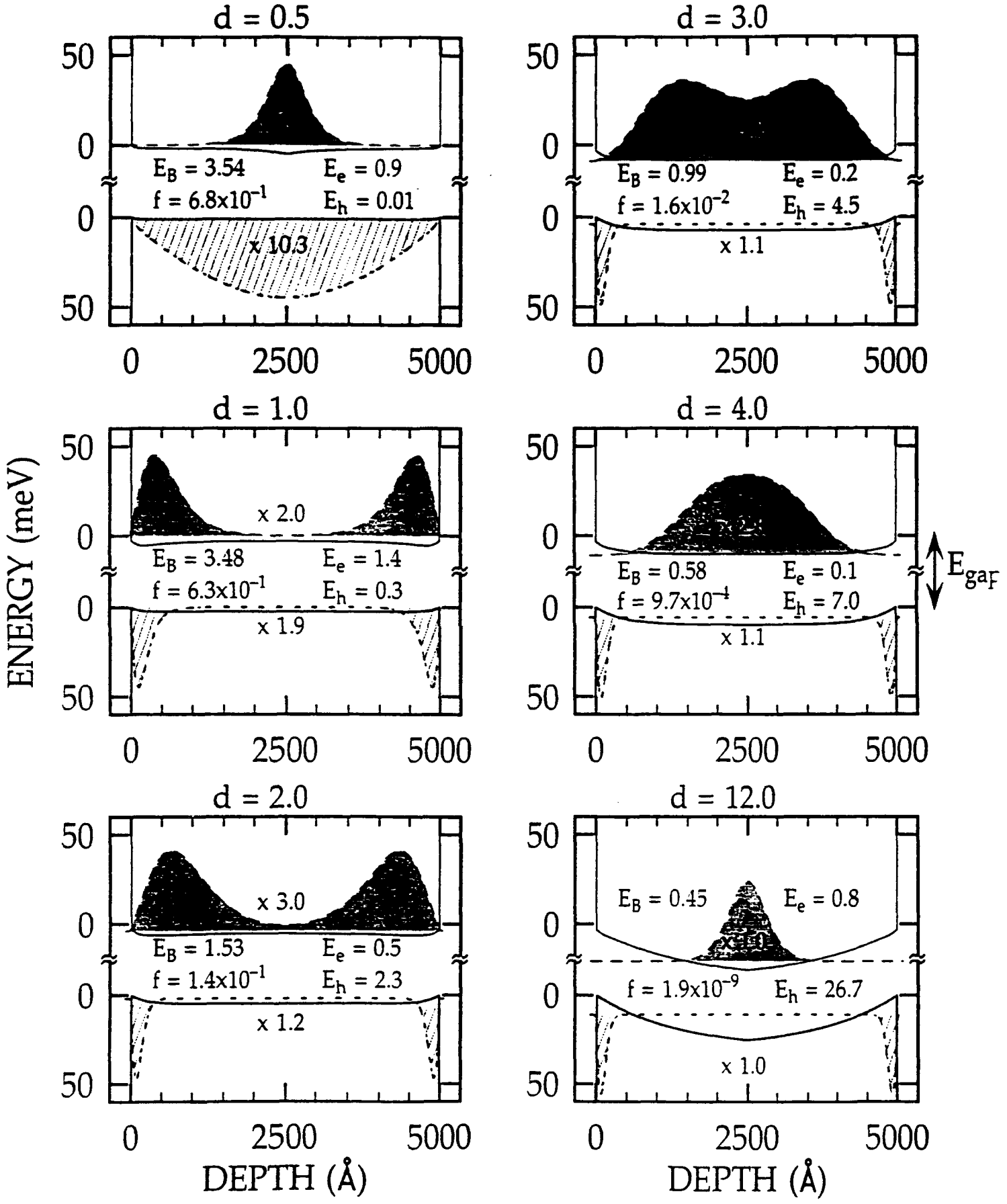
d = 0.5
50
0
E_B = 3.54
E_e = 0.9
f = 6.8x10^{-1}
E_h = 0.01
0
x 10.3
50
0
2500
5000
d = 3.0
50
0
E_B = 0.99
E_e = 0.2
f = 1.6x10^{-2}
E_h = 4.5
0
x 1.1
50
0
2500
5000
d = 1.0
50
x 2.0
0
E_B = 3.48
E_e = 1.4
f = 6.3x10^{-1}
E_h = 0.3
0
x 1.9
50
0
2500
5000
d = 4.0
50
0
E_B = 0.58
E_e = 0.1
f = 9.7x10^{-4}
E_h = 7.0
0
x 1.1
50
E_{gap}
0
2500
5000
ENERGY (meV)
d = 2.0
50
x 3.0
0
E_B = 1.53
E_e = 0.5
f = 1.4x10^{-1}
E_h = 2.3
0
x 1.2
50
0
2500
5000
DEPTH (Å)
d = 12.0
50
E_B = 0.45
E_e = 0.8
0
f = 1.9x10^{-9}
E_h = 26.7
0
x 1.0
50
0
2500
5000
DEPTH (Å)

FIG. 10a.

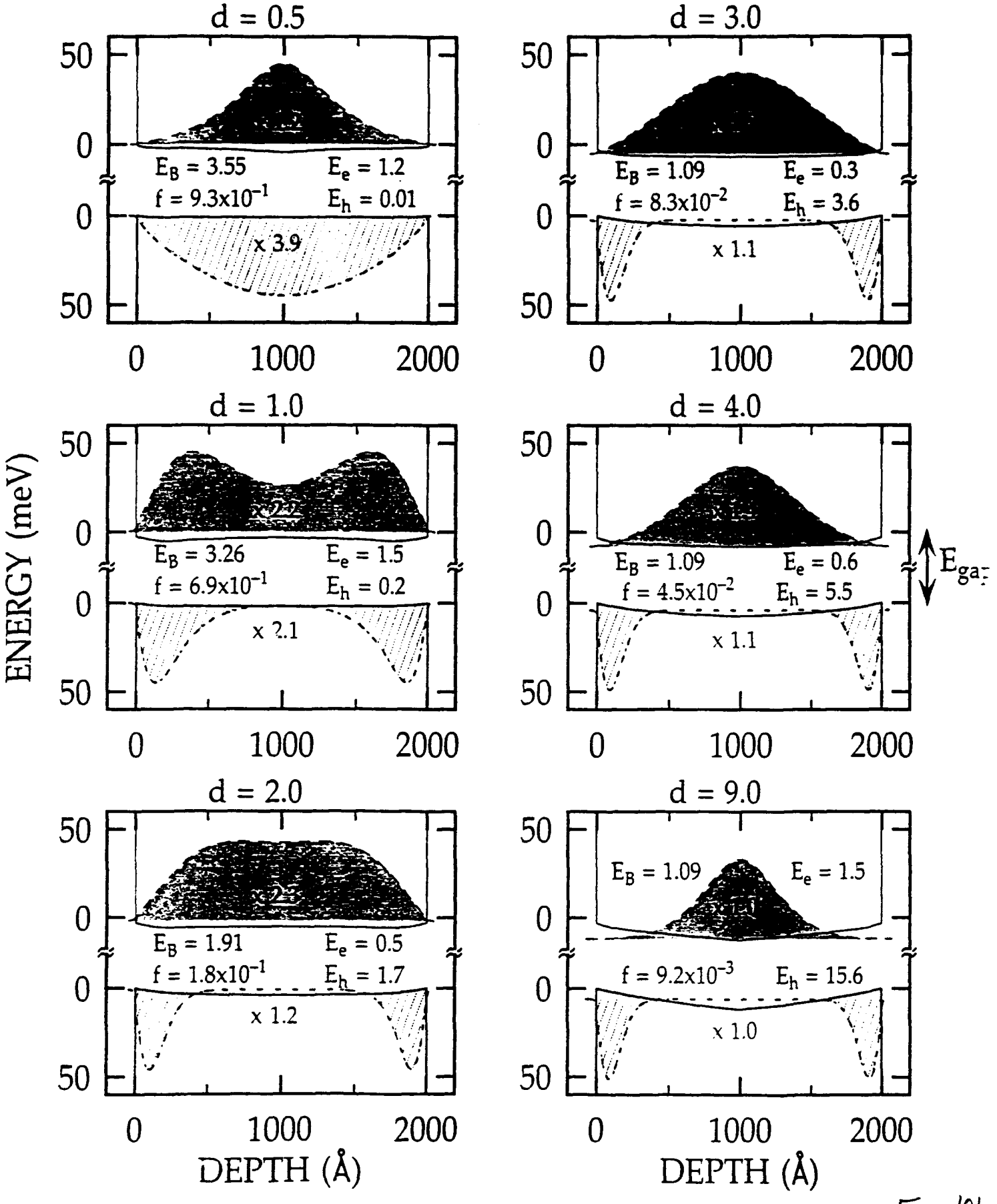
d = 0.5
50
0
E_B = 3.55
E_e = 1.2
f = 9.3x10^{-1}
E_h = 0.01
0
x 3.9
50
0
1000
2000
d = 3.0
50
0
E_B = 1.09
E_e = 0.3
f = 8.3x10^{-2}
E_h = 3.6
0
x 1.1
50
0
1000
2000
d = 1.0
50
0
E_B = 3.26
E_e = 1.5
f = 6.9x10^{-1}
E_h = 0.2
0
x 2.1
50
0
1000
2000
d = 4.0
50
0
E_B = 1.09
E_e = 0.6
f = 4.5x10^{-2}
E_h = 5.5
0
x 1.1
50
0
1000
2000
E_{gap}
d = 2.0
50
0
E_B = 1.91
E_e = 0.5
f = 1.8x10^{-1}
E_h = 1.7
0
x 1.2
50
0
1000
2000
DEPTH (Å)
d = 9.0
50
0
E_B = 1.09
E_e = 1.5
f = 9.2x10^{-3}
E_h = 15.6
0
x 1.0
50
0
1000
2000
DEPTH (Å)
ENERGY (meV)

FIG. 10b.

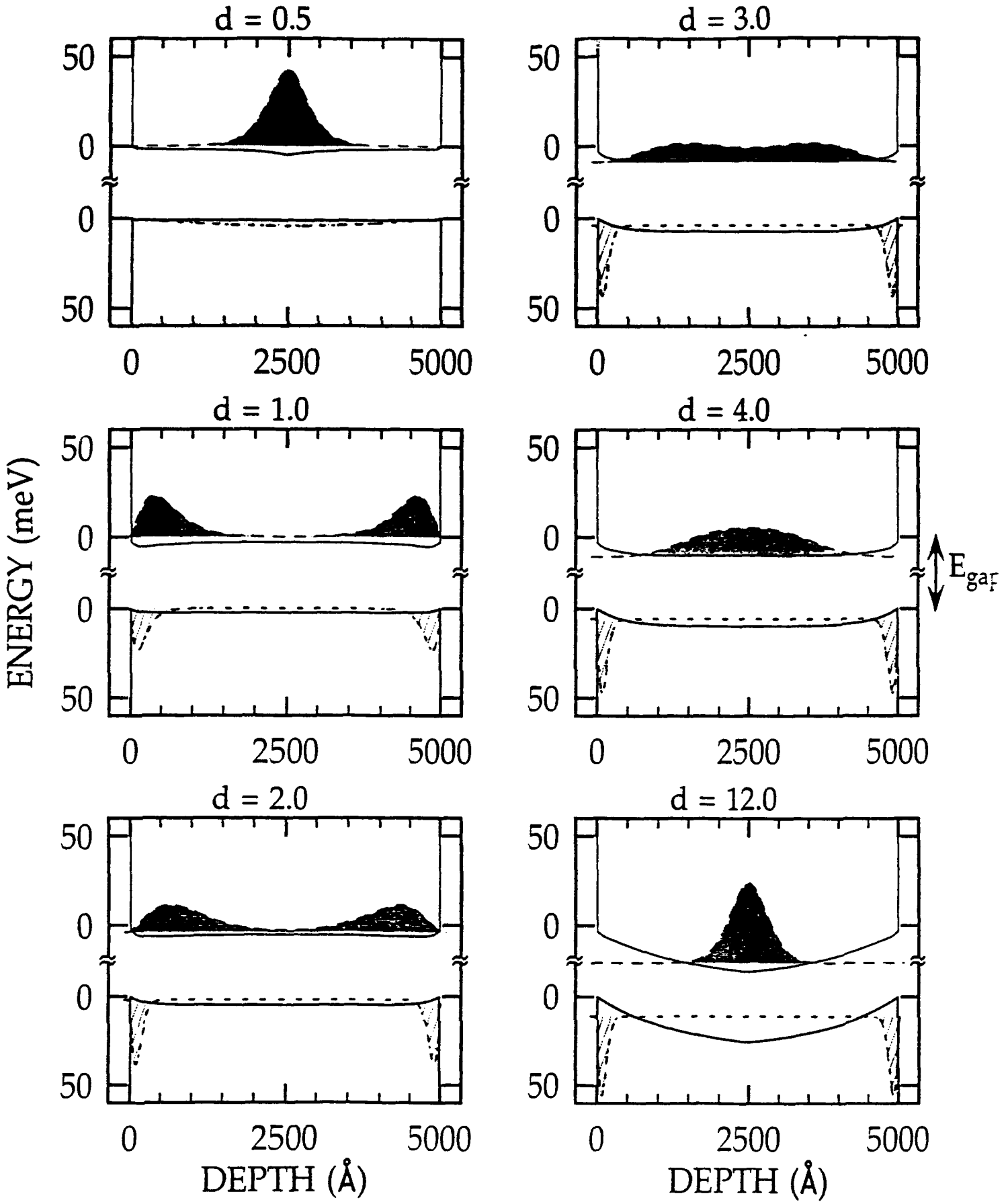
d = 0.5
d = 3.0
d = 1.0
d = 4.0
d = 2.0
d = 12.0
50
0
0
50
0
2500
5000
ENERGY (meV)
E_{gap}
DEPTH (Å)

Fig. 11a.

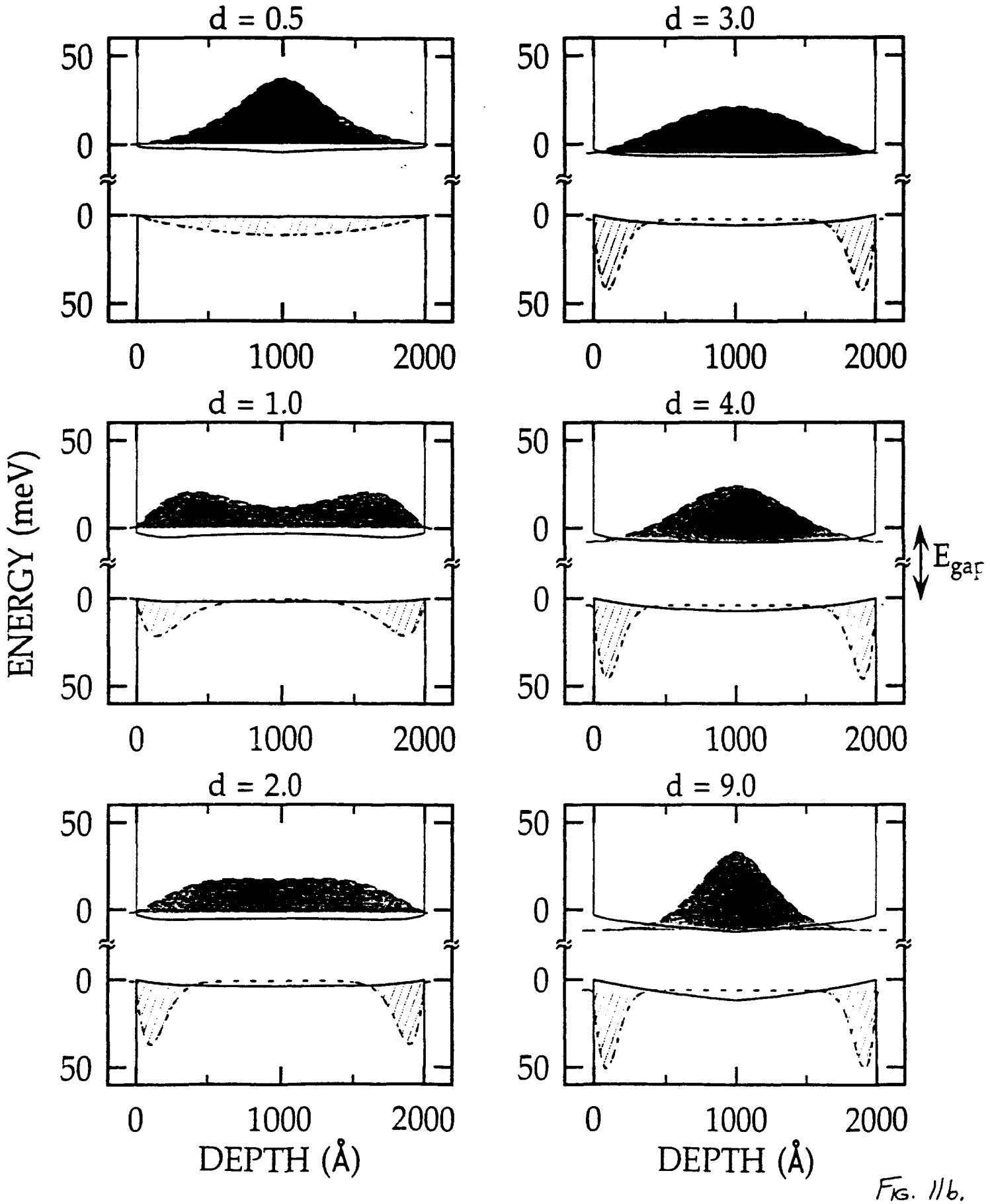
d = 0.5
d = 3.0
d = 1.0
d = 4.0
d = 2.0
d = 9.0
50
0
0
50
0
1000
2000
ENERGY (meV)
E_{gap}
DEPTH (Å)

FIG. 11b.

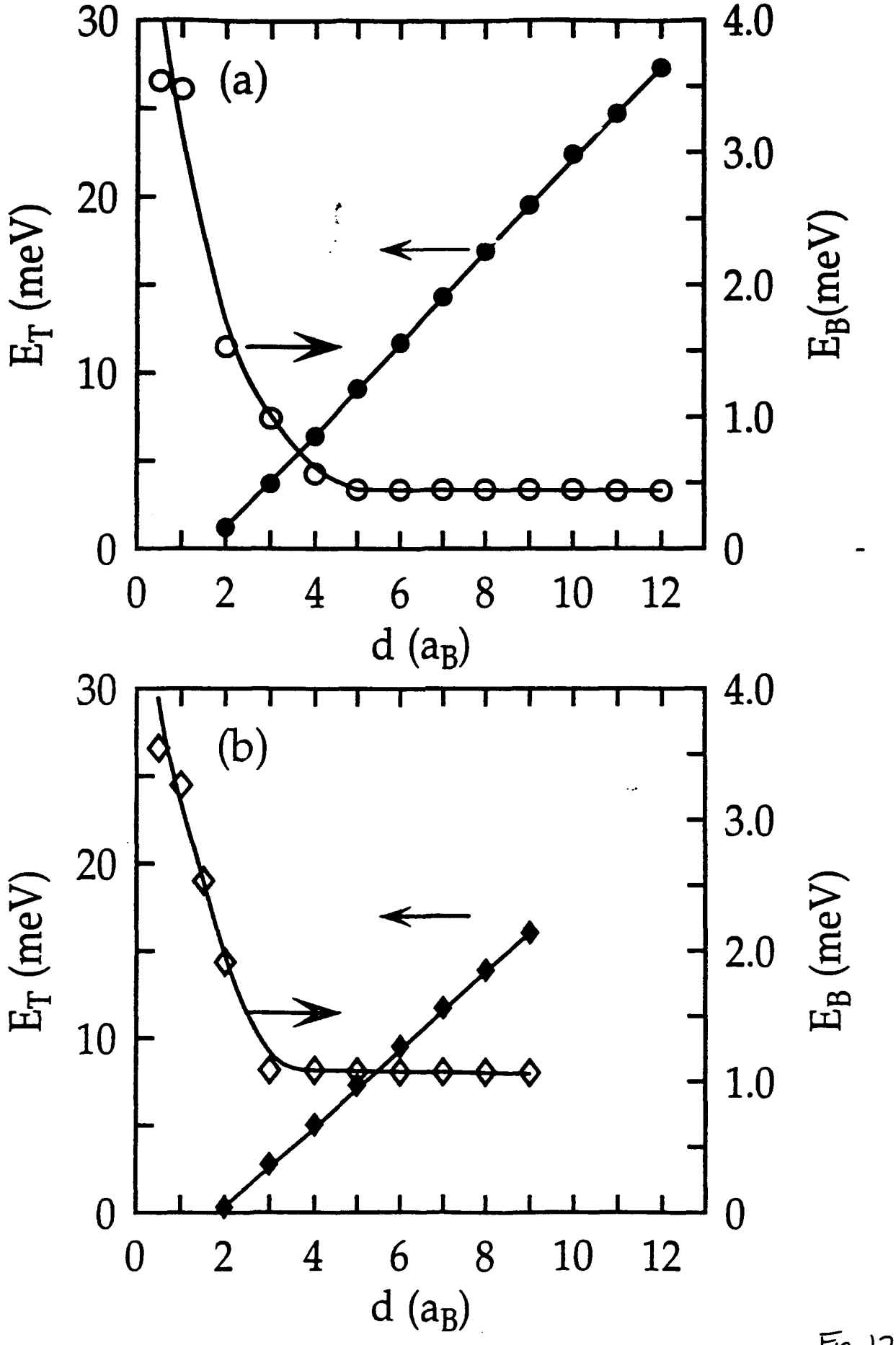

FIG. 12

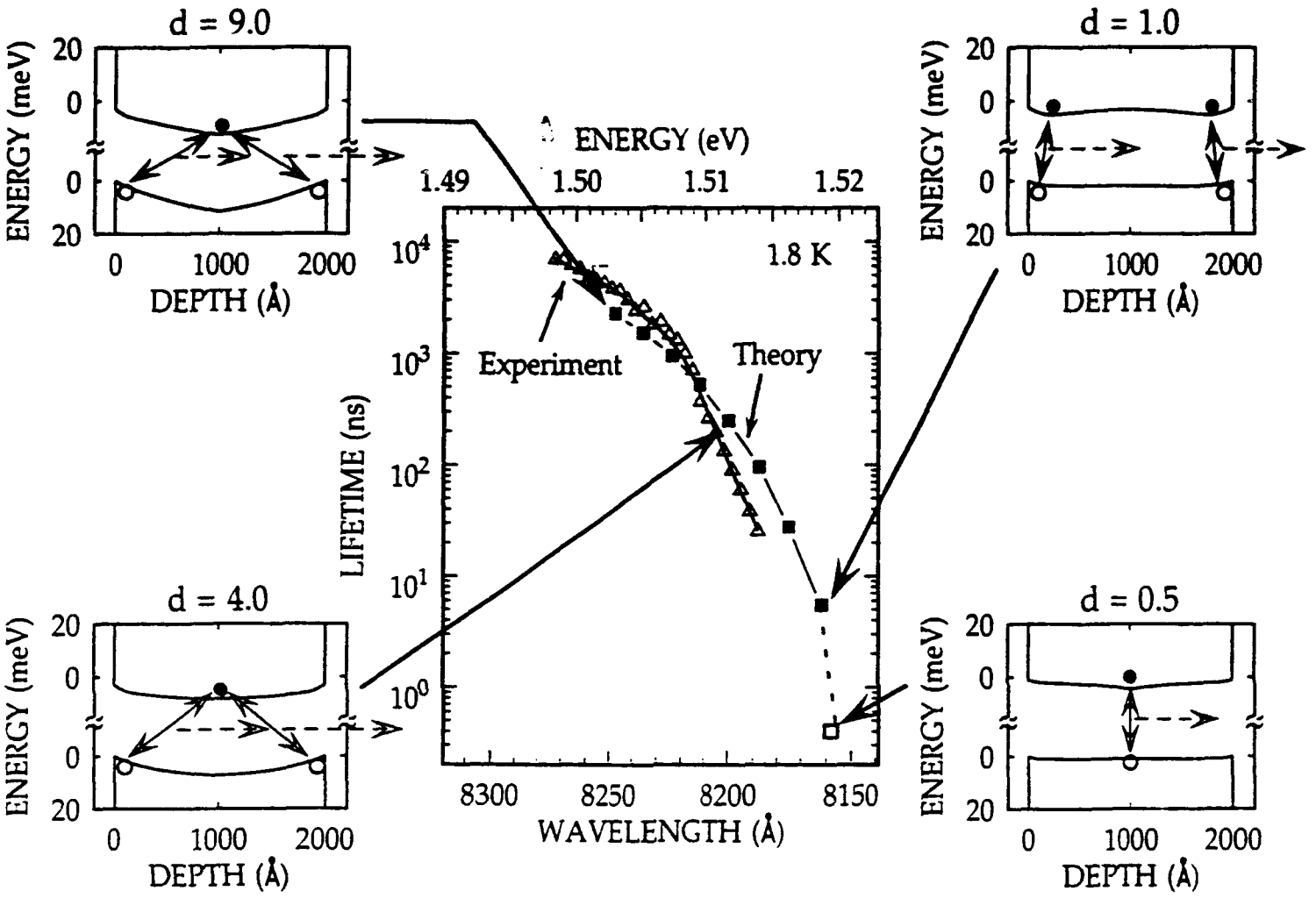
d = 9.0
d = 1.0
d = 4.0
d = 0.5
ENERGY (meV)
DEPTH (Å)
ENERGY (eV)
1.49
1.50
1.51
1.52
1.8 K
Experiment
Theory
LIFETIME (ns)
WAVELENGTH (Å)
8300
8250
8200
8150

FIG. 13

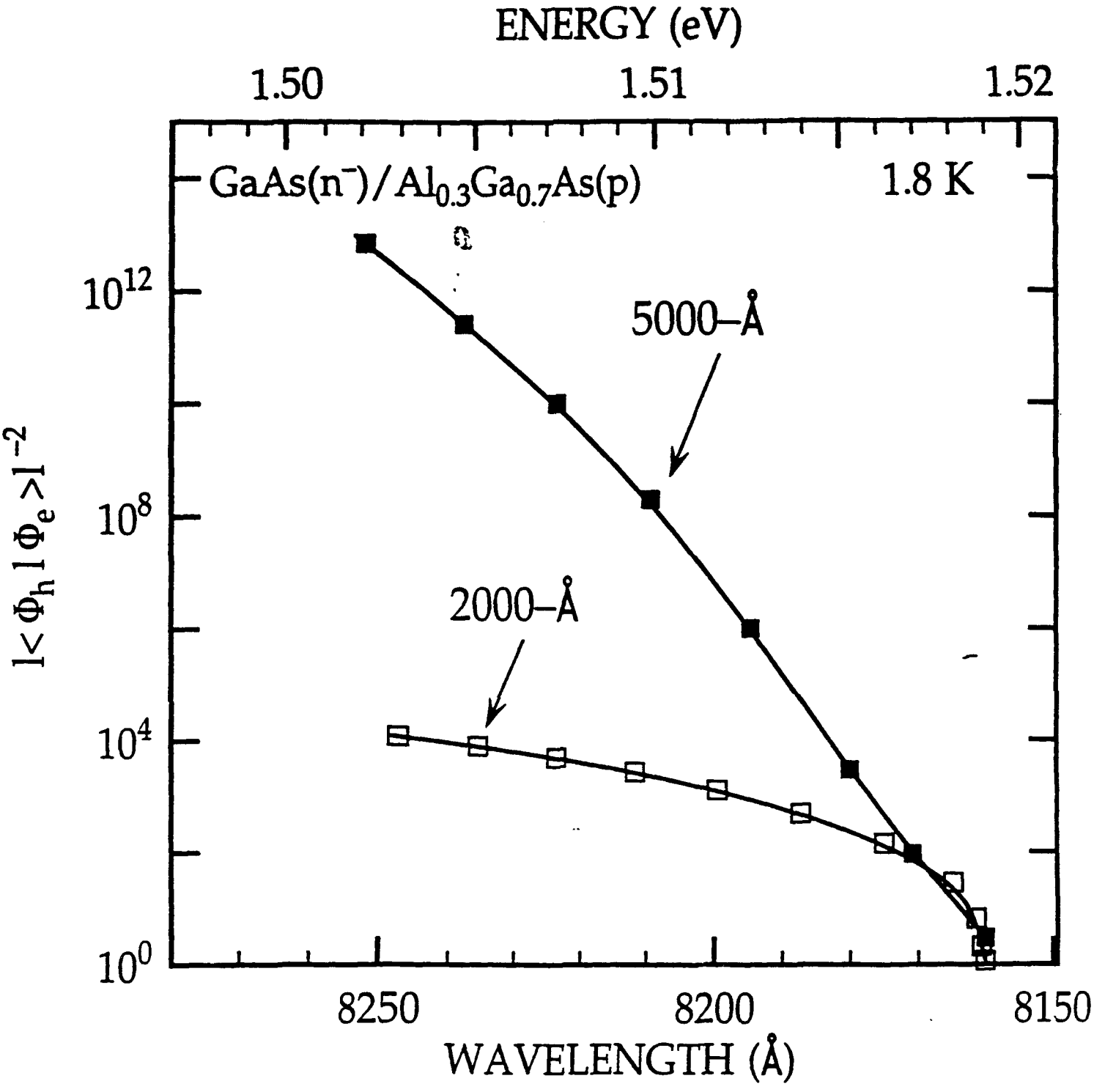
ENERGY (eV)
1.50
1.51
1.52
GaAs(n⁻)/Al0.3Ga0.7As(p)
1.8 K
10^12
10^8
10^4
10^0
5000–Å
2000–Å
|<Φh|Φe>|^-2
8250
8200
8150
WAVELENGTH (Å)

FIG. 14

PUBLICATIONS IN REFEREED JOURNALS

Exciton transport and localization in type-II GaAs/AlAs superlattices

G. D. Gilliland
Emory University, Department of Physics, Atlanta, Georgia 30322

D. J. Wolford and J. A. Bradley
IBM Research Division, T. J. Watson Research Center, P. O. Box 218, Yorktown Heights, New York 10598

J. Klem
Sandia National Laboratories, Albuquerque, New Mexico 87185

M. Jaros
Department of Physics, University of Newcastle upon Tyne, NE1 7RU, United Kingdom

(Received 27 January 1993; accepted 1 April 1993)

We have measured directly the transport of excitons in a type-II short-period GaAs/AlAs superlattice. We find the transport is laser-power dependent, and, at low powers or long times, is diffusive. At low powers, we find diffusion constants which increase monotonically from 2×10^{-3} cm^2/s at 1.8 K to $\sim$7.0 cm^2/s at 30 K. Our results confirm the existence of exciton localization and thermally activated hopping. Implications of these results are discussed.

I. INTRODUCTION

Quantum confinement of free carriers in nanostructured semiconductors was first demonstrated in a GaAs/$Al_xGa_{1-x}As$ quantum well structure in 1975.[1] This materials system is ideal for engineering quantum-confined structures because the conduction and valence band offsets are 68% and 32% of the band gap difference, thus providing sufficient barriers for quantum confinement in both conduction and valence bands for electrons and holes, respectively.[2] Here, carriers are confined in the smaller-gap GaAs layer, and are two dimensional as a result of the removal of a single degree of freedom. After this landmark demonstration of quantum confinement in an artificially grown semiconductor epilayer, more complex, structures were developed. For example, periodic quantum wells with $Al_xGa_{1-x}As$ layers sufficiently thin to allow wave function mixing between different wells were produced in 1976,[3] thereby realizing Esaki *et al.*'s[4] proposed structure called the superlattice. This wave function interaction through the $Al_xGa_{1-x}As$ barrier layers leads to extended states called minibands. More recently, even more complex structures have been engineered to yield exotic electronic and optical properties. For very short-period, periodic multiple quantum well structures, quantum confinement may complicate the electronic structure even further by raising both the GaAs Γ and the $Al_xGa_{1-x}As$ X conduction-band edges. With careful choice of both GaAs and $Al_xGa_{1-x}As$ layer thicknesses (as well as Al composition) a type-II band alignment may result, wherein the lowest energy states for electrons and holes occur in spatially different layers of the structure.[5] This spatial separation of electrons and holes is partially responsible for the dramatically different optical and electronic properties in these structures compared to the quantum wells and superlattices mentioned above, i.e., type-I systems. For a $(GaAs)_m/(AlAs)_n$ structure, a type-II, staggered, band alignment may occur for GaAs-layer thicknesses <35 Å ($m<13$) and AlAs-layer thicknesses >15 Å ($n>6$).[6] Excitons in these type-II systems are thus indirect in real space and in momentum space, since the GaAs layer is direct (Γ edge), whereas the AlAs layer is indirect (X edge).

It is generally agreed that the lowest hole state remains in the GaAs layer for such type-II systems, whereas, in contrast, there is considerable confusion and disagreement about the exact nature of the lowest electronic state.[1,7–13] This confusion arises from the threefold degenerate X-electron states in the AlAs layers. This degeneracy may be removed by several effects, including: the anisotropic X-electron mass [$m_e(X_Z)=1.1\ m_0$ and $m_e(X_{X,Y})=0.19\ m_0$], strain-induced splitting of X_Z and $X_{X,Y}$, $\Gamma-X$ mixing due to the superlattice potential, and localization effects, etc.[7–13] The magnitudes of some of these perturbations may be sample and/or structure dependent, and have been modeled by a variety of methods, including: Kronig–Penney, envelope-function calculations, tight-binding, and local-density calculations.[14–22] As a result, the magnitude of each of these effects, and their effect on the optical and electronic properties is unresolved.

We report here the *first observation* of lateral excitonic transport in type-II $(GaAs)_m/(AlAs)_n$ short-period superlattices.[23] We have used an all-optical, time-resolved photoluminescence (PL) imaging technique to measure exciton transport in a type-II semiconductor nanostructure. This technique, in contrast to the more prevalent electrical techniques, is capable of measuring neutral-particle (i.e., exciton) transport.[24,25] The goal of this study is to increase our understanding of the excitonic states and electronic structure in type-II structures, as well as to elucidate the importance of interfacial effects. Specifically, there has been much speculation concerning the effects of excitonic localization by interface disorder (as inferred indirectly from PL time decay measurements), and we show here, directly, that this hypothesized localization does indeed exist, and is most probably due to heterointerface roughness. Further, we observe dramatic thermal detrap-

 0734-211X/93/11(4)/1647/5/$1.00

ping of these weakly localized excitons, and extract a localization energy from our measurements.

II. SAMPLES AND EXPERIMENT

Our sample was a molecular-beam epitaxy (MBE)-prepared, GaAs(30 Å)/AlAs(50 Å) superlattice with 55 periods. Each GaAs layer was 30 Å thick, whereas AlAs barrier layers were 50 Å thick. Although the nature of the ground electronic state ($X_{X,Y}$ or X_Z) in this structure is disputed somewhat, the prevailing opinion in the literature is that X_Z is the lowest electronic state in this structure.[7]

We have measured time and spatially resolved PL profiles of the carriers generated by pulsed laser excitation using an all-optical analog of the classical Haynes–Shockley experiment.[26–28] PL was excited by a synchronously pumped cavity-dumped dye laser [using Rhodamine 6G(R6G) laser dye] at ~6100 Å, which was pumped by a frequency-doubled continuous-wave (cw) mode-locked Nd^{3+}:YAG laser. Using this experimental setup, under optimal optical alignment, laser spot sizes of ~3–4 μm and PL images extending up to 600 μm are readily obtainable. This laser generated PL is then imaged with a lens system in a confocal manner onto the entrance slits of a triple-grating spectrometer. PL is detected, after being dispersed by the spectrometer, by a multialkali microchannel-plate detector. Imaging the sample (magnified by up to a factor of 40) and using time-correlated single photon counting results in a total system response of ≈3 μm spatially, <1 cm^{-1} spectrally, and <50 ps temporally. The advantage and importance of this technique lies in its sensitivity to neutral-particle (exciton) transport, and the absence of required sample processing. Also, this technique allows the determination and quantification of the details of the possible transport through its spectral sensitivity, and, hence, ability to possibly distinguish the carrier species responsible for the observed transport.

III. RESULTS

Figure 1 shows cw PL spectra for our sample versus temperature, after excitation with the 4579 Å line of a cw argon laser. The excitonic X_Z-Γ no-phonon transition is clearly evident, and its shape is almost completely independent of temperature. We find that the cw PL spectra only decreases slightly in intensity with increasing temperature, whereas time-integrated PL spectra after pulsed excitation decreases by more than three orders of magnitude from 2 to 30 K. Weaker phonon replicas are also evident at all temperatures. Importantly, we do not observe the prominent Boltzmann tail evident in, for example, the free-exciton PL of high-purity GaAs samples, which is indicative of thermalization.[29] Also, the linewidth of the X_Z-Γ transition varies little, from ~5.3 meV at 1.8 K to ~5.9 meV at 30 K (note: kT at 30 K is ~2.6 meV). Figure 2 shows the PL time decays for this sample versus temperature after excitation with the pulsed R6G dye laser described above. (Time decays were found to be independent of laser-power density, and those reported here are for large laser spot sizes—~3 mm—where carrier transport has a negligible influence on the observed decay kinetics.) Here, in contrast to our cw PL spectra, there is a dramatic, monotonic variation in lifetime versus temperature, from 21.5 μs at 1.8 K to ~15 ns at 30 K. Also, the decay kinetics are nonexponential at low temperatures, and rapidly become exponential at higher temperatures (>22 K). (Lifetimes were derived from the exponential long-time tail part of the PL decay kinetics.) These results are consistent with PL time decays reported in the literature for other type-II GaAs/AlAs short-period superlattices.[5,10–12]

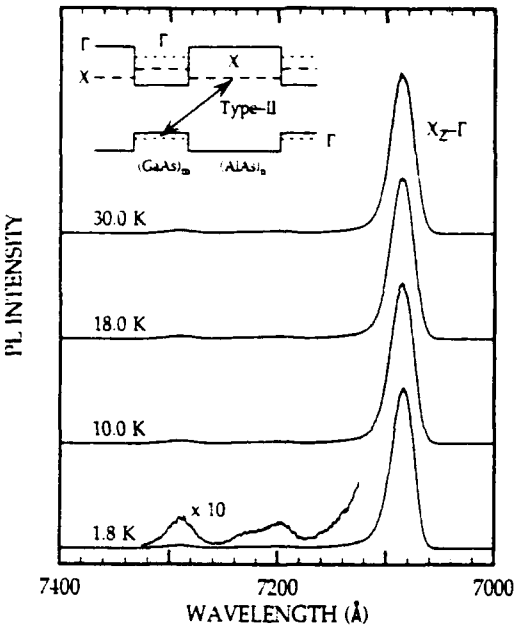

FIG. 1. PL spectra vs temperature after cw excitation at 4579 Å. Inset shows the cross-interface transition responsible for the observed emission.

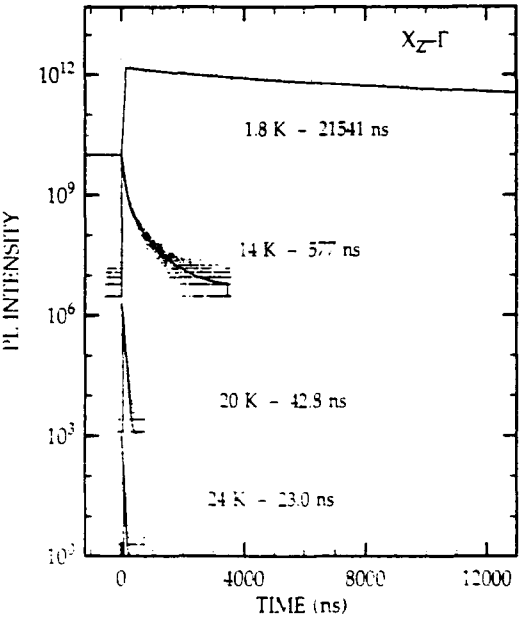

FIG. 2. PL time decays vs temperature after pulsed excitation at 6005 Å. Lifetimes were derived from exponential fits to the long-time tail of the decays.

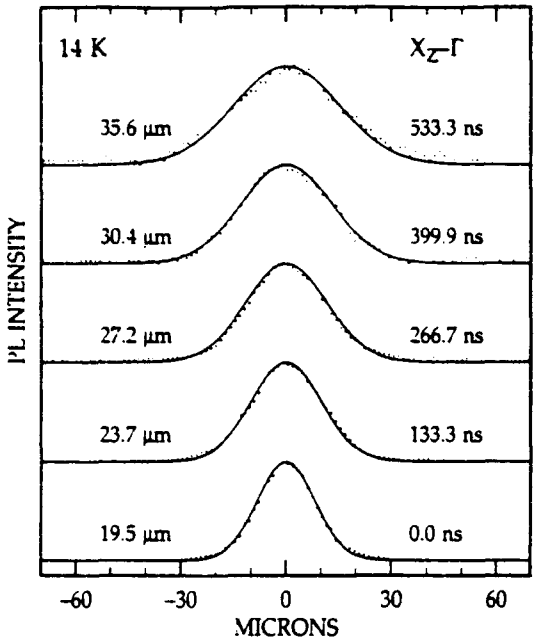

FIG. 3. Time-resolved PL imaging results at 14 K. Solid lines represent Gaussian fits to the data, with the FWHMs shown.

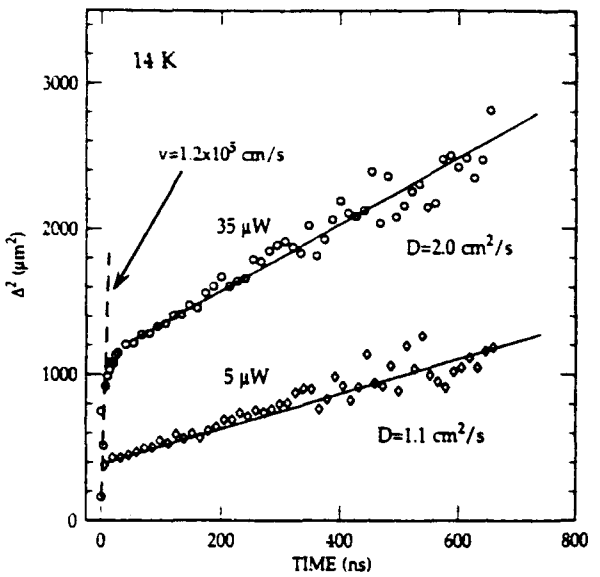

FIG. 4. Δ^2 vs time at 14 K for two different laser powers (average powers shown and the repetition rate is 20 kHz) showing the effect laser power has on the early transport, was obtained from the Gaussian fits as in Fig. 3.

Figure 3 shows the results of our time-resolved PL-imaging experiments at 14 K. The solid lines represent Gaussian fits to the observed line shapes, with the full width at half-maximum [(FWHM) $-\Delta$] taken from such fits, also shown for each time window. These data show unmistakable evidence (a monotonic increase in Δ versus time) for the transport of these cross-interface excitons laterally along the heterointerface. A linear dependence of Δ^2 versus time is possibly indicative of diffusive transport, and this is indeed observed. Moreover, the diffusion coefficient may be calculated from the slope of Δ^2 versus time. Additionally, we also observe a laser-power dependent feature, which is also more prominent at low temperatures, and weaker at high temperatures. At high laser powers the FWHM increases very rapidly in the first several ns, and then saturates to its final slope (approximately equal to that observed at low laser powers—~40 pJ/pulse). Figure 4 shows an example of this power-dependent transport at 14 K. We believe that this is related to the creation of an electron-hole plasma,[30] with its corresponding higher-energy PL emission and short PL lifetime. Nevertheless, our main results are specific to the diffusion of type-II excitons in this structure since all measurements reported in Fig. 3 were made at low powers in an effort to eliminate this complicating high laser-power effect.

Our low-power transport results are summarized in Fig. 5. Here, the diffusion constant, obtained in the manner shown above, is plotted versus temperature. Diffusion constants range from $\sim 2\times 10^{-3}$ cm^2/s at 1.8 K to ~7.0 cm^2/s at 30 K—a 5×10^3 change in just 30 K. Additionally, PL lifetimes versus temperature are shown in this figure. Our PL lifetimes also show a three-order-of-magnitude change over the same temperature range. Importantly, we find that lifetimes decrease while diffusivities increase with temperature, suggestive of a connection between these experimental observations. Indeed, the diffusion length ($L_d = \sqrt{D\tau}$), obtained from our transport and decay kinetics, is constant versus temperature ($L_d \approx 3\mu$m).

IV. DISCUSSION

Studies of type-II excitonic recombination in GaAs/AlAs short-period superlattices are ubiquitous in the literature. In all of these studies,[5,10–12,31] one feature is particularly clear—lifetimes decrease with increasing temperature, although the shape of the decay kinetics is not uniformly the same (i.e., exponential versus nonexponential) for samples grown by molecular-beam epitaxy or organometallic vapor phase epitaxy, MBE or OMVPE, re-

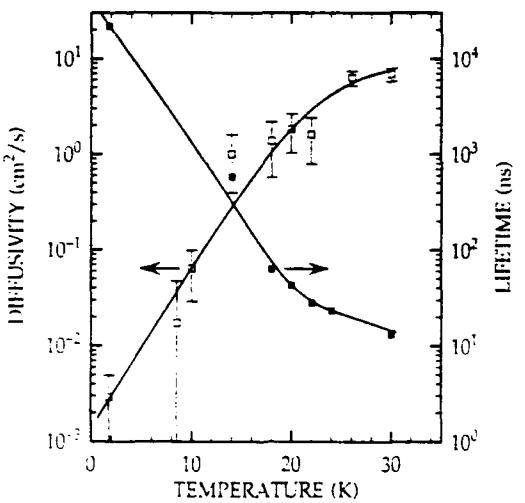

FIG. 5. Diffusion constant and lifetime vs temperature for low laser powers.

spectively. The general conclusion inferred from this is that thermal detrapping of excitons from a distribution of localized states causes the temperature dependence of the observed PL decay kinetics. Further, most authors conclude that this localization results from heterointerface disorder since the cross-interface nature of the excitonic species (the Coulomb potential) forces the electrons and holes to be in intimate contact with the heterointerface.

However, these conclusions have *never—until this report—been directly proven* since the transport of these cross-interface excitons has never been measured. Indeed, if this hypothesis is true, then the observed temperature invariance of the PL line shape suggests that type-II recombination only occurs from localized states, since otherwise, the radiative recombination of excitons in the higher-energy mobile states would result in a pronounced high-energy tail in the PL. We observe no significant change in the PL spectra versus temperature (Fig. 1). This further supports our conclusion regarding the localization. We conclude that localization of the cross-interface excitons at potential fluctuations induced by heterointerface roughness is vital to the recombination mechanism. Further, the PL spectra is indicative of the energy distribution of localization sites. This detrapping may also occur at high excitation powers. Thus, our model for the observed transport and kinetic results is as follows: At low temperatures, excitons are localized in the low-energy heterointerface sites, whereas at higher temperatures, thermal detrapping of a portion of these excitons allows those excitons detrapped from the localized states into mobile states to migrate until they eventually may become trapped at a nonradiative defect, thus shortening the observed lifetime and causing the observed weakening of the PL. cw PL spectra will not become significantly weaker with increasing temperature and concomitant increased trapping and nonradiative decay because a steady state is reached between excitation and trapping. However, time-integrated PL spectra after pulsed excitation should decrease in intensity with increasing temperature, and this decrease is attributable to the reduction in lifetime caused by nonradiative decay. Therefore, both our cw and pulsed, time-integrated PL spectra are consistent with this model. Further, the constant diffusion length versus temperature is consistent with the model since the probability for nonradiative decay depends upon the density of these traps, and, therefore, the diffusion length.

Our transport model relies upon the rapid trapping of excitons in localized states caused by heterointerfacial disorder. In such a system, care must be exercised in modeling the data since different models may yield different results. In particular, models based upon diffusive transport versus dispersive transport should yield discernable differences in the observed transport.[32] Indeed, dispersive transport models have been successful in modeling transport in amorphous systems. We believe that a diffusive model, which approximates thermally activated hopping and is commonly used,[33] is required to model and is consistent with our data. This conclusion is based upon the following observations: (1) the observed transport does not slow down with increasing time, (2) time-resolved PL spectra do not show a redshift in the PL spectra with increasing time, and (3) the PL line shape does not change with increasing temperature. All of these observations rule out a dispersive transport model.

Our transport results are thus the first to definitely and directly show that this localization hypothesis is indeed true. Moreover, we have quantified the magnitude of the diffusive transport versus temperature, and find it to be thermally activated, with an activation energy of -6.8 ± 1.5 meV—20% larger than the PL linewidth. This result is quite peculiar, in light of the observed temperature-invariant PL line shape. We conclude that the temperature-dependent transport results from a temperature-dependent occupation of mobile versus stationary localized states (probably occurring by thermally activated hopping). Additionally, more detailed measurements of type-II exciton transport versus emission energy are currently in progress in an effort to identify a possible mobility edge between these localized and mobile states.

V. CONCLUSIONS

We have measured directly the transport of excitons in a type-II short-period GaAs/AlAs superlattices, for the first time. We have quantified this transport and observe thermalization of excitons from highly localized states to more mobile states. Additionally, our study has further elucidated the electronic structure and recombination mechanism of this type-II superlattice. At high excitation powers, we observe an initial rapid expansion, possibly a result of the formation and transport of an electron-hole plasma, followed by slower diffusive transport at late times. The formation of a higher-energy electron-hole plasma is also confirmed in our time-resolved PL. Our results also serve to characterize the disorder at the heterointerface (5.5 meV linewidth).

ACKNOWLEDGMENTS

Supported in part by the U. S. Office of Naval Research under Contract Nos. N00014-85-C-0868, N00014-90-C-0077, N00014-91-J-1697, and N00014-92-J-1927.

[1] R. Dingle, A. C. Gossard, and W. Wiegmann, Phys. Rev. Lett. **34**, 1327 (1975).
[2] D. J. Wolford, T. F. Kuech, J. A. Bradley, M. A. Gell, D. Ninno, and M. Jaros, J. Vac. Sci. Technol. B **4**, 1043 (1986); D. J. Wolford and J. A. Bradley, Solid State Commun. **53**, 1069 (1985).
[3] A. C. Gossard, P. M. Petroff, W. Weigmann, R. Dingle, and A. Savage, Appl. Phys. Lett. **29**, 323 (1976); J. P. van der Ziel and A. C. Gossard, J. Appl. Phys. **48**, 3018 (1977); L. L. Chang, A. Segmuller, and L. Esaki, Appl. Phys. Lett. **28**, 39 (1976).
[4] L. Esaki and R. Tsu, IBM J. Res. Dev. **14**, 61 (1970); L. Esaki and L. L. Chang, Thin Solid Films **36**, 285 (1976).
[5] E. Finkman, M. D. Sturge, M. H. Meynadier, R. E. Nahory, M. C. Tamargo, D. M. Hwang, and C. C. Chang, J. Lumin. **39**, 57 (1987).
[6] K. J. Moore, P. Dawson, and C. T. Foxon, Phys. Rev. B **38**, 3368 (1988).
[7] P. Dawson, C. T. Foxon, and H. W. van Kesteren, Semicond. Sci. Technol. **3**, 54 (1990).
[8] W. Ge, M. D. Sturge, W. D. Schmidt, L. N. Pfeiffer, and K. W. West, Appl. Phys. Lett. **57**, 55 (1990).
[9] H. W. van Kesteren, E. C. Cosman, P. Dawson, K. J. Moore, and C. T. Foxon, Phys. Rev. B **39**, 13426 (1989).

[10]D. Scalbert, J. Cernogora, C. Benoit a la Guillaume, M. Maaref, F. F. Charfi, and R. Planel, Surf. Sci. **229**, 464 (1990).
[11]F. Minami, K. Hirata, K. Era, T. Yao, and Y. Masumoto, Phys. Rev. B **36**, 2875 (1987).
[12]E. Finkman, M. D. Sturge, and M. C. Tamargo, Appl. Phys. Lett. **49**, 1299 (1986).
[13]J. Ihm, Appl. Phys. Lett. **50**, 1068 (1987).
[14]R. L. de Kronig and W. J. Penney, Proc. R. Soc. London Ser. A **130**, 499 (1930).
[15]G. Bastard, Phys. Rev. B **25**, 7584 (1982).
[16]J. N. Schulman and Y. C. Chang, Phys. Rev. B **24**, 2445 (1981).
[17]J. N. Schulman and T. C. McGill, Phys. Rev. **19**, 6341 (1979).
[18]W. Andreoni and R. Car, Phys. Rev. B **21**, 3334 (1980).
[19]M. A. Gell, D. Ninno, M. Jaros, and D. C. Herbert, Phys. Rev. B **34**, 2416 (1986); L. D. L. Brown, M. Jaros, and D. J. Wolford, *ibid.* **40**, 6413 (1989).
[20]T. Nakayama and H. Kamimura, J. Phys. Soc. Jpn. **54**, 4726 (1985).
[21]D. M. Bylander and L. Kleinman, Phys. Rev. B **36**, 3229 (1987).
[22]R. Eppenga and M. F. H. Schuurmans, Phys. Rev. B **38**, 3541 (1988).
[23]G. D. Gilliland, D. J. Wolford, J. A. Bradley, and J. Klem, *Proceedings of the 21st International Conference on the Physics of Semiconductors*, Beijing China (World Scientific, Singapore, in press).
[24]G. D. Gilliland, D. J. Wolford, T. F. Kuech, and J. A. Bradley, Appl. Phys. Lett. **59**, 216 (1991).
[25]D. J. Wolford, G. D. Gilliland, T. F. Kuech, J. A. Bradley, and H. P. Hjalmarson (unpublished).
[26]J. R. Haynes and W. Shockley, Phys. Rev. **81**, 835 (1951).
[27]D. J. Wolford, G. D. Gilliland, T. F. Kuech, J. A. Bradley, and H. P. Hjalmarson, Inst. Phys. Conf. Ser. **120**, 271 (1992).
[28]G. D. Gilliland, D. J. Wolford, G. A. Northrop, M. S. Petrovic, T. F. Kuech, and J. A. Bradley, J. Vac. Sci. Technol. B **10**, 1959 (1992).
[29]G. D. Gilliland, D. J. Wolford, T. F. Kuech, and J. A. Bradley, J. Vac. Sci. Technol. B **9**, 2377 (1991).
[30]J. L. Mackay, J. D. Sturge, M. H. Meynadier, M. D. Tamargo, and J. L. deMiguel, J. Lumin. **48**, 731 (1991).
[31]P. Dawson, K. J. Moore, C. T. Foxon, G. W. 'tHooft, and R. P. M. van Hal, J. Appl. Phys. **65**, 3606 (1989).
[32]K. W. Böer, *Survey of Semiconductor Physics* (Van Nostrand Reinhold, New York, 1990).
[33]V. M. Agranovich and M. D. Galanin, *Electronic Excitation Energy Transfer in Condensed Matter* (North-Holland, New York, 1982).

Minority-carrier recombination kinetics and transport in "surface-free" GaAs/$Al_xGa_{1-x}As$ double heterostructures

G. D. Gilliland, D. J. Wolford, T. F. Kuech, and J. A. Bradley
IBM Research Division, T. J. Watson Research Center, P. O. Box 218, Yorktown Heights, New York 10598

H. P. Hjalmarson
Sandia National Laboratories, Albuquerque, New Mexico 87185

(Received 9 April 1992; accepted for publication 18 February 1993)

We have measured room-temperature band-to-band recombination decay kinetics in superior quality GaAs heterostructures, and have observed the longest lifetime (2.5 μs) observed for any GaAs/$Al_xGa_{1-x}As$ structure to date. Additionally, using a novel time-resolved optical photoluminescence imagining technique, analogous to the Haynes–Shockley experiment, we have also measured room-temperature minority-carrier transport in this series of "surface-free" GaAs/$Al_{0.3}Ga_{0.7}As$ double heterostructures, measurements only possible in high-quality samples with long lifetimes and intense photoluminescence. We find the transport to be diffusive with diffusion lengths of $\gtrsim 100$ μm. Further, we find, for thick structures, minority-carrier transport is hole-dominated ambipolar diffusion, as expected for high-purity *n*-type material. However, for thinner structures, we find that the minority-carrier transport is time dependent, changing from ambipolar diffusion at early times, as in thick structures, to electron-dominated diffusion at later times. We show that these structures become *effectively p-type modulation doped* due to the relative "impurity" and thickness of the $Al_xGa_{1-x}As$ compared to the GaAs. As a result, the minority-carrier species changes from holes to electrons for decreasing GaAs layer thicknesses. Cumulatively, we show the band-to-band recombination decay kinetics and carrier transport results to be in excellent qualitative and quantitative agreement. Moreover, our results are in excellent agreement with electrical transport measurements of electron and hole mobilities. Finally, with our measured room-temperature lifetimes and minority-carrier transport measurements versus GaAs layer thickness, we accurately calculate the interface recombination velocity for these structures, with the result $S \sim 40$ cm/s, among the lowest ever reported for any GaAs/$Al_xGa_{1-x}As$ structure.

I. INTRODUCTION

Studies of intrinsic band-to-band recombination kinetics in direct-gap semiconductors such as GaAs[1-10] have met with limited success, due, primarily, to the overwhelming effects of surface or interface recombination and residual dopants which may mask intrinsic decay kinetics. Among the most systematic, but nonetheless limited studies of these kinetics to date is that of Nelson and Sobers in 1977,[1-3] in which the effects of intentional dopant impurity concentration on the recomoination kinetics were measured in liquid-phase-epitaxy prepared (LPE) GaAs/$Al_xGa_{1-x}As$ double heterostructures. Despite this serious attempt at examining band-to-band recombination kinetics in GaAs structures, the effects of many other parameters remain largely unexplored (due, again, in part to these deleterious effects). These parameters may be catagorized as relating to the structural parameters (such as surface conditions, $Al_xGa_{1-x}As$ composition, impurity concentration, and thickness, etc.) or growth parameters (growth temperature, growth rate, and V-III ratio, etc.).

Modern epitaxial growth techniques, such as molecular beam epitaxy (MBE)[7,11-20] or organometallic vapor phase epitaxy (OMVPE),[6,21-27] may reduce, if not eliminate, some of these overwhelming, detrimental effects through the preparation of higher-quality semiconductor heterostructures than those available with other growth techniques, thereby allowing studies of the effects these other parameters may have on band-to-band recombination kinetics. Specifically, these epitaxial heterostructures may be superior to LPE-prepared heterostructures in several aspects. First, purities of 10^{14} cm^{-3} have been achieved,[7,16,21,25] with some of these more recent state of the art techniques, comparable to or better than the best LPE material.[1,2,9] Second, truly atomically abrupt heterointerfaces are readily achieved with these growth techniques,[18-20,26-28] in contrast to the graded interfaces (over several thousand angstroms) typical in LPE material.

Despite the advantages of these modern growth techniques, kinetic studies in GaAs, since the early work of Nelson and Sobers[1-3] have largely been inconclusive.[14,16,22-25,29] Complete and systematic studies of the band-to-band recombination kinetics, unencumbered by the issues of interface recombination and other competing and unwanted nonradiative decay processes, have not been forthcoming, with (1) reported band-to-band recombination lifetimes spanning many orders of magnitude, from a few ns to hundreds of ns, and (2) generally inconsistent results.[7,9,11,15,22,24] There have, only lately, been scattered reports[5,7,21,30] of μs lifetimes in MBE- or OMVPE-grown GaAs heterostructures, indicating that some of these more

 0021-8979/93/128386-11$06.00

recent growth techniques are now capable of producing truly high-quality GaAs heterostructures. Recently, we have obtained samples in which band-to-band recombination lifetimes are extremely long (2.5 μs) and consistent and reproducible for many samples,[30–32] whereas samples grown only a few months earlier in the same reactor had lifetimes shorter by a factor of ~ 50. This series of samples, thus provides a unique view of superior GaAs/$Al_xGa_{1-x}As$ heterostructures, while also possibly providing some insight into the important growth and structural parameters essential for producing such high-quality GaAs structures.

In particular, we have measured room-temperature band-to-band recombination time decays in a series of OMVPE-prepared GaAs/$Al_{0.3}Ga_{0.7}As$ double heterostructures. We observe a systematic variation in decay kinetics from bimolecular to single-exponential decays for decreasing GaAs-layer thicknesses. We have also measured the lateral spatial transport (parallel to the heterointerfaces) of minority carriers in these same samples using a novel, time-resolved photoluminescence (PL) imaging technique. Our spatial transport measurements exhibit a transition from ambipolar to electron-dominated minority-carrier diffusion versus GaAs-layer thickness.

By correlating the results of these measurements, we may deduce the effects various material parameters have on the carrier dynamics and recombination kinetics. We find that not only does the GaAs purity critically affect the band-to-band recombination kinetics, as Nelson and Sobers[1–3] have shown, but also the $Al_{0.3}Ga_{0.7}As$ purity and thickness, relative to that of the GaAs, may critically affect these kinetics. Specifically, since OMVPE-prepared $Al_xGa_{1-x}As$ is, in general, not as pure as OMVPE-prepared GaAs,[24] structures with thin GaAs layers, relative to $Al_xGa_{1-x}As$ layers, may become *effectively p-type modulation doped*. These results are fully understood and our interpretation of the data is corroborated by both experiments. Moreover, from such PL kinetic and transport measurements we may *accurately* calculate interface recombination velocities in these structures. Cumulatively, we show that many factors may affect free-carrier recombination kinetics, and hence, measurements and calculations of interface recombination velocities must be carefully performed in thick structures, as we have done here. Finally, we show that previous measurements[9,12,14,15,22,25,29] of interface recombination velocities may be ambiguous since adequate measurements of the carrier dynamics have not been performed.

II. EXPERIMENT

Samples used in this study were OMVPE-prepared $Al_{0.3}Ga_{0.7}As$/GaAs/$Al_{0.3}Ga_{0.7}As$ heterostructures. $Al_{0.3}Ga_{0.7}As$ layers cladding the GaAs layer were 0.5 μm thick in all samples and p-type with a residual doping of $\sim 3\times 10^{16}$ cm^{-3}. GaAs layers were n-type with a residual doping, determined by capacitance-voltage profiling on thick GaAs layers, of $\sim 1\times 10^{15}$ cm^{-3}. GaAs-layer thicknesses ranged over almost three orders of magnitude, from 25 nm to 10 μm, and were determined through scanning electron microscope (SEM) and transmission electron microscope (TEM) measurements. Samples were grown at 750 °C on semi-insulating substrates with a thin GaAs buffer layer between the substrate and double heterostructure. To promote interfacial abruptness, all growths were performed with interruptions (30 s) at each heterointerface.

PL spectra and time-decay measurements were performed using a synchronously pumped (by a frequency-doubled cw mode-locked Nd^{3+}:YAG laser) cavity-dumped dye laser. Resulting laser pulses had a pulse width of 1.0 ps and were tunable from 6400 to 8400 Å using DCM (4-dicyanomethylene-2-methyl-6-*p*-dimethylaminostyryl-4*H*-pyran), styryl 8 (2-(4-(4-dimethylaminophenyl)-1,3-butadienyl)-3-ethylbenzothiazolium Perchlorate), and styryl 9 (2-(6-(*p*-dimethylaminophenyl)-2,4-neopentylene-1,3,5-hexatrienyl)-3-methylbenzothiazolium perchlorate) in the dye laser, with a variable repetition rate from 76 MHz to ~ 1 kHz. The laser beam was focused to a spot size of 3 mm on the sample surface, with an energy of ~ 0.1 nJ per pulse. This essentially effected an uniform "bulk" excitation (the entire layer is excited; the excitation wavelength was chosen to be near resonant with the band gap of the sample at the sample temperature, i.e., for a 10 μm sample at 300 K $\lambda_{exc} \cong 8400$ Å) with the smallest incident laser fluence possible (for the above example of the 10 μm sample this corresponds to a photon flux of $\sim 5\times 10^{11}$ cm^{-2}), while still allowing a reasonable signal-to-noise ratio for photon counting. The sample was mounted "strain-free" to the sample probe in a variable temperature (1.8–300 K) He-gas flow optical cryostat. The results presented here were all performed at room temperature. Luminescence was collected and then dispersed by a 0.85-m double-grating spectrometer and detected by a chilled RCA C31034A photomultiplier tube. PL and time-resolved measurements were performed using the time-correlated single photon counting technique, with a total system response of $\lesssim 0.5$ ns.

Carrier-transport measurements were performed by combining our time-resolved PL measurement technique with a specially designed microscope to discriminate spatially. This technique, analogous to the classical Haynes–Shockley experiment, has many unique advantages over other transport measurement techniques, in that it is (1) "contactless," (2) entirely optical, thus characterizing minority-carrier transport, (3) may distinguish between diffuse and nondiffusive motion, (4) is capable of distinguishing the transport of different particles (electrons, holes, excitons, etc.), and (5) has high time resolution. The experimental apparatus is shown in Fig. 1. The laser beam was expanded and collimated, by lenses $L1$ and $L2$, and then focused tightly onto the sample, by $L3$ inside the cryostat. Resulting spot sizes of ~ 3 μm were readily achieved. Subsequent PL was collected, by $L3$, and then refractively scanned, in a stepwise fashion, back and forth across the optic axis by rotating a thick Plexiglas block. Lenses $L4$ and $L5$ then image the PL onto the entrance slits of the spectrometer. The combination of lenses $L3$, $L4$, and $L5$ magnifies the PL image at the sample by a

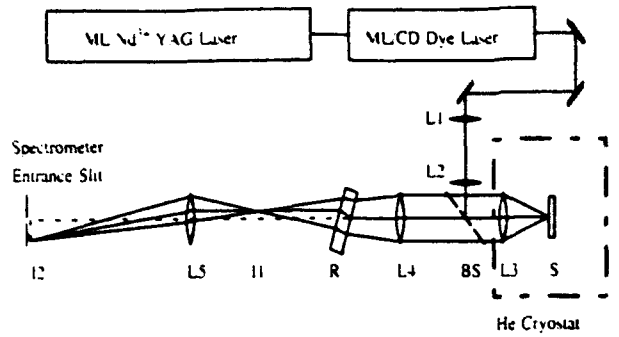

FIG. 1. Experimental design for spatially resolved PL measurements (*S* sample, *L1–L5* lenses, BS beamsplitter, *I1–I2* PL images, and *R* refractory Plexiglas block).

factor of ~20 at the entrance slit of the spectrometer, and is designed to match the spectrometer $f/\#$. The result is a high-resolution spatial image of the laser beam or the sample PL. Figure 2 shows the spatial calibration of our system. By imaging a back-lit quartz disk onto which aluminum squares 115 μm on a side and 50 μm apart were photolithographically defined and evaporated, and simultaneously focusing the laser beam onto one of the squares, we obtain the spatial calibration of the system and the system spatial resolution. It is clear that our system response is near the diffraction limit for visible light (~2.5 μm). With this system, our total system response is $\simeq 3$ μm spatially, < 1 cm^{-1} spectrally, and $\lesssim 500$ ps temporally.

III. RESULTS AND DISCUSSION

Band-to-band recombination in direct-gap semiconductors exhibits a characteristic high-energy Boltzmann tail with a characteristic carrier temperature. PL spectra of four typical samples are shown in Fig. 3. The solid line in the figure represents a fit to the high-energy side of the PL spectra with the Boltzmann expression

$$I(\lambda) = I_0 e^{-hc/\lambda kT_e}. \quad (1)$$

The resulting electronic temperatures T_e are in reasonable agreement with the lattice temperature (300 K), indicating that we are indeed measuring the recombination of thermalized carriers and band-to-band recombination. In addition, the PL peak position is identical for all bulk structures, whereas thinner structures ($\lesssim 500$ Å) show the anticipated effects of quantum confinement. We find the PL in these samples to thus be intrinsic. Further, PL in thick structures ($\gtrsim 0.1$ μm) (where quantum confinement effects are unimportant) are virtually identical with only minor variations in PL intensities.

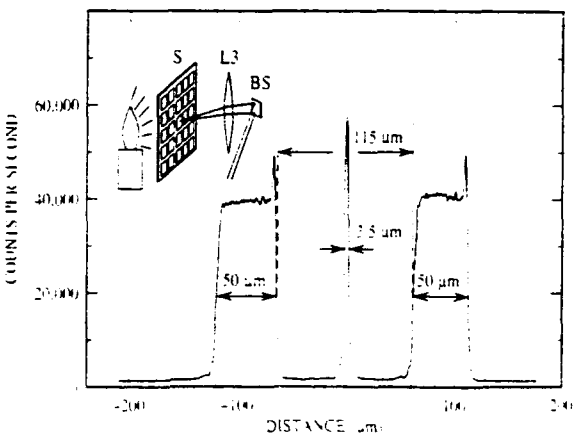

FIG. 2. Spatial calibration was obtained with a quartz disk, onto which aluminum squares (115 μm × 115 μm, and 50 μm apart) were evaporated (inset); this was then backlighted and imaged in place of the sample, while simultaneously focusing the laser to a 3.5 μm spot size on one of the aluminum squares.

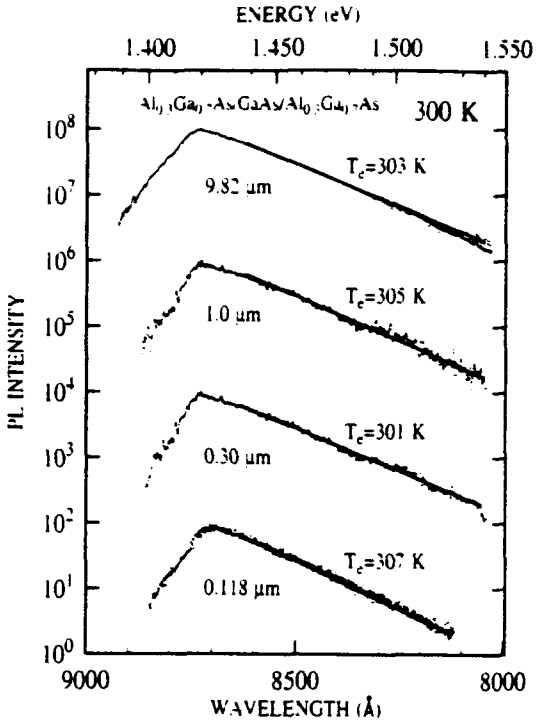

FIG. 3. Room-temperature PL spectra for GaAs/$Al_{0.3}Ga_{0.7}$-As double heterostructures with 9.82 μm, 1.0 μm, and 0.30 μm GaAs layer thicknesses. Maxwell–Boltzmann fits to the high-energy side of the PL spectra are shown as solid lines. These fits yield electronic temperatures identical to the lattice temperature.

A. Recombination kinetics

Figure 4 shows the room-temperature PL time decays for samples with GaAs-layer thicknesses of 9.82, 1.00, 0.30, and 0.118 μm. In contrast to the corresponding PL spectra, there is a large variation in decay kinetics and lifetimes for these samples. These decay kinetics were fit to the rate equation for band-to-band recombination[2–4,8,10]

$$\frac{dp}{dt} = -B(np + n_0 p - p_0 n) - \frac{p}{\tau_{nr}} - \frac{S_1 + S_2}{d} p, \quad (2)$$

where $p(n)$ is the photoexcited hole (electron) density, $p_0(n_0)$ is the built-in hole (electron) density, τ_{nr} represents

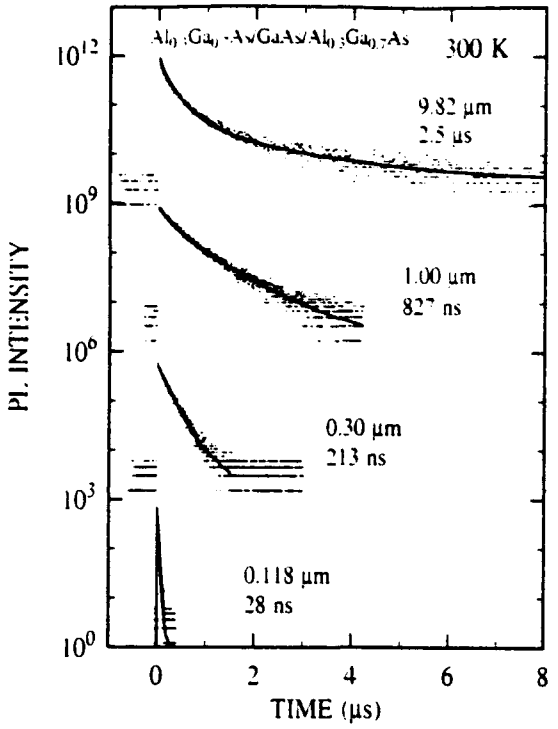

FIG. 4. Decay kinetics for $GaAs/Al_{0.3}Ga_{0.7}As$ double heterostructures with 9.82 μm, 1.00 μm, 0.30 μm, and 0.118 μm GaAs layer thicknesses at room temperature. Lifetimes shown represent the $1/e$ constant for the exponential tails of the decays, and were obtained through least-squares fits of the data to Eq. (3).

the contributions of bulk nonradiative decay to the overall decay rate of minority carriers, d is the GaAs layer thickness (the distance between heterointerfaces), and S_1 and S_2 are the interface recombination velocities at each heterointerface. B is the bimolecular decay constant (2×10^{-10} cm^3/s).[3] This equation represents the decay kinetics in n-type GaAs where holes are minority carriers. For p-type GaAs the decay kinetics are described by the same equation but with the roles of electrons and holes reversed. Equation (2) may lead to several different types of decay kinetics, including (1) bimolecular decays in which $n=p$ and $n,p>n_0,p_0$ and the last two terms in Eq. (2) are small, (2) single exponential decays in which either the last two terms in Eq. (2) dominate over the first term and/or $p_0>p$ or $n_0>n$, and (3) a combination of exponential and bimolecular decays.

The general solution of the rate equation, Eq. (2) is

$$p(t)=\frac{Ae^{-t/\tau}}{1+C[1-e^{-t/\tau}]}, \tag{3}$$

where

$$\frac{1}{\tau}=\frac{1}{\tau_{nr}}+\frac{2S}{d}+B(n_0+p_0). \tag{4}$$

The constant C ($C=Bp_i\tau$ and $A=p_i$, where p_i is the initial photoexcited minority-carrier density) represents the relative importance of the bimolecular decay to the overall decay rate. PL decays are rigorously exponential for $C=0$, whereas the decays become increasingly bimolecular for larger C. The data shown in Fig. 4 were fit using Eq. (3) with A, C, and τ as adjustable parameters. The lifetimes, shown in Fig. 4, are those obtained from these fits and represent the exponential decay constant of the decay tail (the more than three decade decay kinetics measured here confirm that these decay kinetics have truly become exponential at long times). In particular, the 2.5 μs decay observed for our 9.82 μm sample represents the sum of all monomolecular rates as shown in Eq. (4). For relatively high-purity material and moderate photoexcitation ($n=p\gtrsim n_0, p_0\simeq0$), the initial decay is bimolecular, but as the free carriers recombine the photoexcited carrier density will decrease and eventually become less than the built-in carrier densities (n_0, p_0), thereby yielding exponential decays. Thus, decay kinetics which initially are bimolecular will in reality (since S, τ_{nr}, n_0, and p_0 are never zero), eventually, and always, become exponential. Thus, under the experimental conditions mentioned above, these fits lead to well-defined and mutually comparable decay lifetimes.

We find that lifetimes obtained in these samples decrease with decreasing GaAs-layer thickness. This is readily understood and modeled by the rate equations and is generally[2,3,10] identified with the effects of nonradiative interface recombination, $[(S_1+S_2)/d]$. Moreover, the results show (Fig. 4), that these decay kinetics gradually change from highly nonexponential, bimolecular decays to rigorously single-exponential decays for decreasing GaAs-layer thicknesses. Importantly, although the minority-carrier decay kinetics depend upon the relative carrier densities, and thus may be influenced by both minority- and majority-carrier transport, these effects should be negligible for our experimental conditions for PL kinetics measurements (defocused laser spot, $\simeq3$ mm in diameter). The thickness dependence of these decay lifetimes also suggests that bulk nonradiative decay in these samples is negligible. Low-temperature measurements also suggest $\tau_{nr}\gtrsim50$ μs.[33–37] The systematic change in the form of the decay kinetics versus GaAs-layer thickness for identical experimental conditions is not, however, simply understood with the rate equations alone. Thus, we find that all decays in all samples eventually become exponential at long times, as they must, and that the thick structures are dominated at long times by nonradiative interface recombination, whereas the thinner structures (<1 μm) are dominated by majority-carrier recombination (Bn_0).

B. Minority-carrier transport

Despite our assertions concerning the effects of carrier transport on the decay kinetics, we have measured minority-carrier transport in an effort to gain further insight into the kinetics of free-carrier recombination, and the observed systematics. We have measured the spatial transport of minority carriers using the novel PL imaging technique mentioned above. Since the PL intensity at each spatial point reflects the minority-carrier density at that point, the spatial profile of minority carriers versus time after the laser pulse is obtained by measuring the time-

resolved and spatially resolved PL distributions. (Here, the long μs lifetimes and intense room-temperature PL observed in our samples, compared to the $\sim$1 ns lifetimes and weak PL observed in "typical" GaAs structures enable these time-resolved studies.) If the minority-carrier transport is diffusive, and the diffusion coefficient and lifetime are independent of carrier density, then the carrier transport is governed by the traditional diffusion equation.[38,39] The solution of the cylindrically symmetric, two-dimensional diffusion equation

$$\frac{\partial p(\mathbf{r},t)}{\partial t} = D\nabla^2 p(\mathbf{r},t) - \frac{p(\mathbf{r},t)}{\tau} \tag{5}$$

gives the minority-carrier distribution versus time t, and the position in the x-y plane, $\mathbf{r}$, as

$$p(\mathbf{r},t) = \frac{\Delta_0^2 p_0}{4Dt+\Delta_0^2} \exp\left(\frac{-r^2}{4Dt+\Delta_0^2}\right) \exp\left(-\frac{t}{\tau}\right), \tag{6}$$

where D is the diffusion coefficient and Δ_0 is the initial minority-carrier spatial distribution characteristic width. Equation (6) shows that the decay kinetics affect only the overall intensity of the PL, whereas the spatial diffusion of carriers affects the spatial width of the carrier distribution and hence the PL image. Additionally, the spatial profile of the PL should be Gaussian. The spatial diffusion of minority carriers may be further quantified by their characteristic widths, the full width at half maximum (FWHM) of the Gaussian distributions, squared:

$$\Delta^2(t) = [16\ln(2)]D_a t + 4\ln(2)\Delta_0^2. \tag{7}$$

Equation (7) shows that the $(\text{FWHM})^2$ increases linearly with time with a slope of $16\ln(2)D_a$, thus allowing determination of the diffusion coefficient.

Figures 5 and 6 show the PL spatial distribution versus time obtained from samples with GaAs-layer thicknesses of 9.82 and 0.30 μm, respectively. Clearly, the PL, and hence minority-carrier spatial distribution expands significantly during the decay lifetime, and the spatial distributions are approximately Gaussian, as indicated by the fits to the data with Eq. (6), shown as solid lines. This is possibly indicative of diffusive carrier transport. Comparison of Figs. 5 and 6 evidences remarkable differences. The minority-carrier distribution for the 0.30 μm structure expands $\sim$three times further than the 9.82 μm structure in one-third the time (300 μm in 800 ns vs 120 μm in 1.8 μs). Thus, minority carriers are evidently moving *$\sim$nine times faster*. As a means of quantifying this behavior and extracting diffusion constants from the data, Fig. 7 shows the squared FWHM obtained by fitting the data to Eq. (6) versus time. The data are clearly not linear versus time for samples, but do exhibit unmistakable systematics versus GaAs-layer thickness.

For relatively high-purity samples, such as these, minority-carrier diffusion should be ambipolar. Physically, this reflects the fact that charge separation cannot occur due to the Coulomb interaction between carriers. As a result, both species of carriers, electrons and holes, must move together. In effect, the faster moving electrons are

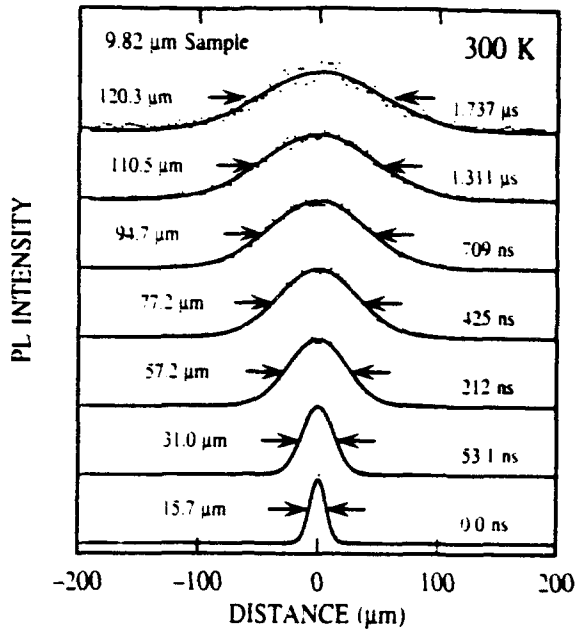

FIG. 5. Room-temperature time-resolved PL distributions for the 9.82-μm-thick double heterostructure. Solid lines represent Gaussian fits to data, with FWHM vs time shown.

forced, by the Coulomb interaction, to "drag" the heavier holes along with them, yielding a slower moving neutral gas of carriers.[40] The diffusion coefficient of this neutral gas of carriers may be expressed as[39]

$$D_a = \frac{[(n+n_0)+(p+p_0)]D_e D_h}{(n+n_0)D_e+(p+p_0)D_h}, \tag{8}$$

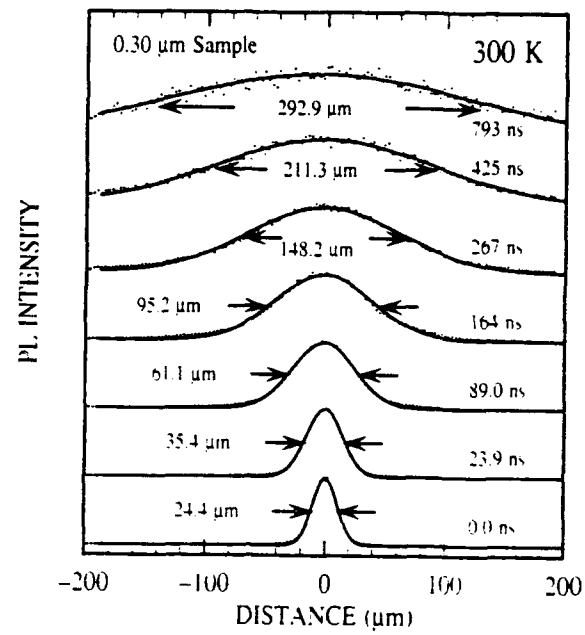

FIG. 6. Room-temperature time-resolved PL distributions for the 0.30-μm-thick double heterostructure. Solid lines represent Gaussian fits to data, with FWHM vs time shown.

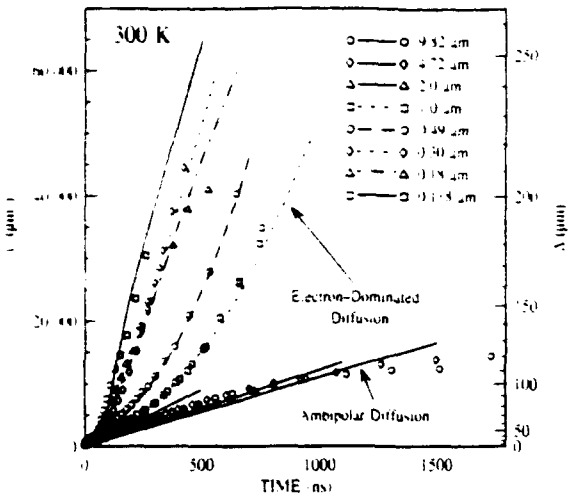

FIG. 7. Room-temperature transport results obtained from Gaussian fits to time-resolved PL spatial distributions. The Gaussian PL FWHM squared is plotted vs time, $\Delta(t)^2$, for all GaAs/$Al_{0.3}Ga_{0.7}As$ double heterostructures; lines represent fits to the data.

where D_e(D_h) is the electron (hole) diffusion constant. The ambipolar diffusion constant is thus related to the electron and hole diffusion constants and the relative, time-dependent densities of each species of carrier. For high-purity material ($n_0, p_0 \simeq 0$), $D_a \simeq D_h$. D_a may thus be carrier density dependent, contrary to the assumptions used in solving the diffusion equation. Our decay kinetics in thicker samples ($\gtrsim 0.5\ \mu m$) are also density dependent, leading to bimolecular decays. Consequently, Eqs. (5) and (6) do not completely and accurately model the dynamics in our structures. As an approximation, we have chosen to include the density dependence of the decay kinetics in the diffusion coefficient, Eq. (8), and neglect any effect these complications may have on the spatial PL profile. A more rigorous model should include a bimolecular decay term in Eq. (5); however, with this additional complexity, Eq. (5) cannot be solved analytically. However, this more complex diffusion equation may be solved numerically, leading to spatial minority-carrier profiles which are very nearly Gaussian.[38] Indeed, we find that the Gaussian fits to the spatial PL profiles are quite good. Importantly, the time dependence of the minority-carrier densities, n and p, may lead, under appropriate circumstances, to time-dependent diffusion constants. Therefore, our detailed decay kinetics measurements provide the means to model the observed minority-carrier transport kinetics.

With this simple model, the results of our PL spatial expansion measurements may be analyzed. The solid lines in Fig. 7 are fits to the spatial expansion data using Eqs. (7) and (8), together with the minority-carrier decay kinetics shown in Fig. 4 (here we have been careful to measure the decay kinetics and transport under identical excitation conditions: laser power and wavelength. In particular the transport was measured at low laser powers, typically a fraction of a μW average power. Importantly, we do not observe any power dependence to the observed minority-carrier transport at these temperatures, and high excitation densities only affect the initial portion of the PL decay kinetics, and the long-time tail is identical to the low excitation density result.) Fits to the data in Fig. 7 are quite good, and were obtained treating p_0, D_e, and D_h as adjustable parameters. The built-in electron density n_0 was estimated from the capacitance-voltage measurements mentioned above, whereas the photoexcited carrier densities are determined by the laser power and spot size. We find that the "effective" built-in hole density in the GaAs layer increases roughly inversely with the GaAs-layer thickness and can reach densities of approximately 1×10^{18} cm^{-3}. Moreover, since $n_0 p_0 =$ constant, as p_0 increases, n_0 must correspondingly decrease.

The physical interpretation of minority-carrier spatial diffusion may now be understood. The GaAs layer is inherently n type, whereas the $Al_{0.3}Ga_{0.7}As$ layers are p type, 0.5 μm thick, with a residual doping level about one order of magnitude higher than in the GaAs. The depletion width at each p-n junction in the GaAs is approximately 0.5 μm,[41] thus, for GaAs-layer thicknesses less than about 1 μm, total depletion (two interfaces), holes may begin to accumulate in the GaAs layer, from the $Al_{0.3}Ga_{0.7}As$ layers. Thus, as GaAs-layer thicknesses decrease, they may change from inherently n type to effectively p type, with the hole density increasing with the inverse GaAs-layer thickness, with a corresponding change in minority carriers from holes to electrons. This results in slow, ambipolar diffusion in the thick structures, and faster, electron-dominated diffusion in the thin structures ($\lesssim 1\ \mu m$). These results, with the known material parameters for these structures, are analogous to modulation doping,[42] wherein majority-carriers in the active, conducting layer originate from either intentional or residual dopants in a different layer of the structure. Physically, this *effective p-type modulation doping* relaxes the constraints of the Coulomb interaction on the ambipolar diffusion. The electrons move in a higher density sea of holes, so charge neutrality is preserved without the constraints of ambipolar transport.

The nonlinear time dependence of Δ^2 in Fig. 7 results from the time dependence of the photoexcited carrier density. Initially, the photoexcited carrier density in our experiments may be as high as $\sim (2\text{–}3) \times 10^{18}$ cm^{-3} (due to the small laser spot size), which is much larger than the built-in carrier density in the GaAs layer for all of our samples. However, these carriers decay, mostly radiatively, and their characteristic lifetime decreases with the GaAs-layer thickness. The initial slope is indicative of ambipolar diffusion, and, for thin samples ($\lesssim 0.5\ \mu m$), the asymptotic slope is indicative of electron-dominated diffusion. We find that the time decay, after the "delta-function-like" excitation pulse, at which the carrier transport changes from ambipolar to electron-dominated diffusion decreases with GaAs-layer thickness. This characteristic time is determined by the time delay at which the photoexcited carrier and built-in carrier density are approximately equal. Thus, the change in slope of the data for each structure in Fig. 7 occurs at earlier times after pulsed photoexcitation for decreasing GaAs-layer thicknesses, due to the increas-

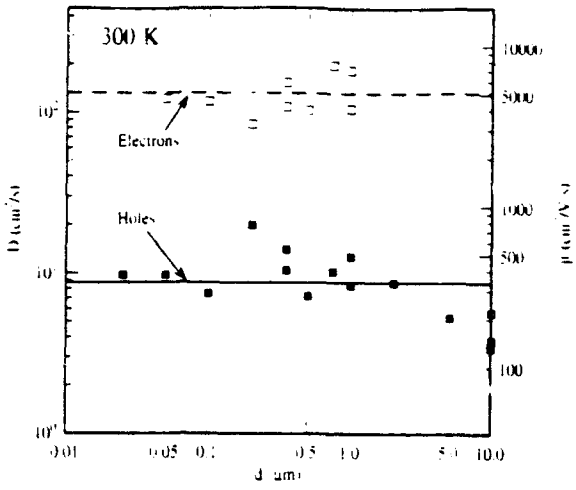

FIG. 8. Room-temperature electron and hole diffusion constants vs GaAs layer thickness obtained from analysis of data in Fig. 7. Corresponding mobilities were obtained using nondegenerate Einstein relation. Horizontal lines represent reported electron and hole mobilities obtained electrically in high-purity-n- and p-type GaAs (see Refs. 51 and 52).

ing hole density accompanying the p-type modulation doping. This change in slope is indicative of a transition from ambipolar to free-electron-dominated diffusion. Earlier, we noted a factor of ~nine difference in the observed transport in our 9.82 and 0.30 μm samples. This results primarily from the difference in minority-carrier mass in these samples, holes versus electrons, respectively.

These results may also be compared and contrasted with electrical transport measurements in GaAs. These electrical measurements quantify the majority-carrier transport properties and are usually reported as mobilities, whereas, in contrast, optical measurements of carrier transport are dominated by the minority carriers. Electrical measurements of majority-carrier electron transport in n type GaAs may thus be compared to optical measurements of minority-carrier electron transport in p-type GaAs, and vice versa. Using the nondegenerate Einstein relation[41]

$$\mu = \frac{D|e|}{kT}, \tag{9}$$

our measurements of carrier diffusion can be correlated with electrical transport measurements. The results of our fits to the data of Fig. 6 using Eqs. (7) and (8) are shown in Fig. 8, yielding average electron and hole mobilities of ~5000 cm^2/V s and ~350 cm^2/V s, respectively. Typical results for electron and hole mobilities, obtained electrically,[41-52] are shown as horizontal lines in Fig. 8. Our results are therefore reasonably consistent with electrical measurements of mobilities reported in the literature. In addition, 300 K Hall measurements in our 9.82 μm structure yield electron mobilities of 5800 cm^2/V s, in excellent agreement with our optical results.

An important quantity characterizing minority-carrier transport is the minority-carrier diffusion length, $L_D = \sqrt{D\tau}$. This may be calculated as a by-product of our minority-carrier kinetic and transport measurements. Table I shows the obtained values of lifetime, diffusion coefficient, mobility, and diffusion length for these samples. These diffusion lengths are also shown in Fig. 9. The decrease in L_d as d decreases results from the decrease in minority-carrier lifetime due to modulation doping. L_d is large enough in all samples such that the carriers may scatter from both heterointerfaces many times during their lifetimes (especially for the thin structures), indicative of high heterointerfacial quality. Our results indicate that minority carriers scatter from heterointerfaces up to ~200 times during their lifetime, thus proving the exceptional quality of these heterointerfaces.

TABLE I. Summary of experimental results vs GaAs-layer thickness.

GaAs thickness (μm)	Lifetime (ns)	Diffusion constant (cm^2/s)	Mobility (cm^2/V s)	Diffusion length (μm)	Interface scattering events
9.82	2511.3	5.7	219.7	37.8	3.9
4.72	1181.7	5.3	205.0	25.0	5.3
2.00	1117.5	8.7	335.8	31.1	15.6
1.00	827.7	183.7	7104.9	123.3	123.3
0.49	297.3	103.4	3997.9	55.43	113.1
0.30	213.2	108.1	4182.4	48.0	160.0
0.15	100.1	84.2	3256.4	29.0	193.5
0.118	28.1	116.3	4496.9	18.1	153.1
0.0575	3.5	121.3	4692.3	6.5	113.4
0.0310	1.7	9.7	374.5	1.3	41.3

C. Carrier dynamics and recombination kinetics

We may now correlate these minority-carrier diffusion dynamics with the decay kinetics to verify consistency. First, consider our thickest structure, the 9.82 μm structure. We find the decay kinetics are bimolecular, whereas

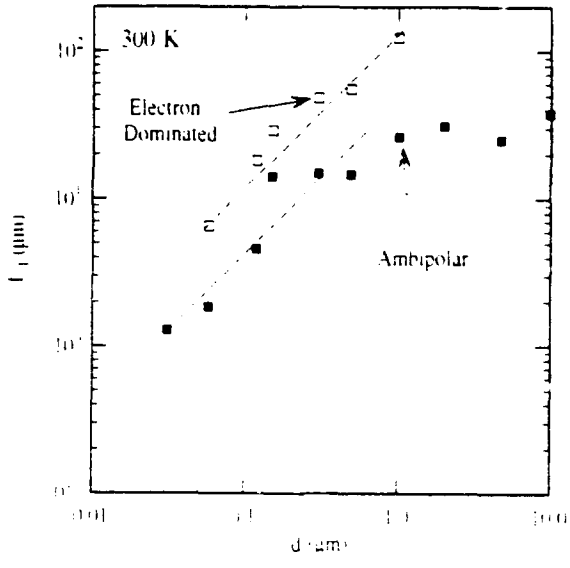

FIG. 9. Room-temperature diffusion lengths obtained from our transport and time-decay results for all GaAs/Al$_{0.3}$Ga$_{0.7}$As double heterostructures. Dashed lines represent a slope of 1, and are indicative of majority-carrier limited lifetimes, and hence diffusion lengths.

the diffusion is ambipolar and slow. For this structure the effects of "p-type modulation doping" mentioned above are negligible since the GaAs layer thickness is larger than twice the depletion width for a single p-n junction. Therefore, the rate equation for the decay kinetics, Eq. (2), may be simplified and reduced to

$$\frac{dp}{dt} = -Bp^2 - \frac{p}{\tau_{nr}} - \frac{S_1+S_2}{d}p, \tag{10}$$

yielding initial bimolecular decays for the minority holes and an exponential tail governed by interface recombination. The corresponding ambipolar diffusion equation, Eq. (8), becomes

$$D_a = \frac{2D_eD_h}{D_e+D_h}, \tag{11}$$

with the diffusion dominated by the slow, diffusing holes, in agreement with our data.

Now consider one of the thinner structures, the 0.30 μm structure. We find the decay kinetics are rigorously exponential, whereas the diffusion is initially slow but drastically increases after about 100 ns. In this case the effects of effective p-type modulation doping are very important. (The built-in hole density p_0 is large.) The rate equation for the decay kinetics for minority carriers, now electrons, may be simplified and reduced to

$$\frac{dp}{dt} = -Bp_0n - \frac{n}{\tau_{nr}} - \frac{S_1+S_2}{d}n, \tag{12}$$

yielding rigorously exponential decays with a lifetime dominated by the term Bp_0. The corresponding simplification of the carrier diffusion equation yields

$$D_a \sim D_e. \tag{13}$$

Thus, the diffusion at late times is electron dominated and fast, again consistent with our data.

D. Interface recombination velocity

Before any calculations of interface recombination velocities are made, the validity of our phenomenological treatment of interface recombination must be confirmed. The term $[(S_1+S_2)/d]$ in the recombination rate equation represents the nonradiative decay of carriers at each heterointerface. This simple phenomenological term arises from the boundary conditions to the solution of the *classical* diffusion equation, yielding a term

$$\left(\frac{d^2}{\pi^2 D}+\frac{d}{S_1+S_2}\right)^{-1}$$

(actually an approximation accurate within 5%).[10] By assuming that the distance between heterointerfaces is small compared to the minority-carrier diffusion coefficient, $(S_1-S_2) \ll \pi^2 D/d$, this may be approximated as $(S_1+S_2)/d$. Essentially this approximation holds in the limit of thin structures (compared to the diffusion length), whereas the term $d^2/\pi^2 D$ becomes important in thick structures (comparable to the diffusion length). The results shown in Table I confirm this approximation. We find that the smallest

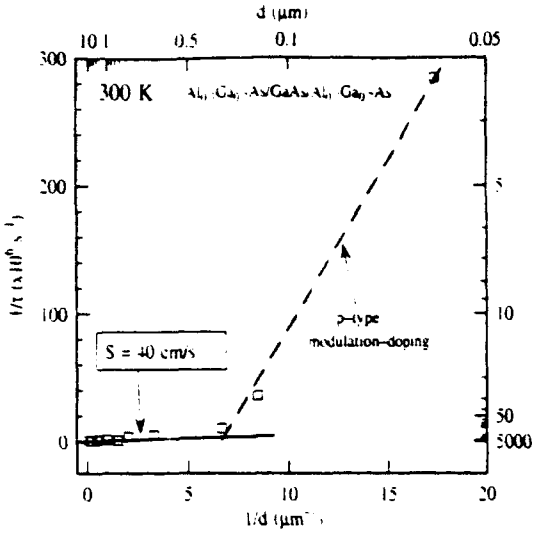

FIG. 10. Plot of the room-temperature lifetimes obtained from fits to the decay kinetics with Eq. (3) vs inverse GaAs layer thickness. Dashed line represents decay kinetics dominated by p-type modulation doping, whereas solid line represents surface recombination. Linear fits to the data for thick structures yield an interface recombination velocity of $\simeq$40 cm/s.

obtained value of $(\pi^2 D/d)$ is $\simeq$43 000 cm/s (in the 9.82 μm structure). So, as long as (S_1+S_2) is much less than 43 000 cm/s, this approximation is valid.

In the limit of thin structures, i.e., the quantum limit, this phenomenological picture of interface recombination is clearly not sufficient. Here, the carriers, actually excitons, are affected by the potential barriers and any interfacial decay at the same time. Thus, d becomes a meaningless quantity. The dynamics of carrier transport influenced by quantum confinement *cannot* be modeled classically. Further, lifetime comparisons between bulk and quantum well systems are meaningless to calculations of interface recombination velocities.[25] An adequate model of interface recombination in the quantum limits does not, to our knowledge, exist, and the plethora of reports in the literature[12-15,17,53,54] of interface recombination velocities in quantum wells are without foundation.

With our room-temperature decay kinetics and lifetime measurements in these structures, together with our minority-carrier transport results, we may calculate the interface recombination velocity for our samples. Equation (4) shows that by plotting the inverse lifetime versus $1/d$, the GaAs-layer thickness, the average interface recombination velocity $[S=\frac{1}{2}(S_1-S_2)]$ may be calculated from the slope of the *linear* fit. In Fig. 10, our lifetimes are plotted in this manner, and the data clearly do not lie on a straight line. The effective p-type modulation doping which is important for structures thinner than 1 μm, causes the first term on the right-hand side of Eq. (4) to become dominant, with p_0 now varying inversely with GaAs-layer thickness. The linear behavior (dashed line) observed for thin structures is therefore determined by this thickness-dependent term, yielding a different slope than the lifetime results for samples dominated by interface recombination (solid line). Equation (4) may lead to three different cases: (1) Bp_0 dominant, leading to the steep slope shown in Fig.

10 as a dashed line. (2) S dominant, leading to the shallow slope (in our case) depending on the magnitude of the nonradiative interface recombination, and (3) τ_{nr} dominant, leading to lifetimes independent of GaAs-layer thickness. Consequently, the interface recombination velocity should only be calculated from the measured lifetimes for the thick structures ($d \gtrsim 1$ μm).

The longest band-to-band recombination lifetimes reported by Nelson and Sobers,[2,3] were for a 16-μm LPE-grown $Al_{0.3}Ga_{0.7}As/GaAs/Al_{0.3}Ga_{0.7}As$ double heterostructure. The kinetics were exponential over four decades with a lifetime of 1.3 μs. In contrast, decay kinetics for our thickest structure, 9.82 μm, were bimolecular with an asymptotic lifetime of ~ 2.5 μs. Hence, our results are effectively $\simeq$ four times longer than those of Nelson and Sobers.[2,3] Further, their reported interface recombination velocities are somewhat ambiguous. As noted earlier, LPE-grown heterostructures have graded interfaces, so carriers do not see a well-defined distance between the two heterointerfaces. This is a flaw in their otherwise excellent experiments.

We have shown here that the kinetics of band-to-band recombination in GaAs structures are very complicated. So while there are reported lifetimes as long as 14 μs in some GaAs structures,[21] no complete study of the kinetics has been attempted. Our detailed and systematic study demonstrates that a single lifetime measurement is not sufficient to fully characterize the recombination kinetics of a sample. Moreover, measurements of lifetimes and subsequent reports of interface recombination velocities in thin structures, such as quantum wells and superlattices, are entirely meaningless. There are many effects such as the reduced dimensionality of these structures, which significantly alter the oscillator strengths and hence recombination lifetimes. Further, the concept of "distance between heterointerfaces," which is critical to calculations of interface recombination velocities, becomes ill-defined for quantum structures.

E. Photon recycling

Some have suggested that the band-to-band recombination kinetics in thick GaAs structures may be significantly affected by photon recycling (PR).[2,3,55–57] This resonant radiative reabsorption and subsequent reemission of photons may cause a lengthening of the observed lifetime, and increases in importance as the GaAs-layer thickness increases. The effects of PR are quite complicated and the possibly drastic change in decay kinetics are critically dependent on experimental and sample geometry. Because of the thickness dependence of several factors which may affect the recombination kinetics, the effects of PR are extremely difficult to isolate. PR is, however, generally recognized to be negligible for GaAs-layer thicknesses less than the characteristic absorption length.

Here, we consider the importance of PR in our samples, especially our thickest samples ($\gtrsim 1$ μm). Samples with GaAs-layer thicknesses less than ~ 1 μm are unambiguously unaffected by PR. Because PR depends critically on the absorption length at each wavelength, PR manifests itself as a red shift in the PL spectra for increasing GaAs-layer thicknesses.[58] We have not observed any shift or differences in the PL spectra for samples with GaAs thickness from 0.1 to 10.0 μm, as is evidenced in Fig. 3. PR should also affect our measurements of minority-carrier transport, leading to anomalously high results for the minority-carrier diffusivities and corresponding mobilities. Our minority-carrier transport results are well understood and in excellent agreement with electrical mobility measurements. Consequently, we find no evidence for PR in these samples. Additionally, lifetime measurements at low temperatures in thin samples ($\lesssim 1$ μm), where PR is clearly and unambiguously negligible, yield lifetimes up to 15 μs.[31] Thus, there is a clearcut case for long lifetimes in samples where PR is completely negligible. Finally, our kinetic measurements were performed with a defocused laser beam (~ 3 mm), and the backscattered PL was detected only over a narrow range of this spot (200 μm spectrometer slits and $\sim 4\times$ magnification of the PL image), thus, excluding possible detection and measurement of PR effects in the direction parallel to the heterointerfaces. Thus, not only do we find no evidence for PR in these samples, we find that all of these results, taken together, definitively exclude the possibility of PR from affecting our measured results.

F. Shockley–Read–Hall recombination

Ahrenkiel *et al.*[57] have shown, quite convincingly, that Shockley–Read–Hall recombination at impurities may be dominant in some structures under some excitation conditions. This recombination mechanism involves the nonradiative recombination of free carriers at midgap or other defect levels. They find anomalous decay kinetics at high excitation densities in moderately doped structures ($\gtrsim 10^{17}$ cm^{-3}), wherein the effective observed lifetime becomes the sum of majority- and minority-carrier lifetimes. They thus observe an intensity-dependent increase in lifetimes with injection level, and model these effects as resulting from the saturation of recombination centers. In our experiments we find these effects are entirely and completely negligible for several reasons. First, our samples were of relatively high purity (~ 100 times more pure than those of Ahrenkiel *et al.*[57]). Second, our optical injection levels were $\gtrsim 150$ times smaller than their smallest pump powers (3 mm spot size and 0.1 nJ per pulse versus 1 mm spot size and $\cong 5$ nJ per pulse). Under these experimental conditions, even they do not observe the effects of Shockley–Read–Hall recombination. Thus, our room-temperature decay kinetics are truly intrinsic, and not defect mediated. Further, our measured lifetimes reflect the true minority-carrier lifetime.

IV. SUMMARY

In summary, we have shown that the room-temperature decay kinetics and spatial transport of carriers in our $GaAs/Al_{0.3}Ga_{0.7}As$ double heterostructures are well understood. We have observed decay kinetics which systematically change from bimolecular to exponential versus time and decreasing GaAs-layer thickness. We find all minority-carrier transport to be diffusive, and in agreement

with corresponding electrically determined mobilities. We observe carrier distributions that expand macroscopically from ~ 3 μm to over 300 μm FWHM. Further, we find differences in the minority-carrier diffusion among the samples, which are interpreted and understood in terms of the carrier kinetics and the effects of *effective p-type modulation doping*. Carrier diffusion in thick structures is ambipolar, whereas in thin structures ($\lesssim 0.5$ μm) it is time dependent, becoming electron dominated, and much faster (by a factor of ~ 10) than in the thicker structures. Diffusion lengths of $\gtrsim 100$ μm in these samples indicate that carriers may scatter many times from both heterointerfaces during their lifetime, indicative of superior heterointerfacial quality. The decay kinetics and spatial expansion of carriers qualitatively and quantitatively agree and concur with electrical measurements of carrier transport. We find no evidence for the effects of photon recycling in our results, and assert that these effects are negligible in our samples. Further, we have shown that measurements of interface recombination velocities may be ambiguous if the carrier dynamics and recombination kinetics are not studied in detail, as we have done here. Our resulting interface recombination velocity ($\simeq 40$ cm/s) and lifetimes (2.5 μs for the 9.82 μm structure) are among the *lowest* and *longest*, respectively, for any GaAs/$Al_xGa_{1-x}As$ structure to date.

ACKNOWLEDGMENTS

We thank G. A. Northrop, L. M. Smith, and J. Martinsen for useful discussions and assistance in computer aided data acquisition. The IBM work was supported, in part, by the Office of Naval Research, under Contract Nos. N00014-85-C-0868, N00014-90-C-0077, and N00014-91-J-1697. The work at Sandia was supported by the U.S. Department of Energy under Contract No. DE-AC04-76DP00789.

[1] R. J. Nelson, J. Vac. Sci. Technol. **15**, 1475 (1978).
[2] R. J. Nelson and R. G. Sobers, Appl. Phys. Lett. **32**, 761 (1978).
[3] R. J. Nelson and R. G. Sobers, J. Appl. Phys. **49**, 6103 (1978).
[4] G. Lasher and F. Stern, Phys. Rev. **133**, A553 (1964).
[5] E. Yablonovitch, T. J. Gmitter, and R. Ghat, Phys. Rev. Lett. **61**, 2546 (1988).
[6] L. M. Smith, D. J. Wolford, R. Venkatasubramanian, and S. K. Ghandi (unpublished).
[7] E. Yablonovitch, R. Bhat, J. P. Harbison, and R. A. Logan, Appl. Phys. Lett. **50**, 1197 (1987).
[8] H. C. Casey, Jr. and F. Stern, J. Appl. Phys. **47**, 631 (1976).
[9] G. W. 'tHooft and C. van Opdorp, Appl. Phys. Lett. **42**, 813 (1983).
[10] G. W. 'tHooft and C. van Opdorp, J. Appl. Phys. **60**, 1065 (1986).
[11] P. Dawson and K. Woodbridge, Appl. Phys. Lett. **45**, 1227 (1984).
[12] B. Sermage, M. F. Pereira Jr., F. Alexandre, J. Beerens, R. Azoulay, C. Tallot, A. M. Jean-Louis, and D. Meichenin, J. Phys. (Paris) Colloq. **C5**, 135 (1987).
[13] K. Fujiwara, A. Nakamura, Y. Tokuda, T. Nakayama, and M. Hirai, Appl. Phys. Lett. **49**, 1193 (1986).
[14] T. J. deLyon, J. A. Kash, S. Tiwari, J. M. Woodall, D. Yan, and F. H. Pollak, Appl. Phys. Lett **56**, 2442 (1990).
[15] H. Iwata, H. Yokoyama, M. Sugimoto, N. Hamao, and K. Onabe, Appl. Phys. Lett. **54**, 2427 (1989).
[16] J. P. Salerno, E. S. Koteles, J. V. Gormley, B. J. Sowell, E. M. Brody, J. Y. Chi, and R. P. Holmstrom, J. Vac. Sci. Technol. B **3**, 618 (1985).
[17] D. Bimberg, J. Christen, A. Werner, M. Kunst, G. Weimann, and W. Schlapp, Appl. Phys. Lett. **49**, 76 (1986).
[18] S. Munnix, R. K. Bauer, D. Bimberg, J. S. Harris Jr., R. Köhrbrück, E. C. Larkins, C. Maierhofer, D. E. Mars, and J. N. Miller, J. Vac. Sci. Technol. B **7**, 704 (1989).
[19] R. Köhrbrück, S. Munnix, D. Bimberg, E. C. Larkins, and J. S. Harris, Jr. Appl. Phys. Lett. **54**, 623 (1989).
[20] A. Ourmazd, D. W. Taylor, J. Cunningham, and C. W. Tu, Appl. Phys. Lett. **62**, 933 (1989).
[21] J. M. Olson, R. K. Ahrenkiel, D. J. Dunlavy, B. Keyes, and A. E. Kibbler, Appl. Phys. Lett. **55**, 1208 (1989).
[22] R. K. Ahrenkiel, D. J. Dunlavy, J. Benner, R. P. Gale, R. W. McClelland, J. V. Gormley, and B. D. King, Appl. Phys. Lett. **53**, 598 (1989).
[23] H. Matsueda and K. Hara, Appl. Phys. Lett. **55**, 362 (1989).
[24] L. W. Molenkamp and H. F. van't Blik, J. Appl. Phys. **64**, 4253 (1988).
[25] A. Hariz, P. D. Dapkus, H. C. Lee, E. P. Menu, and S. P. DenBaars, Appl. Phys. Lett. **54**, 635 (1989).
[26] K. Wada, A. Kozen, Y. Hasumi, and J. Temmyo, Appl. Phys. Lett. **54**, 436 (1989).
[27] D. Bimberg, J. Christen, T. Fukunaga, H. Nakashima, D. E. Mars, and J. N. Miller, J. Vac. Sci. Technol. B **5**, 1191 (1987).
[28] R. C. Miller, R. D. Dupuis, and P. M. Petroff, Appl. Phys. Lett. **44**, 508 (1984).
[29] V. M. Andreev, A. M. Allakhverdiev, V. D. Rumyantsev, O. M. Fedorova, and S. S. Shamukhamedov, Sov. Phys. Semicond. **19**, 1121 (1985).
[30] G. D. Gilliland, D. J. Wolford, T. F. Kuech, J. A. Bradley, C. F. Tsang, and J. Martinsen (unpublished).
[31] D. J. Wolford, G. D. Gilliland, T. F. Kuech, L. M. Smith, J. Martinsen, J. A. Bradley, C. F. Tsang, R. Venkatasubramanian, S. K. Ghandi, and H. P. Hjalmarson, J. Vac. Sci. Technol. B **9**, 2369 (1991).
[32] D. J. Wolford, G. D. Gilliland, T. F. Kuech, J. Martinsen, C. F. Tsang, J. A. Bradley, and H. P. Hjalmarson, *Proceedings of the 18th International Symposium on Gallium Arsenide and Related Compounds, Seattle, WA, Sept. 9–12, 1991*, Institute of Physics Conference Series 120, edited by G. B. Stringfellow (IOP, London, 1991), p. 401.
[33] G. D. Gilliland, D. J. Wolford, T. F. Kuech, and J. A. Bradley, Phys. Rev. B **43**, 14251 (1991).
[34] G. D. Gilliland, D. J. Wolford, T. F. Kuech, and J. A. Bradley, in *Proceedings of the 20th International Conference on the Physics of Semiconductors*, Thessaloniki Greece, edited by S. Pantelides (World Scientific, Singapore, 1990), p. 1577.
[35] G. D. Gilliland, D. J. Wolford, T. F. Kuech, and J. A. Bradley, J. Vac. Sci. Technol. B **9**, 2377 (1991); G. D. Gilliland, D. J. Wolford, G. A. Northrop, M. S. Petrovic, T. F. Kuech, and J. A. Bradley, J. Vac. Sci. Technol. B **10**, 1959 (1992).
[36] G. D. Gilliland, D. J. Wolford, T. F. Kuech, and J. A. Bradley (unpublished).
[37] G. D. Gilliland, D. J. Wolford, G. A. Northrop, T. F. Kuech, and J. A. Bradley, *Proceedings of the 18th International Symposium on Gallium Arsenide and Related Compounds, Seattle, WA, Sept. 9–12, 1991*, Institute of Physics Conference Series 120, edited by G. B. Stringfellow (IOP, London, 1991), p. 413.
[38] A. Olsson, D. J. Erskine, Z. Y. Xu, A. Schremer, and C. L. Tang, Appl. Phys. Lett. **41**, 659 (1982).
[39] W. van Roosbroeck, Phys. Rev. **91**, 282 (1953).
[40] N. Kawamoto, A. Nakamura, and K. Fumiwara, Jpn. J. Appl. Phys. **28**, L1715 (1989).
[41] S. M. Sze, *Physics of Semiconductor Devices* (Wiley, New York, 1981).
[42] R. Dingle, H. L. Stormer, A. C. Gossard, and W. Wiegmann, Appl. Phys. Lett. **33**, 665 (1978).
[43] W. I. Wang, E. E. Mendez, and F. Stern, Appl. Phys. Lett. **45**, 639 (1984).
[44] E. E. Mendez, P. J. Price, and M. Heiblum, Appl. Phys. Lett. **45**, 295 (1984).
[45] E. E. Mendez and W. I. Wang, Appl. Phys. Lett. **46**, 1159 (1985).
[46] L. Pfeiffer, K. W. West, H. L. Stormer, and K. W. Baldwin, Appl. Phys. Lett. **55**, 1888 (1989).
[47] M. I. Nathan, W. P. Dumke, K. Wrenner, S. Tiwari, S. L. Wright, and K. A. Jenkins, Appl. Phys. Lett. **52**, 654 (1988).
[48] A. C. Gossard, J. H. English, M. Miller, and R. J. Simes, J. Cryst. Growth **95**, 247 (1989).
[49] H. Ito and T. Ishibashi, J. Appl. Phys. **65**, 5197 (1989).
[50] C. M. Hurd, S. P. McAlister, W. R. McKinnon, C. E. Falt, D. J. Day, C. J. Miner, and A. J. Springthorpe, J. Appl. Phys. **65**, 3487 (1989).

[51] J. D. Wiley, Semiconductors and Semimetals, **10**, 137 (1975).
[52] C. M. Wolfe, G. E. Stillman, and W. T. Lindley, J. Appl. Phys. **41**, 3088 (1970).
[53] J. E. Fouquet and A. E. Siegman, Appl. Phys. Lett. **46**, 280 (1985).
[54] P. Dawson, G. Duggan, H. I. Ralph, and K. Woodbridge, in *Proceedings of the 17th International Conference on Physics of Semiconductors*, San Francisco, CA, edited by W. Harrison (World Scientific, Singapore, 1984), p. 551.
[55] J. L. Bradshaw, W. J. Choyke, R. P. Devaty, and R. L. Messham, J. Appl. Phys. **67**, 1483 (1990).
[56] B. Bensaid, F. Raymond, M. Leroux, C. Verie, and B. Fofana, J. Appl. Phys. **66**, 5542 (1989).
[57] R. K. Ahrenkiel, B. M. Keyes, and D. J. Dunlavy, J. Appl. Phys. **70**, 225 (1991).
[58] S. D. Lester, T. S. King, and B. G. Streetman, J. Appl. Phys. **63**, 853 (1988).

Optically determined minority-carrier transport in GaAs/$Al_xGa_{1-x}As$ heterostructures

D. J. Wolford, G. D. Gilliland, T. F. Kuech,* and J. A. Bradley
IBM Research Division, Thomas J. Watson Research Center, P.O. Box 218, Yorktown Heights, New York 10598

H. P. Hjalmarson
Sandia National Laboratories, Albuquerque, New Mexico 87185
(Received 8 April 1992)

We have studied minority-carrier electron and hole transport versus temperature (30–300 K) in a series of undoped, "interface-free," GaAs/$Al_{0.3}Ga_{0.7}$As double heterostructures prepared by organometallic vapor-phase epitaxy, with GaAs thicknesses from 0.1 to 10 μm. This was achieved using an all-optical, time-resolved photoluminescence-imaging technique with a spatial resolution of $\lesssim 3$ μm, temporal resolution of ~ 50 ps, and spectral resolution of < 1 cm^{-1}. This technique allows direct determination of minority-carrier transport properties, and is superior to electrical transport measurement techniques in that it is contactless, may distinguish between diffusive and nondiffusive carrier motion, and has high temporal and spectral resolution. We find all transport (electron and hole) in these structures to be diffusive. Specifically, transport in thick structures ($\gtrsim 0.5$ μm) is hole-dominated ambipolar diffusion, whereas in thinner structures ($\lesssim 0.5$ μm) we observe a *time-dependent* transition from ambipolar to electron-dominated diffusion. Minority-carrier mobilities derived from these diffusion measurements, from 300 to ~ 30 K, are in excellent agreement with both electron and hole majority-carrier mobilities. Furthermore, fits to the temperature-dependent mobilities yield deformation potentials in agreement with published electrically derived values.

I. INTRODUCTION

Carrier transport in semiconductors is most commonly studied through Hall measurements.[1–8] This technique has been used ubiquitously to study majority-electron and -hole transport in high-purity, bulk GaAs,[3] undoped GaAs/$Al_xGa_{1-x}As$ quantum wells (QW's),[9,10] modulation-doped GaAs/$Al_xGa_{1-x}As$ QW structures,[11] and two-dimensional (2D) electron and hole gas (2DEG and 2DHG, respectively) transport in modulation-doped single GaAs/$Al_xGa_{1-x}As$ heterojunction structures.[12–19] Despite the obvious accomplishment of the Hall technique, there are other measurement techniques equally capable of quantifying carrier transport. Recently, an all-optical photoluminescence (PL) imaging technique, analogous to the classical Haynes-Shockley experiment,[20] has been used to measure, directly, carrier transport;[21–24] however, here, in contrast to electrical measurement techniques, the observed transport is dominated by *minority carriers* (rather than majority carriers). Many varieties of this PL-imaging technique, each with distinct advantages and disadvantages, have been used to measure transport, including time-of-flight measurements,[23] masked-PL imaging,[22] and direct-PL imaging.[21,24]

In this paper we use an all-optical, time-resolved PL-imaging technique to study electron and hole transport in ideal, "interface-free" GaAs structures. We measure, directly, the transport of minority carriers and examine, side by side, our optically determined diffusivities, as equivalent mobilities, with electrically determined mobilities in comparable structures. Our results, from ~ 30 K to room temperature, are in excellent agreement with classically derived majority-carrier mobilities. Thus, we find *minority-carrier* and *majority-carrier* transport, i.e., holes in *n*-type GaAs and holes in *p*-type GaAs, *quantitatively identical*, contrary to some predictions.[25]

II. EXPERIMENT

Our samples were simple GaAs/$Al_{0.3}Ga_{0.7}As$ double heterostructures. Such structures were chosen for several reasons. First, the wider band-gap $Al_{0.3}Ga_{0.7}As$ layers effectively confine photoexcited carriers to the GaAs layer, thereby eliminating major nonradiative decay processes which may occur at the substrate and free surface. In addition, we find nonradiative decay at GaAs/$Al_{0.3}Ga_{0.7}As$ heterointerfaces to be *virtually nonexistent* in these ideal structures,[26] yielding minority-carrier lifetimes which are extremely long (> 2.5 μs) and PL efficiencies which are very high (10^3–10^4 greater than for bare GaAs epilayers). Second, $Al_{0.3}Ga_{0.7}As$ layers are transparent to near-resonant excitation of the GaAs layer. Therefore, photoexcited carriers are generated solely in the GaAs layer, and our measured results characterize the transport in the active-GaAs layer only—thereby eliminating the common difficulty in Hall measurements of determining the location of the conducting layer or channel. Lastly, such simple structures ease the interpretation of results. The samples were grown by organometallic vapor-phase epitaxy (OMVPE) at 750 °C, at a calibrated growth rate of $\simeq 350$ Å/min. All layers were nominally undoped; $Al_{0.3}Ga_{0.7}As$ layers were *p* type ($\sim 3\times10^{16}$ cm^{-3}) and 0.5 μm thick, while GaAs layers were *n* type ($\sim 1\times10^{15}$ cm^{-3}) with thicknesses ranging from 0.1 to 10.0 μm.

0163-1829/93/47(23)/15601(8)/$06.00

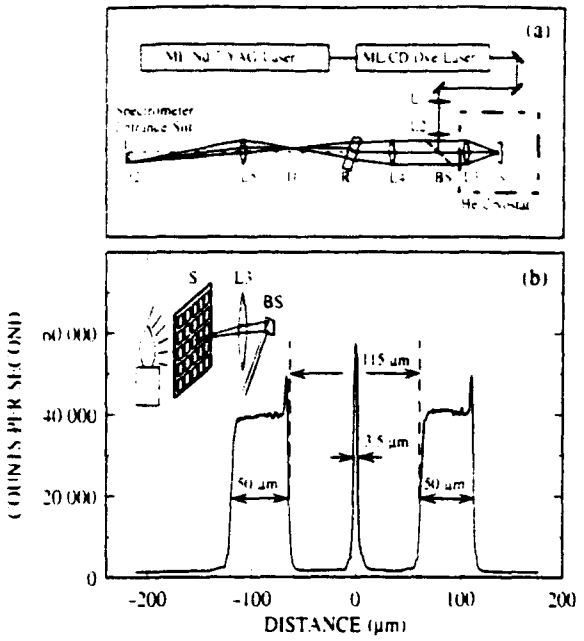

FIG. 1. (a) Experimental setup for spatially resolved PL measurements ($L1$–$L5$, lenses; BS, beamsplitter; S, sample; $I1$,$I2$, PL images; and R, refractory block). (b) Spatial calibration of our system, obtained using a quartz disk in place of the sample, onto which aluminum squares (115×115 μm^2, and 50-μm spacing) were evaporated (inset); this was then backlighted and imaged, while simultaneously focusing the laser to a 3.5-μm spot size on one of the aluminum squares.

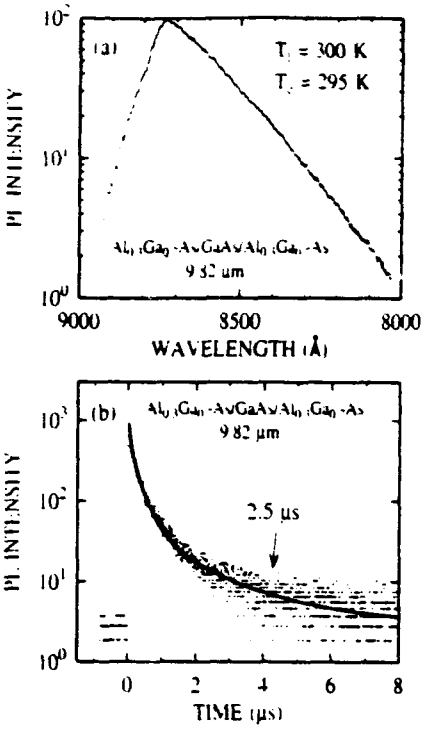

FIG. 2. (a) Room-temperature PL spectrum for the 9.82-μm GaAs-layer thickness double heterostructure. Solid line represents a Maxwell-Boltzmann fit, yielding the electronic temperature T_e. (b) Room-temperature PL time decay for the 9.82-μm double heterostructure. Solid line represents least-squares fit to the data with a bimolecular rate equation, yielding the 2.5-μs lifetime characteristic of the exponential tail.

Our all-optical technique for time-resolved PL imaging of minority-carrier transport requires excitation and imaging, in a confocal manner, through a specially designed microscope. Figure 1(a) illustrates the experimental apparatus. A mode-locked, synchronously pumped cavity-dumped dye laser (tunable from 6400–8400 Å) with a pulse width of ~1 ps was used as a source of photoexcitation, with peak excitation densities possibly reaching $\sim5\times10^{18}$ cm^{-3}. Lenses $L3$, $L4$, and $L5$ form our "PL-imaging microscope," whereas lenses $L1$, $L2$, and $L3$ form our "laser focusing microscope." The system was designed with near-diffraction-limit focusing of the laser beam, magnification (of the PL image) of $\sim20\times$, and light-collecting f-number matched for the composite optical-imaging system, including the spectrometer. Scanning of the PL image across the spectrometer entrance slit was performed through rotation of a Plexiglas block, R, and its corresponding refraction of the back-scattered luminescence. Linearity in the imaging plane was confirmed over a sample spatial range of ±400 μm; Fig. 1(b) shows such spatial calibration of this system. For this calibration, a quartz disk, onto which aluminum squares were photolithographically defined and evaporated, was placed in the sample position. This calibration disk was then back lit with white light, while simultaneously focusing the laser beam onto one of the aluminum squares—thus yielding a "negative" image of the squares with a "δ-function" spike in the center (distance$=0$ μm) corresponding to the focused laser-beam spot. The resulting overall spatial resolution was ~3 μm—thus near diffraction limit.

III. ROOM-TEMPERATURE RESULTS

A typical room-temperature PL spectrum, together with the corresponding time decay from the same 9.82-μm-thick double heterostructure sample, is shown in Fig. 2. We find relatively intense PL resulting from free-carrier, band-to-band recombination. Fits to the high-energy side with the Maxwell-Boltzmann expression—indicative of thermalized band-to-band recombination—yield electronic temperatures virtually equal to the measured and known lattice temperature. Decay kinetics for these structures are somewhat more complicated and dependent upon the GaAs-layer thickness, but independent of PL-emission energy. We find that all decay kinetics, at all temperatures, are well understood and accurately modeled by rate equations for free-carrier recombination[27] (optical properties are dominated by *minority carriers*). Further, lifetimes obtained from fits to the data, representing the exponential tail of the decay, are extremely long ($\gtrsim2.5$ μs).[26,27] These fully understood decay kinetics, long lifetimes, and high PL efficiencies are crucial in making possible studies such as ours discussed below.

Figures 3(a) and 3(b) show time- and spatially-resolved PL distributions for our 9.82- and 0.30-μm-thick double heterostructures at 300 K. These data clearly show that the PL distribution, and, hence, minority-carrier spatial distribution, expands spatially with increasing time. If this minority-carrier transport should be diffusive, then

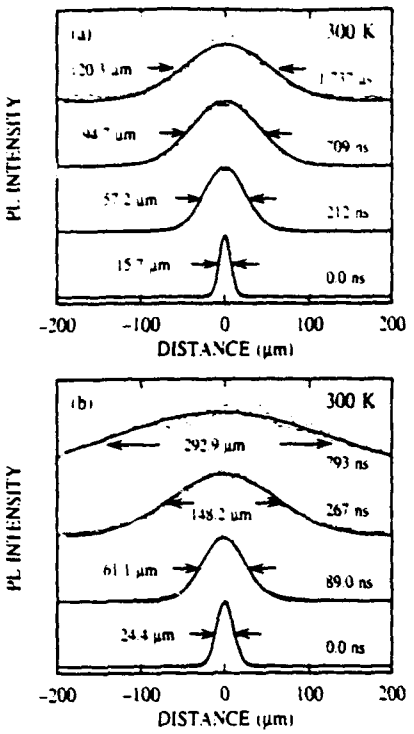

FIG. 3. Room-temperature time-resolved PL distributions. Solid lines represent Gaussian fits to data, with FWHM vs time shown. (a) Results for double heterostructure with 9.82-μm GaAs-layer thickness; (b) results for double heterostructure with 0.30-μm GaAs-layer thickness.

its spatial distribution should evolve in time according to the appropriate diffusion equation. Because our imaging technique only resolves the in-plane (parallel to the heterointerface) motion of carriers and our observed transport occurs over distances much larger than the GaAs-layer thickness, we use the cylindrically symmetric, two-dimensional diffusion equation,

$$\frac{\partial p(\mathbf{r},t)}{\partial t} = D\nabla^2 p(\mathbf{r},t) - \frac{p(\mathbf{r},t)}{\tau} , \tag{1}$$

to model the observed transport. The time-dependent minority-carrier spatial distributions may be obtained analytically from Eq. (1) as

$$p(\mathbf{r},t) = \frac{\Delta_0^2 p_0}{4Dt+\Delta_0^2} \exp\left[\frac{-r^2}{4Dt+\Delta_0^2}\right] \exp\left[-\frac{t}{\tau}\right] , \tag{2}$$

where Δ_0 is the initial ($t=0$) minority-carrier distribution, D is the diffusion constant, and τ is the minority-carrier lifetime. Here, we have assumed, for simplicity, that minority carriers decay exponentially. This is clearly not the case for all of our structures at all temperatures (e.g., bimolecular decays—see Fig. 2). However, we find, through numerical modeling, that with our experimental conditions these additional complexities yield virtually negligible modifications to the spatial distributions, in agreement with Olsson *et al.*[21] Further, such Gaussian distributions accurately model our data, indicated by the solid lines in Fig. 3. Most conspicuously, observed minority-carrier distributions expand macroscopically

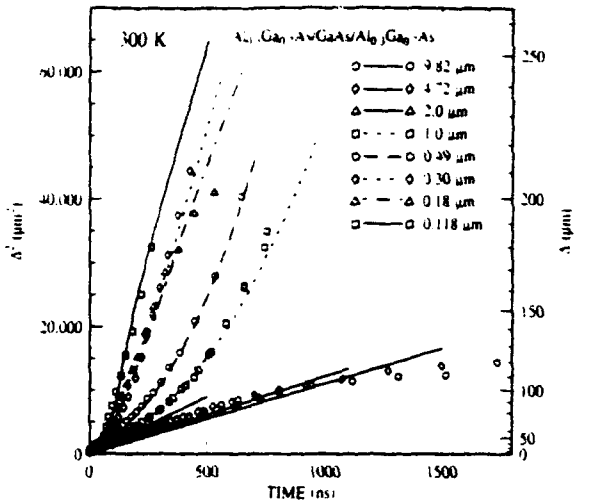

FIG. 4. Gaussian PL FWHM squared vs time $\Delta(t)^2$, for all GaAs/$Al_{0.3}Ga_{0.7}As$ double heterostructures at room temperature; lines represent fits to the data, as discussed in text.

from an initial full width at half maximum (FWHM), Δ_0, of ~ 4 μm to over *300 μm* during the minority-carrier lifetime.

We may further quantify these data by plotting the squared PL FWHM versus time, $\Delta^2(t)$, after the laser pulse, with results for all samples studied shown in Fig. 4. For diffusive transport, and corresponding Gaussian spatial distributions, Δ^2 should vary linearly with time as

$$\Delta^2(t) = [16\ln(2)]D_a t + 4\ln(2)\Delta_0^2 . \tag{3}$$

Figure 4 shows that our transport data are not linear versus time for all samples, but are for some, with clear, *systematic* trends for decreasing GaAs-layer thicknesses.

Results in Figs. 3 and 4 seem, initially, to be somewhat contradictory. The rigorously Gaussian PL distributions of Fig. 3 reflect the occurrence of diffusive transport for the relatively wide structures of GaAs thickness $\gtrsim 0.30$ μm, whereas more nonlinear behavior found in Fig. 4 for some narrower GaAs layers does not. All of these results may, nonetheless, be understood in the context of Eqs. (1)–(3), by taking into account the time-dependent (and carrier-density-dependent) ambipolar diffusion constant D_a. The ambipolar diffusion constant may be expressed as

$$D_a = \frac{[(n+n_0)+(p+p_0)]D_e D_h}{(n+n_0)D_e+(p+p_0)D_h} , \tag{4}$$

where D_e (D_h) is the electron (hole) diffusion constant, n (p) is the photoexcited electron (hole) density, and n_0 (p_0) is the built-in electron (hole) density. Equation (4) shows that D_a depends not only on the electron and hole diffusion constants, but the "relative" densities of electrons and holes. For nearly intrinsic or high-purity material ($n=p$ and $n_0 \simeq p_0 \simeq 0$), D_a is dominated by the smaller diffusion constant D_h. Additionally, Eq. (4) shows that D_a may be time dependent due to the time-dependent electron and hole densities and the nonzero built-in carrier densities. Such carrier-density- and time dependences may be accounted for by including (1) the

time-dependent photoexcited carrier densities obtained in our kinetic measurements, and (2) the static built-in carrier densities. In so doing, we find that the data in Fig. 4 may be accurately modeled in this way, with best fits shown as lines in the figure—thus reconciling the initial apparent discrepancies between Figs. 3 and 4, and confirming truly *diffusive* motion. We also find that the built-in hole density in the GaAs layer is not constant versus GaAs-layer thickness, but drastically increases inversely with GaAs thickness to $\sim 1\times 10^{18}$ cm^{-3} for sufficiently thin structures ($\lesssim 0.1$ μm), whereas $p_0 < n_0$ for thicker structures, consistent with our estimated compensation ($\simeq 40\%$).[28]

In totality, these results are consistent with the material parameters we have independently determined for these structures, and are interpretable as an *effective p-type modulation doping*. With the known doping level and thickness of each layer of our structures, the *p-n* junction depletion width in the GaAs layer is ~ 0.5 μm. Thus, holes from $Al_{0.3}Ga_{0.7}As$ layers may accumulate in the GaAs layer for GaAs layers thinner than approximately twice this depletion length (two interfaces). This is analogous to modulation doping, wherein majority carriers in the active layer originate from dopants (either intentional or residual) in another layer of the heterostructure. Accordingly, thick structures ($\gtrsim 0.5$ μm) are *inherently n type*, whereas thinner structures ($\lesssim 0.5$ μm) are *modulation-doped p type*, and the minority-carrier species changes from holes to electrons for sufficiently thin structures ($\lesssim 0.5$ μm). Thus, we observe a time-dependent transition from ambipolar- to electron-dominated transport.

From such analyses of our data, we calculate the electron and hole diffusion constants, shown in Fig. 5. Additionally, using the nondegenerate Einstein relation, $\mu = D\,e\,/kT$, both electron and hole mobilities may be obtained. (We will discuss later, in more detail, our justification in using the nondegenerate form of the Einstein relation below.) We find both electron and hole mobilities which are independent of GaAs-layer thickness, and *quantitatively* in agreement with electrical measurements on these same samples—$\mu = 5800$ cm^2/V s for electrons (majority carriers in the *n*-type GaAs layer)—and with reported values for both electron and hole mobilities obtained electrically at room temperature (horizontal lines in the figure).[3,29]

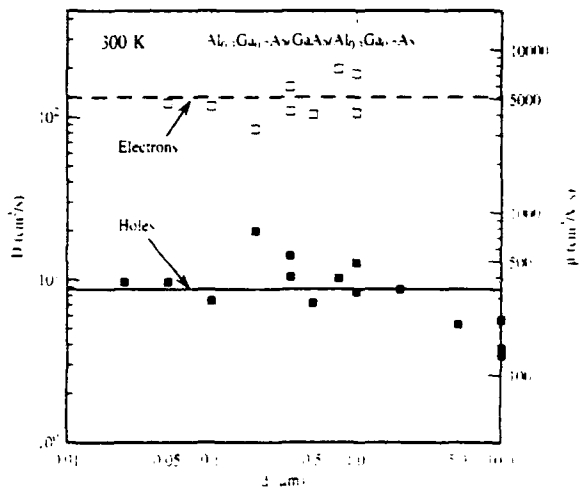

FIG. 5. Room-temperature electron and hole diffusion constants, and corresponding mobilities, vs GaAs-layer thickness obtained from analysis of data in Fig. 4. Horizontal lines represent typical electron and hole mobilities obtained electrically in high-purity *n*- and *p*-type GaAs.

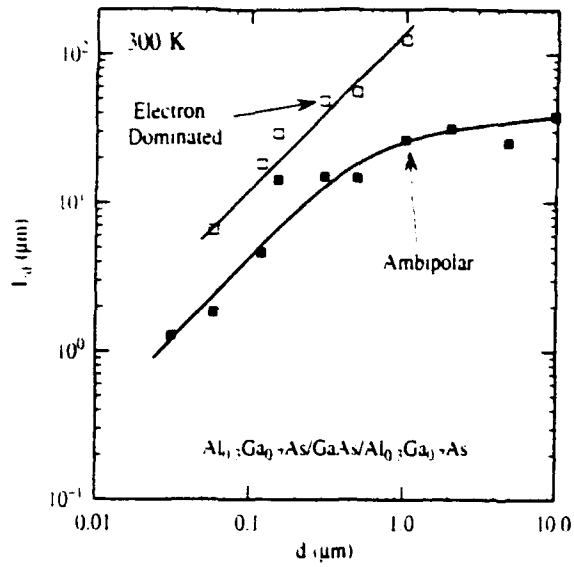

FIG. 6. Diffusion lengths vs GaAs-layer thickness at room temperature.

Minority-carrier diffusion lengths may be obtained as by-products of our decay kinetics and transport measurements. Defined as $L_d = \sqrt{D\tau}$, we find minority-electron diffusion lengths greater than *100 μm*, and minority-hole diffusion lengths of *~35 μm*—among the largest diffusion lengths reported for any GaAs structure.[30] These lengths shown in Fig. 6 also decrease with decreasing GaAs-layer thicknesses ($\lesssim 1.0$ μm), and this steady diminution may be attributed to the rapid decrease in minority-carrier lifetime we find for decreasing GaAs-layer thickness,[31] and is consistent with our asserted *p*-type modulation doping. Using this information, the heterointerfacial quality of our structures may also be characterized. We thus find that carriers move extreme distances during their lifetime, and, thus, may scatter from each heterointerface many times *without decaying nonradiatively*. Thus, our data indicate that carriers scatter from these high-quality heterointerfaces up to *~200 times* during their lifetime—signifying that these high-density heterointerfaces are "mirrorlike," reflecting carriers without suffering and/or competitive nonradiative decay.

IV. TEMPERATURE DEPENDENCE (300–30 K)

Figures 7 and 8 show, respectively, the temperature dependencies of the PL and PL decay kinetics for our 9.82-μm double heterostructure. As previously found at room temperature, the observed emission results from thermalized carriers and, thus, radiative band-to-band recombination. We find, again, these temperature-

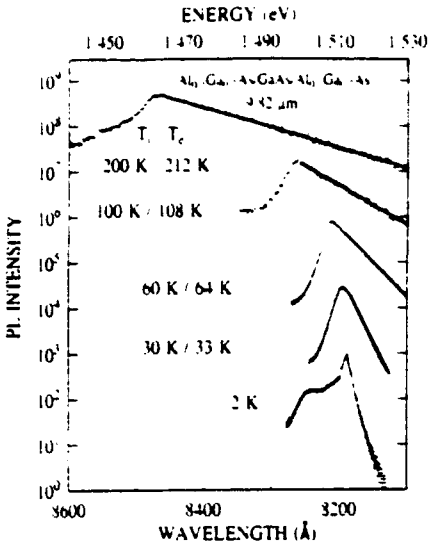

FIG. 7. PL spectra vs temperature for the 9.82-μm-thick double heterostructure. Electronic temperatures were obtained from Maxwell-Boltzmann fits to the spectra.

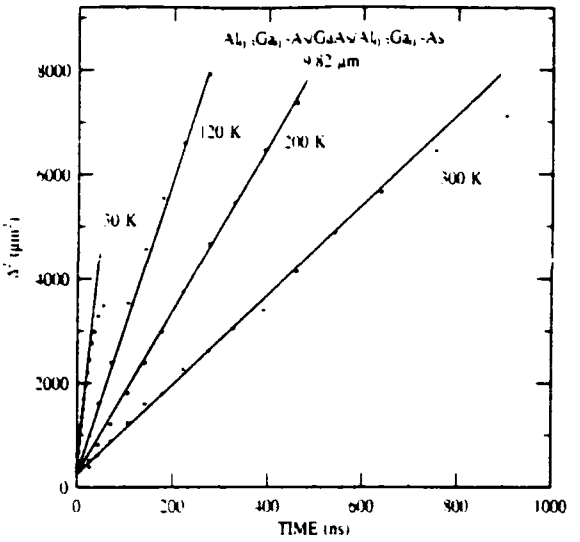

FIG. 9. Temperature dependence of Gaussian PL FWHM squared $\Delta^2(t)$ vs time for the 9.82-μm double heterostructure. Solid lines represent linear least-squares fits to data.

dependent kinetics, for all structures, are fully described by the appropriate temperature-dependent rate equations—taking into full account possible carrier freezeout.

The temperature dependence of the minority-carrier transport may be characterized and quantified in the same manner as our room-temperature results. We find Gaussian PL-spatial distributions at all temperatures (300–30 K). Figure 9 shows Δ^2 versus time obtained from such Gaussian fits to the data. These results, for our thickest heterostructure (9.82 μm), are *linear* at all temperatures, and thus represent the genuine diffusive transport of minority holes. Using Eq. (3), we find that the derived diffusion constant for this minority-hole transport increases with decreasing temperature. Similar measurements for our 0.30-μm structure versus temperature (300–30 K) yield results consistent with the *p*-type modulation doping found at room temperature, thus allowing a determination of *both* minority-electron and minority-hole transport, as shown in Fig. 10. Here also, we find diffusion constants [from fits to Eq. (4)], for both electrons and holes, which *increase* with decreasing temperature.

Figure 11 shows the temperature-dependent minority-hole mobility obtained from the 9.82-μm-thick heterostructure using the nondegenerate Einstein relation. Here, the carrier temperature is assumed equal to the lattice temperature—thus, justified from our findings that, at these temperatures, minority-carrier lifetimes are sufficiently long to allow complete carrier cooling to the lattice temperature, as has been evidenced in the PL

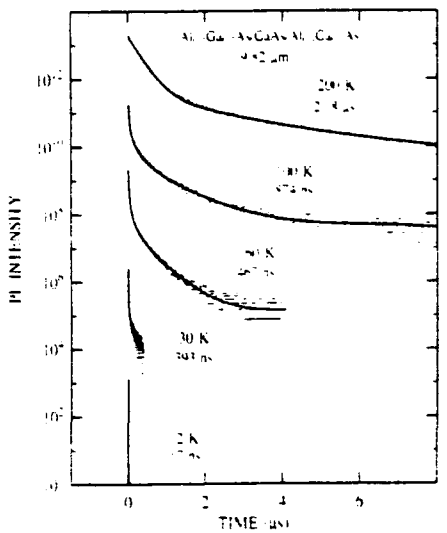

FIG. 8. PL decay kinetics vs temperature for the double heterostructure with a 9.82-μm GaAs-layer thickness. Lifetimes were obtained from fits, and correspond to the exponential tail of the decay.

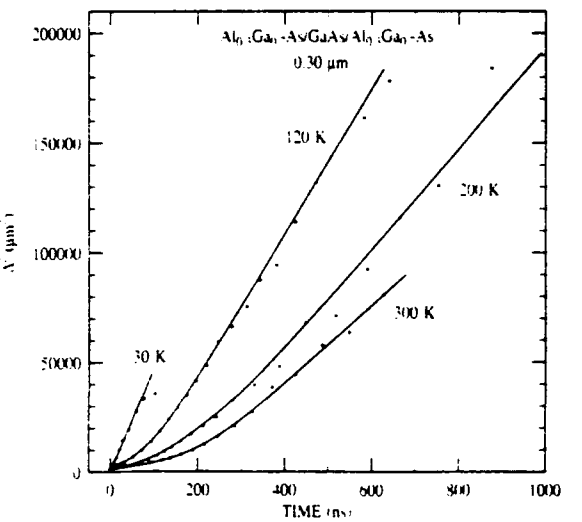

FIG. 10. Temperature dependence of Gaussian PL FWHM squared $\Delta^2(t)$ vs time for the 0.30-μm double heterostructure. Solid lines represent least-squares fits to data using Eq. (4).

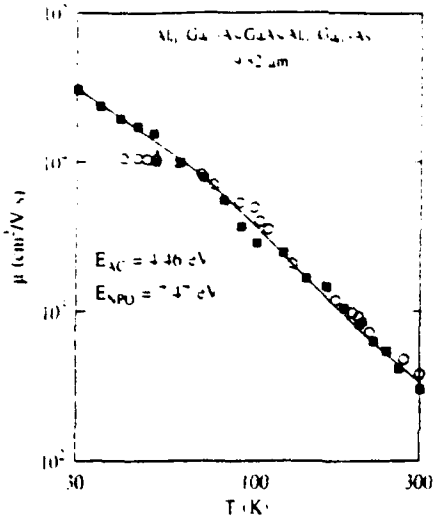

FIG. 11. Temperature dependence of minority-hole mobility in the 9.82-μm double heterostructure (■). Mobilities were obtained from the measured diffusion constants using the nondegenerate Einstein relation. Solid line represents best fit to data, yielding acoustic-phonon and nonpolar-optic-phonon deformation potentials. Hill's results (Ref. 34) for majority holes in p-type GaAs are also shown (○) with excellent agreement.

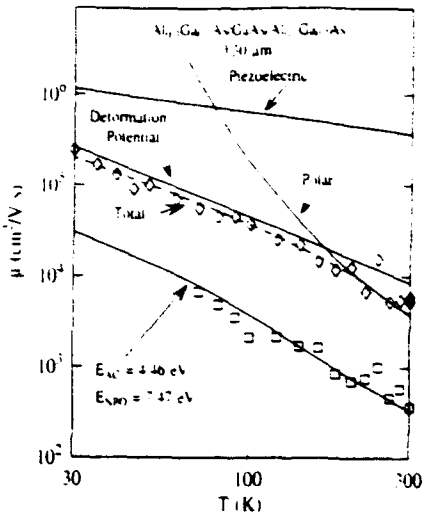

FIG. 12. Temperature dependence of minority-hole (□) and minority-electron (◇) mobilities in the 0.30-μm double heterostructure. Mobilities were obtained from the measured diffusion constants using the nondegenerate Einstein relation. Solid lines represent best fits to the data, as discussed in the text.

high-energy Maxwell-Boltzmann tails and their derived electronic temperatures, of Fig. 7. Further, utilization of the nondegenerate form of the Einstein relation is warranted by the relatively high lattice temperatures which preclude degeneracy and exciton formation.

Hole mobilities in GaAs, at these temperatures, are dominated by acoustic-phonon and nonpolar optical-phonon scattering. Using Wiley's formalism,[29,32,33] the combined mobility is

$$\mu_{\mathrm{AC,NPO}} = 3.1727\times10^{-5}\frac{r^{5/2}(1-r^{1/2})}{(1+r^{3/2})^2} \times \frac{\rho\bar{u}^2}{(m_l^*/m_0)^{5/2}E_{\mathrm{AC}}^2} S(\theta,\eta,T)T^{-3/2}, \quad (5)$$

where

$$S(\theta,\eta,T) = \int_0^\infty \frac{xe^{-x}dx}{1+C[(1+\theta/xT)^{1/2}-e^{\theta/T}(1-\theta/xT)^{1/2}]}, \quad (6)$$

$$C=(\theta/T)\eta/2(e^{\theta/T}-1), \quad (7)$$

$$\eta=(E_{\mathrm{NPO}}/E_{\mathrm{AC}})^2, \quad (8)$$

$r=m_1/m_2$ is the ratio of heavy- and light-hole masses, ρ is the density of the material, $\bar{u}$ is the average sound velocity, and m_l^* is the effective mass of the charged carriers. We find acoustic and nonpolar optical deformation potentials of 4.5 and 7.5 eV, respectively. These results are in good quantitative agreement with other estimates[29] (3.5 and 6.5 eV, respectively), and our least-squares fit to the data (solid line) is in excellent agreement with the totality of our data. Further, these results show that, at high temperatures ($T\gtrsim 70$ K), hole mobilities increase as $\mu\sim T^{-2.4}$—quantitatively identical to Hill's results[34] for majority-hole mobilities in high-purity p-type material obtained electrically, and also shown in Fig. 11. Here, again, we find minority-carrier mobilities *virtually identical* to those of majority-carrier mobilities, and our results and analysis are consistent with phonon-scattering limited transport.

Figure 12 shows the temperature dependence of both minority-hole and minority-electron mobilities, obtained as above, for our 0.30-μm heterostructure. In thin samples, such as this, where the influences of p-type modulation doping become significant—if not dominant ($\lesssim 0.3$ μm)—as demonstrated at room temperature, we obtain mobilities for both species of minority-carrier electron and hole. Below 70 K, all transport in these structures is totally minority-electron dominated, at these excitation levels. We find that the resulting temperature-dependent minority-hole mobilities are identical, both qualitatively and quantitatively, with our 9.82-μm sample results and reported hole mobilities in high-purity, p-type GaAs.[34] Indeed, the lower solid line in Fig. 12 was obtained exactly as for Fig. 11, using Eq. (5).

Electron mobilities in GaAs are more complex than hole mobilities, with the dominant scattering mechanisms being polar-optical, acoustic-deformation-potential phonon (i.e., intrinsic), and piezoelectric scattering.[3] The dashed line in the figure represents the best, least-squares fit to our data using all three of these scattering mechanisms (and Mattheison's rule), together with each of these mechanisms individually indicated (solid lines).[3] Such fitting yields an acoustic-phonon deformation potential of 15.2 eV—with this as the only adjustable fitting parameter. Corresponding reported acoustic-phonon deformation potentials range from 7.0 to 18.0 eV.[3-6,35-37] Our result is, therefore, slightly higher than the most widely accepted value (13.5 eV),[5] and may be a result of differences in measurement technique and/or minority-

carrier versus majority-carrier mobilities.

In totality, our results indicate that minority-carrier transport is quantitatively identical to majority-carrier transport in these high-quality samples. Theoretically, minority-carrier mobilities may be expected to be smaller than majority-carrier mobilities, since impurity scattering may be more dominant for minority carriers (minority carriers have a lower Fermi energy than the same species as majority carrier, for the same doping levels).[25] However, we find that our minority-carrier mobilities, at these temperatures, are lattice limited, and are therefo e truly intrinsic (phonon scattering), thus yielding minority-carrier mobilities comparable or even equal to corresponding majority-carrier mobilities.

V. CONCLUSIONS

We have used an all-optical PL-imaging technique to directly measure the transport of minority-carrier electrons and holes. Significantly, we find *all transport to be diffusive at all temperatures.* Also, both minority-electron and minority-hole mobilities obtained from our measured diffusion constants are in excellent quantitative agreement with electrical measurements of majority-electron and majority-hole mobilities. Additionally, our resulting temperature-dependent mobilities yield appropriate deformation potentials—indeed, ones in good agreement with majority-carrier, electrically determined values. Lastly, these results prove that our all-photoluminescence-based[24,26,27] carrier-transport-measurement technique is (1) fully analogous (but contactless) to the seminal, early optical Haynes-Shockly measurement[20] of transport, and (2) yields both qualitative and quantitative agreement with traditional all-electrical transport methods,[21–23] thus confirming its utility and accuracy.[38–40] Further, as will be discussed in future publications, this method performs equally well for both qualitative and quantitative measurement of neutral-particle (e.g., free excitons and plasmas) transport—an invaluable and complementary result which electrical-transport methods are entirely incapable of determining. Hence, for example, we may now study in detail, at all temperatures (e.g., 1.6–300 K), the spatial and temporal transport of both free carriers and free excitons, and, especially, their possible temperature-dependent joint (or coupled) transport properties.

ACKNOWLEDGMENTS

We thank L. M. Smith, G. A. Northrop, and J. Martinsen for useful discussions and assistance in computer-aided data acquisition. The IBM work was supported, in part, by the Office of Naval Research, under Contracts Nos. N00014-85-C-0868, N00014-90-C-0077, and N00014-91-J-1697. The work at Sandia was supported by the U.S. Department of Energy under Contract No. DE-AC04-76DP00789.

---

*Present address: Department of Chemical Engineering, University of Wisconsin, 1415 Johnson Drive, Madison, WI 53706.

[1]M. I. Nathan, W. P. Dumke, K. Wrenner, S. Tiwari, S. L. Wright, and K. A. Jenkins, Appl. Phys. Lett. **52**, 654 (1988).
[2]C. Guillemot, M. Baudet, M. Gauneau, A. Regreny, and J. A. Portral, Phys. Rev. B **35**, 2799 (1987).
[3]C. M. Wolfe, G. E. Stillman, and W. T. Lindley, J. Appl. Phys. **41**, 3088 (1970).
[4]B. Vinter, Phys. Rev. B **33**, 5904 (1986).
[5]P. J. Price, Phys. Rev. B **32**, 2643 (1985).
[6]P. J. Price, Surf. Sci. **143**, 145 (1984).
[7]J. P. Harrang, R. J Higgins, R. K. Goodall, P. R. Jay, M. Laviron, and P. Delescluse, Phys. Rev. B **32**, 8126 (1985).
[8]C. T. Foxon, J. J. Harris, D. Hilton, J. Hewett, and C. Roberts, Semicond. Sci. Technol. **4**, 582 (1982).
[9]H. Sakaki, T. Noda, K. Hirakawa, M. Tanaka, and T. Matsusue, Appl. Phys. Lett. **51**, 1934 (1987).
[10]R. Gottinger, A. Gold, G. Abstreiter, G. Weimann, and W. Schlapp, Europhys. Lett. **6**, 183 (1988).
[11]R. Dingle, H. L. Störmer, A. C. Gossard, and W. Wiegmann, Appl. Phys. Lett. **33**, 665 (1978).
[12]H. Shtrikman, M. Heiblum, K. Seo, D. E. Galbi, and L. Osterling, J. Vac. Sci. Technol. B **6**, 670 (1988).
[13]B. J. F. Lin, D. C. Tsui, M. A. Paalanen, and A. C. Gossard, Appl. Phys. Lett. **45**, 695 (1984).
[14]J. H. English, A. C. Gossard, H. L. Störmer, and K. W. Baldwin, Appl. Phys. Lett. **50**, 1826 (1987).
[15]E. E. Mendez and W. I. Wang, Appl. Phys. Lett. **46**, 1159 (1985).
[16]R. Dingle, H. L. Störmer, A. C. Gossard, and W. Wiegmann, Appl. Phys. Lett. **55**, 1888 (1989).
[17]E. E. Mendez, P. J. Price, and M. Heiblum, Appl. Phys. Lett. **45**, 295 (1984).
[18]A. C. Gossard, J. H. English, M. Miller, and R. J. Simes, J. Cryst. Growth **95**, 247 (1989).
[19]W. I. Wang, E. E. Mendez, Y. Iye, B. Lee, M. H. Kim, and G. E. Stillman, J. Appl. Phys. **60**, 1834 (1986).
[20]J. R. Haynes and W. Shockley, Phys. Rev. **81**, 835 (1951).
[21]A. Olsson, D. J. Erskine, Z. Y. Xu, A. Schremer, and C. L. Tang, Appl. Phys. Lett. **41**, 659 (1982).
[22]H. Hilmer, A. Forchel, S. Hansmann, M. Morohashi, E. Lopez, H. P. Meier, and K. Ploog, Phys. Rev. B **39**, 10 901 (1989).
[23]R. K. Ahrenkiel, D. J. Dunlavy, D. Greenberg, J. Schlupmann, H. C. Hamaker, and H. F. MacMillan, Appl. Phys. Lett. **50**, 1329 (1987).
[24]G. D. Gilliland, D. J. Wolford, T. F. Kuech, and J. A. Bradley, Appl. Phys. Lett. **59**, 216 (1991); L. M. Smith, D. J. Wolford, J. Martinsen, R. Venkatasubramanian, and S. K. Ghandi, J. Vac. Sci. Technol. B **8**, 787 (1990).
[25]E. O. Kane, Solid State Electron. **28**, 3 (1985).
[26]G. D. Gilliland, D. J. Wolford, T. F. Kuech, J. A. Bradley, C. F. Tsang, and J. Martinsen (unpublished).
[27]D. J. Wolford, G. D. Gilliland, T. F. Kuech, L. M. Smith, J. Martinsen, J. A. Bradley, C. F. Tsang, R. Venkatasubramanian, S. K. Ghandi, and H. P. Hjalmarson, J. Vac. Sci. Technol. B **9**, 2369 (1991).

[28]We have assumed n_0 is constant, equal to the thick structure value, however allowing n_0 to vary—decreases as p_0 increases—($p_0 n_0$ = const) will not quantitatively alter our results.
[29]J. D. Wiley, in *Semiconductors and Semimetals*, edited by R. K. Willardson and A. C. Beer (Academic, New York, 1975), Vol. 10.
[30]R. J. Nelson, in *Gallium Arsenide and Related Compounds*, IOP Conf. Proc. No. 45 (Institute of Physics, Bristol, 1979), p. 256.
[31]L. Jastrzebski, J. Lagowski, H. C. Gatos, and W. Walukiewicz, in *Gallium Arsenide and Related Compounds* (Ref. 30), p. 437.
[32]J. D. Wiley and M. DiDomenico, Jr., Phys. Rev. B 2, 427 (1970).
[33]J. D. Wiley, Phys. Rev. B 4, 2485 (1971).
[34]D. E. Hill, J. Appl. Phys. 41, 1815 (1970).
[35]H. J. Lee, J. Basinski, L. Y. Juravel, and J. C. Woolley, C Phys. 47, 233 (1979).
[36]J. A. Vergés, D. Glötzel, M. Cardona, and O. K. Anc Phys. Status Solidi B 113, 519 (1982).
[37]S. J. Manion, M. Artaki, M. A. Emanuel, J. J. Colema K. Hess, Phys. Rev. B 35, 9203 (1987).
[38]G. D. Gilliland, D. J. Wolford, G. A. Northrop, T. F. K and J. A. Bradley, in *Gallium Arsenide and Related pounds*, IOP Conf. Proc. No. 120 (Institute of Physics tol, 1992), p. 413.
[39]D. J. Wolford, G. D. Gilliland, T. F. Kuech, J. A. Br and H. P. Hjalmarson, in *Gallium Arsenide and Relatec pounds* (Ref. 38), p. 271.
[40]G. D. Gilliland, D. J. Wolford, G. A. Northrop, M. S. vic, T. F. Kuech, and J. A. Bradley, J. Vac. Sci. Tech 10, 1959 (1992).

PRINTED TECHNICAL REPORT & NON-REFEREED PAPERS

Proc. of 21st Int. Conf. on the Physics of Semiconductors, Beijing, China, (World Scientific 1992), p. 241.

FREE-EXCITON RECOMBINATION IN GaAs

D.J. Wolford, G.D. Gilliland,†, T.F. Kuech,‡ and J.A. Bradley
IBM Research Division, T.J. Watson Research Center
P.O. Box 218
Yorktown Heights, New York 10598
and
H.P. Hjalmarson
Sandia National Laboratories
Albuquerque, NM 87185

We have studied the kinetics of free-exciton recombination in "ideal" GaAs structures. Our studies include detailed photoluminescence kinetics measurements versus laser excitation power, temperature, sample structure, and surface treatment. The primary goal in these studies is to understand the mechanism precipitating free-exciton recombination, and the role, if any, that polaritons play. Additionally, we have assessed the effects free-carriers and a variety of different sample structures and surface treatments have on these kinetics.

I. Introduction

It is widely believed that the properties of Coulomb-correlated electrons and holes — excitons — in direct-gap semiconductors are well-understood, both theoretically and experimentally.[1] However, thorough examination of the current literature on this subject, for the prototypical direct-gap semiconductor, GaAs, shows that this is clearly not the case. In particular, theoretical predictions of the oscillator strength, and the corresponding radiative lifetime range from μs[2] to ns.[3] As an example, recently an experimental 2.0 K excitonic lifetime of 3.2 ns has been reported,[3] and widely quoted. The magnitude of this lifetime was interpreted in terms of a "coherence volume,"[3,4] whereas the observed modest increase in lifetime with temperature was believed to be due to the temperature-dependent change in excitonic population within the homogeneous linewidth near K=0, preserving K-selection. Just after this report, another interpretation of the same data based on the concept of exciton-polaritons was published.[5] Even more recently, a 4.0 ns free-exciton lifetime has been reported.[6] In view of these discrepancies, we have studied free-exciton kinetics in high-quality GaAs double heterostructures, in an attempt to definitively test these models, as well as other free-exciton properties (i.e., role of residual strain, interfacial "dead-layer" effects, and the influence of free-carriers on free-exciton kinetics).

II. Samples and Experiment

Our samples were OMVPE- and MBE-prepared $Al_{0.3}Ga_{0.7}As/GaAs/Al_{0.3}Ga_{0.7}As$ heterostructures, with GaAs layer thicknesses ranging from 50 Å to 10 μm. Prior to this study, these samples were fully characterized at 300K.[7] We found that our OMVPE structures are truly "interface-free," as quantified by their 300-K lifetimes (> 2.5 μs) and corresponding record-equivalent interfacial recombination velocities (< 40 cm/s), whereas interfacial results for the MBE-structures still remain somewhat inferior, but still quite good (S ≈ 250 cm/s). Importantly, at low-temperatures (< 25 K), photoluminescence (PL) is uniformly dominated by free-exciton emission in all samples, with impurity-related emissions being weak.

III. Results and Discussion

We have thus measured[8] spectrally resolved free-exciton PL decay kinetics (with 50 ps temporal resolution) versus temperature (1.8 - 40 K), versus GaAs layer thickness, and versus emission wavelength. All decays, in all bulk structures, are short and exponential at 1.8 K, but become progressively and systematically longer and more nonexponential with increasing temperature above 4.0 K. We find, in some structures, a striking thickness-dependent lifetime increase with temperature, varying by more than 5 orders-of-magnitude, from ~ 200 ps at 1.6 K to ~ 14 μs at 25 K. In contrast, decay

kinetics in quantum wells remain exponential with corresponding lifetimes which only increase modestly with temperature. These lifetimes for all of our OMVPE samples are shown in Figure 1. Additionally, we find that variation of the GaAs layer thicknes by over three orders-of-magnitude (from 50 Å to 10 μm) increases the low-temperature free-exciton lifetime from, at most ~ 200 ps to ~ 800 ps — thus, only a factor of four, shown in Fig. 2. Another striking observation is that the 2 K lifetimes do not change with the emission energy, as shown in Fig. 3.

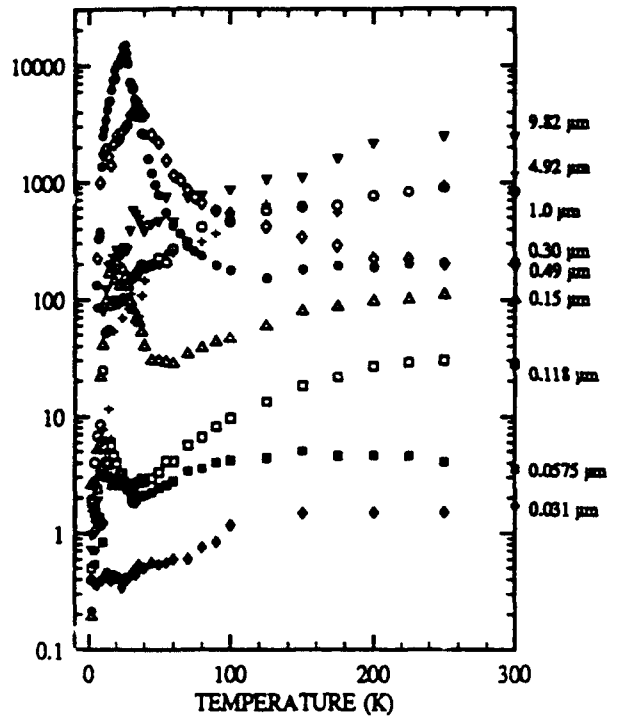

Fig. 1. Lifetimes versus temperature for our OMVPE-prepared structures.

Our results are thus inconsistent with the ns lifetimes reported elsewhere,[3,6] which in some cases may result from high excitation densities. Instead we find a lifetime of ~ 200 ps, with the lifetime increasing with GaAs-layer thickness (possibly due to reabsorption effects[4]). Moreover, these results are not only incompatible with oscillator-strength predictions based on the coherence volume[3,4] model for either excitons or exciton-polaritons, but are also over 10^4 larger than currently existing, accepted models by Elliott[2] for simple free-excitons.

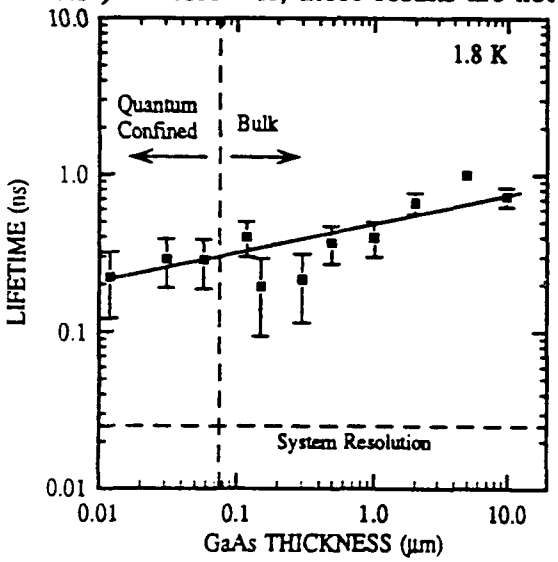

Fig. 2. 1.8 K free-exciton lifetime versus GaAs-layer thickness.

We find[8] that our lifetimes versus temperature are accurately and quantitatively described by coupled rate equations for each species of carrier present, at each temperature (i.e., free-excitons, free electrons and holes). Here, we have included the temperature-dependent density of states, residual impurities, and differences in binding energies for bulk versus quantum structures. Our model also includes the effects of free-exciton localization at a small binding-energy "radiative-defect" which serves to break K-selection, thus precipitating free-exciton recombination. Figure 4 shows calculated lifetimes versus temperature together with our experimental results for a 9.82 μm thick sample, thus demonstrating the excellent agreement. Our model fully explains our observed temperature-dependent lifetimes, lifetimes versus emission energy, and differences between bulk and quantum structures.

Our observed lifetimes versus GaAs-layer thickness and versus emission energy are incompatible with exciton-polariton theories,[5] all of which predict lifetimes which must

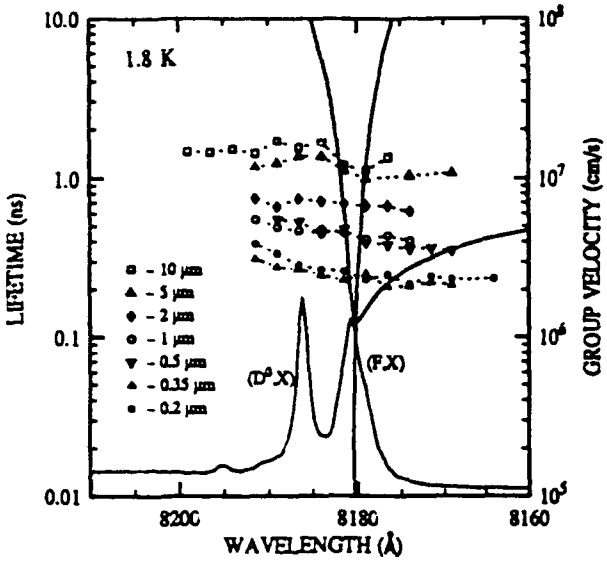

Fig. 3. 1.8 K lifetimes versus PL emission energy and GaAs-layer thickness. Exciton-Polariton group velocities are shown with thick solid lines.

scale directly with layer thickness (for bulk structures) and vary rapidly with emission energy.[9] For quantum-wells, the thickness dependence is not as prominent, and Andreani, et al.[9] have calculated a 25 ps lifetime for a 100 Å quantum well. In an effort to understand the possible role exciton-polariton dynamics may have in such excitonic recombination kinetics, we have undertaken a detailed study of the exciton-polariton dispersion curves through Resonant Brillouin Scattering. We have thus duplicated Weisbuch and Ulbrich's[10] GaAs exciton-polariton dispersion curves, thus demonstrating the existence of exciton-polaritons in these samples. The longitudinal-transverse exciton-polariton splitting is 0.08 meV, whereas the free-exciton linewidth is clearly much larger. Thus, we conclude that damping processes (scattering to other points in the exciton dispersion curve) are dominant over the exciton-photon interaction (polariton effects). In total, we conclude that the exciton recombination kinetics and oscillator strength are entirely dominated by thermalization between free-excitons and free carriers, and that these effects completely mask the anticipated effects of exciton-polaritons.

We have also examined the so-called interfacial "dead-layer" effects[11] commonly observed in GaAs samples. This was accomplished by chemically-etch removing the top $Al_{0.3}Ga_{0.7}As$ layer in these structures, and then probing with extremely high-resolution (< 0.01 meV) PL spectroscopy. We find that with removal of the top, high-quality $Al_{0.3}Ga_{0.7}As$ interface, PL lifetimes and intensities abruptly drop by > 10^3; and the remaining, now-weak free-exciton emission is replaced by even weaker "upper and lower polariton-branch" structure.[12] This dramatic degradation we attribute to loss of the high-quality interface and "native" reoxidation, of the bare GaAs surface — thus leading to the so-called "dead-layer."[11] Figure 5 shows 2 K PL spectra and lifetimes for a 2.0 μm

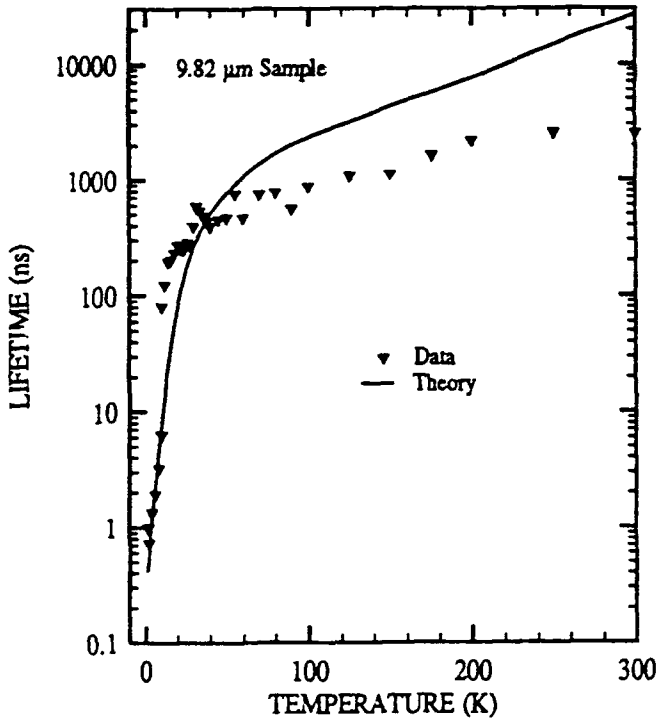

Fig. 4. Calculated lifetimes, solid line, versus temperature together with experimental results for 9.82 μm structures. Calculation does not include surface recombination, thus overestimating high-temperature lifetimes.

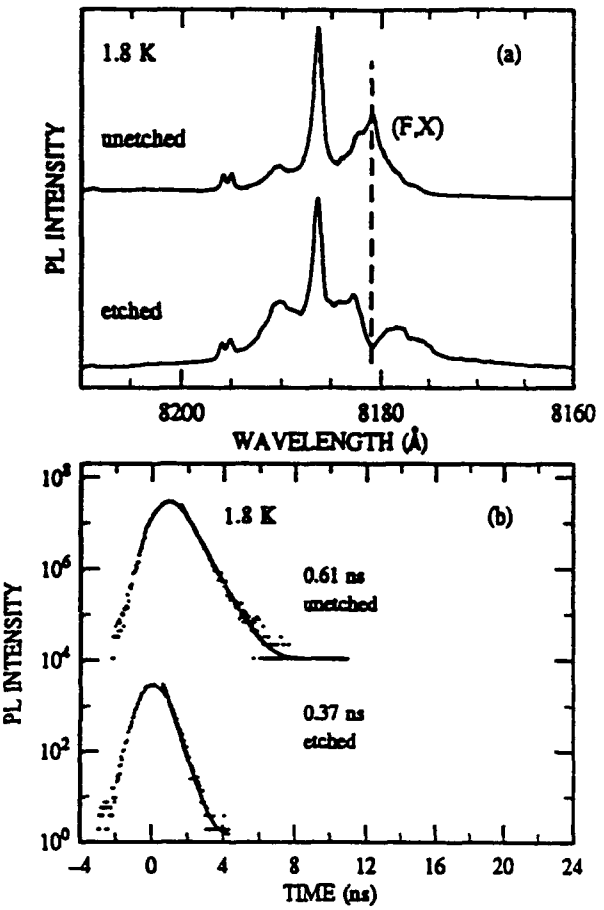

Fig. 5. (a) 1.8 K PL spectra of 2.0 μm structure (top) and same structure after etching off top $Al_{0.3}Ga_{0.7}As$ layer (bottom). (b) 1.8 K free-exciton PL time decays corresponding to PL spectra in (a).

structure, and this same structure after etch-removing the top $Al_{0.3}Ga_{0.7}As$ layer, leaving exposed a bare GaAs surface. Thus, 2 K PL spectra are sensitive to the GaAs surface, whereas the corresponding lifetimes are less so. Additionally, we find that not only is the free-exciton PL sensitive to heterointerface quality, but we also find that residual strain in sample mounting inside our cryostat, and/or from In-backing materials applied to the substrate (during growth — typically done in MBE growth) shift the excitonic resonance. This is the subject of future study.

IV. Conclusion

We have thus established the dominate factors governing excitonic decay in high-purity, virtually "interface-free" GaAs heterostructures. We have demonstrated that the temperature-dependent free-exciton lifetime is determined almost entirely by thermalization with free-carriers, and find that the low-temperature (1.8-K) kinetics are completely unexplainable with any current exciton or exciton-polariton theoretical models.[5]

Supported in part by ONR under contracts N00014-85-C-0868, N00014-90-C-0077, and N00014-91-J-1697, and the US DOE under contract DE-AC04-756DP00789.

REFERENCES

†Present Address: Emory Univ., Dept. of Physics, Atlanta, GA 30322
‡Present Address: Univ. of Wisconsin, Dept. of Chem. Eng., Madison, WI 53706

1. D.C. Reynolds and T.C. Collins, *Excitons Their Properties and Uses*, (Academic Press, New York 1981).
2. R.J. Elliott, Phys. Rev. **108**, 1384 (1957).
3. G.W. 't Hooft, W.A.J.A. van der Poel, L.W. Molenkamp, and C.T. Foxon, Phys. Rev. B **35**, 8281 (1987).
4. J. Feldmann, G. Peter, E.O. Gobel, P. Dawson, K. Moore, and C.T. Foxon, Phys. Rev. Lett. **59**, 2337 (1987).
5. W.J. Rappel, L.F. Feiner, and M.F.H. Schuurmans, Phys. Rev. B **38**, 7874 (1988).
6. J. Aaviksoo, I. Reimand, V.V. Rossin, and V.V. Traunikov, Phys. Rev. B **45**, 1473 (1992).
7. D.J. Wolford, G.D. Gilliland, T.F. Kuech, L.M. Smith, J. Martinsen, J.A. Bradley, C.F. Tsang, R. Venkatasubramanian, S.K. Ghandi, and H.P. Hjalmarson, J. Vac. Sci. Technol. B **9**, 2369 (1991).
8. D.J. Wolford, G.D. Gilliland, T.F. Kuech, J.A. Bradley, and H.P. Hjalmarson, American Physical Society Meeting, Cincinnati, OH, March 1991. Bull. Am. Phys. Soc. **36**, 648 (1991).
9. L.C. Andreani, F. TAssone, F. Bassani, Solid State Comm. **77**, 641 (1991).
10. R.G. Ulbrich and C. Weisbuch, Phys. Rev. Lett. **38**, 865 (1977).
11. E.S. Koteles, J. Lee, J.P. Salerno, and M.O. Vassell, Phys. Rev. Lett. **55**, 867 (1985); T. Steiner, M.L.W. Thewalt, E.S. Koteles, and J.P. Salerno, Phys. Rev. B **34**, 1006 (1986).
12. D.D. Sell, S.E. Stokowski, R. Dingle, and J.V. DiLorenzo, Phys. Rev. B **7**, 4568 (1973).

Proc. of 21st Int. Conf. on the Physics of Semiconductors, Beijing China, (World Scientific 1992), p. 289.

ANOMALOUS LOW-TEMPERATURE FREE-EXCITON TRANSPORT IN GaAs STRUCTURES

D.J. Wolford, G.D. Gilliland,†, T.F. Kuech,‡ and J.A. Bradley
IBM Research Division, T.J. Watson Research Center
P.O. Box 218
Yorktown Heights, New York 10598
and
H.P. Hjalmarson
Sandia National Laboratories
Albuquerque, NM 87185

Using an optical analogue to the classical Haynes-Schockley experiment, we have studied low-temperature free-exciton transport in several "ideal" GaAs structures. We find the observed diffusion constants to be laser excitation power dependent below 50 K, and independent of laser power at higher temperatures. We observe peak 2 K diffusivities of > 1000 cm^2/Vs. Possible mechanisms are discussed.

I. Introduction

At low temperatures, free carriers may condense into free-excitons, which are electrically neutral, and are thus unobservable with conventional electrical transport techniques. In recent years some have resorted to optical means for studying exciton transport properties.[1-8] For example, Hillmer, et al.[2] have studied free-exciton transport in GaAs quantum wells using an opaque mask technique. Here, in contrast, we have used an all-optical, time-resolved PL imaging technique which relies on the direct confocal imaging of the photoexcited PL spot, and has the advantage of requiring no sample processing. This technique is sensitive to both charged and neutral-particle transport, and has high spatial, spectral, and temporal resolution (< 3 μm, < cm^{-1}, and ≈ 50 ps, respectively).[5,6]

II. Samples and Experiment

Our samples were OMVPE-prepared $Al_{0.3}Ga_{0.7}As$ (p ~ $10^{16}cm^{-3}$)/GaAs (n ~ $10^{15}cm^{-3}$)/$Al_{0.3}Ga_{0.7}As$ (p ~ $10^{16}cm^{-3}$) heterostructures with GaAs layer thicknesses ranging from 50 Å to 10 μm. Our time-resolved PL-imaging technique is described elsewhere.[5,6] We have utilized this technique to quantify free-carrier (electron and hole) transport at higher temperatures (50 K - 300 K) in these same structures, and find remarkable agreement with electrically measured majority-carrier mobilities in comparable structures. Additionally, we find[6] excellent agreement in our derived deformation potentials (obtained from fitting the temperature-dependent diffusivities converted into mobilities using the Einstein relation) and reported deformation potentials. Thus, we have demonstrated the utility and accuracy of this technique.

III. Results and Discussion

We find, after focussed, above-gap, laser excitation (3 μm laser spot), PL distributions which spread radially with increasing time, with Gaussian spatial profiles, possibly indicative of "diffusive motion." Figure 1 shows these spatially and temporally resolved distributions for our 9.82 μm thick sample at 10 K.

If the observed transport is indeed diffusive, then the characteristic width of the Gaussian distribution (the Full-Width at Half-Maximum — FWHM — Δ) squared should be directly proportional to time. Figure 2 shows Δ^2 versus time and temperature for our 9.82 μm thick structure. The diffusivity, obtained from the slope, clearly increases with decreasing temperature. Figure 3 shows Δ^2 versus laser excitation power at 2 K for this same sample. The power dependence is clear and unmistakable. Diffusion constants increase monotonically with laser power, and at 2 K range from ~ 1 cm^2/Vs to over 1200 cm^2/Vs.

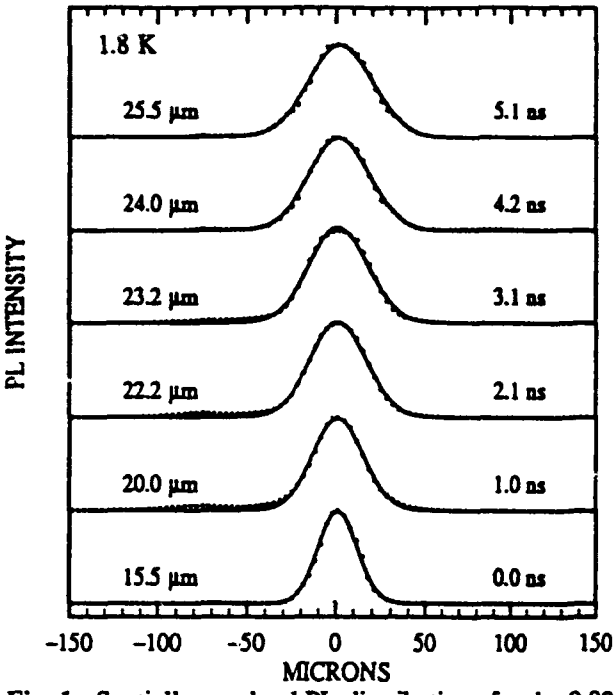

Fig. 1. Spatially-resolved PL distributions for the 9.82 μm sample at various times after the laser pulse at 1.8 K. FWHM at each time is indicated.

Since most transport is measured electrically,[9-11] transport properties are most commonly reported as mobilities. Here, we measure diffusion constants directly, not mobilities. These diffusion constants may be converted into mobilities through application of the Einstein relation. However, caution must be exercised for the following reasons: (1) degeneracy effects may become important at these low-temperatures and high excitation densities, (2) excitons may not be in thermal equilibrium with the lattice, (3) free-carriers may still exist, even at these low temperatures, and may play a role in the observed transport, (4) radiative absorption and reemission of photons may distort the observed measurements, and (5) excitons are bosons, not fermions. These difficulties are very hard to address, and are the current subject of study. To date, we have observed the following regarding these issues:[12] (1) The degeneracy effects of bosons act in an opposite direction to that of fermions, and if the transport involves both species (free-excitons and free carriers), then degeneracy effects become quite complicated, (2) in some structures free-exciton lifetimes are > 15 μs at ~ 25 K, and have most probably reached thermal equilibrium with the lattice. However, at 2 K, the free-exciton lifetime is < 1 ns, possibly precluding complete thermalization with the lattice. (3) Our detailed free-exciton PL decay kinetics measurements and modeling substantiate our hypothesis that free-carriers play a significant role in the dynamics of free-exciton emission even at 4 K. (4) Photon recycling at the free-exciton resonance may occur, but has only a minor effect on free-exciton kinetics (factor of < 2 in lifetime).[13]

Figure 4 shows all of our measured diffusivities converted into into mobilities (using the Einstein relation), for comparison purposes, versus temperature and laser power for our 9.82 μm and 0.30 μm thick GaAs structures. At high temperatures (> 50 K) the transport is of free-carriers. In our 9.82 μm structure we observe hole-dominated ambipolar transport, whereas in our 0.30 μm structure we observe a time-dependent change from electron-dominated to hole-dominated ambipolar transport.[5,6] These results

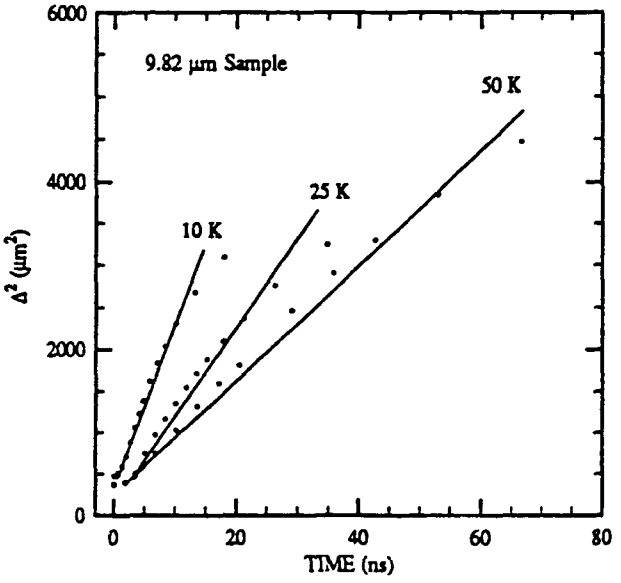

Fig. 2. Full-width at Half-Maximum squared versus time and temperature for the 9.82 μm thick structure.

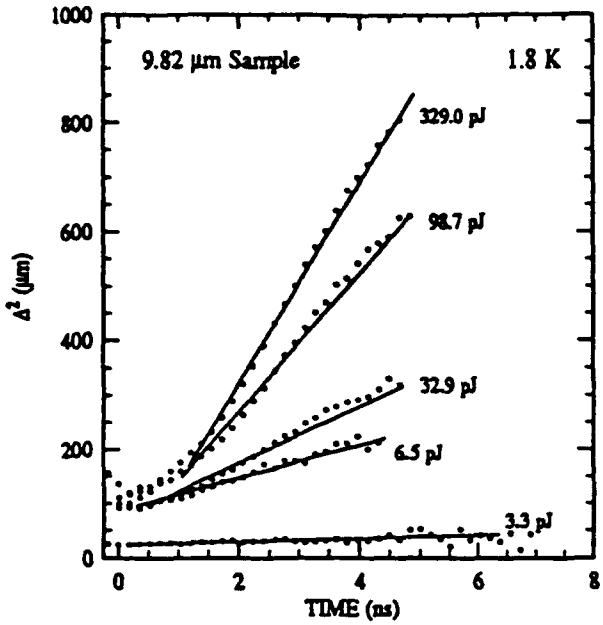

Fig. 3. Laser excitation power dependence of Δ at 1.8 K. Energies are per laser pulse.

are well-understood and in excellent agreement with our PL decay kinetics.[6] However, the power-dependent diffusivities at low-temperatures are not understood.

One possible mechanism for this power-dependent transport may be the "phonon-wind".[7,8] This mechanism has been conclusively shown to play an important role in the transport of excitons and electron-hole droplets in Si and Ge.[7,8] Tightly focussed laser excitation generates a high-density of phonons and carriers localized at this spot. These phonons (primarily low-frequency acoustic phonons) may then couple to the excitons, transferring their momentum, and driving the excitons away from this spot. This leads to a characteristic spatial distribution for this transport mechanism, a *shell-shaped* distribution.[8] Figure 5 shows a gedanken experiment, de- signed to clarify this issue. Here, a slit and crossed-slit scan are performed on both a normally-diffusing and phonon-driven exciton distribution.

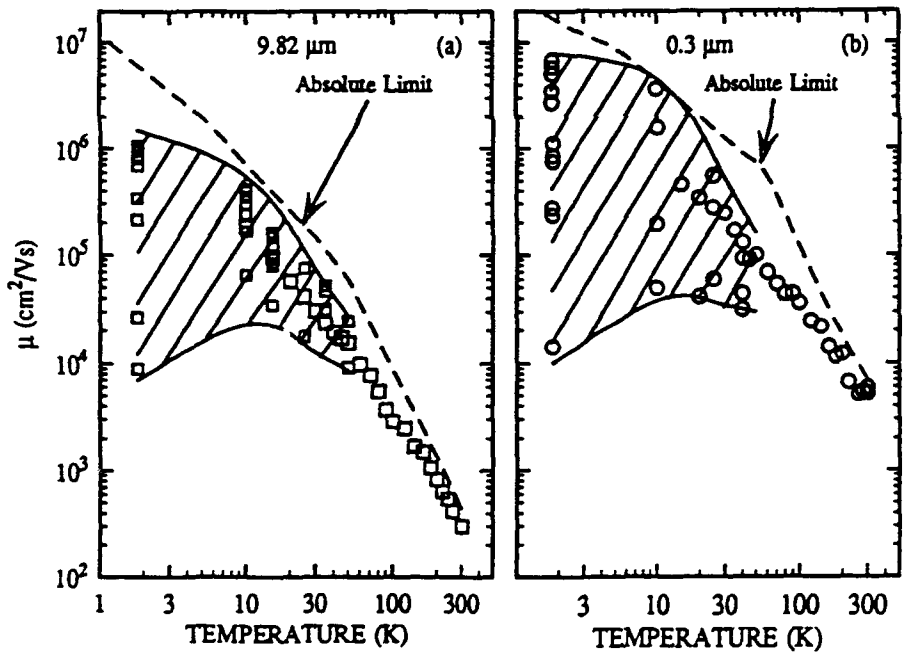

Fig. 4. Temperature dependence of mobilities derived from measured diffusivities and the Einstein relation for our (a) 9.82 μm and (b) 0.30 μm structures. Absolute mobility limits are taken from Ref. 14.

Clearly the correct technique for distinguishing these two mechanisms is with a crossed-slit scan. We have measured the detailed two-dimensional, space- and time-resolved PL (just as was done by Wolfe, et al.[8]), and do not observe the double peaks as in Fig. 5, and thus may conclusively rule-out "phonon-wind" driven-transport as a causative mechanism for these extremely large, power-dependent diffusivities.

Another, possibly more plausible mechanism, for this anomalous transport is the joint diffusion of free-excitons and free-carriers, coupled through temperature-dependent capture and ionization.[12] This mechanism relies on the same physics as our model

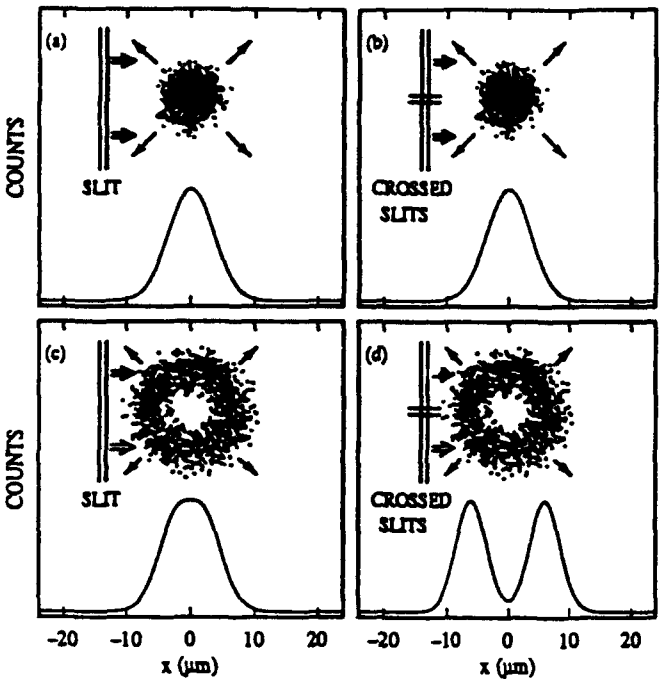

Fig. 5. Gedanken experiment simulating slit scan and crossed-slit scans of both a normally-diffusing (a) and (b) and phonon-wind driven (c) and (d) exciton distribution.

for free-exciton decay kinetics, and involves the solution of coupled, power-dependent free-carrier and free-exciton rate equations. In this context, free-carriers quickly condense into free-excitons, which then diffuse and decay radiatively with a lifetime of < 1 ns; simultaneously, remaining free-carriers diffuse and then condense into free-excitons, which then recombine. Therefore, our measured transport, though spectrally resolved, may actually represent the joint motion of both free-excitons and free-carriers. At this point the importance of photon-recycling is unclear, and is being studied.

IV. Conclusion

We have observed anomalous, low-temperature, laser power dependent transport of free-excitons in GaAs structures. We find peak 2 K diffusivities of > 1000 cm^2/s. The apparent mechanism for these transport results is connected to the interaction between the transport of both free-excitons and free-carriers, which is both laser-power and temperature-dependent. Future research to further clarify our results includes resonant excitation experiments.

Supported in part by ONR under contracts N00014-85-C-0868, N00014-90-C-0077, and N00014-91-J-1697, and the US DOE under contract DE-AC04-756DP00789.

REFERENCES

†Present Address: Emory Univ., Dept. of Physics, Atlanta, GA 30322
‡Present Address: Univ. of Wisconsin, Dept. of Chem. Eng., Madison, WI 53706

1. A. Olsson, D.J. Erskine, Z.Y. Xu, A. Schremer, and C.L. Tang, Appl. Phys. Lett. 41, 659 (1982).
2. H. Hilmer, A. Forchel, S. Hansmann, M. Morohashi, E. Lopez, H.P. Meier, and K. Ploog, Phys. Rev. B 39, 10901 (1989).
3. R.K. Ahrenkiel, D.J. Dunlavy, D. Greenberg, J. Schlupmann, H.C. Hamaker, and H.F. MacMillan, Appl. Phys. Lett. 50, 1329 (1987).
4. L.M. Smith, D.J. Wolford, J. Martinsen, R. Venkatasubramanian, and S.K. Ghandi, J. Vac. Sci. Technol. B 8, 787 (1990).
5. G.D. Gilliland, D.J. Wolford, T.F. Kuech, and J.A. Bradley, Appl. Phys. Lett. 59, 216 (1991).
6. G.D. Gilliland, D.J. Wolford, T.F. Kuech, and J.A. Bradley, J. Appl. Phys., to be published.
7. M. Greenstein and J.P. Wolfe, Phys. Rev. Lett. 41, 715 (1978).
8. J.P. Wolfe, J. Lumin. 30, 82 (1985).
9. M.I. Nathan, W.P. Dumke, K. Wrenner, S. Tiwari, S.L. Wright, and K.A. Jenkins, Appl. Phys. Lett. 52, 654 (1988).
10. C. Guillemot, M. Baudet, M. Gauneau, A. Regreny, and J.A. Portal, Phys. Rev. B 35, 2799 (1987).
11. C.M. Wolfe, G.E. Stillman, and W.T. Lindley, J. Appl. Phys. 41, 3088 (1970).
12. D.J. Wolford, G.D. Gilliland, T.F. Kuech, J.A. Bradley, and H.P. Hjalmarson, Inst. Phys. Conf. Ser. 120, (IOP Bristol, 1992), p. 271.
13. D.J. Wolford, G.D. Gilliland, T.F. Kuech, J.A. Bradley, and H.P. Hjalmarson, Bulletin of the American Physical Society 36, 648 (1991).
14. W. Walukiewicz, J. Appl. Phys. 59, 3577 (1986); W. Walukiewicz, H.E. Ruda, J. Lagowski, and H.C. Gatos, Phys. Rev. B 30, 4571 (1984).

Proc. of 21st Int. Conf. the Physics Semiconductors, Beiji China, (World Scient 1992), p. 1250.

OPTICALLY-DETERMINED EXCITONIC TRANSPORT IN TYPE-II GaAs/AlAs SUPERLATTICES

G.D. Gilliland,†, D.J. Wolford, and J.A. Bradley
IBM Research Division, T.J. Watson Research Center
P.O. Box 218
Yorktown Heights, New York 10598
and
J. Klem
Sandia National Laboratories
Albuquerque, NM 87185

We have, for the first time, directly measured the transport of excitons in a Type-II superlattice. Our results confirm the existence of exciton localization and thermally-activated hopping. Implications of these results are discussed.

I. Introduction

Quantum-confinement effects leading to excitonic localization in one-dimension have been thoroughly demonstrated in GaAs/$Al_xGa_{1-x}As$ quantum well structures.[1] For periodic structures with sufficiently thin $Al_xGa_{1-x}As$ layers, wavefunction interaction through the $Al_xGa_{1-x}As$ barrier layer may lead to extended states, i.e. superlattice minibands. Additionally, for very short-period multiple-quantum-well structures, the quantum-confinement effects may raise both the GaAs Γ and the $Al_xGa_{1-x}As$ X conduction-band-edges. With judicious choice of both GaAs and $Al_xGa_{1-x}As$ layer thicknesses (as well as $Al_xGa_{1-x}As$ composition) a Type-II band alignment may result, wherein the lowest energy states for electrons and holes occur in different layers of the structure.[2] Specifically for the $(GaAs)_m/(AlAs)_n$ system, this may occur for GaAs-layer thicknesses < 35 Å (m < 13) and AlAs-layer thicknesses > 15 Å (n > 6).[3] Excitons in these Type-II systems are thus indirect in real-space and in momentum-space.

Generally, it is agreed that the lowest hole-state remains in the GaAs-layer for such Type-II systems, whereas, in contrast, there is considerable confusion and disagreement about the nature of the lowest electronic state.[1,4-10] This confusion arises in part from the three-fold-degenerate X-electron states in the AlAs layers. This degeneracy may be removed by several effects, including: the anisotropic X-electron mass ($m_e(X_Z)$ = 1.1 m_0 and $m_e(X_{X,Y})$ = 0.19 m_0), strain-induced splitting of X_Z and $X_{X,Y}$, Γ-X mixing due to the superlattice potential, and short-range lattice disorder resulting in excitonic localization, etc..[4-10]

We report here the <u>first observation</u> of lateral excitonic transport in a Type-II $(GaAs)_m/(AlAs)_n$ (m=11 and n=19) short-period superlattice. This was accomplished using an all-optical time-resolved photoluminescence (PL) imaging technique, which is unique (compared to electrical techniques) in its sensitivity to neutral-particle transport.[11,12] The goal of this study is to further understanding of nature of the excitonic states in Type-II structures, as well as the importance of interfacial atomic and electronic structure. In particular, there has been much speculation in the literature concerning the effects of excitonic localization by interface disorder (as inferred <u>*indirectly*</u> from PL time decay measurements), and we show here <u>directly</u> that this localization does indeed exist. Further, we find significant thermal detrapping of these weakly localized excitons, and extract a localization energy.

II. Samples and Experiment

Our sample was a MBE-prepared, short-period GaAs(30 Å)/AlAs(50 Å) superlattice, with 55 periods. Most studies[4,5,6,7,13] although not all[2,9,10] have concluded that the lowest electron bound state is X_Z for most structures, whereas for structures with AlAs barriers < 60 Å it is $X_{X,Y}$. Indeed, Jaros, et. al[13] have found that X_Z is always

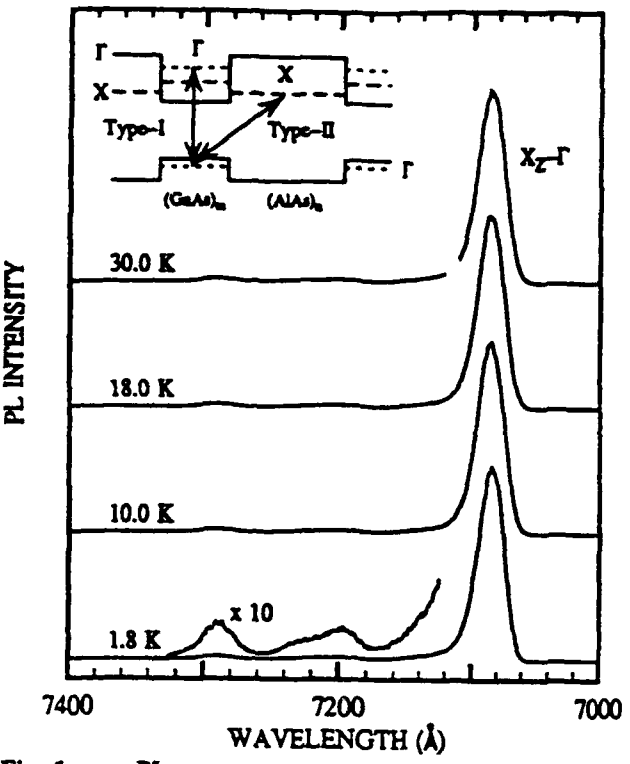

Fig. 1. cw PL spectra versus temperature. Inset shows schematic band diagram, with confinement energies (dotted line).

lowest in energy. For our structure, it is safe to conclude that X_Z is the lowest electronic state.

Using an all optical analog of the Haynes-Shockley experiment, we have measured time- and spatially-resolved PL profiles. PL was excited by a synchronously pumped cavity-dumped dye laser pumped by a frequency-doubled cw mode-locked Nd^{3+}:YAG laser. With our experimental setup, laser spot sizes of ~ 3 - 4 μm and PL images extending over 600 μm are obtainable. By imaging the sample (magnified by up to a factor of 40) and using time-correlated single photon counting, our total system response is ≈ 3 μm spatially, < 1 cm^{-1} spectrally, and < 500 ps temporally. The advantage and utility of this technique lies in its sensitivity to neutral-particle (exciton) transport, and the absence of required sample processing.

III. Results

Figure 1 shows cw PL spectra for our sample versus temperature. The excitonic no-phonon transition which we attribute to X_Z-Γ states is clearly evident, and substantially unchanging at all temperatures. Weaker phonon replicas are also evident at all temperatures. The linewidth of the X_Z-Γ transition varies little, from ~ 5.4 meV at 1.8 K to ~ 6.0 meV at 30 K. Figure 2 shows the PL time-decays for this sample versus temperature. Here, in contrast to our cw PL spectra, there is a dramatic variation in lifetime, from 21.5 μs at 1.8 K to ~ 20 ns at 30 K. Also, the decay kinetics are *nonexponential* at low-temperatures (lifetimes were derived from the exponential long-time tail part of the kinetics), and rapidly become *exponential* at higher temperatures (> 24 K).

Figure 3 shows our time-resolved PL-imaging results at 30 K. The solid lines represent fits to the data with Gaussian lineshapes, and the full-width at half-maximum (FWHM — Δ) is also shown for each "time window." These data show unmistakable evidence for the spatial transport of these Type-II excitons laterally along the heterointerfaces. A linear dependence of Δ^2 versus time is indicative of diffusive

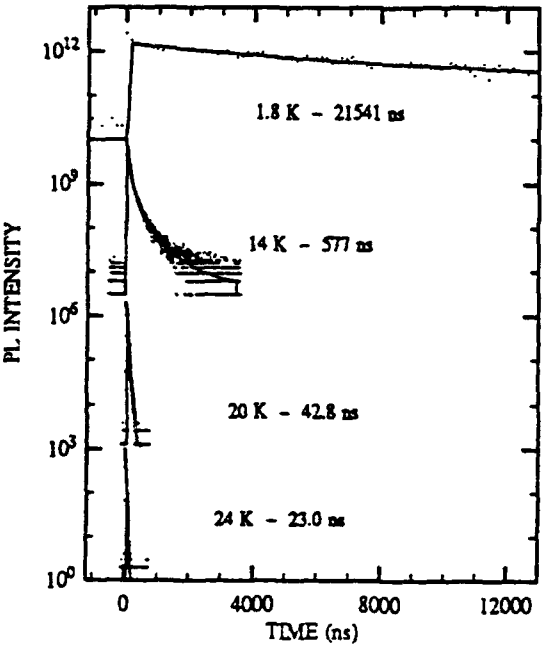

Fig. 2. PL time decays versus temperature.

transport, and this is indeed observed. We also observe a laser-power-dependent feature, which is also more prominent at low-temp- eratures, and negligible at high temperatures and low laser-powers (as used here). Specifically, at high laser-powers the FWHM increases very rapidly in the first several ns, and then saturates to its final slope (equal to that observed at low laser-powers — ~ 40 pJ/pulse). This is maybe related to the creation of an indirect-gap electron-hole plasma.[14] Nevertheless, our results are specific to the diffusion of Type-II excitons in this structure, since all measurements were made at low powers.

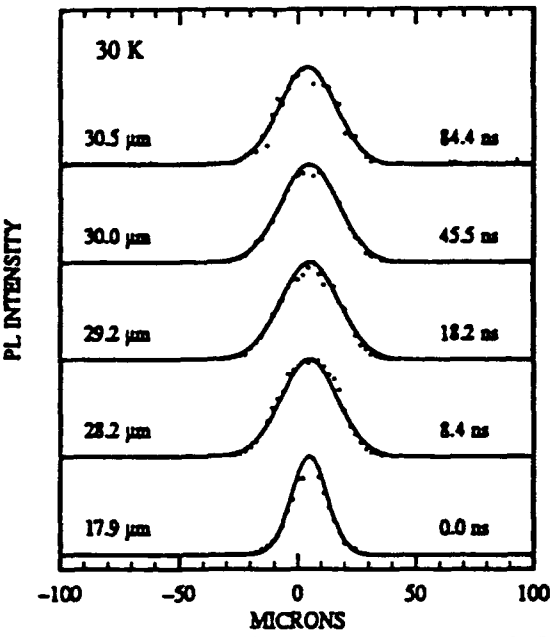

Fig. 3. Spatially and temporally-resolved X_Z-Γ PL distributions at 30 K.

These transport results are summarized in Fig. 4. Here, the diffusion constant obtained as shown above is plotted versus temperature. Diffusion constants range from ~ 2×10^{-3} cm^2/s at 1.8 K to ~ 7.0 cm^2/s at 30 K — a $\underline{5 \times 10^3}$ change in just 30 K. Additionally, PL lifetimes versus temperature are shown in this figure. Importantly, we find that lifetimes decrease while diffusivities increase with temperature.

IV. Discussion

Time-resolved studies of Type-II excitonic recombination in GaAs/AlAs short-period superlattices[2,7-9,15] and $GaAs/Al_xGa_{1-x}As$ superlattices under pressure[16] are ubiquitious in the literature. In all of these studies,[2,7-9,14-16] one feature is particularly clear — *lifetimes decrease with increasing temperature*. The general conclusion inferred from this is that the temperature-dependence is caused by the thermally-induced detrapping of excitons from a distribution of localized states resulting from possible interface disorder. At low-temperatures, excitons are localized in the low-energy sites at the heterointerface, whereas at higher temperatures, thermal detrapping of these excitons allows them to migrate until they eventually become trapped at a nonradiative defect, thus shortening the observed lifetime. However, these conclusions have <u>never</u> been directly proven. Indeed, if this hypothesis is true, then the observed temperature invariance of the PL lineshape suggests that Type-II radiative recombination predominantly occurs from localized states. Thus, the PL spectra is indicative of the energy distribution of localization sites. This detrapping may also occur at high excitation powers.

Our transport results are the <u>first</u> to definitely and directly show that this localization hypothesis is indeed true. Moreover, we have quantified the magnitude of the diffusion versus temperature, and find thermally activated transport, with an activation energy of ~ 8.6 meV — 40 % larger than the PL linewidth. We conclude the temperature-dependent transport is due to a temperature-dependent occupation of mobile versus stationary "localized states." The transport most probably occurs by thermally-activated hopping. Additionally, more detailed measurements of Type-II exciton transport versus emission energy are currently in progress, in an effort to identify a possible "mobility edge."

These results may also permit examination of heterointerface quality. Our temperature-dependent transport is most likely indicative primarily of this thermal occupa-

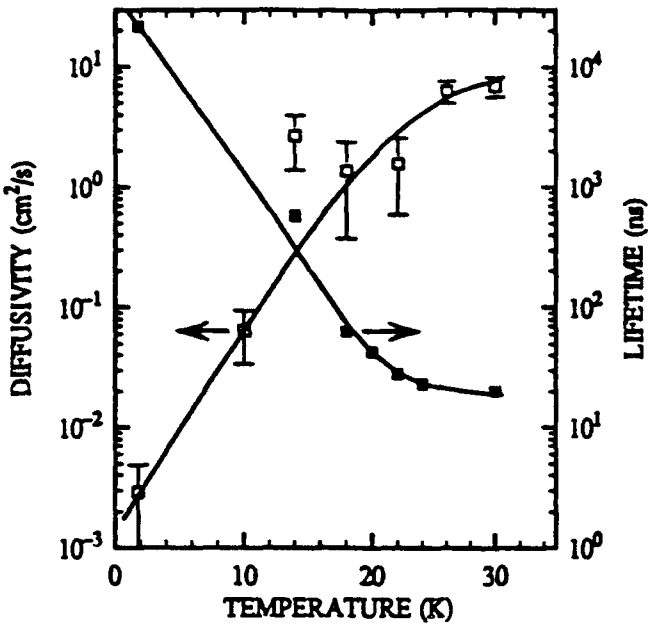

Fig. 4. Diffusion constants and PL lifetimes versus temperature.

tion of mobile versus localized states, instead of a temperature-dependent mobility of the delocalized excitons. Thus, a realistic scattering model would include significant localization and a temperature-dependent occupation of the mobile versus localized states — leading to quantification of scattering or capture times into the localized states. This scattering time may also be related to the "dephasing" of the excitonic ensemble, since it represents one of many contributions to the total dephasing. These issues will be addressed in the future through detailed modeling and possibly direct measurements of the dephasing rate.

V. Conclusion

We have directly measured the transport of excitons in Type-II short-period GaAs/AlAs superlattices, for the first time. We have quantified this transport and find thermalization from highly-localized states. At high powers, we observe an initial rapid expansion followed by slower transport at late times. This results from the formation and transport of an indirect electron-hole plasma, and is also confirmed in our time-resolved PL. Our results also quantify the heterointerface disorder (8 meV localization energy).

Supported under ONR contracts N00014-85-C-0868, N00014-90-C-0077, and N00014-91-J-1697.

REFERENCES

†Present Address: Emory Univ., Dept. of Physics, Atlanta, GA 30322

1. R. Dingle, A.C. Gossard, and W. Wiegmann, Phys. Rev. Lett. 34, 1327 (1975).
2. E. Finkman, M.D. Sturge, M.H. Meynadier, R.E. Nahory, M.C. Tamargo, D.M. Hwang, and C.C. chang, J. of Lumin. 39, 57 (1987).
3. K.J. Moore, P. Dawson, and C.T. Foxon, Phys. Rev. B 38, 3368 (1988).
4. P. Dawson, C.T. Foxon, and H.W. van Kesteren, Semicond. Sci. Technol. 3, 54 (1990).
5. W. Ge, M.D. Sturge, W.D. Schmidt, L.N. Pfeiffer, and K.W. West, Appl. Phys. Lett. 57, 55 (1990).
6. H.W. van Kesteren, E.C. Cosman, P. Dawson, K.J. Moore, and C.T. Foxon, Phys. Rev. B 39, 13426 (1989).
7. D. Scalbert, J. Cernogora, C. Benoit a la Guillaume, M. Maaref, F.F. Charfi, and R. Planel, Surface Science 229, 464 (1990).
8. F. Minami, K. Hirata, K. Era, T. Yao, Y. Masumoto, Phys. Rev. B 36, 2875 (1987).
9. E. Finkman, M.D. Sturge, and M.C. Tamargo, Appl. Phys. Lett. 49, 1299 (1986).
10. J. Ihm, Appl. Phys. Lett. 50, 1068 (1987).
11. G.D. Gilliland, D.J. Wolford, T.F. Kuech, and J.A. Bradley, Appl. Phys. Lett. 59, 216 (1991).
12. D.J. Wolford, G.D. Gilliland, T.F. Kuech, J.A. Bradley, and H.P. Hjalmarson, Phys. Rev. B, unpublished.
13. L.D.L. Brown, M. Jaros, and D.J. Wolford, Phys. Rev. B 40, 6413 (1989).
14. J.L. Mackay, J.D. Sturge, M.H. Meynadier, M.D. Tamargo, and J.L. deMiguel, J. Lumin. 48,49, 731 (1991).
15. P. Dawson, K.J. Moore, C.T. Foxon, G.W. 'tHooft, and R.P.M. van Hal, J. Appl. Phys. 65, 3606 (1989).
16. T.W. Steiner, D.J. Wolford, T.F. Kuech, and M. Jaros, Superlattices and Micro. 4, 227 (1988); D.J. Wolford, T.F. Kuech, J.A. Bradley, M.A. Gell, D. Ninno, and M. Jaros, J. Vac. Sci. Technol. B 4, 1043 (1986).

Proc. of 21st Int. Conf. on the Physics of Semiconductors, Beijing, China, (World Scientific 1992), p. 1743.

INTRINSIC AND INTERFACIAL RECOMBINATION IN OMVPE- AND MBE-PREPARED $GaAs/Al_xGa_{1-x}As$ HETEROSTRUCTURES

G.D. Gilliland,† D.J. Wolford, T.F. Kuech,‡ and J.A. Bradley
IBM Research Division, T.J. Watson Research Center
P.O. Box 218
Yorktown Heights, New York 10598
and
J. Klem and H.P. Hjalmarson
Sandia National Laboratories
Albuquerque, NM 87185

We have studied intrinsic free-carrier recombination in a variety of GaAs structures, including: OMVPE- and MBE-prepared $GaAs/Al_xGa_{1-x}As$ double heterostructures, Na_2S passivated GaAs structures, and bare GaAs structures. We find OMVPE-prepared structures are superior to all of these other structures with 300 K lifetimes of ~ 2.5 μs and negligible nonradiative interface and bulk recombination, and thus are truly surface-free ($S < 40$ cm/s). Moreover, we observe systematic trends in optical properties versus growth conditions. Lastly, we find that the presence of free-exciton recombination in the low-temperature photoluminescence spectra is a necessary but not sufficient condition for optimal optical properties (i.e. long minority-carrier lifetimes).

I. Introduction

Bare GaAs surfaces are notorious for the large number of dangling bonds and the corresponding high-density of recombination centers, which results in poor electronic and optical properties.[1-6] These surface states act as sinks for nonradiative recombination of minority-carriers, and, consequently, may have a huge negative impact on the optical properties of minority-carriers, including photoluminescence (PL) efficiencies and lifetimes.[1-6] Fortunately, there are techniques to improve the minority-carrier properties through the reduction of the nonradiative surface states.[5,7-9] This passivation may be achieved by a variety of means; however, the most successful of these techniques is by epitaxial growth of $Al_xGa_{1-x}As$ layers on both sides of the active GaAs layer. In this paper we report our attempts at optimizing minority-carrier properties, and our success at the almost total elimination of the competing and spurious nonradiative decay at any surface or interface states. This was achieved through systematic variation of growth parameters and subsequent full characterization of various optical properties. Thus, we have discovered the optimal growth conditions which yield the best optical properties, and, as a result, may compare OMVPE- and MBE-growth as well as heterointerfacial quality.

II. Samples and Experiment

In the last few years we have studied the optical properties of OMVPE-prepared, nominally-undoped, symmetric $GaAs/Al_{0.3}Ga_{0.7}As$ double heterostructures.[8-12] After systematic growth parameter variation, we arrived at this optimal set of growth conditions: $T_g \approx 750°C$, V/III ratio of ≈ 40, 30 second growth interruptions at each interface, and 35 nm/min. growth rate. Resulting GaAs layers were n-type ($10^{15}cm^{-3}$) with thicknesses from 50 Å to 10 μm. $Al_{0.3}Ga_{0.7}As$ layers were p-type ($10^{16}cm^{-3}$) with a 0.5 μm thickness.

Here, our goal is to conduct a parallel study for MBE-prepared structures, and then to compare the optical quality of MBE versus OMVPE structures. Our canonical sample for optimization was an undoped, symmetric double heterostructure with each of the 3 layers 0.5 μm thick. We have systematically varied the growth temperature, growth temperature profile, growth rate, and interruption time to achieve optimal results. Following this we varied the GaAs-layer thickness (4.0 μm to 50 Å) to determine the surface recombination velocity for these structures.

Our optical characterization involved measurements of room-temperature PL spec-

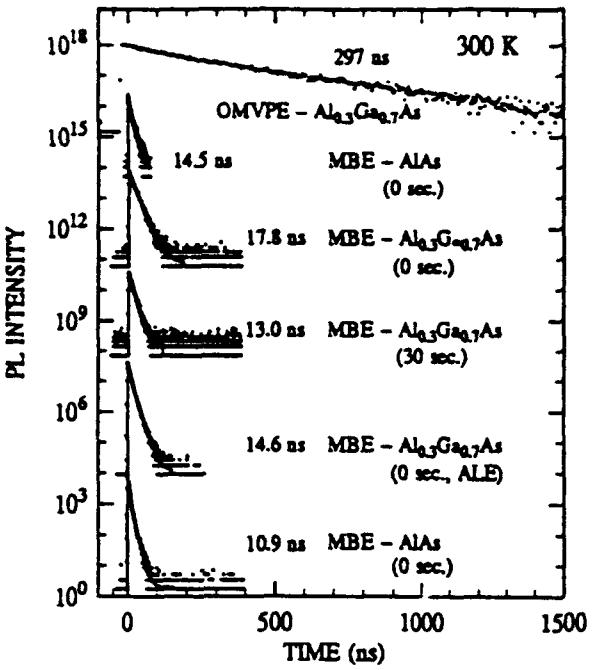

Fig. 1. 300 K PL time decays for 0.5 μm OMVPE and MBE structures. MBE samples were grown with $Al_xGa_{1-x}As$ barriers and growth interrupts as shown, with one using Atomic Layer Epitaxy (ALE).

tra, PL time-decays, all-optical PL imaging of minority-carrier transport, and 2 K PL spectra and time decays. All time-resolved PL was carried out with 50 ps resolution. Laser excitation beams were defocussed to ≈ 3 mm and attenuated to < 0.1 nJ/pulse energy for PL time decay measurements.

III. Results and Discussion

PL time decay kinetics are determined by the time-dependence of the minority-carrier density. This, in turn, is governed by the rate equations describing all possible radiative and nonradiative decay channels.[8] These equations may be then used to fit PL decay kinetics, thereby assessing the importance of each contribution to the minority-carrier decay.

A. OMVPE-Prepared Samples

We have extensively studied the kinetics of free-carrier and free-exciton recombination and the dynamics of free-carrier transport in our series of OMVPE-prepared double heterostructures (thicknesses from 50 Å to 10 μm) versus temperature (2 K - 300 K).[8-12] In total we find the quality of these samples to be quite remarkable, and almost unequalled. These results are summarized as follows:

(1) Very long minority-carrier lifetimes — > 2.5 μs for a 10 μm thick sample.
(2) Extremely low surface recombination velocities — < 40 cm/s.
(3) Negligible bulk nonradiative decay — $\tau_{nr} > 3$ μs.
(4) Long minority-carrier diffusion lengths — $L_d > 100$ μm.
(5) Prominent free-exciton PL at low temperatures.

Importantly, we find that all decay kinetics, including versus temperature, may be readily understood by a set of coupled rate equations describing the temperature-dependent free-carrier decay and capture by impurities and free-excitons. Moreover, all kinetics results agree quantitatively with all of our transport measurements.

B. MBE-Prepared Samples

Before attempting to assess the absolute quality of the MBE-prepared double heterostructures (i.e. surface recombination velocities from detailed thickness-dependent measurements), we chose to optimize the observed optical properties of a canonical 0.5 μm thick structure through variation of various growth parameters. This also enables a detailed comparison with our 0.5 μm thick OMVPE-prepared structures. The possible growth parameters which may be varied include: growth temperature, growth rate, $Al_xGa_{1-x}As$ barrier composition, growth temperature profile, interruption time at each heterointerface, and use of atomic layer epitaxy.

Figure 1 shows room temperature PL time-decays for several MBE-prepared samples compared to our canonical, best 0.5 μm thick OMVPE-prepared sample. Here the growth parameters varied include $Al_xGa_{1-x}As$ barrier composition ($Al_{0.3}Ga_{0.7}As$ and AlAs), growth interrupt time at each heterointerface, and use of atomic layer epitaxy. None of these parameters had any significant impact on our results. Clearly these results are inferior to our OMVPE results, possibly indicative of larger nonradi-

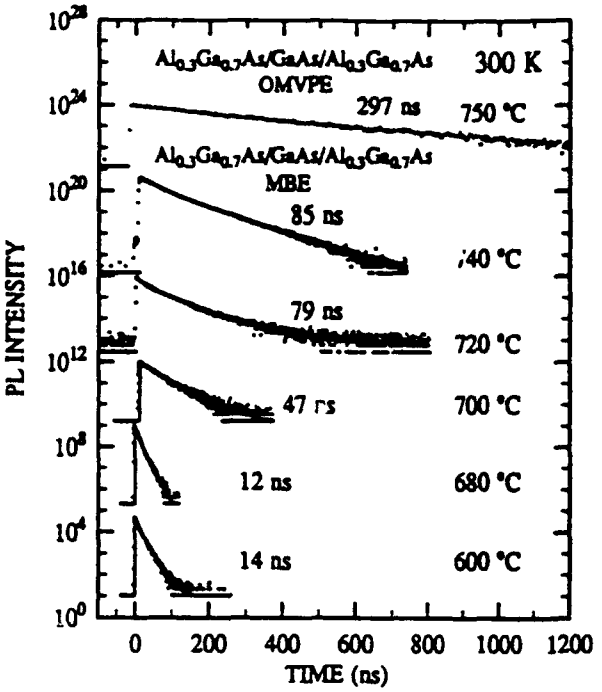

Fig. 2. 300 K PL time decays versus MBE growth temperature compared to our canonical OMVPE 0.5 μm sample. Lifetimes represent exponential tail of decay.

ative interface recombination. These results are surprising since these samples were grown in reactors routinely capable of producing 1 x 10^6 cm^2/Vs mobility modulation-doped structures — considered to be indicative of high heterointerfacial quality.

Figure 2 shows 300 K PL time decays versus growth temperature. Here, there is a clear and systematic trend with lifetimes increasing with growth temperature. The maximum lifetime of 85 ns is achieved at the highest growth temperature possible in this system (~ 740°C), limited by the As flux required to keep the surface As stabilized. Thus, growth temperature appears to be an important factor in improving the optical properties, and hence minority-carrier properties, in these structures. Further study of other growth parameters is currently in progress.

C. Surface Recombination Velocities

At this point we may proceed with a detailed GaAs-layer thickness dependent study of kinetics in these optimized, high-growth temperature MBE samples. Figure 3 shows the results of all of our measurements in all of our structures. Here τ is plotted versus GaAs-layer thickness, and the solid lines represent fits to the lifetimes yielding the surface recombination velocities and bulk nonradiative decay rates. Our OMVPE samples are clearly superior to all others, with the MBE samples next. The Na_2S passivated OMVPE structures are inferior to both of these other *permanent* growth techniques (Na_2S is hygroscopic). Further, all of these passivation techniques show dramatic improvement over the single bare GaAs surface. Additionally, we find that these changes in lifetimes are quantatitively reflected in the PL efficiencies.

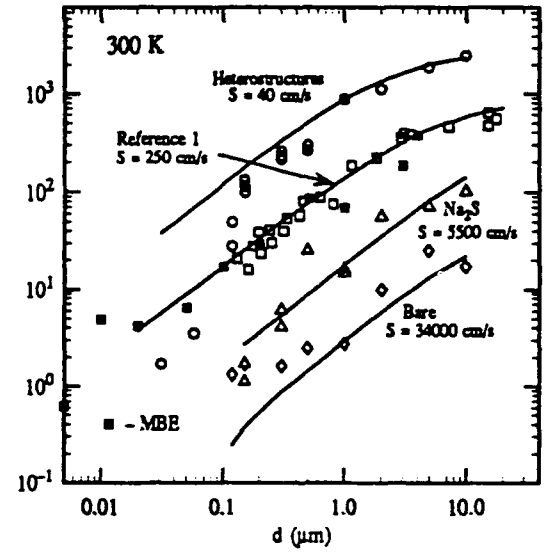

Fig. 3. 300-K lifetimes for OMVPE GaAs/$Al_{0.3}Ga_{0.7}As$ double heterostructures (o), etched and Na_2S repassivated structures (Δ), "bare" heterostructures (◊), MBE heterostructures (□), and LPE double heterostructures (from Ref. 1) (□) — all versus GaAs-layer thickness. Lines represent least-squares fits yielding interface recombination velocities shown.

D. Free-Exciton Recombination

After such thorough characterization of heterointerfacial quality, we examined the low-temperature PL spectra and time-decays for these OMVPE- and MBE-prepared samples. We find all spectra in all high-heterointerfacial qual-

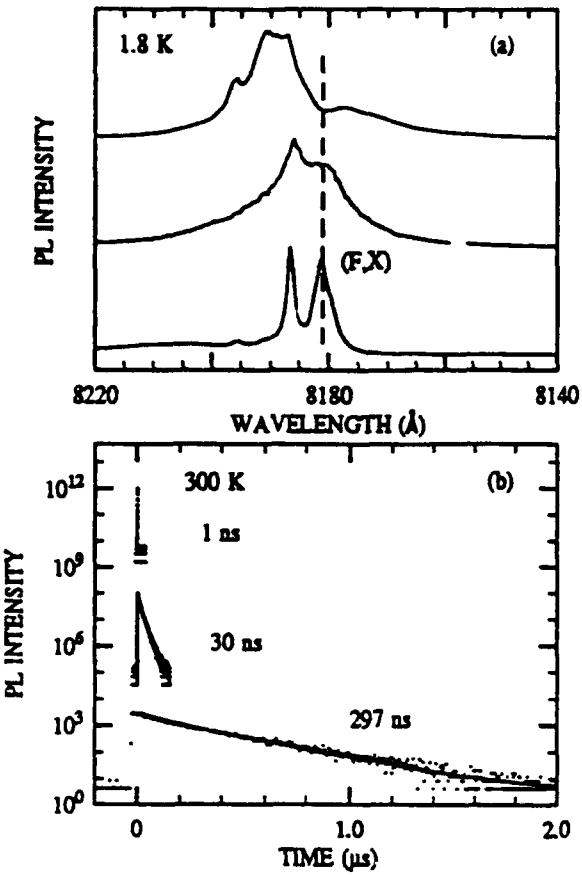

Fig. 4. (a) 1.8 K PL spectra for (top) poor, (middle) fair, and (bottom) good GaAs heterostructures. Note appearance of dip at free-exciton resonance in poor sample. (b) Corresponding lifetimes to same samples in (a) at 300 K.

ity samples (as determined by 300 K lifetime measurements) uniformly exhibit free-exciton emission, as opposed to the common occurrence of the dip and so-called "upper and lower exciton-polariton branches."[13] This appears to be *a necessary, but not sufficient* condition for long free-carrier lifetimes and low interface-recombination velocities. The "dead-layer" which is thought to be responsible for the above mentioned PL dip may also influence the minority-carrier kinetics. Figure 4 demonstrates this connection between dead-layer effects and short free-carrier lifetimes.

IV. Conclusion

We have demonstrated the possibility of preparing truly "surface-free" structures through the growth of GaAs/$Al_{0.3}Ga_{0.7}As$ heterostructures and have found the optimal growth conditions for such ideal samples. We have also found that OMVPE-prepared structures are ~ 3 times superior to MBE-prepared structures. This appears to be the result of increased bulk and interface recombination. Lastly, we have observed that high-quality heterointerfacial properties are always accompanied by prominent free-exciton emission.

Supported in part by ONR under contracts N00014-85-C-0868, N00014-90-C-0077, and N00014-91-J-1697, and the US DOE under contract DE-AC04-756DP00789.

REFERENCES

†Present Address: Emory Univ., Dept. of Physics, Atlanta, GA 30322
‡Present Address: Univ. of Wisconsin, Dept. of Chem. Eng., Madison, WI 53706

1. R.J. Nelson and R.G. Sobers, J. Appl. Phys. 49, 6103 (1978).
2. M.G. Mauk, S. Xu, D.J. Arent, R.P. Mertens, and G. Borghs, Appl. Phys. Lett. 54, 213 (1989).
3. B.J. Skromme, C.J. Sandroff, E. Yablonovitch, and T. Gmitter, Appl. Phys. Lett. 51, 2022 (1987).
4. L.M. Smith, D.J. Wolford, J. Martinsen, R. Venkatasubramanian, and S.K. Ghandi, J. Vac. Sci. Technol. B 8, 787 (1990).
5. R.K. Ahrenkiel, B.M. Keyes, and D.J. Dunlavy, J. Appl. Phys. 70, 225 (1991).
6. G.B. Lush, D.H. Levi, H.F. MacMillan, R.K. Ahrenkiel, M.R. Melloch, and M.S. Lundstrom, submitted to Appl. Phys. Lett.
7. L.W. Molenkamp and H.F.J. van't Blik, J. Appl. Phys. 64, 4253 (1988).
8. G.D. Gilliland, D.J. Wolford, T.F. Kuech, and J.A. Bradley, J. Appl. Phys., to be published.
9. G.D. Gilliland, D.J. Wolford, T.F. Kuech, J.A. Bradley, C.F. Tsang, and H.P. Hjalmarson, unpublished.
10. D.J. Wolford, G.D. Gilliland, T.F. Kuech, L.M. Smith, J. Martinsen, J.A. Bradley, C.F. Tsang, R. Venkatasubramanian, S.K. Ghandi, and H.P. Hjalmarson, J. Vac. Sci. Technol. B 9, 2369 (1991).
11. D.J. Wolford, G.D. Gilliland, T.F. Kuech, J. Martinsen, C.F. Tsang, J.A. Bradley, and H.P. Hjalmarson, Inst. Phys. Conf. Ser. 120, (IOP Bristol, 1992), p. 401.
12. G.D. Gilliland, D.J. Wolford, T.F. Kuech, and J.A. Bradley, Appl. Phys. Lett. 59, 216 (1991).
13. D.D. Sell, S.E. Stokowski, R. Dingle, and J.F. DiLorenzo, Phys. Rev. B 7, 4568 (1973).